On-line Monitoring and Controlling of Batch Crystallisation Using Rapid Heating and Cooling

Najah Battikh

Submitted for the degree of Doctor of Philosophy

Heriot-Watt University

School of Engineering and Physical Sciences
Institute of Mechanical, Process and Energy Engineering

April 2017

Abstract

Batch crystallisation is a common operation in the pharmaceutical and fine chemical industries for purification and separation. With the advent of industrially robust instruments to monitor crystallisation, it is now possible to develop more sophisticated control systems, to better control the crystal size and shape. However, with batch cooling crystallisation, the number of control handles that can be used in any control system is limited; a stirrer speed and heating/ cooling rates are the two that are readily available.

The work carried out in this PhD project aims to demonstrate that an online video imaging technique can be used to both monitor and control batch cooling crystallisation. The measuring technique has been developed using low-cost readily available camera and has been utilised to perform measurements of meta-stable zone width (MSZW) at different operating conditions and other key properties of L-glutamic acid and glycine solutions. Nucleation kinetics parameters for both the polythermal and isothermal experiments were calculated according to KBHR method. The outcomes of these experiments exhibited a good agreement with previous workers using more sophisticated measuring methods.

Traditional laboratory scale batch cooling systems use one hot/cold source in order to study crystallisation. When information from laboratory is applied to industrial scale, there is inherent issue with heat transfer related to the time constant which industrial systems can respond to. Therefore, in this thesis, a system which has the advantage of introducing a method to rapidly heat and cool a batch crystalliser has been developed. This was achieved by switching the water flow through the crystalliser jacket between hot and cold water baths using six solenoid valves. Different variables were examined; those included the switching frequency and duration as well as the temperature set point of the two baths. It was found that the switching duration had a little effect on the nucleation time and temperature. In contrast, the switching frequency had impact which was more obvious when the ratio became higher either for the cold bath duration to the hot one or vice versa. Moreover, the temperature set point of the hot and cold baths showed to be of great potential for switching effectiveness.

For the first time, a comparison of the switching technique, crash cooling and constant linear cooling rate effects on the nucleation point of glycine was presented. It was found that the switching mechanism gives controllable profile by selecting the hot and cold bath temperatures set point and the switching frequency. Therefore, switching method adds an additional level of control not possible with one water bath which is used in traditional cooling profiles (crash and linear).

Understanding the heat transfer phenomena in processes that are temperature limited, for instance cooling crystallisation, is of great importance for the overall process efficiency. Consequently, a simple heat transfer model of agitated vessel was developed in this work and showed its ability to predict the vessel temperature in the case of switching between hot and cold baths, programmed heating/cooling rates and crash heating/cooling. The evaluation of the different heat transfer resistances was also considered by using Wilson method.

There has recently been increasing emphasis on the control of crystallisation process to obtain particular physical properties for the produced crystals as this has a major effect on the effectiveness of the downstream processes. Accordingly, a control approach that integrated the process video imaging system with the switching technique was developed in this thesis. The experimental findings showed that the developed PVI-switching control system was able to control the crystallisation of LGA and glycine as it improved the overall quality of the crystals produced in terms of size and presence of fines over conventional methods. This was proved by analysing the images captured of the crystals at the end of experiment. In addition, the sensitivity and robustness of the developed control approach were also verified.

Dedication

This thesis is dedicated to my parents (Ghazy&Naima) and the memory of my dear aunt (Huda) who always supported me and believed that I would complete this PhD successfully.

Acknowledgements

There are a number of different individuals, groups and organisations whom I would like to thank for their support during my PhD study. First of all, I would like to express my deep gratitude and sincere thanks to Prof. Graeme White who supervised this PhD and provided continuous support throughout the research period, great encouragement and extensive feedback on drafts from the early days and up to the final stages of writing up this thesis. I am also grateful to Dr. Matthew Dunnigan, my second supervisor, for his invaluable advice.

Also, I would like to thank all the academic staff and technicians at the Chemical Engineering Department, Heriot-Watt University for their continuous support during my studies. I am most grateful to Eileen McEvoy for her special support. I take special pleasure in thanking my home university, Al-Baath University in Homs, Syria which offered me this great opportunity to pursue higher education (MSc and PhD) at Heriot-Watt University.

What I have achieved would not have been possible without the support of my family who have shown undying patience and support throughout my PhD journey and have always believed in my ability to persevere and achieve. Major thanks to my friends whose unremitting encouragement has been essential for me throughout this journey.

ACADEMIC REGISTRY
Research Thesis Submission

Name*:*	NAJAH BATTIKH		
School:	EPS-IMPEE		
Version: *(i.e. First, Resubmission, Final)*	Final	Degree Sought:	PhD in Chemical Engineering

Declaration

In accordance with the appropriate regulations I hereby submit my thesis and I declare that:

1) the thesis embodies the results of my own work and has been composed by myself
2) where appropriate, I have made acknowledgement of the work of others and have made reference to work carried out in collaboration with other persons
3) the thesis is the correct version of the thesis for submission and is the same version as any electronic versions submitted*.
4) my thesis for the award referred to, deposited in the Heriot-Watt University Library, should be made available for loan or photocopying and be available via the Institutional Repository, subject to such conditions as the Librarian may require
5) I understand that as a student of the University I am required to abide by the Regulations of the University and to conform to its discipline.
6) I confirm that the thesis has been verified against plagiarism via an approved plagiarism detection application e.g. Turnitin.

* *Please note that it is the responsibility of the candidate to ensure that the correct version of the thesis is submitted.*

Signature of Candidate*:*		Date:	

Submission

Submitted By *(name in capitals):*	NAJAH BATTIKH
Signature of Individual Submitting:	
Date Submitted:	

For Completion in the Student Service Centre (SSC)

Received in the SSC by *(name in capitals):*			
Method of Submission *(Handed in to SSC; posted through internal/external mail):*			
*E-thesis Submitted (**mandatory for final theses**)*			
Signature:		Date:	

Please note this form should be bound into the submitted thesis.
Academic Registry/Version (1) August 2016

Table of Contents

List of Tables

List of Figures

Nomenclature

Symbols	Definition	Units
A	Crystal surface area	m^2
B	Rate of secondary nucleation	nuclei/cm^3.s
b	Cooling rate	ºC/min
C^*	Equilibrium saturation concentration	g/l
C_c	Crystal concentration	g/ml
C_e	Solute concentration in equilibrium with particle of infinite radius size	kg/kg
C_i	Solute concentration at the crystal-solution interface	kg/kg
C_r	Solubility of crystal of radius r	kg/kg
ΔC_{max}	Maximum supersaturation at maximum possible super cooling	g/l
D	Solute diffusion coefficient	kg/m.s
G	Growth rate	m/s
g	Crystal growth order	--
ΔG	Overall free energy change	J
ΔG_{crit}	Free energy change for a nucleus of critical size	J
ΔG_{Homo}	Free energy change corresponds to homogeneous nucleation	J
ΔG_{Hetro}	Free energy change corresponds to heterogeneous nucleation	J
ΔG_S	Surface excess free energy	J
ΔG_V	Volume excess free energy	J
ΔG_v	Free energy change associated with the phase transition per unit volume	J/m^3
ΔH_f	Solute molar latent heat of fusion	J/mol
IDI	Area under intensity distribution curve at any time	$pixel^2$
IDI_{Max}	Maximum area under the intensity distribution curve	$pixel^2$
IDI_{Min}	Minimum area under the intensity distribution curve representing 0 g/ml crystal concentration	$pixel^2$
J	Nucleation rate	nuclei/cm^3.s
K	Boltzmann constant = 1.3805×10^{-23}	J/K

K	Nucleation rate constant	--
K_d	Diffusion mass transfer coefficient	$kg/s.m^2$
K_G	Overall crystal growth coefficient	$kg/s.m^2$
K_m	Mass transfer coefficient	$kg/s.m^2$
K_r	Surface reaction rate coefficient	$kg/s.m^2$
M_T	Suspension density	kg/m^3
m	Nucleation order	--
N	Agitation speed	rpm
$m_{r,LGA}$	Mass of recovered LGA as crystals	g
R	Universal gas constant = 8.314	J/mol.K
r	nucleus radius	m
r_c	critical nucleus radius	m
S	Supersaturation	--
T	Solution temperature	K
T_0	Temperature at the start of the process	ºC
T_{dis}	Dissolution temperature	ºC
T_{cry}	Crystallisation temperature	ºC
T_f	Temperature at the end of the process	ºC
T_f	Solute fusion temperature	K
T_{sat}	Saturation temperature	ºC
T_t	Temperature at time t during the process	ºC
ΔT_{max}	Meta-stable zone width	ºC
V	Vessel volume	ml
W%	White Pixels Percentage	%
W%_SP	White pixels percentage set-point	%
x	Solute mole fraction	--

Greek Letters

γ	Activity coefficient	--
γ	Interfacial tension	N/m
ε	Correction factor for the change in concentration for the hydrated salts	--
Θ	Contact angel	degree
σ	Relative supersaturation	--
υ	Molecular volume	m^3
δ	Stationary film thickness	m
Φ	Free energy ratio between homogeneous and heterogeneous nucleation	--
Ω	Molar volume of the particle in solution	m^3/mol

Abbreviations

ADNC	Automated Direct Nucleation Control
APIs	Active Pharmaceutical Ingredients
ATR-FTIR	Attenuated Total Reflection Fourier Transform Infrared
CCD	Charged Coupled Device
CFD	Computational Fluid Dynamic
CLD	Chord Length Distribution
CSD	Crystal Size Distribution
DNC	Direct Nucleation Control
DSC	Differential Scanning Calorimetry
FBRM	Focused Beam Reflectance Measurement
IDI	Intensity Distribution Integral
IR	Infrared
KBHR	Kashchiev, Borissova, Hammond and Roberts
LDS	Laser Diffraction Spectroscopy
LED	Light-Emitting Diode
LGA	L-glutamic Acid
MSZW	Meta-stable Zone Width
NRTLSAC	Non-Random Two-Liquid - Segment Activity Coefficient
OBC	Oscillatory Baffled Crystalliser
PAT	Process Analytical Technology
PC	Personal Computer
PIV	Particle Image Velocimetry
PVI	Process Video Imaging
PVM	Particle Vision and Measurement
RCI	Retreat Curve Impeller
SDC	Smallest Detectable Crystal
SSC	Supersaturation Control
UNIFAC	Universal Functional Activity Coefficient
UV-VIS	Ultra-Violet Visible Spectroscopy

List of Publications

- N. Battikh, G. White, “On-line Video Imaging System for Controlling Batch Crystallisation”, 1st IMPEE Conference, Heriot-Watt University, Edinburgh, UK, June. 2013.

- N. Battikh, G. White, “Optical Monitoring of Crystallisation- Impeller Characteristics”, 2nd IMPEE Conference, Heriot-Watt University, Edinburgh, UK, July. 2014.

- N. Battikh, G. White, “Optical Monitoring of Crystallisation: Determination of L-Glutamic Acid Metastable Zone Width (MSZW)”, in APACT 15, Manchester, UK, April. 2015.

Chapter 1
Introduction

This thesis concerns the development of a real-time video imaging system combined with a novel thermal switching technique, to control the batch crystallisation of two model compounds. Optical methods for determining the nucleation, growth and identification of crystals have been developed by a number of workers and have proved useful to detect, for example, the change in polymorphic form of crystals which exhibit polymorphism. The imaging technique here is based on this published work, using an external digital camera and PC to process images in real time.

Control of batch crystallisation has recently focused on methods to monitor the chemistry and events within the crystalliser using techniques such as ATR-FTIR and FBRM. These control systems are normally linked to manipulate the set point of single heater/cooler units in an attempt to produce better crystals. However, temperature manipulation is characterised by relatively long response times, far longer than the kinetic rate of nucleation. This means that responding to changes in nucleation and spontaneous growth of crystals is not feasible by only adjusting the temperature set point of a single water bath. Therefore, this thesis presents a novel method to quickly change the crystalliser wall temperature by switching between hot and cold baths in an attempt to affect the nucleation and the growth rate of crystals in a faster way. This method provides additional level of control for cooling crystallisation.

This chapter highlights the motivation behind this work, where the importance of controlling the quality of crystals in terms of size, shape and morphology is mentioned. The application of an optical technique in monitoring and controlling the crystallisation process is introduced. The chapter closes with outlining the structure of the thesis, pointing out the main aspects that were investigated in this work.

1.1 Research Background and Motivation

Crystallisation from solution has widespread use in the pharmaceutical, food and fine chemical industries to obtain substances in a pure form. It has an advantage of lower energy consumption compared with other separation processes, such as, filtration and distillation. Crystallisation itself can be achieved by evaporation of the solvent, addition

of anti-solvent that changes the solubility within a crystalliser, and by cooling a solution which is at a high temperature. However, in cooling crystallisation the process can be highly affected by different factors, such as, cooling rate, mixing hydrodynamics, concentration and impurities. This is of great impact on the products properties. These properties, namely crystal size distribution (CSD), polymorphic form and purity, in turn, have major effect on the efficiency of the subsequent downstream processes, especially filtration and drying (Mullin, 2001). They also influence the product effectiveness, notably stability, dissolution rate and bioavailability in the pharmaceutical industry where over 90% of the active pharmaceutical compounds (APIs) are produced in crystalline form (Variankaval et al., 2008). Accordingly, crystallisation control has an economic significance.

Over the last twenty years, the availability of process analytical technology (PAT) tools opens up the possibility of on-line monitoring of crystallisation process which has advantages over traditional offline methods in terms of accuracy, time and the ability to react if undesired events or properties during the process are discovered. Examples of these techniques are: Attenuated Total Reflection Fourier Transform Infrared (ATR-FTIR) (BORISSOVA et al., 2009; Khan, 2008; Groen and Roberts, 2001), Focused Beam Reflection Measurement (FBRM) (Barrett and Glennon, 2002; Kougoulos et al., 2005; Abu Bakar, 2010) and optical techniques (Simon et al., 2009b; Simon et al., 2010; Brown, 2012). Most of these tools are probe-based which require inserting probe inside the crystalliser. In spite of their effectiveness, these types of tools have their disadvantages that they only monitor a very small area, influence the hydrodynamics of the system (i.e. mixing profiles and intensity) and introduce the possibility of contamination if not cleaned properly. In some cases insertion optical-based probes and FTIR probes become fouled with solids depositing on the probe's window that can give a wrong signal for the controller. Regarding the optical techniques, despite the fact that they are considered as non-invasive ones, they still require the crystals to be at specific minimum size to be detectable causing post-nucleation detection rather than actual one.

Nowadays, the combination of the PAT with a control approach led to improve the quality of the products and promote the process efficiency in terms of reducing the number of failed batches, minimising the variability between batches and as a result decreasing the manufacturing cost and time. Different control strategies have been reported in the literature. Some of them were based on maintaining the supersaturation

level constant through changing the temperature profile (Grön et al., 2003; Khan et al., 2011). In other words, the feedback control loop uses measurements of supersaturation to manipulate the temperature set point of the heater/cooler. Temperature cycling approach based on heating and cooling cycles, has also been used to keep the target number of counts/s measured by FBRM constant to achieve the desired CSD. These cycles were carried out either at constant heating/ cooling rates (Abu Bakar, 2010) or by proportional control (Saleemi, 2011) that adjusts the jacket temperature according to the value of the error signal using one water bath. The results were good in terms of products quality. However, when this demonstrated at 100 L pilot plant scale, it was not easy to achieve the immediate heating and cooling rates resulting in a delayed response, more significant overshoots and longer batch times (Saleemi, 2011). This is expected as it would depend on the capacity of the heater/ cooler system.

Process Video Imaging (PVI) techniques have been previously used to monitor the crystallisation process (Wang et al., 2005; Simon et al., 2009a; Brown, 2012). However, to best of our knowledge, it has not been used in combination with control strategy to improve the products quality. Moreover, all the control systems that previously applied were based on using one water bath to change the temperature profile. In this case, the efficiency is limited to the capacity of the water bath. Scaling up the process will then have inherent issue with heat transfer related to the time constant that the system can respond to.

Reflecting on the above considerations, the development of a system which has the ability to monitor and control the crystallisation process of different compounds and is more close to the setup industry can use, was the motivation of the work present in this thesis. Therefore, switching between hot and cold water baths as a method to manipulate the crystalliser's temperature was introduced. This means that fluid of different temperatures could be supplied to the jacket and the resulting wall temperature can be quickly changed. This would affect the nucleation and possibly the growth rate of crystals in ways that are not achievable by a single water bath using linear or non-linear cooling profiles.

In summary, this thesis presents a novel method to control the temperature inside batch crystalliser using a relatively inexpensive monitoring tool combined with a twin hot /cold temperature source. A number of experiments have been done during the

development of these tools to evaluate the system and to make sure it is robust and can demonstrate repeatability.

1.2 Research Objectives

The main objectives of this thesis were as follows:

- To develop a simple heat transfer model for an agitated vessel to predict the vessel temperature as a result of applying different heating/ cooling profiles and test its reliability.

- To introduce the switching technique that provides hot and cold water to the crystalliser's jacket for a non-crystallising system and study how it can affect the temperature inside the vessel.

- To develop an on-line process video imaging system to monitor and characterise batch cooling crystallisation. This includes the measurement of Meta-stable Zone Width (MSZW) at different operating conditions and the estimation of the nucleation kinetics parameters. L-glutamic acid (LGA) was chosen as material for examination because of the availability of data in the literature which helped validate the results obtained in this work using the developed PVI system. Adding to that, it has low solubility in water compared with the second material used in this study; glycine which exhibits high solubility in water.

- To prove the validity of the developed on-line process video imaging system as a monitoring technique for crystallisation processes in different systems.

- To assess the effect of the novel switching technique on the cooling crystallisation of glycine compared with the conventional (i.e. linear and crash) cooling profiles.

- To develop a control strategy that combines the on-line process video imaging and switching techniques to improve the quality of LGA and glycine crystals formed in unseeded batch cooling crystallisation, in terms of size and presence of fines in comparison with the traditional systems.

1.3 Thesis Structure

The thesis consists of this introduction and six further chapters that are outlined as follows:

Chapter 2 reviews in detail the fundamental principles of crystallisation processes with the emphasis on batch cooling crystallisation process. A description of different process analytical techniques and their application for monitoring and controlling crystallisation process is also presented, with the focus on the optical techniques as they share similarity with the one used in this work. Furthermore, the standard methods used in industry and in the laboratory are highlighted.

Chapter 3 demonstrates the development of a simple heat transfer model of agitated vessel to predict the temperature inside the vessel. The reliability of the model is examined by comparing the model results with experimental data. The chapter also discusses the heat transfer phenomenon in the 2 L agitated vessel in terms of different aspects, which are the maximum feasible heating/cooling rates, dead time, time constant and the effectiveness of the water baths used. The switching system supplying hot and cold water to the vessel jacket and its effect on the temperature inside the vessel are also presented.

Chapter 4 describes the materials used and the experimental set-up and procedures implemented in this work. It also discusses the application of the developed on-line video imaging system to measure the MSZW of LGA in a 2 L batch crystalliser under various operating conditions; different cooling rates and stirring speeds. The impact of the type of material used for the impeller is also investigated. The nucleation kinetics parameters are retrieved using Nývlt method whereas the apparent rate of overall solute mass transfer is calculated by analysing recorded images. After initial testing on LGA, the monitoring technique was applied to glycine. Glycine was selected following a search for a material that exhibits different solubility characteristics from LGA. The reliability of the findings obtained by this technique is tested by comparing them with those from literature (Liang, 2002; Rajoub, 2014). Adding to that, the effect of applying the switching technique to the cooling crystallisation of aqueous solutions of glycine in a 2 L batch crystalliser is investigated. This involves the study of the impact of various variables, such as, switching frequency and duration as well as the temperature set-point of each water bath. A comparison between the effect of the

switching method and the traditional cooling profiles on the cooling crystallisation of glycine is also shown.

Chapter 5 details the implementation of the novel control system developed which combines the optical and switching techniques on unseeded cooling crystallisation of LGA and glycine as model systems. The robustness and the reliability of the strategy are also tested.

Finally, **Chapter 6** summarises conclusions from each chapter to make recommendations for further work.

Chapter 2

Literature Review

The scope of this chapter is to review the underlying principles in the crystallisation field with emphasis on batch cooling crystallisation. Process Analytical Technology (PAT) and its application in crystallisation process monitoring and control are highlighted.

Crystallisation is one of the most important and arguably complex operations in the chemical industries, which is mainly utilised in separating and purifying chemicals. Crystallisation is as old as the chemical industry itself and a main unit operation that is used especially in the pharmaceutical, fine chemical, and food industries (Myerson, 2002; Zhang et al., 2010).

In spite of the fact that the crystallisation process can be conducted in different types of crystallisers for examples: batch, semi-batch or continuous one, the batch configuration, that until recent times is not well understood, is still the most widely used in pharmaceutical industries (Korovessi, 2005; Saleemi, 2011). Batch crystallisation is used within the pharmaceutical and speciality chemical industry because firstly, many of the processes do not involve large volumes of material; the low volume of active pharmaceutical ingredients (API) lends itself to a batch operation rather than continuous one. In addition, batch is employed where losses are kept at a minimum due to the high cost of the raw materials (Myerson, 2002) and for traceability and batch identity requirements. Secondly, the crystallisation of different compounds can be performed by using the same crystalliser. As long as different operating conditions and control recipes are necessary to produce these compounds, the batch mode has the ability to carry out that relatively easily (Costa and Maciel Filho, 2005).

2.1 Crystallisation Mechanism and Theory

This section highlights in detail the fundamental theories and mechanisms that govern the crystallisation process.

2.1.1 Solubility

Solubility, in definition, represents the maximum amount of solute that can be dissolved in a solvent at equilibrium and is often expressed as a function of temperature. This relationship is of great influence on the choice of the crystallisation method, for example, cooling crystallisation is preferable for systems of strong relationship (i.e. materials of high solubility) , whereas anti-solvent crystallisation is for those of a weak relation (i.e. materials of low solubility). Solubility data for some systems are available in the literature (Stephen et al., 1963; Seidell, 1940; Mullin, 1997), but caution should be taken as impurities can seriously affect the solubility (Mullin, 1997).

Different methods can be used to experimentally measure solubility, for example:

- Isothermal method: it is based on the measurement of the solubility (determination of the equilibrium amount of solute dissolved in a solvent) at a constant controlled temperature with stirring employed. In this technique, a known amount of solvent is heated to the desired temperature in a jacketed vessel. The solute is then added in excess (i.e. the total amount of solute added should be known) and the solution is agitated at the constant temperature for 4-24 hours. A sample is then taken and analysed for the solute concentration. If the solute concentration is not accurate, the solution should be filtered and the remaining undissolved solute should be dried and weighed. The latter is then subtracted from the total amount of solute added (Myerson, 2002).
- Differential scanning calorimetry (DSC): it depends on determining the saturation (equilibrium) temperature from extrapolating the DSC profiles measured at different heating rates to zero heating rate. The DSC profile shows the dynamic relationship between temperature and heat and thus the dissolution temperature can be defined at the point where the greatest change in the heat flow curve occurs (Mohan et al., 2000).
- Use of attenuated total reflection Fourier transform infrared (ATR-FTIR) (Dunuwila and Berglund, 1997).
- Use of a modified formula of van't Hoff equation that includes an activity coefficient γ to fit for non-ideal solutions (Mullin, 2001):

$$\ln x\gamma = \frac{\Delta H_f}{R}\left[\frac{1}{T_f} - \frac{1}{T}\right] \quad \textbf{(2.1)}$$

Where x is the mole fraction of the solute in the solution, ΔH_f is the molar latent heat of fusion of the solute (J/mol), R is the gas constant (8.314 J/mol.K), T_f is the fusion temperature of the solute (K) and T is the solution temperature (K). In order to be able to use equation (2.1), activity coefficient γ should be estimated. This can be accomplished by using activity coefficient models, for example, Universal Functional Activity Coefficient (UNIFAC) (Gmehling et al., 1978) and the Non-Random Two-Liquid – Segment Activity Coefficient (NRTLSAC) (Chen and Song, 2004).

2.1.2 Meta-stable Zone

For crystallisation processes, the meta-stable zone is located between the material solubility and supersolubility curves. The distance between these curves, represented by the line 23, is called metastable zone width (MSZW).

Figure 2.1 illustrates the solubility-supersolubility diagram of a two-component system that consists of three zones (Mullin, 2001):

1. Stable zone, where the solution is unsaturated and the crystallisation cannot occur.
2. Meta-stable zone, where spontaneous nucleation is impossible, but growth would occur if crystal seeds were added.
3. Unstable zone, where spontaneous nucleation can occur.

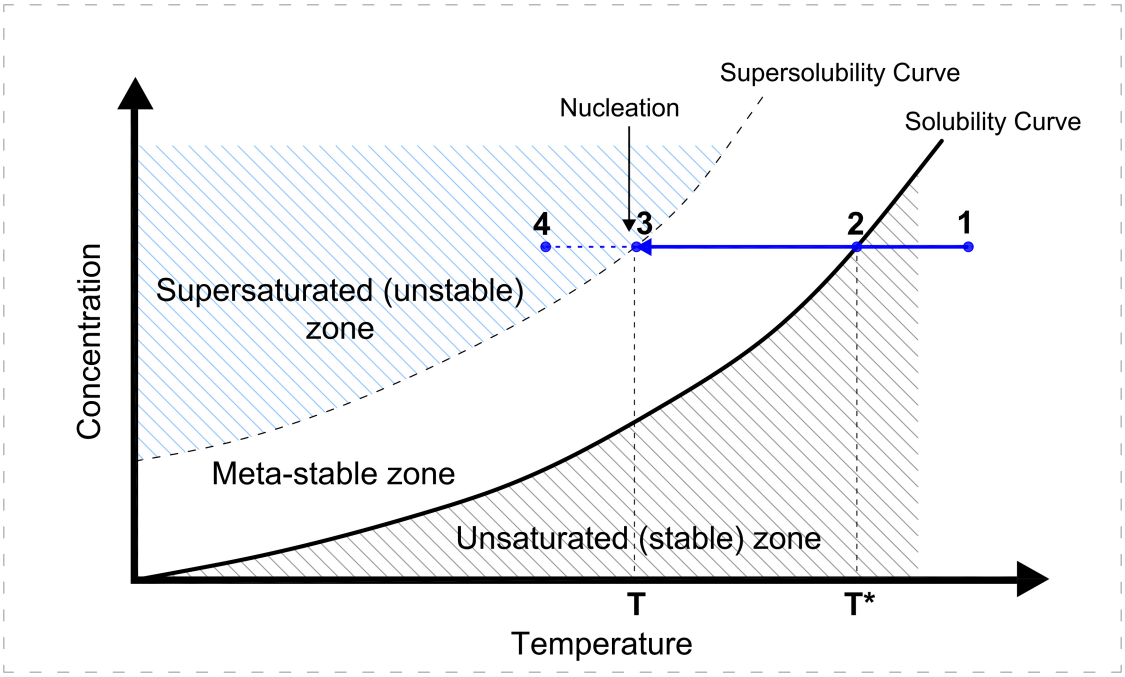

Figure 2.1: Classical description of solubility-supersolubility diagram.

Assuming a solution represented by point 1 in Figure 2.1 is cooled (line 123); spontaneous nucleation can only occur if conditions represented by point 3 are achieved. However, further cooling to point 4 would be required to initiate crystallisation, especially with very soluble substances because the solution may become very viscous so the crystallisation is hindered (Mullin, 2001). For the system described in Figure 2.1, the MSZW can be calculated in terms of the maximum supercooling required to initiate nucleation as:

$$MSZW = T^* - T \tag{2.2}$$

Where T^* is the saturation temperature and T is the crystallisation temperature.

Determination of MSZW is of high importance for estimating nucleation kinetics of the crystallisation process (Kubota, 2008; Barrett and Glennon, 2002) as well as controlling the growth rate which can be achieved by keeping the operating point within the meta-stable zone throughout the whole process (Barrett and Glennon, 2002).

It is worth pointing out that nucleation can take place in the meta-stable zone after a certain time interval. This time delay is called an induction time and is a function of the material type. Different factors can govern the induction time; such as, supersaturation level, fluid mechanics and impurities (Liang, 2002).

Various techniques have been utilised to measure the MSZW which are:

- Naked eye (Nývlt, 1968; Fujiwara et al., 2002; Mullin and Jancic, 1979; Nagy et al., 2008);
- Attenuated total reflection-Fourier transform infrared (ATR-FTIR) spectroscopy (Dunuwila and Berglund, 1997; Groen and Roberts, 2001; Lewiner et al., 2001b; Févotte, 2002; Fujiwara et al., 2002; Borissova et al., 2008; Nagy et al., 2008; Trifkovic et al., 2009);
- Turbidity (Borissova et al., 2008; Liang, 2002; Kadam et al., 2011; Mitchell and Frawley, 2010; Ni and Liao, 2008; Ni and Liao, 2010; Marciniak, 2002; Graber et al., 1999);
- Focused beam reflectance measurement (FBRM) (Nagy et al., 2008; Fujiwara et al., 2002; Barrett and Glennon, 2002; Liotta and Sabesan, 2004; Liotta, 2001; Barrett et al., 2005);
- Particle vision and measurement (PVM) (Barrett and Glennon, 2002);
- A densitometer (Marciniak, 2002);
- Bulk video imaging (Simon et al., 2009a);
- Ultrasonic velocity (Gürbüz and Özdemir, 2003; Marciniak, 2002; Al-Jibbouri et al., 2002; Titiz-Sargut and Ulrich, 2003) and
- Electrical conductivity (Graber et al., 1999; Lyczko et al., 2002).

These techniques used to measure the MSZW can be split into two groups based on the physical property employed for the first nuclei detection: the first group depends on monitoring the change in grown nuclei quantity, such as naked eye, turbidity and PVM, while the second one takes into consideration the change in solution concentration; for instance, FTIR spectrometer, ultrasound sensor and electrical conductivity (Kubota, 2008). The measured MSZW can be affected by the technique applied resulting in determining an apparent MSZW (Marciniak, 2002; Kubota, 2008; Mullin and Jancic, 1979). Determination of MSZW experimentally is time-consuming. To overcome this problem, (Mersmann and Bartosch, 1998) have developed a new theoretical model to predict the MSZW of seeded batch crystallisation based on the birth of nuclei on the crystals surface present in the solution and their outgrowth. The accuracy of the model was better for steep solubility curves than that of flat ones. As known, the unseeded crystallisation is widely used in the chemical industries. Therefore, (Kim and Mersmann, 2001) derived different theoretical models to predict the MSZW based on the nucleation mechanism occurring in the crystalliser.

2.1.2.1 Factors affect the Meta-stable Zone Width

Unlike dissolution, MSZW is a nucleation kinetic-limited parameter that is highly affected by the process conditions such as cooling rate, solution concentration (Borissova et al., 2008), agitation speed, stirrer's material (Liang et al., 2004) and presence of impurities (Sangwal and Mielniczek-Brzóska, 2004).

The effect of impeller materials on crystallisation process has been firstly studied by (Garside and Davey, 1980; Ness and White, 1976). (Ness and White, 1976) investigated the impact of using two different materials (stainless steel and plastic) for Rushton impellers on the collision nucleation of seeded crystallisation of aqueous magnesium sulphate ($MgSO_4.7H_2O$). They found that the nucleation rate has significantly influenced by the stirrer speed between 310 and 460rpm at different cooling rates. Moreover, they established a relationship between stirring rate and nucleation rate for both impeller materials. They concluded that the nucleation rate decreased by four to six times using plastic impeller compared with a stainless steel one at the same cooling rate.

Based on the previous works, (Liang et al., 2004) studied the effect of using Perspex and stainless steel retreat curve impellers on the primary nucleation of aqueous L-glutamic acid solutions in 450 ml batch crystalliser at different stirring speeds. They found that the relationship between MSZW and agitation speed was similar for both impeller materials where the MSZW decreased as the stirrer speed increased until this speed reached around 400rpm where the nucleation was retarded because of the central vortex which draws air bubbles into the solution that hinder the nucleation point. However, the nucleation using stainless steel impeller was much easier than the one using Perspex impeller. Moreover, nucleation order was higher in the case of stainless steel impellers than in the case of Perspex ones. But, the opposite was for the nucleation rate constant.

Regarding the cooling rate impact on MSZW, (Liang et al., 2004) found that MSZW is directly proportional to the cooling rate which agrees with the nucleation theory. The same finding was observed by (Borissova et al., 2008) by studying the crystallisation of L-glutamic acid aqueous solutions in 500L and 20L crystallisers. They also concluded that MSZW is inversely proportional to the solution concentration.

In classical crystallisation studies, since experiments measure MSZW at different cooling rates, the results from a series of cooling rates are usually plotted and extrapolated to 0 to give the true MSZW. However in practice, lab and industrial scale crystallisers will have to achieve a higher depression in temperature than the MSZW in order to generate primary nucleation.

2.1.3 Supersaturation

Supersaturation, by definition, is the driving force for crystallisation to occur (Mullin, 2001). A supersaturated solution contains more dissolved solids than its capacity at a certain temperature. In industrial processes, high supersaturation level is the main announcer to induce primary nucleation. Thus, the start of crystallisation process is conditioned by the solution supersaturation level (Patchigolla, 2007). In general, the degree of solution supersaturation is given in terms of solution concentration as follows (Mullin, 2001):

- Concentration driving force:

$$\Delta C_{max} = C - C^* \tag{2.3}$$

- Supersaturation ratio:

$$S = \frac{C}{C^*} \tag{2.4}$$

- Relative supersaturation:

$$\sigma = \frac{\Delta C_{max}}{C^*} = S - 1 \tag{2.5}$$

Where C is the actual solution concentration and C^* is the equilibrium saturation concentration at a given temperature.

There are various methods to generate supersaturated solutions, which are: cooling, solvent evaporation, addition of anti-solvent and chemical reaction (Myerson, 2002). Each of these methods has its own advantages. Supersaturation is generated close to heat transfer surface in both cooling and evaporation crystallisations, whereas anti-solvent and reaction crystallisations lead to localise and rapid crystallisation where the

stirring mechanism is of great impact. Certainly, the method choice is mainly based on both the desired product properties and economic requirements.

Supersaturation level can affect the nucleation and growth kinetics which are of significance for crystal's properties; for example, size, shape, polymorphic form and purity. In other words, higher supersaturtion level forms large number of nuclei leading to wider crystal size distribution (CSD), while lower level generates small number of nuclei leading to narrower CSD (Groen, 2001a). The supersaturation, in turn, is influenced by different factors, for example, temperature, agitation, cooling rate and crystalliser hydrodynamics. Therefore, it is of great importance to measure and monitor the solution supersaturation. Different online techniques have been used to measure supersaturation experimentally (Löffelmann and Mersmann, 2002; Qu et al., 2005) as well as by simulation (Yang et al., 2006). In addition, various control strategies have been utilised in industry to control the supersaturation profile in order to meet the product specifications; such as size and shape (Braatz, 2002; Grön et al., 2003).

2.1.4 Nucleation

Nucleation is, by definition, the process of formation small nuclei that play a role as centres of crystallisation. It is the step that immediately follows the supersaturation generation and hence depends on the level of supersaturation. Many different factors can promote nucleation such as agitation, mechanical shock, friction, magnetic fields, ultrasonic radiation and extreme pressures within solutions and melts (Mullin, 1997). Nucleation is of paramount importance in the control of crystal properties and in selective crystallisation of a specific polymorph (Rodríguez-hornedo and Murphy, 1999).

The mechanisms of nucleation are divided into two main categories, as illustrated in Figure 2.2:

1. **Primary Nucleation** is the first step of formation new crystals and can occur spontaneously (homogenous nucleation) or be induced by the presence of foreign particles (impurities) in the system (heterogeneous nucleation).
2. **Secondary Nucleation,** is nucleation that occurs due to something else happening in the crystalliser. Typically, secondary nucleation is induced by the presence of solute particles formed as a result of attrition, breakage, presence of

impurities, interaction with the surrounding; such as, impeller and crystalliser wall (Mullin, 2001).

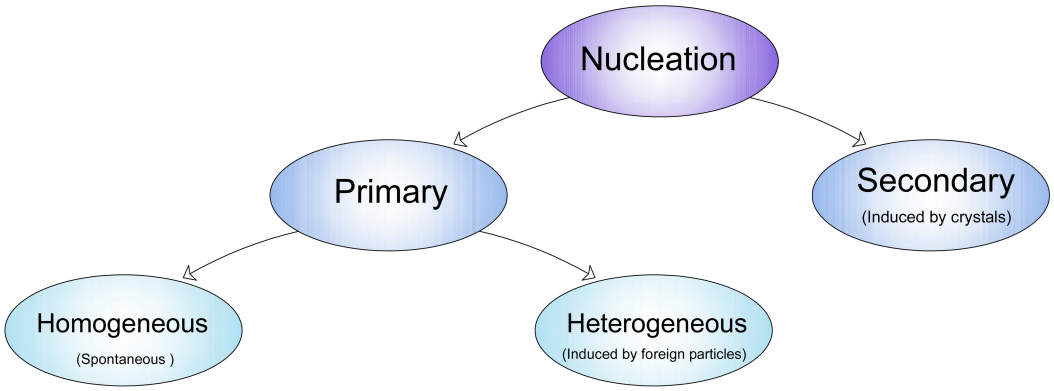

Figure 2.2: Schematic presentation of the different nucleation mechanisms.

2.1.4.1 Primary Homogeneous Nucleation

The classical theory of nucleation states that nuclei are formed in solution by a sequence of gradual attachments of molecules to clusters. These clusters should grow to a size larger than a critical value to be stable and not dissolve back again into the solution (Myerson, 2002). According to this mechanism, the rate of nucleation is given in the form of Arrhenius equation by:

$$J = A \exp\left(\frac{-\Delta G}{k\,T}\right) \tag{2.6}$$

Where A is the pre-exponential factor with value of 10^3 nuclei/cm^3.s, ΔG_{cr} is the free energy change for a nucleus of critical size, T is the temperature and k is the Boltzmann constant, which is equal to 1.3805×10^{-23} J/K.

The thermodynamic approaches for homogenous nucleation were described by the work of (Gibbs et al., 1928; Volmer, 1939; Becker and Döring, 1935). The overall free energy change for a cluster subjected to phase transition ΔG is expressed by:

$$\Delta G = \Delta G_S + \Delta G_V \tag{2.7}$$

For a spherical nucleus, equation (2.7) becomes:

$$\Delta G = 4\pi\, r^2\gamma + \frac{4}{3}\,\pi\, r^3\gamma\, \Delta G_v \tag{2.8}$$

Where

ΔG_S is the surface excess free energy, i.e. the free energy between the surface and the bulk of the particle. It is a positive quantity and proportional to r^2.

ΔG_V is volume excess free energy, i.e. the free energy between very large particle and the solute in the solution. It is a negative quantity and proportional to r^3 and ΔG_v is the free energy change associated with the phase transition per unit volume.

γ is the interfacial tension.

r is the nucleus radius.

As shown in equation (2.8), ΔG_S and ΔG_V are of opposite signs and change differently with the nucleus radius. This causes the overall free energy change ΔG to pass through a maximum value called the critical free energy change, ΔG_{cr} that associates with the critical nucleus radius, r_c, see Figure 2.3. The critical nucleus radius r_c is the minimum radius for stable nucleus, and therefore nuclei smaller than r_c will dissolve and those larger than r_c will continue to grow.

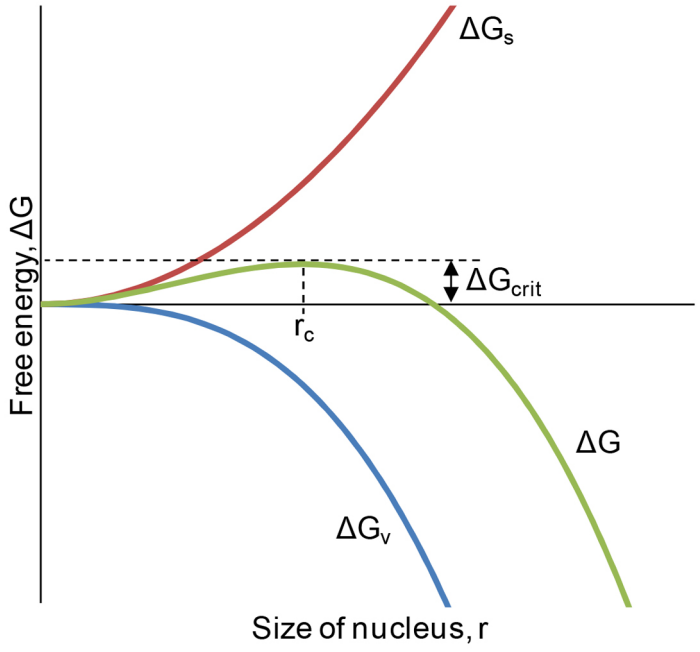

Figure 2.3: Free energy diagram showing for nucleation (Garside and Davey, 2000).

By differentiating equation (2.8) with respect to r and equating the differential to zero, the critical nucleus radius r_c is equal to:

$$r_c = \frac{-2\gamma}{\Delta G_v} \tag{2.9}$$

By substituting equation (2.9) into equation (2.8), the critical free energy change, ΔG_{cr} is obtained:

$$\Delta G_{crit} = \frac{4\pi \gamma r_c^2}{3} \quad \textbf{(2.10)}$$

The Gibbs-Thomson (or Ostwald-Freundlich) relationship between particle size and solubility (Ostwald, 1900; Freundlich and Hatfield, 1926) may be expressed in the form:

$$\ln \frac{C}{C^*} = \ln S = \frac{2 \gamma \upsilon}{kTr} \quad \textbf{(2.11)}$$

Where υ is the molecular volume.
Hence equation (2.10) can be rewritten as:

$$\Delta G_{crit} = \frac{16\pi \ \gamma^3 \upsilon^2}{3(kT \ \ln S)^2} \quad \textbf{(2.12)}$$

Combining equation (2.12) with equation (2.6), the homogenous nucleation rate can be given as:

$$J = A \exp[\frac{-16\pi \ \gamma^3 \upsilon^2}{3k^3 \ T^3 \ (\ln S)^2}] \quad \textbf{(2.13)}$$

It can be seen explicitly from equation (2.13) that the main variables govern the nucleation rate are temperature T, supersaturation S and interfacial tension γ.

The classical nucleation theory has been widely used over the years. However, differences were seen between its prediction of the nucleation rate and the experimental values. This proposed that nucleation in fact does follow more complex routes than those described by the classical theory of nucleation. Therefore, a two-step model has been suggested to take into account this issue. It was firstly used for protein crystallisation, but it showed later its ability to explain most of the crystallisation processes from solution.

A comparison between the classical nucleation theory and two-step model mechanisms is demonstrated in Figure 2.4. The mechanism of two-step model includes the formation of sufficient-sized unordered cluster of solute molecules and then restructuring into ordered cluster (Chen et al., 2011; Vekilov, 2010).

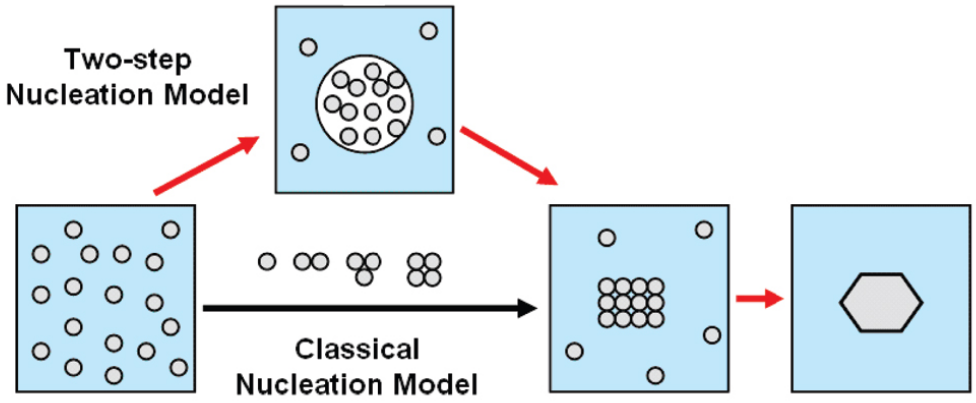

Figure 2.4: A comparison between the classical nucleation theory and two-step model mechanisms (Erdemir et al., 2009).

2.1.4.2 Primary Heterogeneous Nucleation

As mentioned above, homogenous nucleation occurs spontaneously from a clear pure solution. However, in laboratory and industrial crystallisations, it is impossible to prepare solutions that do not have impurities. These impurities, which form substrate for nucleation could be atmospheric dust or tiny crystals retained in minute cracks on the impeller or the crystalliser wall from previous runs. Unlike homogenous nucleation, heterogeneous nucleation requires less energy as a result of the impurities presence and thus takes place at a lower supersaturation (Myerson, 2002).

The overall free energy change corresponds to heterogeneous nucleation can be given by:

$$\Delta G_{Hetro} = \Phi \, \Delta G_{Homo} \tag{2.14}$$

Where Φ is the correction factor and has a value less than unity.

(Volmer, 1939) found a relationship between the contact angle θ between the crystalline deposit and the foreign solid surface (see Figure 2.5 a) and the factor Φ as follows:

$$\Phi = \frac{(2 + \cos\theta)\ (1 - \cos\theta)^{\,2}}{4} \tag{2.15}$$

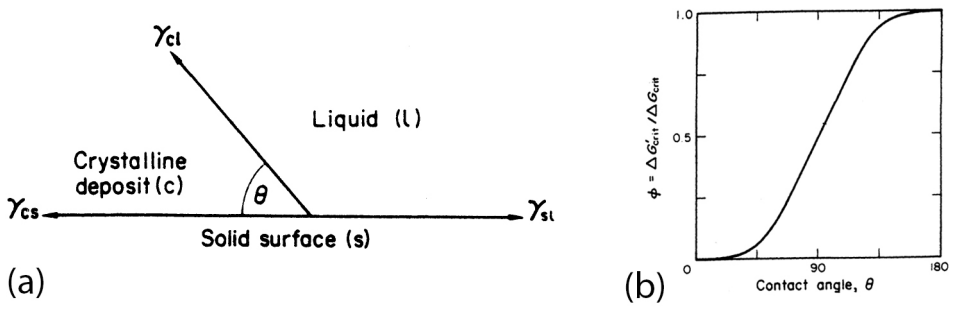

Figure 2.5: (a) Interfacial tensions at the boundaries between three phases (two solids, one liquid). (b) The relationship between the ratio of free energies of homogeneous and heterogeneous nucleation and the contact angels.

Extending Volmer's work from impurities, it is easy to see that objects within the solution can act as nucleation devices – e.g. the impeller, baffle and temperature probe.

2.1.4.3 Secondary Nucleation

Secondary nucleation is thought to occur by the presence of seed crystals in a supersaturated solution, and thus it occurs at a lower supersaturation than that for primary nucleation.

Secondary nucleation can take place by different mechanisms as follows (Mullin, 1997; Myerson, 2002):

1. Initial or dust breeding → crystalline swept away from the surface of seed crystals either during their growth or storage.
2. Needle breeding → Breakage of needle-like or dendritic crystals at high supersaturation level.
3. Polycrystalline breeding → Fragmentation of irregular polycrystalline agglomeration.
4. Collision or contact breeding → Collision of crystal-crystal, crystal-impeller, and crystal- crystalliser internals.
5. Fluid shear → Shear forces due to solution mixing and even solution passing the seed crystals.

The rate of secondary nucleation is given by the semi-empirical equation (Liang, 2002):

$$B = K_n N^i M_T^j \Delta C^n \quad \textbf{(2.16)}$$

Where K_n is constant, N is agitation speed and M_T is suspension density. For the values of exponents: n is between 0.5 and 2.5 (Tavare and Garside, 1986), j lies between 0 and unity. However, the theoretical range for i is from 2 to 4 whereas the experimental one is 0 to 8 (Garside and Davey, 1980; Garside, 1985).

Therefore, it is worth pointing out that both supersaturation and crystalliser hydrodynamics (such as, stirrer speed and type) can affect the secondary nucleation (Thompson and Robson, 2001). Some researchers pointed out that the hardness of the impeller material noticeably promotes the secondary nucleation (Randolph and Sikdar, 1974; Ness and White, 1976). Not only will there be a mass transfer process with solute changing position but there will be thermal processes as the solute changes phase, moving from liquid into a solid state.

Secondary nucleation is considered as the predominant type for moderate or high soluble materials and also in continuous industrial crystalliser (Mullin, 1997). A comparison among the effect of the different nucleation types on MSZW is presented in Figure 2.6.

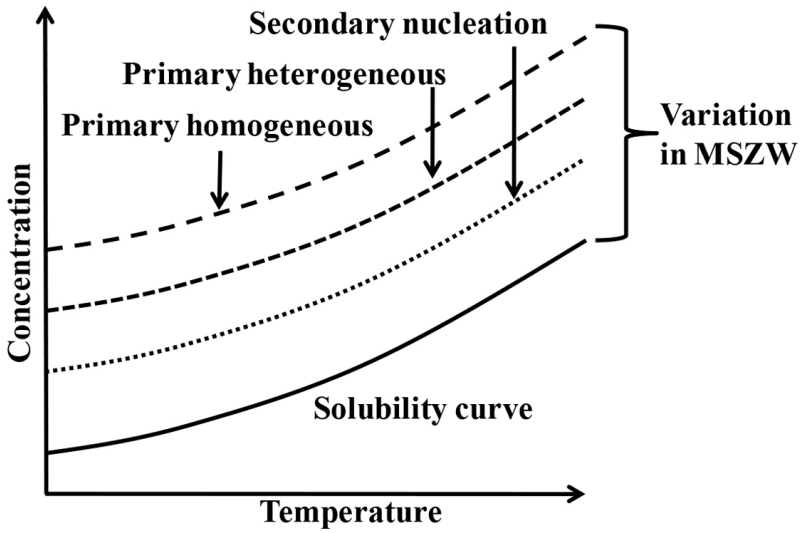

Figure 2.6: The effect of nucleation types on MSZW (Saleemi, 2011).

2.1.4.4 Determination Methods of Nucleation Kinetics:

Nývlt's Method:

Since the classical nucleation theory failed to explain the behaviour of actual crystallisation processes, an empirical relationship was proposed by (Nývlt, 1968) to

evaluate the nucleation kinetics of real systems in which the nucleation rate J was expressed as a function of maximum possible supersaturation ΔC_{max}:

$$J = K \Delta C_{max}^{m} \quad \textbf{(2.17)}$$

Where K is the nucleation rate constant and m is the nucleation order.
ΔC_{max} can also be written in terms of the maximum possible undercooling of the system (MSZW) as:

$$\Delta C_{max} = \left(\frac{dC^*}{dT}\right) \Delta T_{max} \quad \textbf{(2.18)}$$

$$\Delta T_{max} = T_{sat} - T_{cry} \quad \textbf{(2.19)}$$

Where dC^*/dT is the temperature dependence of solubility, T_{sat} is the saturation temperature and T_{cry} is the crystallisation temperature.

The nucleation rate can also be assumed to be equal to the supersaturation rate achieved by cooling:

$$J = qb = -q\left(\frac{dT}{dt}\right) = -\varepsilon \left(\frac{dC^*}{dT}\right)\left(\frac{dT}{dt}\right) \quad \textbf{(2.20)}$$

Where b is the cooling rate ($-dT/dt$), q is the crystal mass deposited per unit mass of free solvent when the solution is cooled by 1ºC and ε is a correction factor for the change in concentration for the hydrated salts.

Substituting equations (2.18) and (2.20) into equation (2.17) yields:

$$-\varepsilon \left(\frac{dC^*}{dT}\right)\left(\frac{dT}{dt}\right) = K \left[\left(\frac{dC^*}{dT}\right) \Delta T_{max}\right]^{m} \quad \textbf{(2.21)}$$

Taking the logarithms of equation (2.21) and rearranging gives:

$$log\left(\frac{-dT}{dt}\right) = (m-1)log\left(\frac{dC^*}{dT}\right) - log(\varepsilon) + log(K) + mlog\,(\Delta T_{max}) \quad \textbf{(2.22)}$$

Equation (2.22) shows a linear relationship between *log (-dT/dt)*, i.e. cooling rate and *log* ΔT_{max} where the slope of the line is the nucleation order m. The nucleation rate constant can be obtained from the intercept. This method was used by (Nývlt et al., 1985; Nývlt, 1968) to process the experimental data for more than 25 inorganic salts. They found that the nucleation order does not depend on the presence of the solid phase or temperature, but it is related to the molecular weight of the solute. In other words, it is inversely proportional to the number of molecules needed for forming a critical nucleus (Nývlt, 1968). The nucleation order has a physical importance for the crystallising system; it reflects the state of the solid-liquid interface. Therefore, the low value of m represents strong solid-liquid interfaces which eases the formation of stable nuclei, while the high value of m means weak solid-liquid interfaces which makes the formation of stable nuclei difficult (Sangwal, 2009b).

Nývlt's method is based on some assumptions and simplifications which are: the nucleation rate is equal to the supersaturation rate at the time of detecting the first nuclei and the nuclei can be detected only if they grow to a certain size (Liang, 2002). Nevertheless, it is still able to provide useful information on the nucleation process. Nývlt's method was used in chapter 4 for the determination of nucleation kinetics of LGA.

Kubota's Interpretation:

To determine the nucleation kinetics using this method, it is required to obtain the detectable number density (N_m/V) to take into account the sensitivity of the detection tool (Kubota, 2008). According to this approach, the detectable number density after time *t* can be calculated as:

$$\frac{N_m}{V} = \int_0^t J(t)dt \qquad \textbf{(2.23)}$$

Assuming that the nucleation rate is given as a function of the maximum possible undercooling by:

$$J(t) = K_n^{`} \Delta T^m \qquad \textbf{(2.24)}$$

Where

$$K_n^{`} = K\,(\frac{dC^*}{dT})^m \qquad \textbf{(2.25)}$$

Assuming that the cooling rate b = (dT/dt), substituting equation (2.24) into equation (2.23) yields:

$$\frac{N_m}{V} = \frac{K_n^{`}}{b}\int_0^{\Delta T_{max}} \Delta T^m dT = \frac{K_n^{`}}{(m+1)b}\,(\Delta T_{max})^{m+1} \qquad \textbf{(2.26)}$$

Taking the logarithms of equation (2.26) and rearranging gives:

$$log\Delta T_{max} = \frac{1}{m+1}\log\left[\left(\frac{N_m}{K_n^{`}V}\right)(m+1)\right] + \frac{1}{m+1}log\,(b) \qquad \textbf{(2.27)}$$

Equation (2.27) shows that a plot of $log\ \Delta T_{max}$ verses $log\ b$ would give a straight line with a slope equal to $1/(m+1)$, where m is the nucleation order. The nucleation rate constant can be calculated from the intercept providing the detectable number density is known.

The induction time, in definition, is the time needed to detect the first nucleation event in a solution kept at a constant supercooling.

Kubota has recently defined the induction time as the time required for the number density of grown nuclei to reach a specific value. Based on that, equation (2.23) can be rewritten as:

$$\frac{N_m}{V} = \int_0^{t_{ind}} J(t)dt \qquad \textbf{(2.28)}$$

Substituting equation (2.24) into equation (2.28) yields:

$$\frac{N_m}{V} = \int_0^{t_{ind}} K_n^{`}\,\Delta T^m dt = K_n^{`}\,(\Delta T)^m t_{ind} \qquad \textbf{(2.29)}$$

Rearranging equation (2.29) gives the induction time as a function of the supercooling ΔT as:

$$t_{ind} = \frac{N_m}{V\,K_n^{`}}\,(\Delta T)^{-m} \qquad \textbf{(2.30)}$$

Equation (2.30) is similar to equation (2.27) for the MSZW. Thus, the nucleation kinetics can be deduced from a trend line of a plot of t_{ind} verses ΔT. Equation (2.30) shows that there is a relationship between the MSZW and the induction time. This is an advantage of Kubota's approach over Nývlt's method which did not give any information about the induction time.

More recently, Sangwal deduced, based on the classical nucleation theory, a linear relation between *ln(b)* and $\frac{1}{(\Delta T_{max})^2}$ which can be used to estimate the nucleation parameters (Sangwal, 2009b; Sangwal, 2009a; Sangwal, 2011). Kashchiev, Borissova, Hammond and Roberts (KBHR) also developed an analytical approach which provided expressions of the dependence of the MSZW on the cooling rate based on the initial evolution of either the number of nuclei or the fraction of crystallised volume. This model allows the determination of the main parameters of the nucleation and the growth processes as well as the nucleation mechanism occurred (Kashchiev et al., 2010b; Kashchiev et al., 2010a) .The KBHR approach was applied by Corzo et al. to determine the nucleation kinetics of methyl stearate from kerosene solutions (Corzo et al., 2014).

2.1.5 Growth Rate

The crystal growth step starts once the nuclei of the critical size have been formed. This step includes the deposition of additional solute molecules from a supresatured solution on the crystal surfaces. Therefore, the structure at the molecular level of each face of a crystal highly affects the growth mechanism. These faces can be divided into three groups, shown in Figure 2.7, which are:

- F (flat) faces:
- S (stepped) faces
- K (kinked) faces

These faces differ in the number of surfaces available for molecules to be attached to. From an energetic point of view, the more the number of available surfaces, the more favourable the face is. As a result, the K faces is the quickest growing faces, followed by the S and F faces respectively (Myerson, 2002).

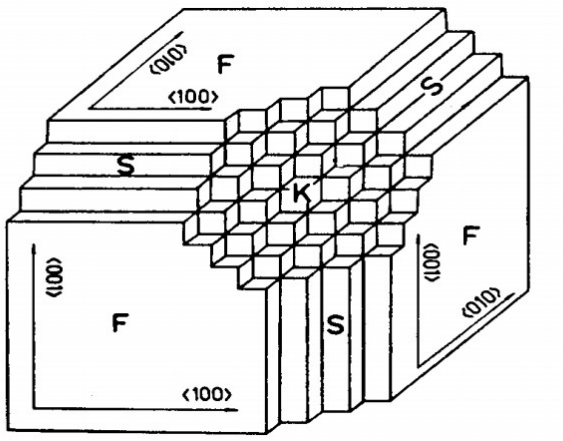

Figure 2.7: The three possible crystal faces.

In general, the crystal growth process involves a series of steps, as schematically illustrated in Figure 2.8, which are:

1. The transport of solute molecules from the bulk to the edge of the boundary layer of the crystal surface.
2. Diffusion of solute molecules through the boundary layer towards the adsorption sites on the crystal surfaces according to Fick's law as a result of concentration gradient near the crystal surface.
3. Molecules adsorption on the crystal surface.
4. Molecules diffusion along the crystal surface to the energetically favourable sites; 4^{*}. Desorption from the crystal surface.
5. Attachment to a step face.
6. Diffusion along the step face.
7. Integration into a kink face on the crystal surface.

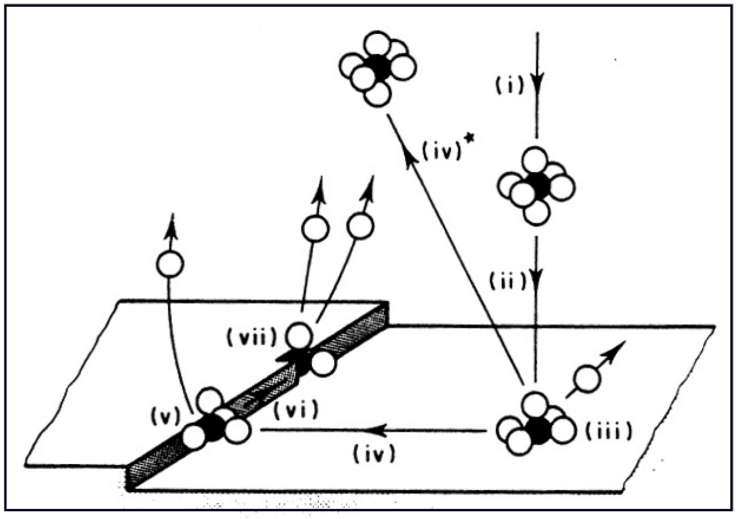

Figure 2.8: Schematic representation of crystal growth steps (Scheel and Elwell, 1975).

Any of the above mentioned steps can be growth rate-limited depending on its speed. Therefore, the growth rate can be diffusion control when steps (1-2) are the slowest while it is surface integration control when steps (3-7) are the slowest. According to this, different models for the crystal growth have been proposed; some of them will be described below.

2.1.5.1 Diffusion-Reaction Model

This model is originally established by (Noyes and Whitney, 1897) who considered the crystal growth was basically a diffusional process and also the crystallisation was the reverse of the dissolution. Moreover, they suggested that the rates of these two processes were controlled by the concentration difference between the bulk of the solution and the crystal surface and expressed as:

$$\frac{dm}{dt} = K_m A (C - C^*) \quad \textbf{(2.31)}$$

Where m is the solid mass deposited over time t, K_m is mass transfer coefficient, A is crystal surface area, C is solute concentration in the solution bulk and C^* is saturation concentration.

Equation (2.31) was modified by (Nernst, 1904), based on the assumption that a thin stationary film of liquid would be found close to the crystal surface through which all the solute molecules should diffuse:

$$\frac{dm}{dt} = \frac{D}{\delta} A (C - C^*) \quad \textbf{(2.32)}$$

Where D is the solute diffusion coefficient and δ is the stationary film thickness.

The thickness of stationary film δ depends on the agitation speed in the system (solution- crystals). Thus, film thickness up to 150 μm was found in stagnant solutions while in well-mixed solutions this thickness dropped to almost zero which could indicate infinite growth rate in agitated solutions. This means that the description of the crystal growth mechanism on the base of film diffusion alone is not enough. Another issue with this theory is that the dissolution process is not always the reverse of the crystallisation because the substance dissolves at a quicker rate is that it crystallises at under the same operational conditions.

As a result of these issues, (Berthoud, 1912; Valeton, 1924) made some modifications to the theory. They suggested that the crystal growth process is governed by two stages: diffusion stage whereby the molecules move from the bulk to the crystal surface, followed by a first-order reaction stage in which the molecules integrate into the crystal lattices. These two stages, schematically illustrated in Figure 2.9, can be expressed as:

$$\text{Diffusion} \qquad \frac{dm}{dt} = K_d\, A\, (C - C_i) \tag{2.33}$$

$$\text{Reaction} \qquad \frac{dm}{dt} = K_r\, A\, (C_i - C^*) \tag{2.34}$$

Where K_d is diffusion mass transfer coefficient, K_r is surface reaction rate coefficient and C_i is solute concentration at the crystal-solution interface.

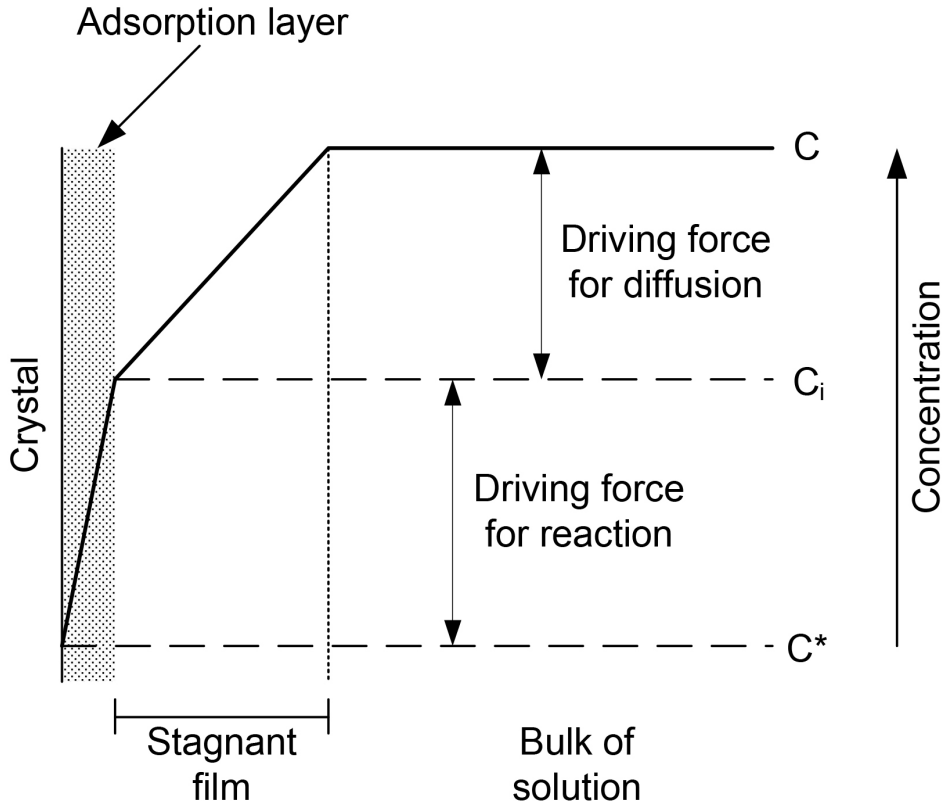

Figure 2.9: Concentration driving forces for diffusion-reaction model in crystallisation from solution.

In fact, the interfacial concentration C_i is difficult to determine in real systems. Therefore, it is more appropriate to remove the term C_i, by taking into account the overall concentration driving force, C- C^*:

$$\frac{dm}{dt} = K_G A (C - C^*)^g \quad \textbf{(2.35)}$$

Where K_G is the overall crystal growth coefficient and g is the order of the crystal growth process and generally between 0 and 2.5. However, some studies showed that there is a third step, so-called heat transfer that takes place at the same time with the surface reaction step. This step includes the heat removal from the crystal surface (i.e. dissipation of crystallisation heat) and then playing a role in crystal growth rate (Hixson and Knox, 1951). The heat transfer step is, in turn, highly affected by the cooling system efficiency.

In general, different factors; for instance, temperature, hydrodynamics, slurry concentration, crystal size and impurities can affect the value of K_G.
The factors affecting each stage involved in the growth process are summarised in Figure 2.10.

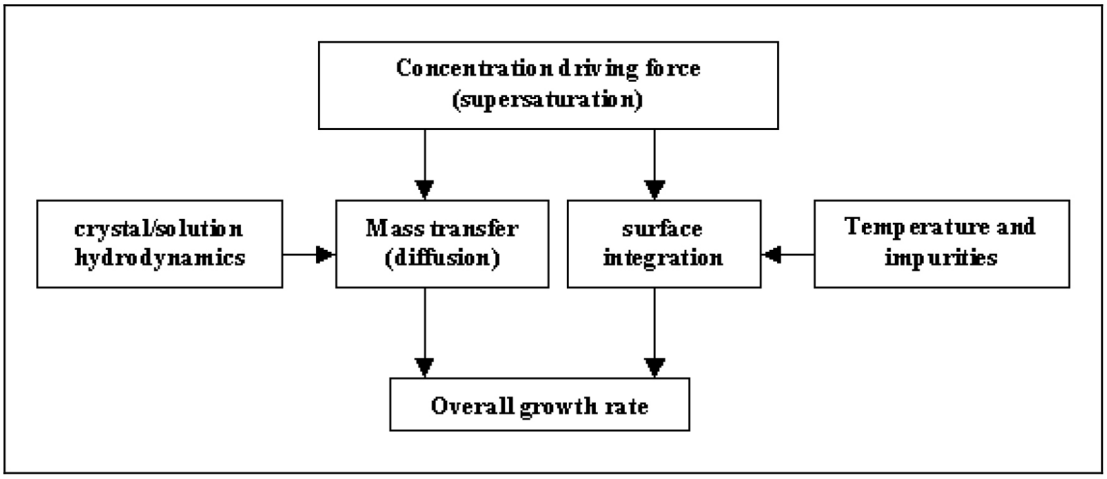

Figure 2.10: Diagrammatic representation of the factors that influence the processes involved in crystal growth (Myerson, 2002).

2.1.5.2 Screw Dislocation Model (BCF)

The BCF model was developed by (Burton et al., 1951) for higher growth rate at low supersaturation level. It is based on the presence of screw dislocation on the crystal surface which supplies necessary kink sites for growth to continue. Figure 2.11 shows the consecutive stages of spiral growth development induced by a screw dislocation.

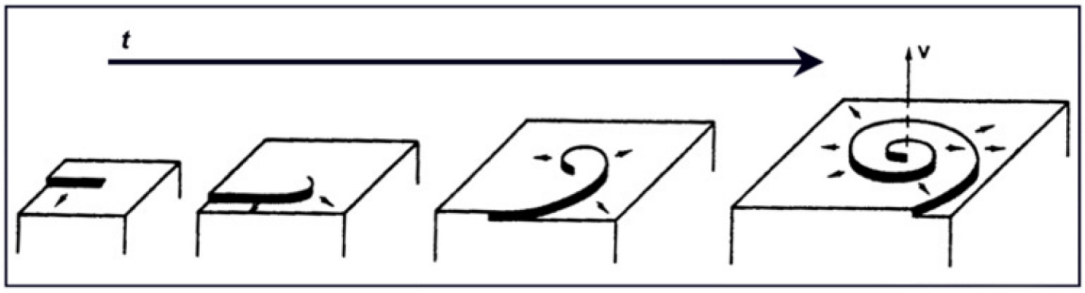

Figure 2.11: Spiral growth development starting from a screw dislocation (Liang, 2002).

The relationship between the growth rate G and the relative supersaturation according to this model is given by:

$$G = A\sigma^2 \tanh\left(\frac{B}{\sigma}\right) \tag{2.36}$$

Where A and B are complex temperature-dependent constants, which consist of parameters determined by step spacing.

Based on the supersaturation level, different relationships can be found between growth rate and supersaturation, as clearly illustrated in Figure 2.12.

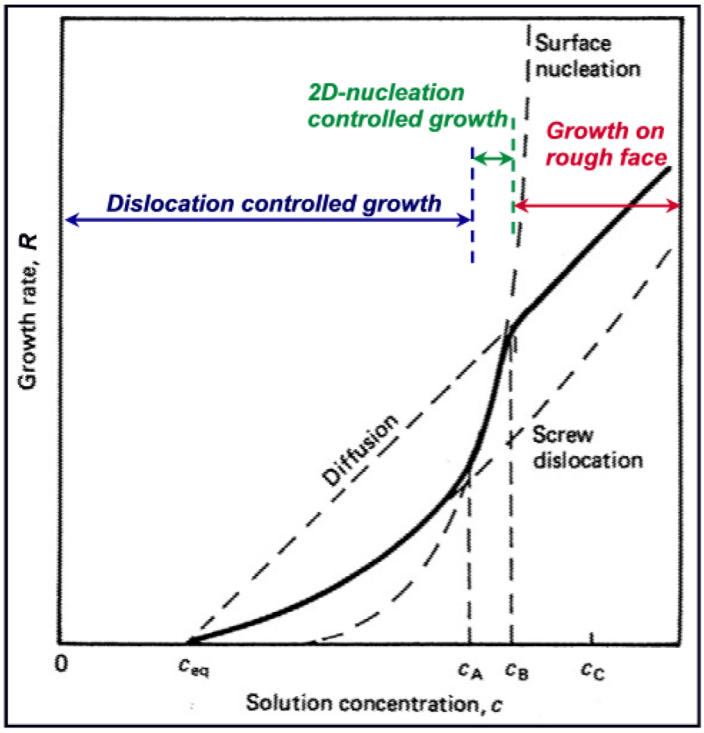

Figure 2.12: Growth rate change from a parabolic to linear growth law as supersaturation increases (Groen, 2001a).

- At low supersaturation: $G \propto \sigma^2$ as tanh $(B/\sigma) \rightarrow 1$, this indicates that the screw dislocation is the growth-controlled mechanism.
- At slightly higher supersaturation: $G \propto \sigma^{5/6} \exp(1/\sigma)$ signifying 2D surface nucleation (B+S).
- At high supersaturation: $G \propto \sigma$ suggesting fast growth on a rough face.

2.1.5.3 Birth and Spread (B+S) Model

It is also called 2D nucleation growth. This model suggests that 2D nuclei will form on the molecularly smooth crystal surface to provide new sites (steps and kinks) for further growth. The model assumes also that the surface nuclei can form at any location on the crystal (i.e. edge, corner or face) and spread at a finite constant rate (Myerson, 2002). This mechanism takes place only at relatively higher supersaturation as mentioned in Figure 2.12, because surface nucleation is stopped by the high energy barrier.

2.1.5.4 Continuous Growth

Continuous crystal growth is also known as rough growth in where a crystal surface is molecularly rough, and thus it provides low energy sites that are favourable for growth. This type of growth is dominant at high supersaturation level as shown in Figure 2.12.

2.1.5.5 Growth Rate Measurement

Growth rate can be measured by different experimental techniques (Garside et al., 2002). One of these techniques is single crystal growth which concentrates on the growth rate of individual face (Lee and Parkinson, 1999; Mullin, 2001). Growth rate measurements are often used in the first step to generate models of the crystallisation process. These models are usually based on population balance that is based on the conservation of mass, energy and crystal population for prediction of overall mass transfer rates under controlled conditions and for observing size-dependent growth or growth rate dispersion (Costa et al., 2007; Mullin, 2001).

2.1.6 Ostwald Ripening

The Ostwald ripening phenomenon, firstly described by (Ostwald, 1901), states that in a saturated solution where crystals of different sizes are suspended, the smaller crystals tend to dissolve and afterward the resultant solute deposits on the larger crystals. This phenomenon happens as a result of a crystal size dependence of solubility (Myerson,

2002). This relationship between crystal size and solubility can be expressed by Gibbs-Thomson equation as (Baldan, 2002):

$$C_r = C_e \ exp\left(\frac{2\gamma\Omega}{R_B T}\frac{1}{r}\right) \cong C_e \left(1 + \frac{2\gamma\Omega}{R_B T}\frac{1}{r}\right) \quad \textbf{(2.37)}$$

Where C_r is the solubility of crystal of radius r, C_e is the solute concentration in equilibrium with particle of infinite radius size, γ is the interfacial tension of the solid particle in contact with the solution, R_B is the universal gas constant, T is absolute temperature and $\boldsymbol{\Omega}$ is the molar volume of the particle in solution.

From equation (2.37), it can be noted that the smaller the particle, the higher its solubility will be. During Ostwald ripening process, there are particles of critical radius r^* which are in equilibrium with the solution. This means that crystals of radius $r > r^*$ will grow, whereas crystals of radius $r < r^*$ will dissolve (Baldan, 2002).

Generally, the Ostwald ripening leads to decease the crystals number present in the system, increase the average crystal size and alter the crystal size distribution (Myerson, 2002). Ostwald ripening can also change the CSD over time at a constant temperature; however its effect can be quicker with temperature cycling (Mullin, 2001).

2.1.7 Polymorphism

Polymorphism in the pharmaceutical field has received a great interest over the last 40 years (Mo et al., 2011). Polymorphism, by definition, is a phenomenon in which the same material is found in different forms. These forms have the same chemical formula but differ in the way in which molecules are arranged. Therefore, polymorphic forms may have different physical properties, which categorise as (Chawla and Bansal, 2004):

- Packaging properties: density, conductivity, and reflective index.
- Thermodynamic properties: heat capacity, solubility, entropy, internal energy and chemical potential.
- Mechanical properties: hardness, tensile strength compatibility and tableting properties.
- Kinetic properties: dissolution rate and stability.

Many substances exhibit polymorphism. For example, L-glutamic acid has two polymorphic forms, metastable α-form which is rhombic and stable β-form which is needle like, whereas glycine can crystallise in five polymorphic forms α, β, γ, ε and δ. The ε and δ-glycine can only be formed at high pressure (Dowling, 2012). However, α, β, γ- glycine are metastable, unstable and stable respectively at ambient conditions (Srinivasan, 2008).

As a consequence, in the control of crystal size and shape, it is desirable to be able to control which particular polymorph will form. In the pharmaceutical industry especially, where the conversion from meta-stable form to the stable form one can change the drug solubility in the human body, leading to a big influence on the bioavailability of the drug (Korovessi and Linninger, 2005; Mangin et al., 2009).

Different factors that can govern the formation of particular polymorph during crystallisation include supersaturation, temperature, heating/cooling rates, solvent, and hydrodynamics (Kitamura, 2002a). Seeding is also considered as an effective technique to form the desired polymorph (Doki et al., 2004; Llinàs and Goodman, 2008; Beckmann, 2000).

In industry, various techniques are applied to identify the polymorph's structure such as IR spectroscopy, X-ray powder diffraction, Raman spectroscopy, microscopy and others (Stephenson et al., 2001).

2.1.8 Breakage and Attrition

Attrition is the generation of many small fragments from crystals suspended in a solution, whereas breakage is the fraction of crystals into a number of relatively large pieces. Both mechanisms take place as a consequence of collision of crystals with each other, with stirrer blades, with baffles, or with crystalliser's wall. Both mechanisms lead to reduce the crystal size, widen the crystal size distribution and change the crystal shape and morphology (Bravi et al., 2003).

2.2 Crystallisation Methods

Different methods can be applied to crystallise materials out of solution, which are:

1. Cooling- decrease temperature to reduce solution solubility, preferable for materials of high solubility.
2. Evaporation- reduction in solvent volume for low solubility materials with temperature stability. However, this method is not applicable in pharmaceutical industries, due to the fact that most APIs have limited temperature stability (Fujiwara et al., 2005).
3. Anti-solvent- adding another solvent to reduce the solute solubility, widely used to crystallise materials that are either of low solubility or thermally degradable (Yu et al., 2006a; Guo et al., 2005). In addition, anti-solvent can be cheaper to implement in terms of energy consumption as no heating or cooling is required compared with other methods. On the other hand, it requires a crystalliser of larger volume and further downstream processes to separate the solvent and anti-solvent mixture (Abu Bakar, 2010). Contamination can also happen which is not desired for an API.
4. Chemical reaction- to generate solute.
5. Change in pH- addition of acid or base.

Of the above methods, cooling crystallisation will be explained in more detail in the next section as it is the technique employed in this work.

2.2.1 Cooling Crystallisation

It is widely applied for materials of high solubility which show a strong relationship between temperature and solubility and are not thermally degradable. In addition, this method does not need any additional raw materials that may affect the crystal purity or require larger crystalliser as the case in anti-solvent operation (Nagy et al., 2006). Supersaturation in cooling crystallisation can be generated using different cooling profiles, for example: linear, natural and programmed cooling (Pöllänen, 2006; Abu Bakar, 2010; Saleemi, 2011), as shown in Figure 2.13.

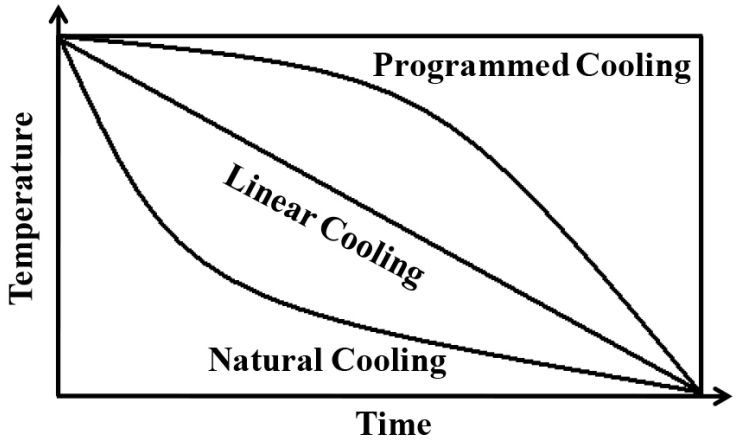

Figure 2.13: Schematic description of different types of cooling profiles.

2.2.1.1 Natural Cooling

Natural cooling here is defined by taking a hot solution and removing it from one container into another that is exposed to air. As seen in Figure 2.13, the solution will be cooled rapidly at the beginning due to the large temperature difference between the solution and the coolant and then slowly at the end as the temperature driving force decreases. The high cooling rate depends on the heat transfer capacity of the system (Abu Bakar, 2010) and also on the heat transfer coefficients. This rapid cooling at the start generates high supersaturation level which leads to form large amounts of fines resulting in poor quality crystals with smaller mean size and wider distribution (Mullin, 1997; Saleemi, 2011).

2.2.1.2 Linear Cooling

In this mode, the cooling rate is constant throughout the process. This rate should be optimised as too low rate is not economic due to long batch time. However, too high rate leads to rapid nucleation with large number of fines (Pöllänen, 2006). Normal linear cooling crystallisation can be done by adding seed crystals that prevent the onset of primary nucleation. One of the advantages of linear cooling is its operational simplicity especially at large scale. Unlike natural cooling, linear mode needs the presence of a temperature control system to be implemented.

2.2.1.3 Programmed Cooling

The programmed (controlled) profile aims to improve the crystals quality in terms of their size and distribution and is often related to the level of supersaturation. At the

beginning of the process, the temperature has to decrease slowly and thus the supersaturation level generated is low in order to be proportional to the small surface area of crystals available for growth and avoid nucleation. The cooling rate gradually increases with time as the surface area of the crystals becomes larger (see Figure 2.13). The first trial for the calculation of programmed cooling curve at different operating condition was done by (Mullin and Nývlt, 1971; Jones and Mullin, 1974) based on supersaturation balance. Due to its difficulty to be implemented in practice, a simplified formula was proposed by (Mullin, 2001) and given as follows:

$$T_t = T_0 - (T_0 - T_f)\left(\frac{t}{\tau}\right)^x \quad \textbf{(2.38)}$$

Where T_0 , T_f , and T_t are the temperatures at the start, end and any time t during the process, respectively, τ is the total batch time, x=3 for seeded crystallisation and x=4 for unseeded crystallisation. The higher value of the exponent (i.e. x=4) is to allow the temperature to decrease more gently at the beginning of the cooling stage. This equation is only applicable under specific circumstances and related to how linear the solubility curve is and that growth rates of formed crystals are independent of supersaturation. This is not always the case for many crystals (Mullin, 2001).

2.3 Techniques for the Characterisation of Crystallisation Process

The characteristics of the end product, such as, size, shape, purity and structure are of great importance due to their effects on the efficiency of downstream processes such as filtration, milling and drying as well as the product effectiveness in terms of bioavailability and stability. These properties themselves can also be affected by the process parameters (temperature, supersaturation and fluid dynamics). For that, nowadays there is a growing need for online characterisation of both process parameters and product properties to meet end-use specifications within the industrial production. In response to these issues, different process analytical techniques have been used for online monitoring and control of the crystallisation process. This section will explain in more detail some of these techniques which share similarities to the process video imaging tool developed in this project:

2.3.1 Focused Beam Reflectance Measurement (FBRM)

Focused beam reflection measurement is a technique that depends on inserting a probe inside a crystalliser to provide online information about the system under investigation. It uses a focused laser beam which projects through a sapphire window of the probe (Alvarez, 2007). This beam is rotated by the optics at a speed of 2 to 6 m/s (Pons et al., 2006) and therefore scans in a circular path. Any particle passing by the window's field of view (Barrett and Glennon, 2002) will reflect the beam back to the probe. This reflection continues until the particle has left the beam (Alvarez, 2007). The beam which crosses the particle on a straight line between two random points on the particles edge giving a distance known as cord length (Abbas et al., 2002a).The cord length can then be calculated from the laser scanning speed and the reflection time. Typically, thousands of chords are measured per second resulting in cord length distribution (CLD) over the range 0.8 to 1000 µm (Richmond et al., 1998). Figure 2.14 shows the Lasentec FBRM probe tip and the measurement mechanism (Worlitschek and de Buhr, 2005).

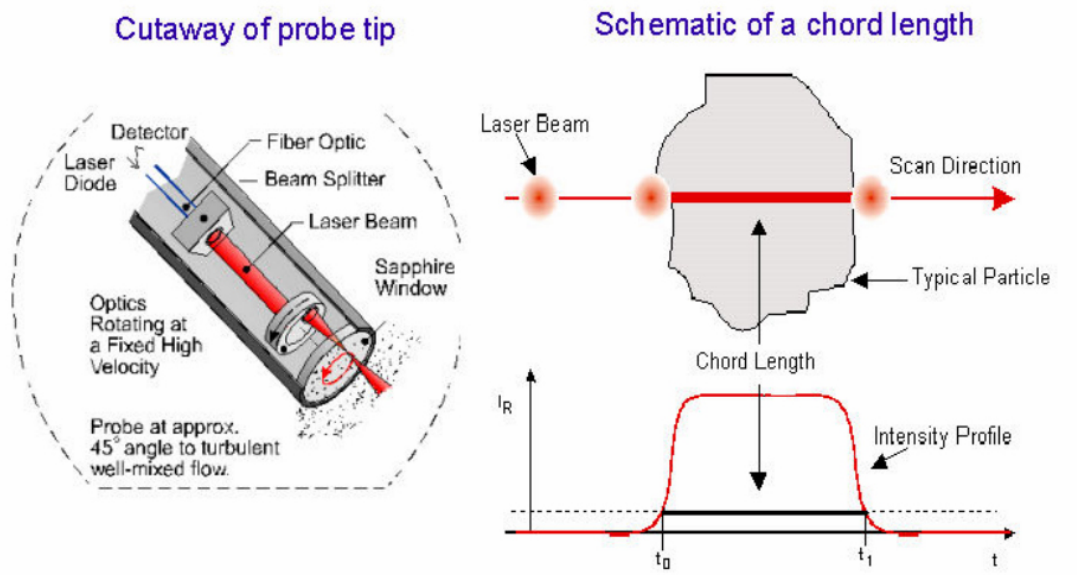

Figure 2.14: FBRM measurement: FBRM probe tip (left), and chord length measurement (right).

FBRM has widely used in the crystallisation field to measure the solubility and MSZW curves (Barrett and Glennon, 2002; Fujiwara et al., 2002; Liotta and Sabesan, 2004),to estimate crystallisation kinetics (Kougoulos et al., 2005), to monitor polymorphs (Barrett and Becker, 2002; Schöll et al., 2006) and as process control tool (Doki et al., 2004; Kim et al., 2005; Abu Bakar, 2010).

In general, FBRM are used to detect the presence of small crystals formed as a result of primary nucleation, and also the change in size distribution of growing crystals. Methods that convert cord length distributions to crystal size distributions are subject of several research papers.

2.3.2 Attenuated Total Reflectance- Fourier Transform Infrared (ATR-FTIR) Spectroscopy

ATR-FTIR is classified as a vibrational spectroscopy. The infrared spectra have the advantage of describing the molecules structure because each functional group has a particular frequency at which the IR energy is absorbed and thus can be used for molecules identification. The basic principles underpinning the ATR probe are presented in Figure 2.15. The infrared beam enters the ATR crystal, which consists of an IR transparent material with a high refractive index, at an angle of 45ºC. The beam is reflected inside the crystal and collected by the IR-detector although it penetrates into the medium through the reflection surface with a depth of few microns. Various crystal materials of different properties are available including diamond, zinc selenide (ZnSe) and germanium. Further information can be found in (BrukerOptics, 2011).

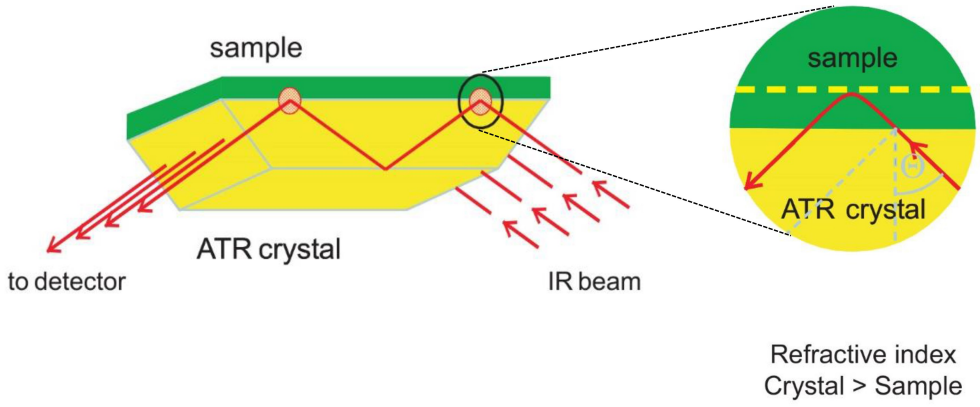

Figure 2.15: ATR principle (BrukerOptics, 2011).

ATR-FTIR has found widespread applications in the crystallisation field, for example, as an online process tool to measure the solution concentration (Lewiner et al., 2001b; Dunuwila and Berglund, 1997; Fujiwara et al., 2002; Feng and Berglund, 2002; Groen and Roberts, 2001) and also to control the cooling and anti-solvent crystallisations of various organic materials in order to improve the crystal size consistency (Braatz, 2002;

Braatz et al., 2002; Chung et al., 2000; Feng and Berglund, 2002; Gutwald and Mersmann, 1990; Lewiner et al., 2001a; Liotta and Sabesan, 2004; Yu et al., 2006a; Fujiwara et al., 2005; Fujiwara et al., 2002; Grön et al., 2003; Zhou et al., 2006; BORISSOVA et al., 2009; Khan, 2008) . However, one of the major problems associated with the ATR-FTIR probe is encrustation phenomenon. The probe is prone to be encrusted with solid due to the nucleation on its surface. This deteriorates the strength of the beam and hence degrades the signals sent for processing. In turn this affects the accuracy of concentration measurement.

2.3.3 Turbidity

Turbidity is a probe-based optical technique that uses light to measure the crystals concentration based on the cloudiness of the solution (Harner et al., 2008; Raphael and Rohani, 1996). Turbidity technique consists of a fibre optic probe that is divided into two parts: the first one for transmitting the light down to the solution where a mirror, positioned typically 1cm far from the probe, reflects the light back to the other part. The intensity of the reflected light defines the solid concentration. The lower the intensity, the higher the concentration is (Liang, 2002). The turbidity probe was used widely to detect the onset of crystallisation and dissolution for different chemicals in cooling crystallisation (Liang, 2002; Jiang, 2012; Mougin, 2001; BORISSOVA et al., 2009), see Figure 2.16.

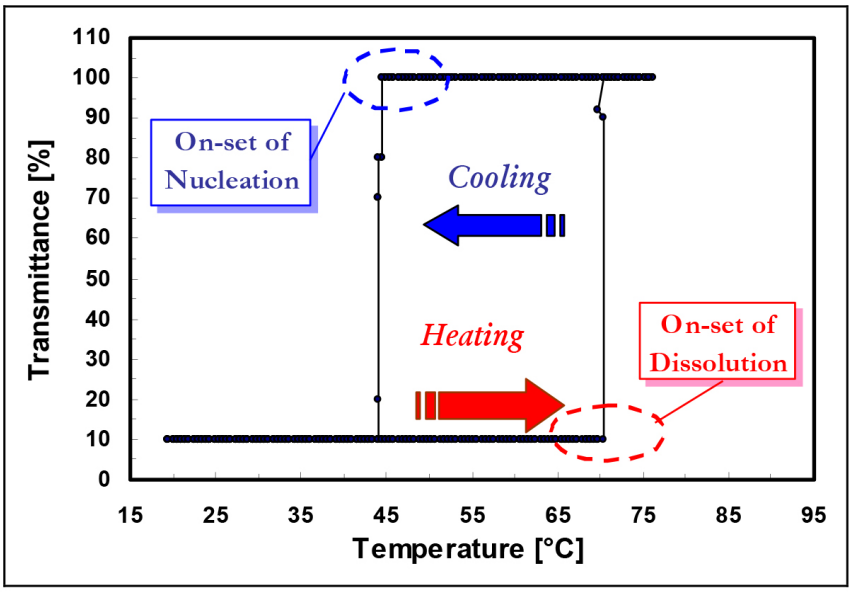

Figure 2.16: Typical measurement of the onset of nucleation and dissolution using turbidity data (Liang, 2002).

Adding to that, turbidity probe was utilised to monitor and control seeded and unseeded batch cooling crystallisation processes (Harner et al., 2008; Moscosa-Santillan et al., 2000).

This technique, as other techniques that are probe-based, can visualise only a small volume equals to the volume in which the beam hits the reflection mirror and thus the solution should be well mixed in order for the measurements to be representative of the entire solution.

2.3.4 Particle Vision and Measurement (PVM):

PVM probe, developed by Lasentec Inc., USA, is an in-situ video microscope that can give information about the shape, size and structure of particles present in a process, eliminating the need for offline sampling (Barrett and Glennon, 2002; Mettler-Toledo AutoChem, 2011). The PVM system consists of a charged coupled device (CCD) camera and light source (six independent lasers sources) to illuminate the area under investigation (Patience, 2002). The PVM probe was utilised to visualise the crystals in the determination of the meta-stable zone width of potash alum water system (Barrett and Glennon, 2002) and in the crystallisation of sodium chlorate (Patience, 2002). The PVM probe can image particles of 5-15µm in size. Due to being a rugged probe, PVM is suitable for industrial applications (Braatz, 2002). PVM showed the ability to identify some unexpected events in crystallisation process such as phase separation (oiling out) and to explore the reasons of these events (Desikan et al., 2005; Deneau and Steele, 2005; Lafferrere et al., 2004). Therefore, inline information provided by PVM about the process can save time and efforts for process development compared to traditional analytical techniques (Mettler-Toledo AutoChem, 2011).

However, the probe can visualise an area of (860 µm x 645 µm) which may not represent the whole bulk solution, leading to limit application in large scale industrial crystallisation (Barrett and Glennon, 2002). In addition, further image processing is required if more information about the crystallisation process is needed.

2.3.5 Particle Image Velocimetry (PIV) Technique:

PIV system is a non-intrusive optical technique that was initially used to measure the instantaneous velocities of the particles in the flow chamber using scanning laser light

sheet for illumination. In principle, two images of the particles should be taken; one every laser scan and then the velocity can be extracted using auto-correlation (Raffel et al., 2007). Because the direction of the moving particles was not defined by this method, the cross-correlation method was used to overcome this problem. The new method included grabbing two images at the same laser scan. The power spectrum or Young`s fringe could be obtained from overlapping the two images in order to gain the velocity vector map (Keane and Adrian, 1992; Wirth and Baritaud, 1996). PIV technique has developed rapidly over the last few years in which the use of digital charged-coupled device (CCD) cameras led to facilitate the process where the captured images are saved to a PC that can generate the vector map in a short time (Lai, 1996).

The use of PIV measurements of the flow field were employed to estimate the instantaneous gradient of Reynolds stresses (Sharp and Adrian, 2001; Sharp et al., 2000), calculate turbulent kinetics energy and kinetic energy dissipation rate (Rajoub, 2014; Buonacucina, 2010), and also validate the numerical flow simulations carried out by computational fluid dynamics (CFD) (Buonacucina, 2010).

Regarding the crystallisation field, the PIV data was employed to measure the velocities of both mother liquor and crystals, detect the nucleation point and record the growth rate of LGA (Rajoub, 2014). Figure 2.17 shows the stereoscopic principles of the PIV system.

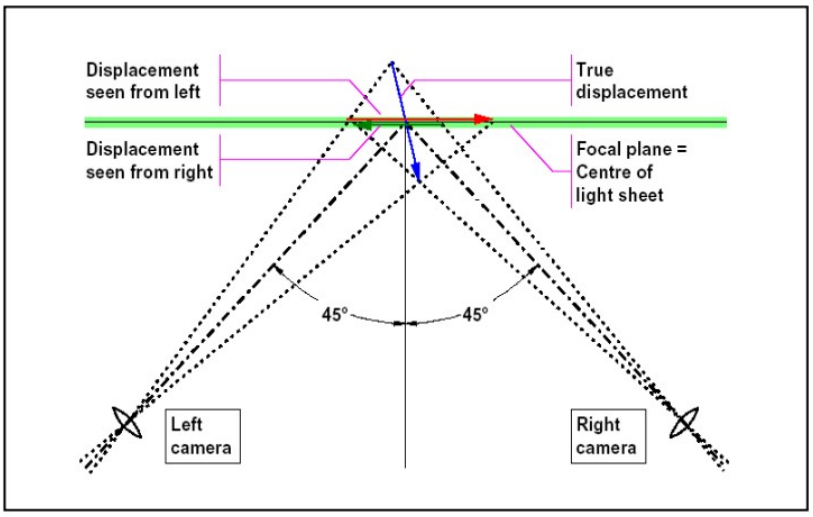

Figure 2.17: stereoscopic representation of PIV system.

2.3.6 Laser Diffraction Spectroscopy (LDS):

This technique is classified as a non-imaging optical system that is widely used in the field of particle sizing. Its principle is based on light scattered by the particles in suspension to get information about the particle size. A schematic representation of the classical laser diffraction technique is illustrated in Figure 2.18 (Abbas et al., 2002a).

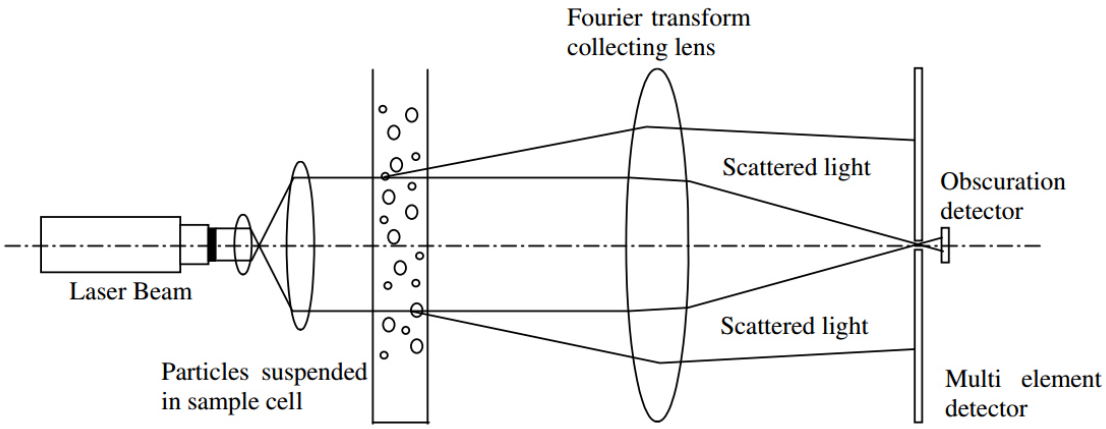

Figure 2.18: Schematic representation of the classical laser diffraction technique.

A low power helium–neon laser is used to pass through the sample whereby the laser beam is scattered by the particles present within the sample at different angles. These angles are inversely proportional the crystal's size; large crystals scatter laser at small angles while small crystals scatter laser at large angles. The light scattered by the particles is gathered a detector. Information about crystal size distribution (CSD) and the sample volume concentration can be obtained through the data collected by the detector via a deconvolution step. However, this technique assumes that the particles are of spherical shape (Abbas et al., 2002b). Furthermore, it can only measure particles in the range 0.05 µm to 9000 µm and require dilution for concentrated solutions and therefore it is widely used as offline particle sizing technique (Patchigolla, 2007).

2.3.7 Microscopy:

Microscopy is still considered as the basic method for quick evaluation of the evolution of liquid and solid particles in dynamic processes. While viewing the particles by the microscope, particle's size, shape and composition can be measured. The particles can be seen directly via the optical lenses where their size can been expressed as the projected area diameter (the diameter of a circle having the same area as the crystal when viewed from above). The accuracy of the measurements of this tool is prone to

overlapping problem effect (Larsen et al., 2007; Larsen and Rawlings, 2008). Consequently, having well dispersed sample of the particles on microscope slide is not an easy matter (Aamir et al., 2010b). In addition, caution should be taken into account whilst preparing samples to avoid the segregation of the particles.

Based on the size of the examined particles, two different microscopes can exist: optical microscope for particles size in the range 0.8 to 150µm, and electron microscope for those in the range 0.001µm to 5µm (Mougin, 2001). Microscopy is usually a complementary technique that can be used to validate the results of other process analytical tools (PAT). However, (Aamir et al., 2010a) showed the possibility of using microscopy as online tool to monitor the crystallisation process of a tripalmitin from melt in which nucleation rate, growth rate and crystal size distributions can be defined.

In essence PVM and microscopy are the same methods, with PVM being based on a digital camera system that can be processed automatically either on-line or off-line.

2.4 Heat Transfer Systems in Stirred Tank

Batch cooling crystallisation is by definition a volume of solvent/solute which is usually cooled by means of an external jacket or internal coil. An agitator is used to keep the solution/solute system well mixed to avoid temperature hot/cold spots from developing. Heat transfer in stirred tanks is of significance in chemical processes. External Jackets are considered as the most popular and robust configurations in the chemical industry in terms of cost and safety. They do not pose any problems in cleaning inside the crystalliser, for example. They are of three different types: plain, limpet coil or half pipe and dimple. The presence of the dimples in the jacket can enhance turbulence leading to improve the heat transfer performance compared with the plain jacket.

Regarding the internal coils, they are cheaper, able to be operated at higher pressures, give a more uniform temperature distribution and better heat transfer performance than jackets. On the other hand, they are not preferred in case of mixing viscous liquids and crystal slurries and also due to the encrustation phenomenon (Lakghomi et al., 2008; McConville, 2002).

The different types of heating/cooling systems are shown in Figure 2.19 (McConville, 2007).

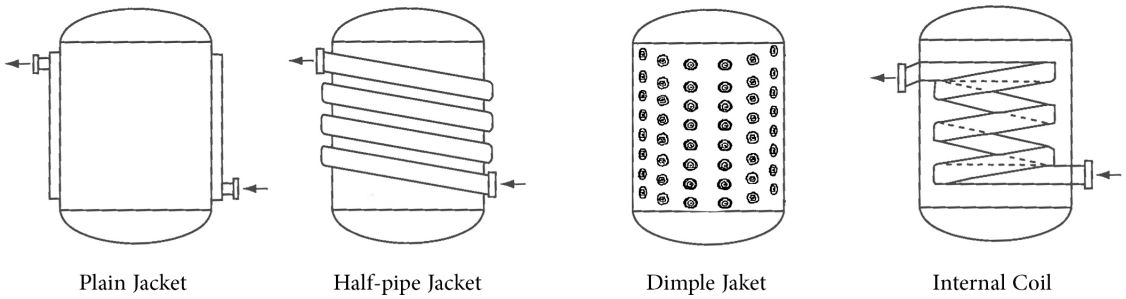

Figure 2.19: Common vessel heating and cooling arrangements.

2.4.1 Heat Transfer and Nucleation in Jacketed Vessels:

According to classical theory, nucleation rate is a function of the supersaturation which is therefore a function of the temperature of the solution and the concentration of dissolved solute (Mullin, 2001). Hence any region inside the batch vessel can exhibit different rates of nucleation depending on the local temperature and concentration.

From work by (Donnelly et al., 2005), although the temperature within the reactor appears uniform, the distribution of solute is not. However, even under the assumption of being well mixed, there must be a small temperature gradient close to the internal wall of the vessel. Therefore, nucleation is more likely to occur close to the internal vessel wall. In addition to temperature difference, the overall heat transfer is affected by the overall temperature difference between the jacket's fluid and the vessel. The overall heat transfer coefficient also has an impact but this is more related to the turbulence inside the jacket and the vessel, and the physical properties of the two fluids. This means that the temperature of heat transfer fluid would have an effect on initiating the formation of crystal nuclei (nucleation).

A schematic diagram of the temperature profile across the crystalliser wall is shown in Figure 2.20. For the jacketed vessel, the overall heat transfer coefficient U consists of three resistances which are the vessel-side (h_v), the vessel wall ($\Delta x/ k$) and the jacket-side (h_j).

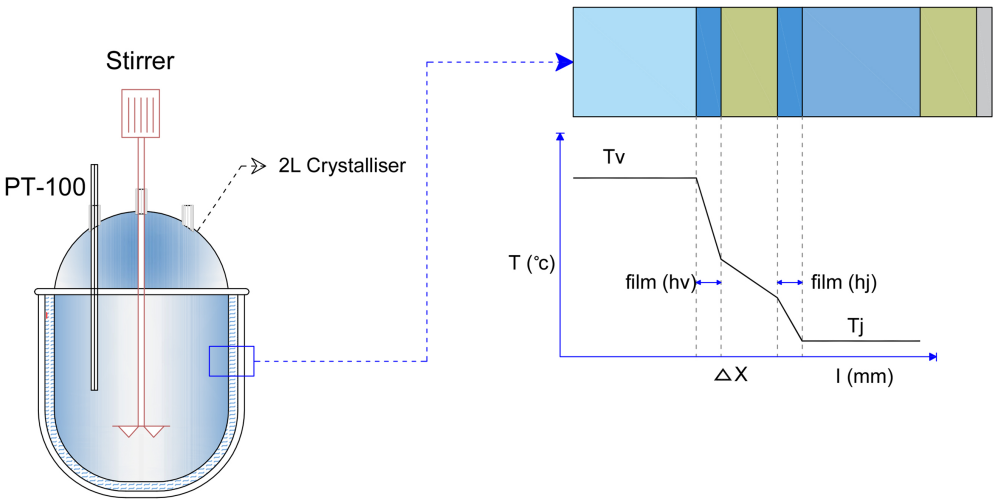

Figure 2.20: A schematic diagram of the temperature profile across the crystalliser wall.

The thermal resistances of the jacket's fluid and the crystalliser wall are generally given by the manufacturer while h_v can be calculated from U value using Wilson method (Choudhury et al., 2016). This will be explained in detail in chapter 3.

In addition to nucleation, crystals' growth is also a function of supersaturation and hence of local temperatures. It is therefore feasible that crystals travelling close to cold spots on the vessel wall will experience higher growth rates than those in the bulk of the crystalliser.

In an attempt to see if surface wall temperatures were of significant issue, Liang (Liang, 2002) carried out a computational fluid dynamic (CFD) study on a 2 litre single baffled crystalliser to predict the temperature profile within the liquid media. The findings showed that 2 litre vessels offered good heat transfer where the mother liquor cooled down quickly (within 24 seconds) to the vessel wall temperature which indicates the temperature variation inside the vessel is an order of fractions of a degree and hence considered negligible. As a result of this, the supersaturation difference between the layer at the sidewall and the bulk liquor was not thought to be significant. However, (Liang, 2002) noted that there was a 'hot spot' observed at the vessel centre near the liquid surface with a temperature higher than the rest of the liquid bulk by a half degree.

Moreover, Bentham (Bentham, 2015) ran CFD simulations for unbaffled jacketed vessels agitated by a pitched blade turbine to better understanding the flow and the heat

transfer inside this type of reactor which is of great importance for very temperature-sensitive processes. Bentham concluded that the flow through the jacket was not uniform and the inlet and outlet ports of the jackets had greater heat transfer. In addition, his results showed hot spots at the top and the bottom of the vessel, particularly close to the toroidal section and in the areas of secondary flow where the flow was minimal. The temperature variation was quite small; about 0.4 ºC.

Regarding the wall temperature, Bentham also found that the coldest wall temperature was noticed at the bottom of the jacket directly below the impeller, where dead zone of low flow was seen regardless the heating or cooling process of the vessel was applied. Although, this area had the higher heat transfer as a result of the presence of the impeller which forced the fluid downwards, the jacket controlled the heat transfer in this area. Bentham's work was focused on how to control rapid runaway chemical reactions using only the heating jacket as means to offset a rapid rise in temperature.

It may then be concluded from the works of Liang and Bentham that a dead zone with a maximum temperature difference of 0.5 ºC can be seen at the wall of the agitated vessel as a result of either crash heating or cooling.

Crystallisation is a balance between the phase change of solute from liquid to solid, and the accompanying liberation of heat that has to be removed. Under initial nucleation which generates a significant number of new nuclei, there is an accompanying liberation of heat. In a process very similar to runaway reactions, to control this rapid nucleation, the heat transfer system in batch crystallisers must be capable of quickly responding to requests to cool or heat the liquid media. Without installing additional heat transfer surface area within the crystalliser, the only method to achieve control is by changing the temperature of the jacket fluid as quickly as possible. This can be achieved using two or more sources where some sources are held at a high temperature, and the other at a cold temperature. Although this method has its advantages, care must be taken. Since the material of the crystalliser is either glass for small scale or glass-lined steel for larger scale, it cannot be subjected to large temperature differences as this could stress the glass and make it crack. The maximum values of ΔT for the standard glass-lined steel vessels are shown in Figure 2.21. These values must be considered to avoid any thermal stress on the vessel (De Dietrich Process Systems, 2015).

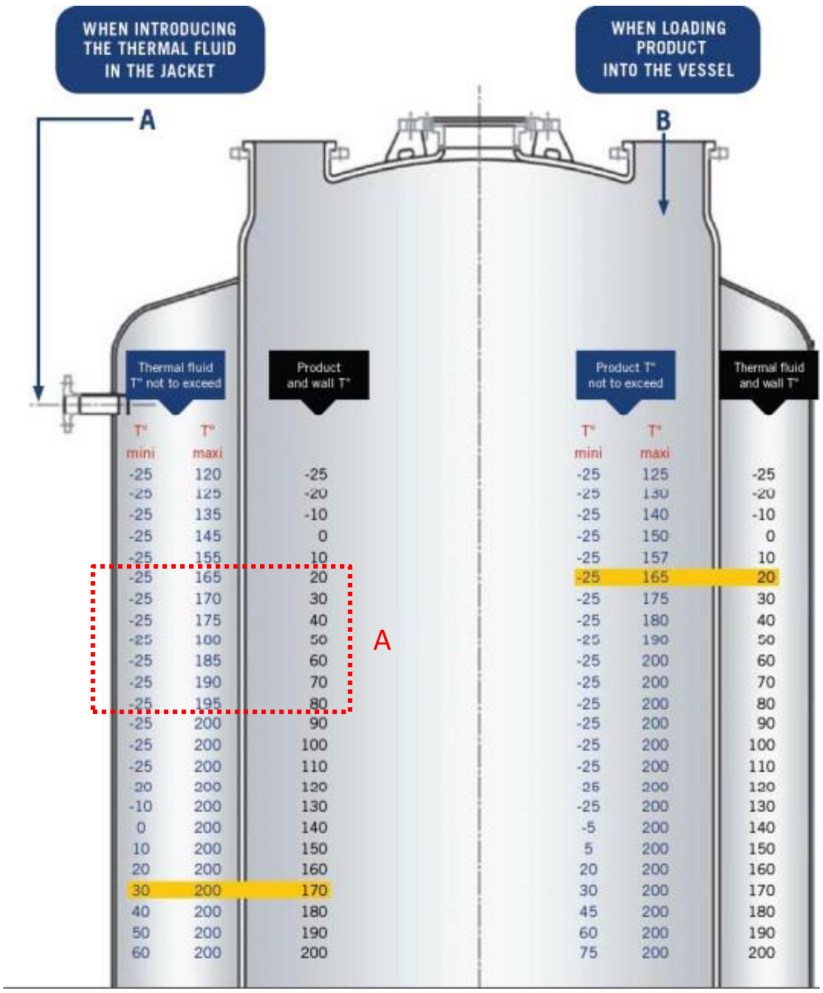

Figure 2.21: The maximum temperature difference between the jacket's fluid and the product for the standard glass-lined steel vessels where region A represents the operational conditions for the systems investigated in this work.

The next chapter will describe the developed "switching" technique where the temperature inside the jacket of a batch crystalliser can be changed quickly so as to rapidly drive the temperature inside the batch crystalliser.

2.4.2 Types of Heat Transfer Fluid Used in Industry:

The characteristics of heat transfer fluids are of great importance, because they affect the selection of devices (i.e. pumps, pipes and heat exchangers) used in the heating/cooling unit and the available temperature range in which can be worked.

The most common heat transfer fluids used in industry are: water, inhibited glycols, mineral oils, silicon based oils and paraffinic oils. Each of them has its advantages and disadvantages. Water is cheap and readily available, but it has low temperature limitation of 0ºC and requires treatment with corrosion inhibitors. $CaCl_2$ and NaCl

brines with inhibitors are popular for applications where a lower than 0°C is needed. However, their specific heat decreases as concentration increases. For temperatures lower than -20°C, ethylene or propylene glycol with inhibitors are the cheapest available fluids and have excellent heat transfer properties. They can be added to water to reduce its freezing point.

Silicon oils are economical choice because they are thermally stable and have long life (up to 10 years) and low toxicity. However, they have low viscosity and thus they can leak in the case of fault in system design. Mineral or paraffinic oils are economical option where they last for long time and work in the range (150-300°C), but they are difficult to pump at low temperature because of their high viscosity. A fluid with a high viscosity also has poor heat transfer properties.

Unlike laboratory scaled heater/chillers, industrial scale heating and cooling systems often use two separate sources; a heating circuit and a cold supply circuit. In some cases a combined heater/chiller is used which is like a laboratory water bath in many ways. Low temperatures can only be achieved in a dedicated chillier with refrigerant undergoing cyclic compression and evaporation (McConville, 2007).

Reciprocating, piston, rotary and screw are some types of compressors used in the cooling system. Compressor type depends on the required temperature range and refrigerants. When refrigerant is selected, many factors should be taken into account such as stability, vapour-temperature behaviour, toxicity and flammability. The widely used refrigerant in large processes is ammonia. However, nowadays the main refrigerants are fully and partly fluorinated FC (McConville, 2007).

2.5 Crystallisation Control

It is well-known that the properties of the final crystals, such as size, shape and morphology have a major effect on downstream processes, like filtration, drying and milling. Much of the cost of producing an API is down to the work-up steps that are needed to take the raw reactants to the final API form; crystallisation is a step often used in work up to separate out the solid that is wanted. Other steps in the workup include filtration and drying. The size of crystals produced in any crystallisation can be critical to the throughput and efficiency of the intermediate drying and filtration stages. In

addition, especially for the API itself, controlling the final form of the API may be critical in order to have the desired solubility of drugs through regulating the dissolution rate of the drug in the human body. Accordingly, there has recently been increasing emphasis on the control of crystallisation process to obtain particular physical properties for the produced crystals.

As mentioned in section 2.4, cooling crystallisation involves reducing the temperature of solution down to a point that nucleation can start, or seed crystals can grow. Therefore, much of the effort of research into controlling crystallisation has been to use techniques that manipulate the set point of the temperature system that regulates the temperature of the solution within the crystalliser. Generally, there are two main approaches used in crystallisation control, which are:

2.5.1 Model-based Approach

Model-based approach has become popular over the last decade. This approach, in principle, depends on selecting one property of the product, for example, the mean crystal size, as a target. Then it applies material and energy balance equations in order to find out the best operating conditions that lead to achieve the desired property (Fujiwara et al., 2005; Braatz, 2002; Rawlings et al., 1993). However, a simplified population balance that characterises the material balance has been widely used in the literature where only nucleation and growth kinetics were considered; i.e. agglomeration, dendritic growth and shape change were neglected (Fujiwara et al., 2005).

Open loop temperature control (T-control), in which the temperature follows pre-set profile, was traditionally utilised in industry to control cooling crystallisation. (Mullin and Nývlt, 1971) applied optimal convex cooling profile to obtain the desired supersaturation .This work was repeated by (Jones, 1974; Jones and Mullin, 1974) who developed a method to calculate the optimal cooling profile using a model described in terms of population, mass and energy balances. However, the theoretical optimal cooling profiles were normally developed for the laboratory and are often only applicable to the laboratory scale due to the power of the heating and cooling sources available. In addition, the larger volume and internal hydrodynamics of industrial scale batch crystallisers lead to spatial variations throughout the reactor volume. Industrial crystallisation is also likely to be affected by impurities inherent within the chemistry

for the reaction stage. By implementing a pre-defined cooling profile from laboratory experiments, this means that the influence of impurities, which differ from batch to batch, cannot be accounted for.

As a consequence of that, different studies have tried to develop more efficient models that could take into account all the parameters that affect the prediction capability (i.e. accuracy) of a model, such as agglomeration (Costa and Maciel Filho, 2005) and thermodynamics and secondary nucleation (Worlitschek and Mazzotti, 2004). As this approach requires considerable expertise in process modelling and optimisation, this limits its use to laboratory studies. Adding to that, both the effects of parameters uncertainties and the disturbances should be considered in the model to ensure accurate prediction leading to more complicated procedure and the need of extra time (Nagy and Braatz, 2004).

Recently, Zhang et al. (Zhang et al., 2009) suggested an iterative learning control (ILC) approach based on the linearised models obtained from process operational data to keep the desired supersaturation profile of a crystallisation process. A similar algorithm for the supersaturation control in batch cooling crystallisation was proposed by Forgione et al. (Forgione et al., 2012). However, they developed the model based on the combination of ILC and PI controllers to neglect the effect of system disturbances. In order to minimise the need for the development of detailed mathematical model and the use of data based linear time varying (LTV) models that have poor extrapolative capability, hybrid models combining the simplified model and data-driven model were proposed by (Hermanto et al., 2011; Zhang et al., 2012). Although, the hybrid models showed good performance, they had only been applied on systems with well-defined mathematical models. More recently, the development of a data-driven approach based on (LTV) model in an (ILC) framework was shown by the work of (Sanzida and Nagy, 2013). This approach defined the supersaturation set point and the corresponding temperature profile for the supersaturation controller by the benefits of the repetitive nature of batch processes in order to produce crystals with the desired properties.

2.5.2 Direct Design (Model-free) Approach

The direct design approach applies feedback control strategies based on online measurement of supersaturation or product properties, for example, the CSD in order to

follow the best operating conditions that lead to attain the desired crystal quality (Zhou et al., 2006).

In recent years, the availability of accurate in-line sensors for the measurement of solution concentration and crystal size has opened the possibility of using these tools such as conductivity (Doki et al., 2001), calorimetric (Monnier et al., 1997) and ATR-FTIR (Lewiner et al., 2001b; Dunuwila and Berglund, 1997; Fujiwara et al., 2002; Feng and Berglund, 2002; Groen and Roberts, 2001) combined with control algorithms to control crystallisation process effectively. Moscosa-Santillan et al. (2000) proposed an alternating cycle of temperature, namely, a succession of cooling and heating periods using a water-glycol bath enclosed in a cryothermostat, based on online information obtained from a spectral turbidimetric method for a seeded batch cooling crystallisation of glycine in water. They found that the alternative profile improved the CSD with 95% of the final product having a large size between 1 and 1.6 mm and only 3% of it as fines. It also reduced secondary nucleation compared with two well-known temperature profiles that are widely used in crystallisation, namely the optimal convex Mullin-Nývlt and linear cooling profiles that form fines. Moreover, (Doki et al., 2004) reported a control strategy for seeded cooling crystallisation of α-form glycine. This strategy used data from an in-situ ATR-FTIR spectrometer and FBRM particle counter to online manipulate the alternating temperature profile in order to keep the crystal count number the same as the original seed crystal value by applying linear heating and cooling rates using one water bath.

With the aim of directly controlling the CSD in a crystallisation process, (Abu Bakar et al., 2009) introduced a new direct nucleation control (DNC) approach for controlling the crystallisation of glycine from a water-ethanol mixture. This approach was based on controlling the amount of nuclei present in the system, measured by FBRM, through either addition of anti-solvent / temperature reduction or addition of solvent / temperature increase. The results showed the ability of the developed control system to produce larger crystals particularly compared to uncontrolled system.

Furthermore, (Bakar et al., 2009) proposed a temperature cycling method that is based on maintaining the target counts of CLD provided by FBRM during the whole crystallisation process via adjusting the heating/ cooling rates to achieve the desired CSD and polymorphic form of sulfathiazole in water and in n-propanol. This alternating

cycles of heating and cooling stages promoted Ostwald ripening as the heating stage dissolved the fine crystals, while the cooling stage accelerated the growth of the larger crystals (Mullin, 2001). Those approaches were utilised later by (Moynihan and Kelly, 2012) for the crystallisation of phenacetin from ethanol. However, Moynihan and Kelly examined two forms of cooling regimes for unseeded and seeded phenacetin crystallisation. In the first regime, turbidity counts were used to switch between heating /cooling stages. While in the second cooling regime, the batch temperature was manipulated to keep the cooling profile within the boundary of the MSZ. They found that pre-defined cyclic temperature profiles gave good quality of crystals if used with seeded batches. This approach for larger reactors would depend on the capacity of the heater/ cooler system and it may not be easy to achieve the immediate heating and cooling rates. However, the seed amount, size and loading are defined based on the requirements of the final products (Kubota et al., 2001; Lung-Somarriba et al., 2004; Yu et al., 2006b) because these factors, if not defined correctly, can lead to the dispersion of the CSD. In addition, it is sometimes not practical to seed the system externally.

The closed-loop concentration control (C-control) method using ATR-FTIR technique, in which the supersaturation set point is set at a constant value, has been widely used and shown its robustness to improve the crystal size consistency in cooling and anti-solvent crystallisation of various organic materials as reported by (Braatz, 2002; Braatz et al., 2002; Chung et al., 2000; Feng and Berglund, 2002; Gutwald and Mersmann, 1990; Lewiner et al., 2001a; Liotta and Sabesan, 2004; Yu et al., 2006a; Fujiwara et al., 2005; Fujiwara et al., 2002; Grön et al., 2003; Zhou et al., 2006; BORISSOVA et al., 2009; Khan, 2008). The supersaturation level is kept close to the solubility curve in order to optimise the crystal growth and prevent secondary nucleation. However, working close to a solubility curve (low supersaturation) has its disadvantages, such as slow growth rate and long batch times. Therefore, the choice of supersaturation profile should guarantee fast growth rate as well as low nucleation rate as illustrated in Figure 2.22. Supersaturation levels of 1.1, 1.2, and 1.3 were able to produce crystals of good quality (Khan et al., 2011).

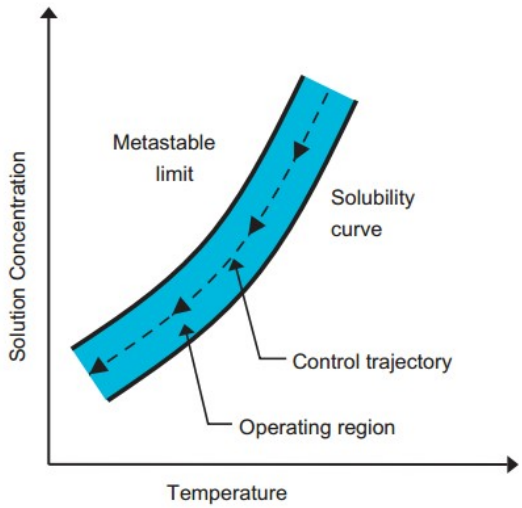

Figure 2.22: The concentration-temperature operating profile (labelled as control trajectory) for batch cooling crystallisation lies between the solubility curve and the metastable limit (Fujiwara et al., 2005).

However, (BORISSOVA et al., 2009; Chew et al., 2007a; Lewiner et al., 2002) found that C-control for unseeded crystallisation produced inconsistent crystals as a result of the irreproducibility of primary nucleation. Added to that, the ATR-FTIR probe was prone to encrustation due to nucleation on its surface, blocking the IR signals and rendering the instrument blind to subsequent measurements. This encrustation phenomenon deteriorates the reliability of the FTIR measurement method.

To overcome this issue, a study by (Chew et al., 2007b) proposed a fully automated control method for unseeded cooling crystallisation of glycine/water and paracetamol/water systems using FBRM measurement. In this work, the author allowed primary nucleation to take place, then raised the temperature using a linear ramp to obtain a pre-determined PSD and finally initiated a linear cooling cycle. Through this method, the initial nucleated crystals were refined (fines dissolved, larger ones better conditioned). The results showed that the product consistency was much better than that for unseeded systems over five runs with a decrease in variability by more than three times.

FBRM is a technique that depends on the optical quality of the measuring sensor and so is also prone to encrustation. The fact that seeds generated were conditioned in Chew's work reduced the likelihood of the FBRM probe being affected by deposits of crystals during the crystallisation process. This strategy was extended to anti-solvent

crystallisation of glycine in ethanol-water mixture by (Hermanto et al., 2010). The results showed good product quality and CSD consistency.

In the drive to improve the robustness of C-control strategy, (Woo et al., 2009) also suggested an adaptive C-control method that used the FBRM as a control signal for both cooling crystallisation and anti-solvent crystallisation. In Woo's work, the nucleation point was detected by FBRM and then the operating curve (temperature or anti-solvent addition rate) was changed to maintain the number of particle counts per unit time at its desired value. This further enhanced the quality of the final product.

In crystallisation processes, undesired events such as, secondary nucleation, accidental seeding from deposited crust on the crystalliser's wall and variations in seed quality, can lead to a poor final CSD. The traditional open loop control system was not able to cope with these events resulting in an undesired CSD. In addition, the aforementioned C-control approaches faced difficulty to remove the effect of these undesired events once they have occurred. To overcome these problems, (Saleemi, 2011; Saleemi et al., 2012) developed an automated direct nucleation control (ADNC) approach using FBRM to yield a better quality product, with a narrow and uniform CSD, for the cooling crystallisation of paracetamol in isopropyl alcohol using either internal seeds generation, external seeding or accidental seeding. This approach was based on temperature cycling to keep the system particles number close to the set point value through dissolving tiny crystals and promoting the growth of large crystals leading to desired the CSD. It proved to be robust and able to correct for the disturbances that could take place during the crystallisation process. The temperature cycling method was used before by (Abu Bakar et al., 2010; Kim et al., 2003) . However, in the work of (Saleemi et al., 2012) , the number of cycles, rate and frequency, heating/cooling rates and temperature limits were defined by an automatic and adaptive feedback control system.

In a move towards process scale up control, (Khan et al., 2011) extended the closed loop supersaturation control system developed earlier by (Grön et al., 2003) , to 20 L lab scale and 250 L industrial pilot-plant crystallisers. They developed a multivariate, chemometric partial least-squares (PLS) FTIR calibration model to monitor the concentration of LGA in seeded batch cooling-crystallisation in order to control the supersaturation at three different levels: 1.1, 1.2, and 1.3 using both internal and

external seeding modes. They found that the average crystal size obtained was inversely proportional to supersaturation level.

Industrial scale crystallisers are often controlled using two or more external heat exchangers taking utility fluid from a loop (Khan et al., 2011). Figure 2.23 shows a typical type of scheme where temperature to the jacket of the crystalliser comes from two exchangers, one supplying heat, and the other supplying cold. The response times for the external exchangers should ideally be faster than the response time of the crystalliser but this depends on flow rates, areas, fouling and the utility systems used.

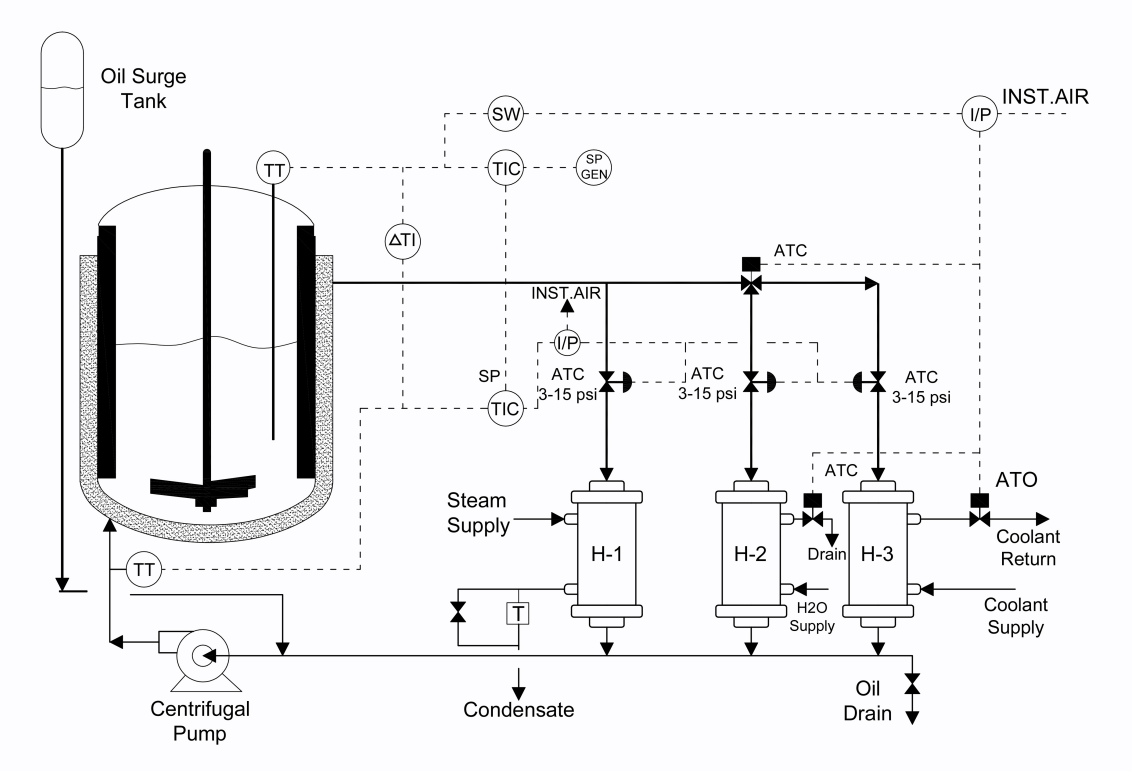

Figure 2.23: Recirculating temperature control with indirect heat transfer (Myerson, 2002).

Saleemi (2011) also applied his ADNC approach to 100 L pilot plant scale for paracetamol/isopropanol and ortho-amino benzoic acid (OABA)/water systems. The results showed better product quality over the traditional linear and crash cooling profiles. Details of the method used to cool the reactor are not clear but it is likely that the control system adopted a standard approach for a small scale unit of this type; a circulating oil which flows through an electrical heater and a cooling coil. A control system would either activate the heater or allow cold utility fluid into the coil thereby regulating the temperature of the oil.

As can be noted, the direct design approach is simple, compared with model-based approach, because neither kinetics information nor modelling is required making it desirable for large scale industry crystallisations. On the other hand, the reliability of this approach depends on the accuracy of the online measurement and the effectiveness of the controller.

Both approaches, model-based and model-free, however, will only manipulate one set point; the temperature set point of the water bath. As will be explained in chapter 4, providing additional control "handles" may give the industry alternative methods to produce crystals. In this thesis, a method is proposed that implements a novel control strategy based on the use of two temperature sources; a hot and cold source, to control the crystallisation of LGA-water and glycine-water systems. A PVI system has been developed to monitor the formation of crystals and combined with the switching technique to control the crystallisation process of LGA and glycine. Chapters 3, 4 and 5 will provide a detailed documentation of the developed system.

2.6 Conclusion

This chapter highlighted the fundamental theories and mechanisms that govern the crystallisation process. In addition, it reviewed the techniques used to monitor the crystallisation process focussing on the optical methods as the monitoring technique developed in this work is classified into this category. An introduction of the control approaches applied to batch cooling crystallisation was given. From the literature review, it is clear that crystallisation particularly for batch cooling is:

1. Process that is governed by mass and heat transfer. The formation of new solid is a process that involves heat that needs to be removed through an external source.

2. That spontaneous primary nucleation is often undesired event that causes the formation of a large number of fines within the solution. Additional seeds can be used to offset primary nucleation but if cooling rate is high then secondary nucleation can take place.

3. In the chemical industry when a control system is implemented, it is taken for granted that the response time for the controller and the associate control valves is

far quicker than the time constant associated with the process. The two areas where this is not the case is a) for runaway reactions where the kinetic rate is much higher than the control system can respond to and, b) for cooling crystallisation where primary and secondary nucleation rates may be also higher than the current cooling control system can respond to.

4. There are various methods to monitor crystallisation ranging from methods associated with the chemistry (e.g. FTIR and XRD) to optical type monitoring. These provide information on the status of the crystallisation and a convenient way of inputting information to control system.

In the following chapters, the development of simple heat transfer model of agitated vessel to predict the vessel temperature as a result of applying different cooling profiles is demonstrated. The application of the developed PVI system for monitoring the cooling crystallisation of two chemicals, namely, LGA and glycine is shown. Moreover, the novel switching technique that supplies hot and cold water to the batch crystalliser jacket and how the key variables of its frequency and duration can influence the cooling crystallisation of glycine are investigated.

Finally, the implementation of the developed control strategy on cooling crystallisation of LGA-water and glycine-water systems to grow crystals with larger size through combining the developed PVI system with the switching technique is demonstrated.

Chapter 3

Heat Transfer for Non Crystallised Systems

Understanding the heat transfer phenomena in processes that are temperature limited, for instance cooling crystallisation, is of great importance for the overall process efficiency and improving the quality of the final product which is the main goal of this work.

This chapter provides simple heat transfer model of agitated vessel which is similar in configuration to the crystalliser used in this work. Adding to that, experimental works carried out in the 2 L vessel to find out the efficiency of the two water baths used in heating/ cooling cycle are presented. Moreover, this part of the thesis investigates the concept of switching between hot and cold water baths and how this can affect the temperature inside the crystalliser which is of influence on the direction of crystallisation process.

3.1 Heat Transfer Model of Agitated Vessel

The aim of generating this model is to predict the temperature inside the 2 L vessel as a result of applying different cooling profiles. The heat transfer model of the agitated vessel was developed from the energy balance on the liquid inside the vessel; which is water in our case.

Heat exchange between the jacket and the vessel is given by:

$$Q = U\,A\,\Delta T_m \tag{3.1}$$

Where U is the overall heat transfer coefficient, A is heat transfer area, and ΔT_m is the logarithmic mean temperature difference which equals to:

$$\Delta T_m = \frac{T_1 - T_2}{ln\frac{T - T_1}{T - T_2}} \tag{3.2}$$

Enthalpy difference between the inlet and outlet streams of the jacket is:

$$Q = \dot{M}\,c_p\,(T_1 - T_2) \tag{3.3}$$

Where $\dot{M}$ is the mass flow rate of fluid passing through the external jacket, c_p is the specific heat capacity of fluid passing through the jacket, and T_1 and T_2 are the inlet and outlet temperatures of the jacket fluid respectively.

Equating equations (3.1) and (3.3) yields:

$$U\ A\ \Delta T_m = \dot{M}\ c_p (T_1 - T_2) \tag{3.4}$$

Substituting equation (3.2) into (3.4) gives:

$$U\ A \frac{T_1 - T_2}{ln\frac{T - T_1}{T - T_2}} = \dot{M}\ c_p (T_1 - T_2) \tag{3.5}$$

Rearranging similar terms and grouping the constants together yields:

$$ln\frac{T - T_1}{T - T_2} = \frac{UA}{\dot{M}\ c_p} \tag{3.6}$$

$$\frac{T - T_1}{T - T_2} = e^{\frac{UA}{\dot{M}\ c_p}} \tag{3.7}$$

Assuming $\boldsymbol{K = e^{\frac{UA}{\dot{M}\ c_p}}}$, equation (3.7) can be simplified as:

$$T_2 = \frac{1}{K} T_1 + T - \frac{1}{K} T \tag{3.8}$$

The rate of change of the vessel temperature can be calculated by:

$$Q = M_T\ c_p^T \frac{dT_T}{dt} \tag{3.9}$$

Where M_T is the mass of the vessel liquid, and $\boldsymbol{c_p^T}$ is the specific heat capacity of the liquid inside the vessel.

Equating equations (3.3) and (3.9) gives:

$$M_T\ c_p^T \frac{dT_T}{dt} = \dot{M}\ c_p\ (T_1 - T_2) \tag{3.10}$$

Substituting equation (3.8) into equation (3.10) yields:

$$M_T\ c_p^T \frac{dT_T}{dt} = \dot{M}\ c_p \left(\frac{K - 1}{K}\right) (T_1 - T_T) \tag{3.11}$$

Rearranging similar terms and grouping the constants together yields:

$$\frac{M_T\, c_p^T}{\dot{M}\, c_p \left(\frac{K-1}{K}\right)} \frac{dT_T}{dt} + T_T = T_1 \tag{3.12}$$

Equation (3.12) is of the form:

$$\tau \frac{dx}{dt} + x = c \tag{3.13}$$

The Laplace transform of this form is known as:

$$X(s) = \frac{1}{\tau s + 1} C(s) \tag{3.14}$$

Hence the time constant is:

$$\tau = \frac{M_T\, c_p^T}{\dot{M}\, c_p (\frac{K-1}{K})} \tag{3.15}$$

This time constant of the process defines the response time of the system to changes in temperature.

Rearranging the definition of the time constant to $\alpha = \frac{\dot{M}\, c_p \left(\frac{K-1}{K}\right)}{M_T\, c_p^T}$

Equation (3.11) becomes:

$$\frac{dT_T}{dt} = \alpha\, (T_1 - T_T) \tag{3.16}$$

Since T_1 is the temperature of the jacket fluid, for a linear heating rate, this temperature changes as:

$$T_1 = T_0 + \beta t \tag{3.17}$$

Where β is the heating rate ºC/min, T_0 is the initial jacket temperature ºC and t is the time in minutes.

However, for a linear cooling rate, the jacket temperature changes as:

$$T_1 = T_0 - \beta t \tag{3.18}$$

Where β is the cooling rate ºC/min.

In order to predict the vessel temperature for a typical programmed cooling and heating rates (for example β=0.3 ºC/min), the fourth order Runge-Kutta method was used to solve equation (3.16) in MATLAB for an estimated value of overall heat transfer coefficient (U=293 $W.m^{-2}\ K^{-1}$).

To see to what extent the experimental data of the vessel temperature for 0.3 ºC/min heating and cooling rates can fit with the mathematical model described in equation (3.16), the experimental and model results are plotted in Figures 3.1 and 3.2 respectively.

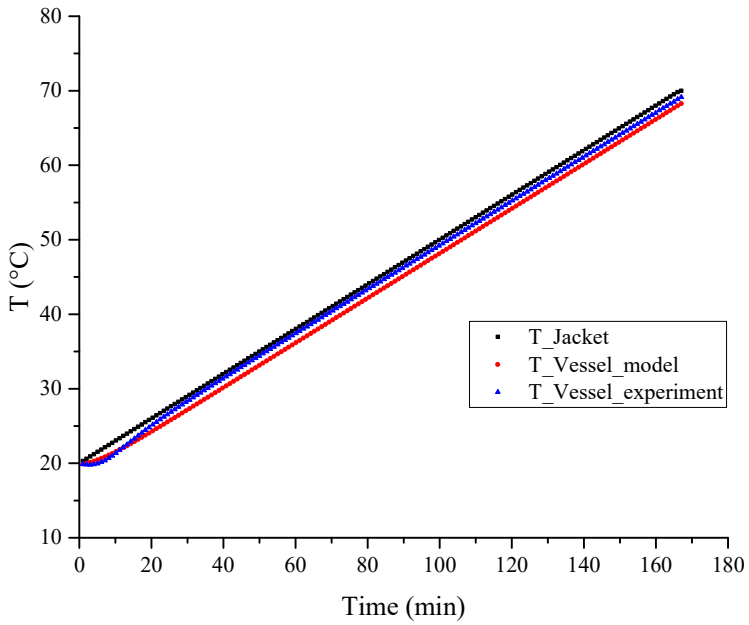

Figure 3.1: A comparison between the experimental data and the model results of the vessel temperature for programmed heating rate of 0.3 ºC/min.

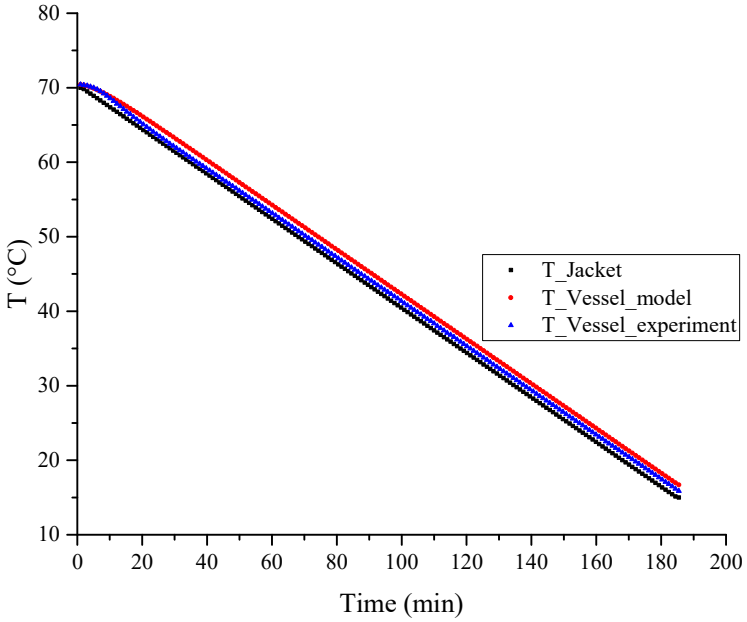

Figure 3.2: A comparison between the experimental data and the model results of the vessel temperature for programmed cooling rate of 0.3 ºC/min.

As seen in Figures 3.1 and 3.2, the model was able to predict the vessel temperature to a good degree if compared with the experimental data.

3.2 Water Bath Effectiveness

Cooling crystallisation involves a balance between mass transfer and heat transfer; mass transfer of solute from the liquid to the solid form, and associated latent heats. The formation of new solid material is modelled as a kinetic process so that the rate of crystallisation involves a rate of heat transfer. When nucleation starts, this could be a rapid process so a potential system that detects and controls nucleation would have to respond with a similar time scale. In order to determine what the response times were of laboratory water baths, a series of experiments were carried out to investigate the effectiveness of the water bath used to heat up or cool down the water inside the agitated vessel.

All the experiments were conducted in a 2 L jacketed round bottom glass vessel equipped with a retreat curve impeller (RCI) driven by an electric motor. A vertical cylinder baffle was also installed inside the vessel because this is the standard configuration used in batch crystalliser (Liang, 2002). To minimise evaporation losses

in the 2 L vessel, the lid of the vessel was attached to the body with a parafilm tape sealing.

The vessel was placed inside a rectangular tank (100x50x50 cm) filled with tap water. Heating-cooling cycles were carried out using a MATLAB programme running on PC connected via RS232 port to the water bath (Haake-F6-C40). The water bath, which was connected to the vessel jacket through hoses and silicon tubes, was fitted with platinum resistance thermometer (PT-100) to measure the temperature inside the vessel. A schematic diagram of the system is illustrated in Figure 3.3.

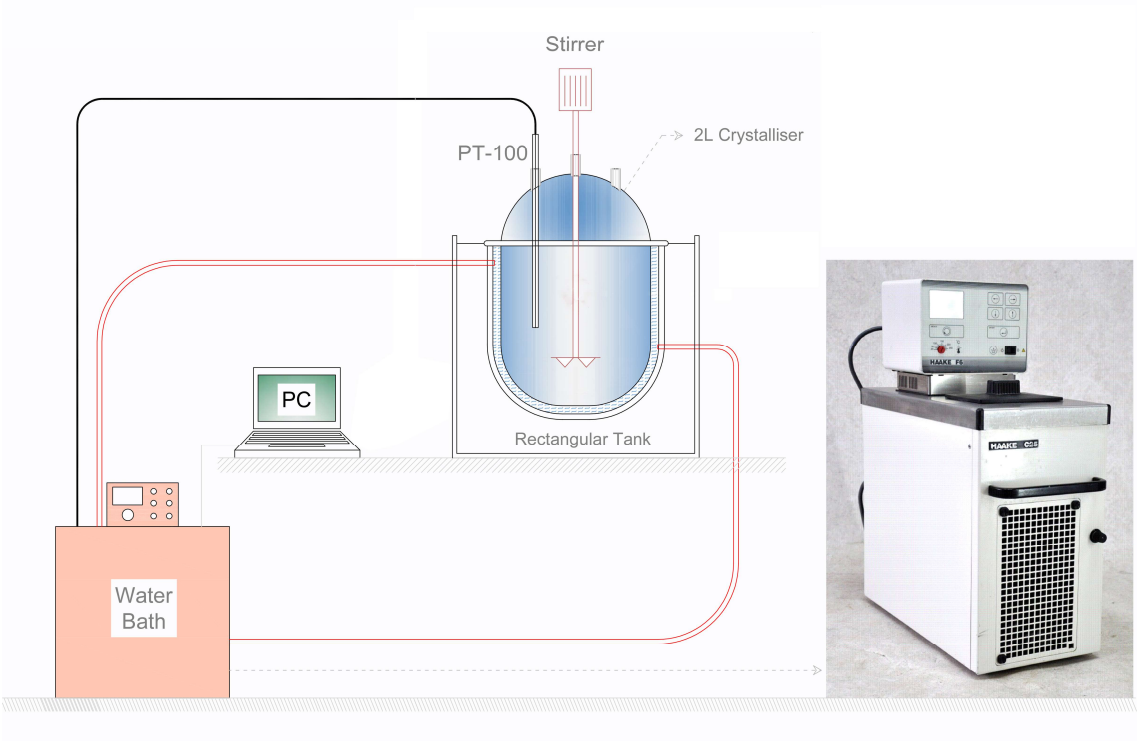

Figure 3.3: Schematic diagram of the laboratory unit.

For the first experiment, the objective was to determine the heating and cooling capacity of the water bath without the additional load of water inside the vessel and inside the rectangular tank. The objective of the second experiment was to find the same loading values but when the vessel and tank were filled. The experimental protocol was as follows:

1. Starting from room temperature conditions, set the water bath temperature set point at 70ºC and allow water to circulate through the jacket.
2. Record the water bath temperature every 30 seconds until reaching 70ºC. In experiment 2, the vessel temperature was also recorded.
3. Set the water bath set point temperature at 5ºC.

4. Record the water bath temperature every 30 seconds until it reaches 5ºC. In experiment 2, the vessel temperature was also measured.

The water bath and vessel temperatures as a function of time are shown in Figures 3.4 and 3.5 for the heating stage and the cooling stage respectively.

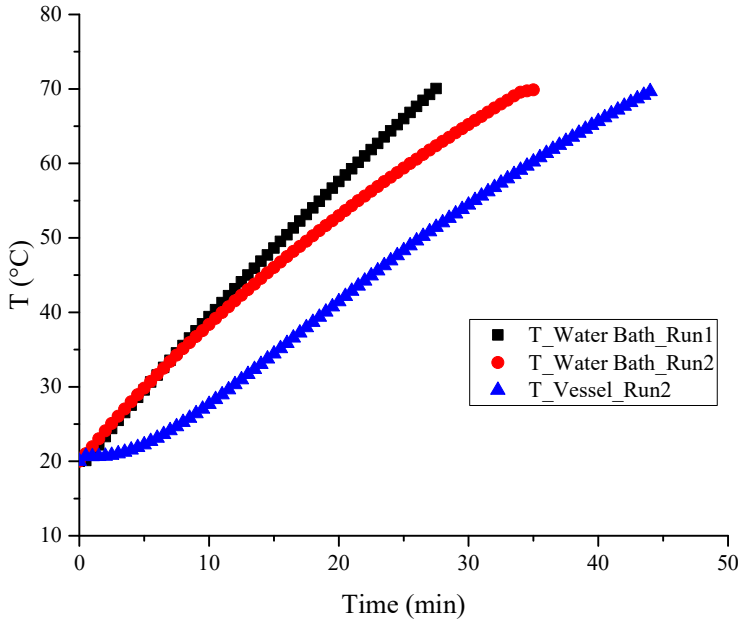

Figure 3.4: Water bath and vessel temperatures as a function of time for the heating stage.

The heating rate for both water bath and vessel between 20ºC and 70ºC is summarised in Table 3.1.

Table 3.1: The heating rate of the water bath and the vessel for both experiments.

Run Number	Experiment Conditions	Water_Bath Heating Rate Between 20 and 70 ºC [ºC/min]	Vessel Heating Rate Between 20 and 70 ºC [ºC/min]
1	Empty Vessel and Rectangular Tank	1.8	N/A
2	Full Vessel and Rectangular Tank	1.4	1.2

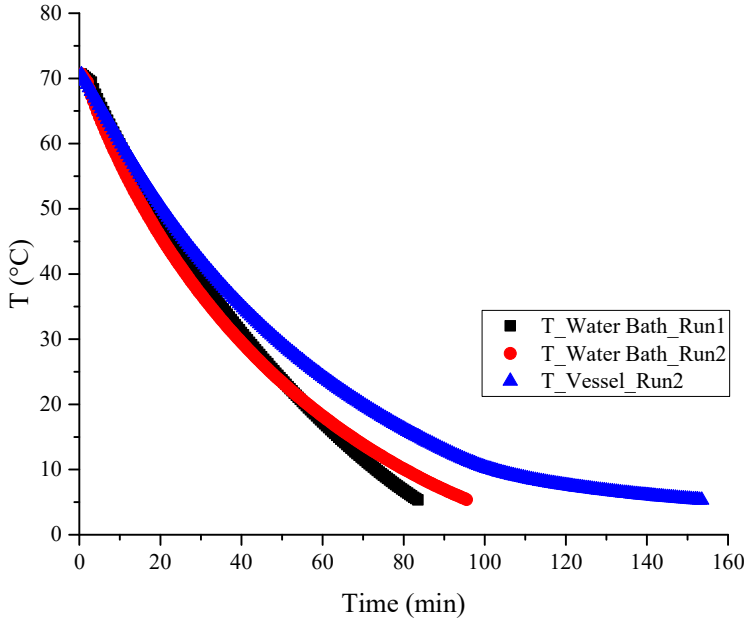

Figure 3.5: Water bath and vessel temperatures as a function of time for the cooling stage.

The cooling rate for both water bath and vessel between 70ºC and 5ºC is summarised in Table 3.2.

Table 3.2: The cooling rate of the water bath and the vessel for both experiments.

Run Number	Experiment Conditions	Water_Bath Cooling Rate [ºC/min]	Vessel Cooling Rate [ºC/min]
1	Empty Vessel and Rectangular Tank	0.8	N/A
2	Full Vessel and Rectangular Tank	0.64	0.4

It is worth noting that the water bath is able to heat the vessel up at a higher rate than to cool it down as seen clearly in Tables 3.1and 3.2. This can be explained as a result that the water bath has higher heating capacity (2000 W) compared against a cooling capacity of (550-700 W) (Artisan, 2000).

Comparing the water bath temperature profile of experiment 1 with that of experiment 2, it is observed that water bath in experiment 1 heated up and cooled down to the desired temperature quicker than that in experiment 2. The reason is simply down to the difference in heat load required to heat/cool the water that was in the vessel and in the

rectangular tank. Nevertheless, the overall difference in time between the experiments 1 and 2 for both heating and cooling stages is small as can be noticed in Figures 3.4 and 3.5. Based on these results, it is sensible to conclude that the presence of water in the rectangular tank surrounding the agitated vessel has a small influence on the capacity of the water bath to deliver the desired temperature profile.

Moving on to the effect of the agitation speed, Figure 3.6 compares the vessel temperature profile during the heating and cooling cycle at different stirring speeds.

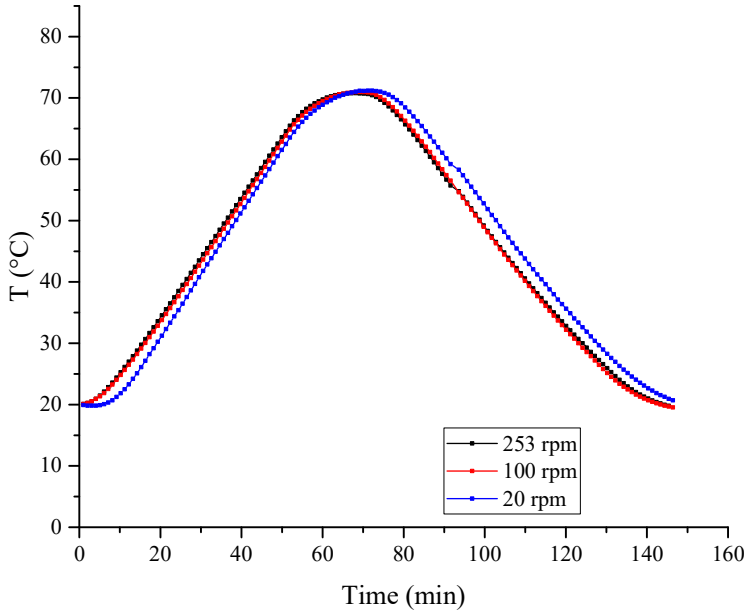

Figure 3.6: Vessel temperature profile during the heating and cooling cycle at different stirring speeds.

As shown in Figure 3.6, there is virtually no influence of stirring speed on the vessel temperature heating and cooling profiles over the range 100-253 rpm. However, there is a delay in temperature response for a lower speed (20 rpm) which is due to the poor mixing that influences the heat transfer efficiency. To investigate deeply the effect of the agitation speed on the overall heat transfer between the jacket and the vessel, Wilson method was used. As known, the overall heat transfer can be expressed as:

$$\frac{1}{U} = \frac{1}{h_v} + \frac{\Delta x}{k} + \frac{1}{h_j} \qquad \textbf{(3.19)}$$

Where U is the overall heat transfer coefficient, h_v is the heat transfer coefficient at the internal wall of the crystalliser, Δx is the thickness of the crystalliser wall, k is the

thermal conductivity of the crystalliser wall and h_j is the heat transfer coefficient at the external wall of the crystalliser. The thermal resistances of the jacket fluid and the vessel wall are constant provided the jacket fluid is at a constant velocity and can be expressed in the term ϕ. Therefore, equation (3.19) can be written as:

$$\frac{1}{U} = \phi + \frac{1}{h_v} \tag{3.20}$$

The relationship between the heat transfer coefficient at the internal wall of the vessel (h_v) and the ratio of the stirrer speed (N) to a reference speed (N_0) is given as (Uhl and Gray, 1966):

$$\frac{1}{h_v} = \beta \left(\frac{N}{N_0}\right)^{-2/3} \tag{3.21}$$

Substituting equation (3.21) into equation (3.20) yields:

$$\frac{1}{U} = \phi + \beta\left(\frac{N}{N_0}\right)^{-2/3} \tag{3.22}$$

The values of U for the different stirring speeds were estimated by fitting the mathematical model described in equation (3.16) to the experimental data (see Table 3.3).

Table 3.3: Summary of the experimental data.

Stirrer Speed N [min^{-1}]	$(N/N_0)^{-2/3}$ [-]	Estimated U [$W/m^2.K$]	1/U [$m^2.K/W$]
20	2.1	220	0.0045
100	0.7	270	0.0037
253	0.4	300	0.0033

Plotting U^{-1} vs. $\left(\frac{N}{N_0}\right)^{-2/3}$ gives Wilson plot as shown in Figure 3.7 and the values for β and ϕ can be determined from the slope and the intercept respectively.

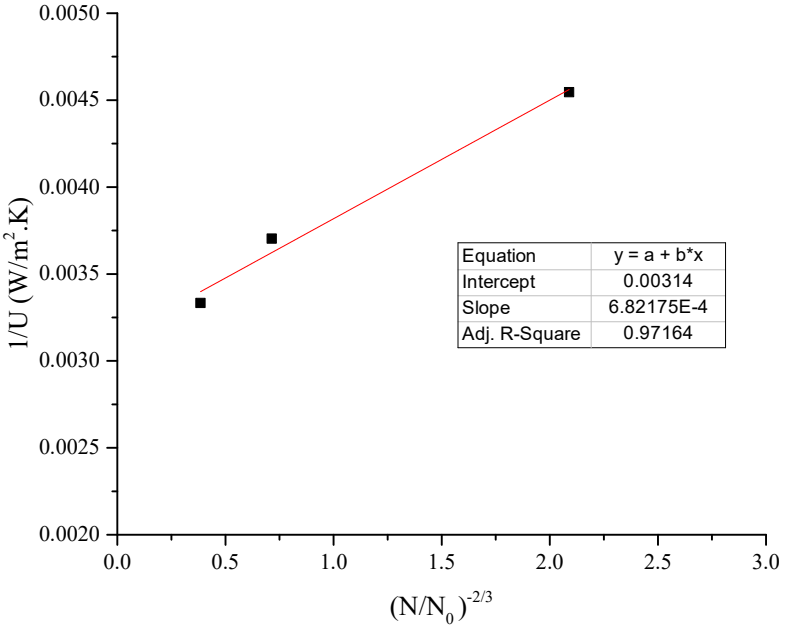

Figure 3.7: Wilson plot of water determined in 2L vessel with RCI impeller.

Using the slope and the intercept of Wilson plot, the heat transfer resistances can be calculated from equations (3.21) and (3.22). Table 3.4 summarises the results of calculated heat transfer coefficients where the wall thickness, Δx is 2mm and the thermal conductivity of the vessel material (i.e. glass), k is 1.14 W/m.K.

Table 3.4: Summary of the calculated heat transfer coefficients for different agitation speeds.

Stirrer Speed N [min^{-1}]	U [$W/m^2.K$]	h_v [$W/m^2.K$]	h_j [$W/m^2.K$]	$k/\Delta x$ [$W/m^2.K$]
20	220	684	743	570
100	270	1999	743	570
253	300	3712	743	570

As can be seen in Table 3.4, the results obtained showed an effect of the stirrer speed on heat transfer coefficient at the internal wall of the vessel (h_v) which is in good agreement with the literature (Perry and Green, 1999). This would suggest that the limitation to heat transfer, the resistance to heat transfer, for the same properties of the vessel and the jacket fluid is related to the speed of the impeller and it decreases with increasing the speed.

3.3 Measuring the Dead Time and Time Constant for the Agitated Vessel

Time constant and dead time terms are key parameters in developing any closed loop control system. In principle, the dead time is the delay in the process variable response due to a change in controller output. The longer the dead time, the worse the control performance is. Contrary to this, the time constant describes how fast the process variable acts in response to the controller output variation. Therefore the shorter it is, the more effective the control is (Smith and Corripio, 1985). Consequently, before beginning the development of the control strategy, it is essential to measure the process characteristics to find out how fast the vessel temperature can be changed due to a step change in temperature. To do that, the following procedure was used:

1. Set the Haake water bath temperature set point at 70ºC.
2. When the Haake temperature was at its set point, the water flow through the vessel jacket was switched from Grant to Haake water bath using solenoid valves. This will be explained in detail in section 3.4. The vessel temperature change because of this switching was recorded every 30 seconds and the Grant water bath temperature set point was set at 15ºC.
3. When the vessel temperature was reached the desired temperature 70ºC, the water flow through the jacket was switched from Haake back to Grant water bath and the vessel temperature change was recorded every 30 seconds as well.

The vessel temperature response as a result of switching to hot and cold water baths is shown in Figures 3.8 and 3.9, respectively.

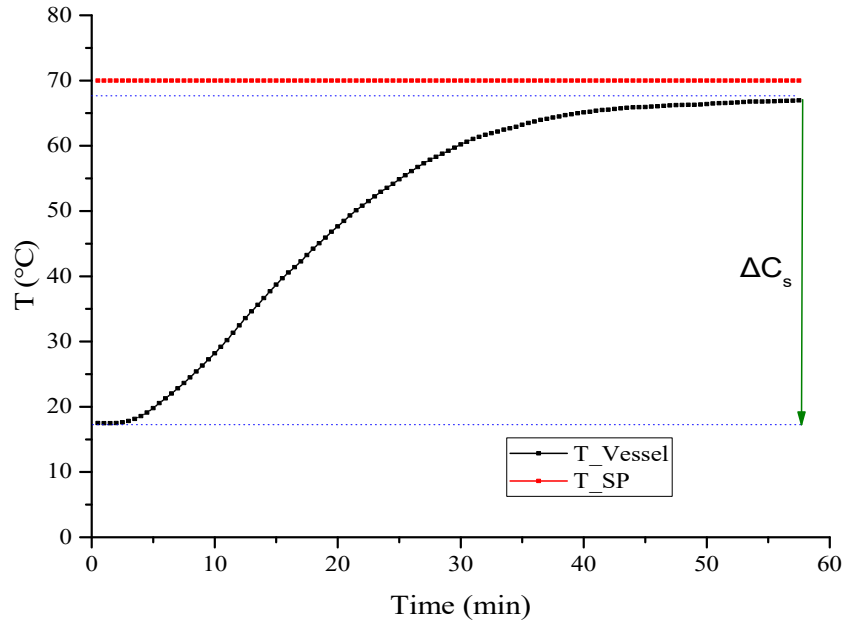

Figure 3.8: Vessel temperature response as a result of switching to hot water bath.

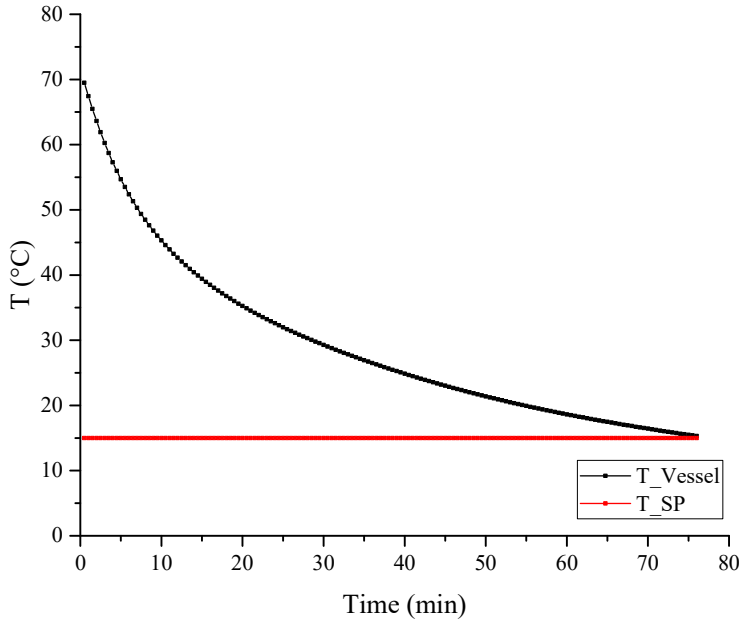

Figure 3.9: Vessel temperature response as a result of switching to cold water bath.

As it can be seen in Figure 3.8, the vessel temperature at the beginning did not change as a result of switching to hot bath and then it started increasing until it levelled off again. Therefore, the dead time represents the period before the temperature begins to increase. However, the time constant is equal to 0.632 of the steady state change in

vessel temperature (ΔC_s) (Smith and Corripio, 1985). Table 3.5 contains the calculated values of the dead time and time constant of the agitated vessel. These measured values show that despite the differences in heating and cooling power of the water baths, the time constants are approximately similar.

Table 3.5: Calculated values of the dead time and time constant of the agitated vessel.

Dead Time [min]	Time Constant for Heating Stage [min]	Time Constant for Cooling Stage [min]
2	18.5	19.5

To check if the mathematical model described in equation (3.16) can also predict the vessel temperature for crash heating and cooling, the fourth order Runge-Kutta method was used to solve equation (3.16) in MATLAB for an estimated value of overall heat transfer coefficient (U=90 $W.m^{-2}$ K^{-1}). The experimental and model results are plotted in Figures 3.10 and 3.11 respectively.

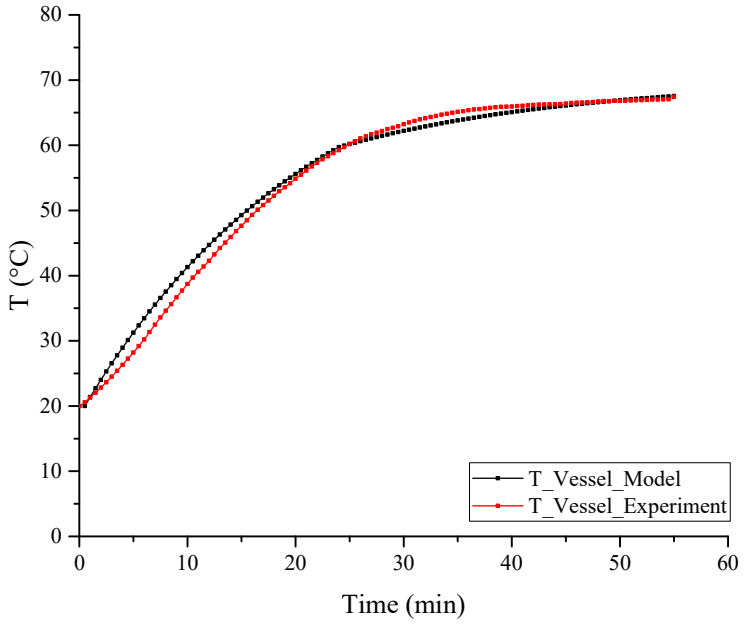

Figure 3.10: A comparison between the experimental data and the model results of the vessel temperature for crash heating.

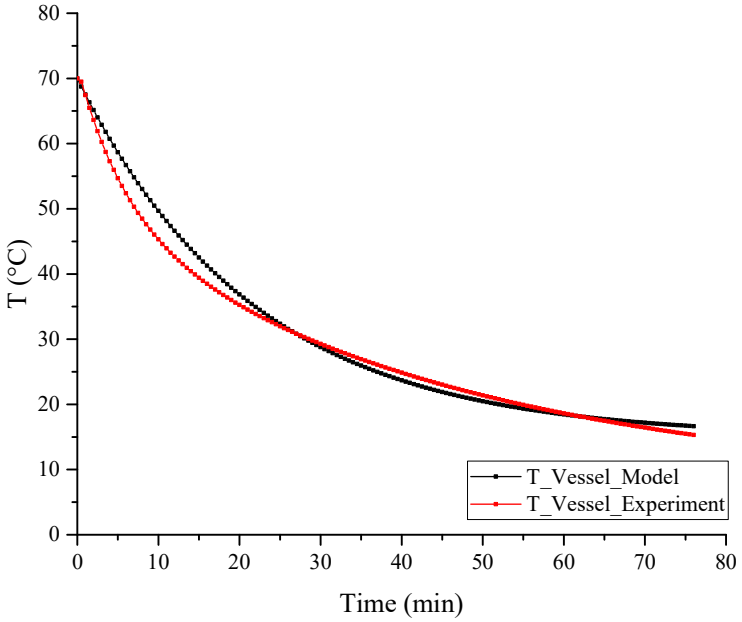

Figure 3.11: A comparison between the experimental data and the model results of the vessel temperature for crash cooling.

As seen in Figures 3.10 and 3.11, there is small deviation between the experimental data and model prediction values. As the vessel was not insulated, there would be thermal losses which were not taken into the account in the model equation. This may explain the difference between the two set of data.

As mentioned earlier, comprehensive knowledge of heat transfer is of crucial importance for controlling the process performance. However, as the process scale goes up, the heat transfer becomes more difficult due to a lower ratio of specific area to volume (Brown, 2012; Liang, 2002). In section 3.1, it was found that the time constant is calculated by:

$$\tau = \frac{M_T \, c_p^T \, e^{\frac{UA}{\dot{M} \, c_p}}}{\dot{M} \, c_p (e^{\frac{UA}{\dot{M} \, c_p}} - 1)} \tag{3.23}$$

This equation implies that the time constant is a function of the overall heat transfer coefficient U, the internal surface area A, the mass flow rate and the specific heat capacity of the heating/cooling fluid, and the mass of fluid inside the vessel. Therefore it is no surprise that the time constants measured and shown in Table 3.5 should be similar since water baths of similar specifications were used for heating and cooling.

The time constant for larger vessel is given by:

$$\tau_2 = \frac{M_{T2}\, c_p^T\, e^{\frac{UA_2}{\dot{M}\, c_p}}}{\dot{M}\, c_p(e^{\frac{UA_2}{\dot{M}\, c_p}} - 1)} \tag{3.24}$$

The mass of the vessel liquid is calculated by:

$$M_T = \rho\, .V = \rho\, \pi \frac{D^2}{4}\, D \tag{3.25}$$

Where ρ is the density of the fluid inside the vessel and D is the diameter of the vessel. For the larger vessel ($D_2 = 2D$), the liquid mass is:

$$M_{T2} = \rho\, .V_2 = \rho\, \pi \frac{(2D)^2}{4}\, 2D \tag{3.26}$$

Substituting equations 3.25 and 3.26 into equations 3.23 and 3.24 respectively yields:

$$\tau = \frac{\rho\, \pi \frac{D^2}{4}\, D\, c_p^T\, e^{\frac{UA}{\dot{M}\, c_p}}}{\dot{M}\, c_p(e^{\frac{UA}{\dot{M}\, c_p}} - 1)} \tag{3.27}$$

$$\tau_2 = \frac{\rho\, \pi \frac{(2D)^2}{4}\, 2D\, c_p^T\, e^{\frac{UA_2}{\dot{M}\, c_p}}}{\dot{M}\, c_p(e^{\frac{UA_2}{\dot{M}\, c_p}} - 1)} \tag{3.28}$$

Thus, the ratio of τ_2 to τ gives:

$$\frac{\tau_2}{\tau} = \frac{\dfrac{\rho\, \pi \frac{(2D)^2}{4}\, 2D\, c_p^T\, e^{\frac{UA_2}{\dot{M}\, c_p}}}{\dot{M}\, c_p(e^{\frac{UA_2}{\dot{M}\, c_p}} - 1)}}{\dfrac{\rho\, \pi \frac{D^2}{4}\, D\, c_p^T\, e^{\frac{UA}{\dot{M}\, c_p}}}{\dot{M}\, c_p(e^{\frac{UA}{\dot{M}\, c_p}} - 1)}} = 8 \qquad ; \quad e^{\frac{UA}{\dot{M}\, c_p}} \gg 1 \tag{3.29}$$

It can clearly be seen in equation (3.29) that the time constant increases by a factor of 8 as a result of doubling the vessel diameter. This means that for the same operating conditions (heat transfer fluid and temperature difference between the vessel and the

heat transfer fluid); the heat transfer dynamics will be slower resulted in a delayed response. Therefore, the process which is temperature limited will take much longer time if the scale size goes up. Thus, the effect of increasing time on stability of the product should be taken into account. In addition to the response time for external heating and cooling systems, the temperature differences across the wall of the vessel would be important. Consequently, a good understanding of heat transfer is important for the success of the scale up process.

3.4 Switching Technique

Industrial temperature control is nowadays accomplished by using external electric heater and heat exchanger taking utility fluid from a loop. Figure 3.12 shows a typical type of scheme of the temperature control unit. As can be seen, the process fluid will flow through either an electrical heater (supplying heat) or heat exchanger (supplying cold) thereby regulating the fluid temperature. The response times for the external exchangers should ideally be faster than the response time of the process but this depends on flow rates, areas, fouling and the utility systems used.

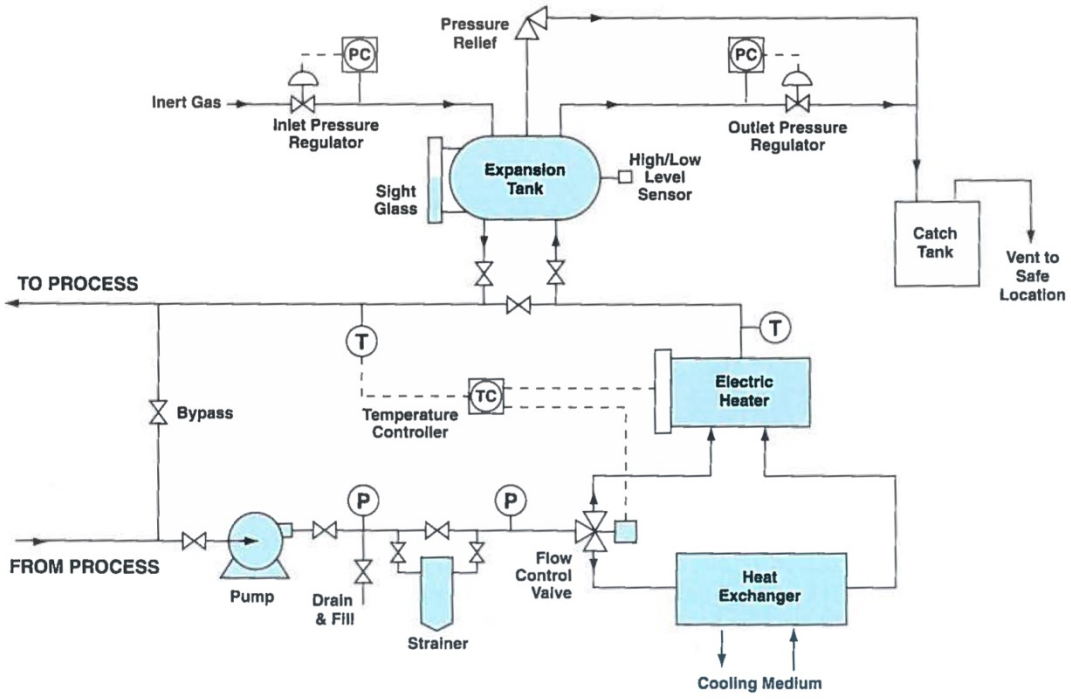

Figure 3.12: Schematic of a typical temperature control unit (TCU) (McConville, 2002).

In the work carried out in this PhD thesis, a switching system supplying hot and cold water to the vessel jacket was developed. This system is more close to the setup

industry uses and different from the traditional cooling system employed at the laboratory scale. From the analysis in section 3.3, the time constants for heating and cooling using a single water bath were shown to be the same. Therefore, using two baths with the same characteristics would also produce the same time constants. Time constants for water baths have been shown to be minutes, yet from literature, nucleation can take place in seconds and therefore there is no possibility of controlling nucleation using a traditional single water bath. However, using two baths, with one bath set to a different temperature than the other would mean that fluid of different temperatures could be supplied to the jacket and the resulting wall temperature can be quickly changed. This change in temperature may affect the nucleation and possibly the growth rate of crystals in ways that are not achievable by a single water bath using linear or non-linear cooling profiles.

Therefore, this section of the thesis introduces a novel switching technique that will be used in the following chapters to change the temperature inside the crystalliser in order to control the crystallisation of two different chemicals. Switching between hot and cold sources and holding the crystalliser at the cold temperature is recognised technique to investigate induction time. This technique is based on changing the water flow through the vessel jacket between hot and cold water baths using solenoid valves. Based on this approach, the work covered in this thesis uses two water baths and six solenoid values to rapidly change the jacket between one temperature and another.

Figure 3.13 shows schematic illustration of the experimental setup. This system was first described in section 3.2. However, another water bath (Grant (GP200-R2)) and six solenoid valves were added to the setup. The purpose of the valves is to change the water flow through the jacket between the two baths. The solenoid valves are shut-off valves that have one inlet port and one outlet port. In the de-energised condition, they are closed. However, they can be activated by a digital control signal comes from MCC USB-1208LS interface box. The heating and cooling sources were Haake (F6-C40) and Grant (GP200-R2) water baths. A MATLAB programme was written specifically to change the flow through the jacket at a designated frequency, see Appendix C.

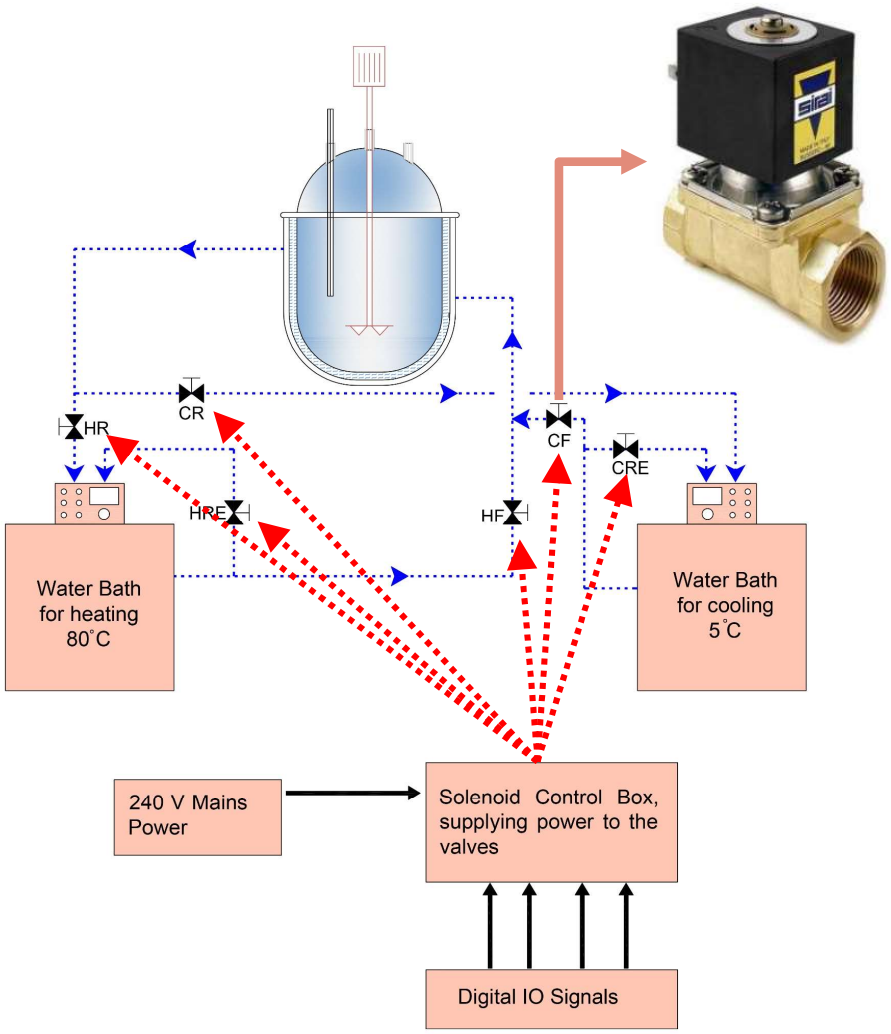

Figure 3.13: Schematic illustration of the experimental set-up of the switching technique.

The switching experimental procedure was as follows:

1. Filling the vessel with 2 L water and heating it up to 70 ºC using Grant (GP200-R2) water bath. At the same time, the Haake water bath, which is the cold source, was kept at 15 ºC.
2. Switching the water flow through the vessel jacket between hot water bath (Grant at 70 ºC) and cold water bath (Haake at 15 ºC) using solenoid valves at different frequencies of Grant: Haake, which are 1:1, 1:3 and 1:8. The vessel, Haake and Grant temperatures were recorded every minute. A Pico Technology TC-08 USB Data Logger fitted with thermocouple type K was used to record the Grant temperature.

The vessel, Haake and Grant temperature profiles as a result of applying a switching frequency of Hot:Cold→1:3 are shown in Figure 3.14.

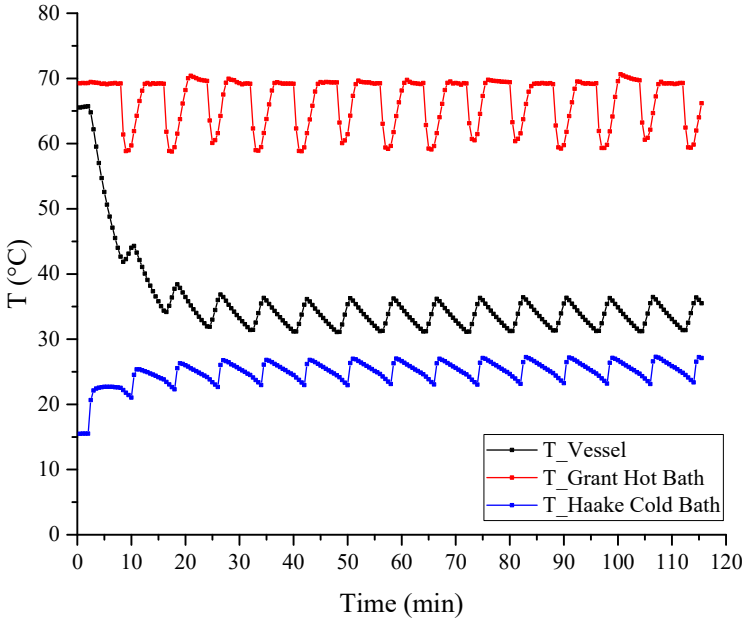

Figure 3.14: The temperature profile of vessel and Haake and Grant water baths as a result of applying switching frequency of Hot: Cold→1:3.

As shown in Figure 3.14, the vessel temperature dropped rapidly at the beginning when switching to the cold source happened due to the big difference between the vessel and the cold bath temperature. The vessel temperature then fluctuates between 31 and 36 ºC due to the switching effect between cold and hot baths respectively.

To see if the vessel temperature profile as a result of applying switching frequency of Hot: Cold→1:3 can also be predicted using the mathematical model described in equation (3.16), the fourth order Runge-Kutta method was used to solve equation (3.16) in MATLAB for an estimated value of overall heat transfer coefficient (U=250 $W.m^{-2}$ K^{-1}). The experimental and model results are plotted in Figure 3.15.

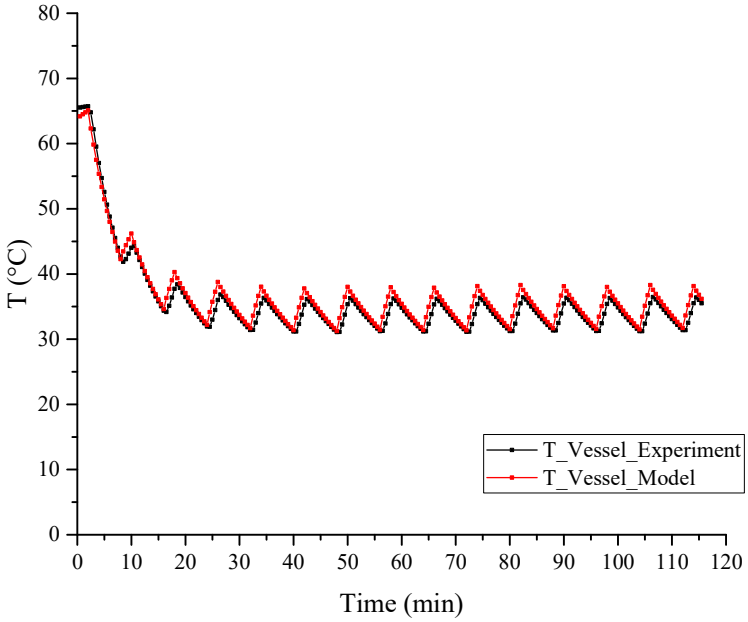

Figure 3.15: A comparison between the experimental data and the model results of the vessel temperature for switching frequency of Hot: Cold→1:3.

As can be seen in Figure 3.15, the model results matched well the experimental data. The optimised value of U was 90 $W.m^{-2}$ K^{-1} in the case of using one water bath and 250 $W.m^{-2}$ K^{-1} in the case of switching (two water baths are used). This would suggest that the resistance to heat transfer is related more to the jacket fluid itself than the internal vessel. As can be noted, less heat resistance is seen by using two water bath compared to the one bath. This adds an advantage to the developed switching technique over the traditional heating/ cooling methods.

The effect of applying different switching frequencies on the vessel temperature is presented in Figure 3.16.

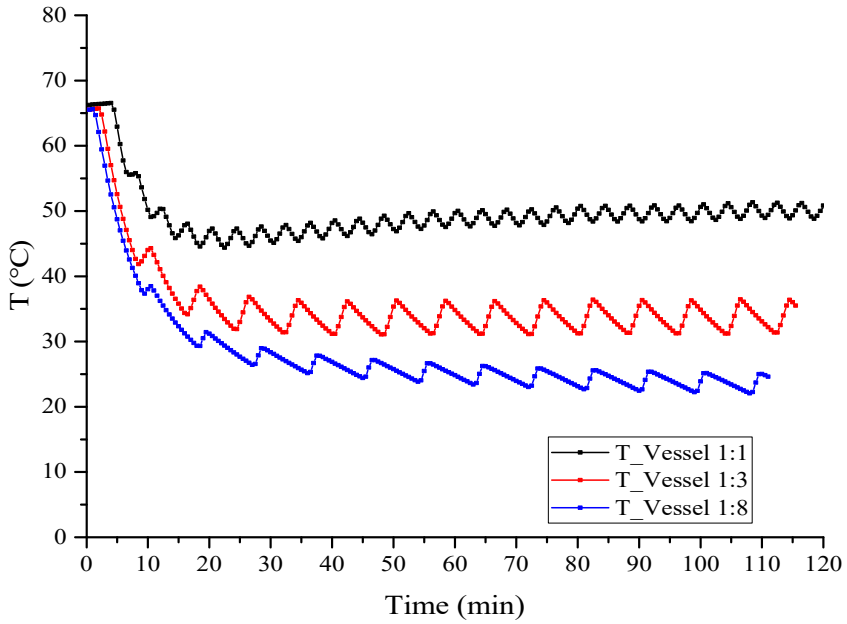

Figure 3.16: The effect of switching frequency on the vessel's temperature.

It can clearly be noted in Figure 3.16 that the switching frequency has a big effect on the average vessel temperature during the switching stage. The lower the frequency (i.e. the longer the cold bath is on compared to the hot one) the lower the vessel temperature achieved. This is, in turn, of great importance on the cooling crystallisation process of glycine as will be seen in chapter 4.

The reason behind choosing Haake and Grant as cold source and hot source respectively is that Haake has higher cooling capacity (700W) compared to Grant capacity (250W) (Artisan, 2000; Grant, 2010) and therefore it was thought that it was better to have higher cooling power as possible. This can also clearly seen in Figure 3.17 where two identical experiments were carried out as explained above. The only difference was that the water bath set up was swapped; the hot bath was now the cold bath and vice versa.

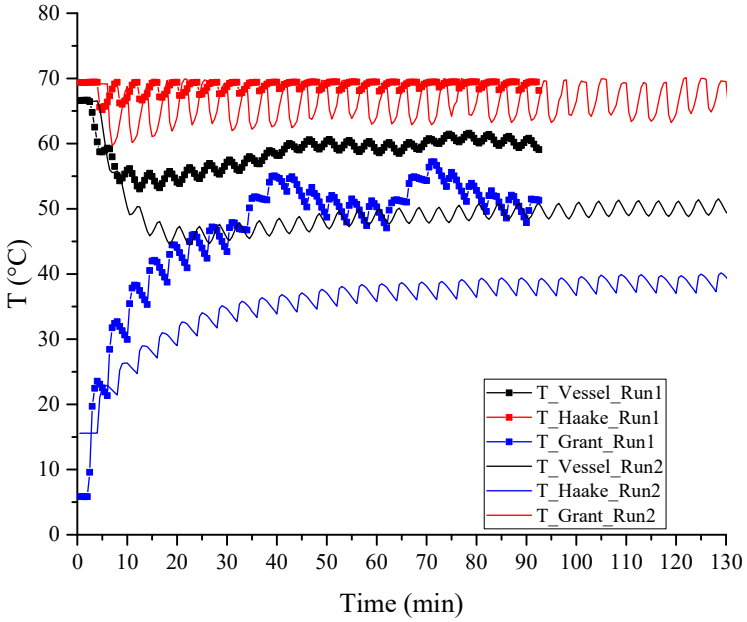

Figure 3.17: A comparison of the vessel, Haake and Grant water baths temperatures as a result of swapping between the two water baths for switching frequency of 1:1.

As seen in Figure 3.17, having Grant bath as a cold source (run1) led to a higher average vessel temperature than that in the case of Haake bath as a cold source (run 2). This is expected because the Haake bath has higher cooling capacity than Grant bath as mentioned above.

3.5 Conclusion

In the light of above discussions, it can be concluded that the agitated vessel used in this work is good for heating and cooling cycle with regard to the heat transfer efficiency. In addition, the scale up influence on heat transfer in terms of time constant was investigated. A simple heat transfer model of agitated vessel was also developed and showed its ability to predict the vessel temperature in the case of programmed heating/cooling rates, crash heating/cooling or switching between hot and cold baths. The evaluation of the different heat transfer resistances was also considered by using Wilson method. The switching technique and how its frequency affects the vessel temperature were also studied. However, the impact of this technique on the cooling crystallisation of glycine and its role to improve the crystals' size of glycine and LGA will be investigated in chapters 4 and 5 respectively.

Chapter 4

Optical Monitoring of Cooling Crystallisation Process and the Effect of Switching Technique on the Characterisation of Glycine/Water System

This chapter demonstrates the potential of using online video imaging technique for monitoring the cooling crystallisation behaviour. Crystallisation behaviour can be affected by various factors; for example, cooling rate, impeller material and stirring speed. This, in turn, affects the properties of the final crystals that are of great importance for the downstream processes as mentioned before.

This chapter will describe in detail the materials, experimental set-up and procedures used in this work. The focus will be on the feasibility of the developed online video imaging system with a flood light source to measure the meta-stable zone width (MSZW) of L-glutamic acid at different operating conditions in a batch crystalliser using two impellers of different material type; Perspex and stainless steel, and estimate both the nucleation kinetic parameters and the overall solute mass transfer rates. The MSZW of glycine will also be measured at different cooling rates and the nucleation mechanism and kinetics will be assessed using the polythermal methodology. Added to that, the crash cooling data for glycine will be analysed by means of the isothermal method to evaluate the nucleation parameters.

The novel switching technique supplying hot and cold water to the crystalliser's jacket and how the key variables of its frequency and duration can influence the cooling crystallisation of glycine will also be investigated in this chapter. Glycine was chosen because its solubility curve is a strong function of temperature, i.e. a small change in temperature can produce a rapid change in supersaturation.

In addition to the performance of trials, it was important to establish the temperatures set point for the two water baths in order to allow them to function as hot and cold sources. Furthermore, a comparison between the switching technique, crash cooling and constant linear cooling rate effects on the nucleation point of glycine is presented.

4.1 Introduction

Process Video Imaging (PVI) techniques include any tool that uses a video camera to observe a process. This tool has been applied in many fields such as crystallisation (Wilkinson et al., 2000) and droplet size distributions in liquid-liquid dispersions (O'Rourke and MacLoughlin, 2005). A typical PVI system consists of a camera connected to a PC with software to grab and save images for either online or offline processing. In addition, this system requires a source of illumination that can be a directed light, LED or focused laser which is particularly useful in the case of monitoring micron scale particles.

In crystallisation, the use of video imaging technique has been reported in the literature; for example, (Wilkinson et al., 2000; Wilkinson et al., 2003) who developed an approach for online crystals length measurements using video imaging. (Wang et al., 2005) monitored and detected the crystallisation onset of 33.3g L-glutamic acid in 500 ml distilled water at different cooling rates. The crystallisation point was detected by image analysis at either earlier or at the same time as would be detected by turbidity probe. They also calculated the crystal growth rates and the polymorphic transformation of L-glutamic acid in water. The possibility of using PVI to determine the crystal size distribution (CSD) was shown by the work of (Caillet et al., 2007) who grabbed images of citric acid crystals in water using CCD camera probe in order to determine the CSD. Yet, this tool had drawbacks with respect to the crystals size and concentration. The size needed to be more than 15μm to be detectable and the concentration kept lower than 10wt% to avoid crystal overlap. Later on, (Eggers et al., 2008) suggested a method to determine the size distribution depending on the axial length distribution. This method showed a high agreement with the results obtained from the traditional methods of CSD determination. This method was further developed by (Kempkes et al., 2010) using two cameras at different angles and 3D CSD and shape information were obtained.

(Simon et al., 2010) utilised a bulk video imaging method to define the MZSW in food and pharmaceutical processes and proved that this technique can compete well other process analytical techniques (PAT): for instance focused beam reflectance measurement (FBRM) and ultra-violet visible spectroscopy (UV-VIS). More recently, (Brown, 2012) also demonstrated the feasibility of applying a PVI system to measure the MSZW of different paracetamol (PA) solutions in a 200 mL oscillatory baffled crystalliser (OBC) as well as measuring the crystal's growth rate and mean size.

In his work, (Brown, 2012) defined so-called the intensity distribution integral term (IDI), which is a function of the white percentage in any grey scale image. Therefore, for the PVI system, 0% represents clear solution with no crystals (black image) and 100% represents the opaque (totally white) one. Figure 4.1 depicts the MSZW determination using PVI system developed by (Brown, 2012).

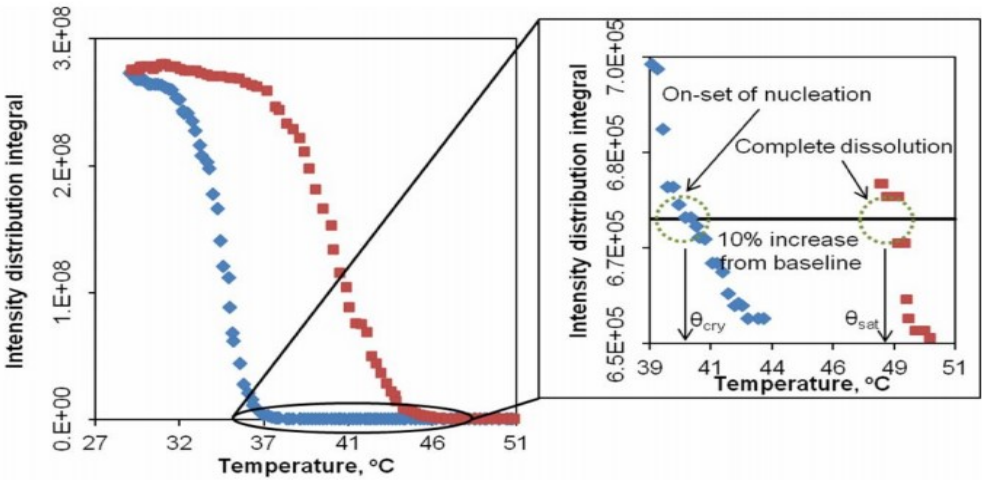

Figure 4.1: Metastable zone width curve showing crystallisation (blue) and dissolution (red) (Brown, 2012).

The onset of nucleation temperature (T_{cry}) was observed when the IDI value of the solution rose above a predefined value (assumed to be 10% above the value for clear solution (0%)). Similarly the dissolution temperature (T_{dis}) was defined when the IDI value drops below the predefined value. Similar procedures were used in turbidity probe measurements (Groen, 2001b; Liang, 2002; BORISSOVA et al., 2009) for the MSZW of L-glutamic acid. However, the % transmittance reading recorded by turbidity probe and the IDI value have opposite relationship with the crystal concentration (the IDI value increases with crystal concentration while the % transmittance reading decreases with crystal concentration).

Supersaturation is the essential driving force of all crystallisation processes which can be achieved through different methods. One of these methods is cooling which is used in this work where temperature reduction leads to decrease in solution solubility and hence transfer of solute from liquid to solid phase. Since the faster the cooling rate, the greater the rate of supersaturation generated, this in turn will affect the nucleation point.

This chapter will therefore describe a "switching" technique where the temperature inside the jacket of a batch crystalliser can be changed quickly so as to rapidly drive the temperature inside the batch crystalliser. The emphasis here will be placed on

investigating the effect of switching technique frequency and duration on the nucleation point of glycine, the impact of the hot and cold sources temperatures set point as well as comparing the switching results with those of the traditional cooling profiles; crash and linear ones. The aim of this comparison is to highlight any effect on the crystallisation characteristics of glycine (in particular the nucleation point) coming from changing the crystalliser's temperature by switching mechanism using two baths (hot and cold) instead of the conventional methods that use one cold bath.

4.2 Materials

To investigate if the switching method would have impact on the crystallisation behaviour, a suitable set of materials was needed that exhibit different features:

1. That the solubility curves are of different slopes. A material with a strong relationship between solubility and temperature and another with a weak relation and thus they would respond differently to low and high cooling rates.
2. Materials which were soluble in water to a similar degree so as not to change the properties (e.g. viscosity and density) of the solution.
3. That had been studied before by conventional means.

After searching the literature, the two selected materials were L-glutamic acid and glycine. L-glutamic acid was chosen because of, firstly, the availability of data in the literature which helped validate the results obtained in this work using the developed PVI system and, secondly, its low solubility in water compared with the second material used; glycine which exhibits high rate of change of solubility with temperature.

4.2.1 L-glutamic Acid

L-glutamic acid (Chemical formula $C_5H_9NO_4$, Molar Mass 147.13 g/mol) is a small amino acid which was firstly found in wheat gluten in 1866 by German chemist Karl Ritthausen. It has one basic amine group and two carboxylic acid groups as shown in Figure 4.2.

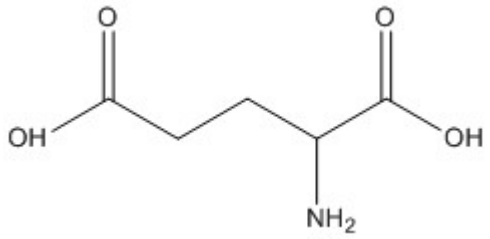

Figure 4.2: Molecular structure of L-glutamic Acid.

L-glutamic acid is formed in the human body during carbohydrate metabolism and has a role in neurotransmission (Patchigolla, 2007). In addition, it is widely used in both pharmaceutical industries as an anti-ulcer drug and food processes as a food enhancer (Hermann, 2003). Molecules of L-glutamic acid in the crystal lattice as well as in acidic solution (pH is between 2.2 and 4.3 as the case in this work) are in a zwitterionic form. Changing the solution pH allows the L-glutamic acid molecules to exist in four different isoelectric forms; -2, -1, 0, +1 (Borissova et al., 2005).

L-glutamic Acid can crystallise into two polymorphic forms; the rhombic meta-stable form (α) and the needle-like stable form (β). These forms are of different solubility, robustness, density and molecular arrangement. The operating conditions in crystallisers play a main role in determination the type of polymorph produced (Cashell et al., 2004; Kitamura, 2002b). Figure 4.3 shows the two distinct polymorphic forms of L-glutamic Acid.

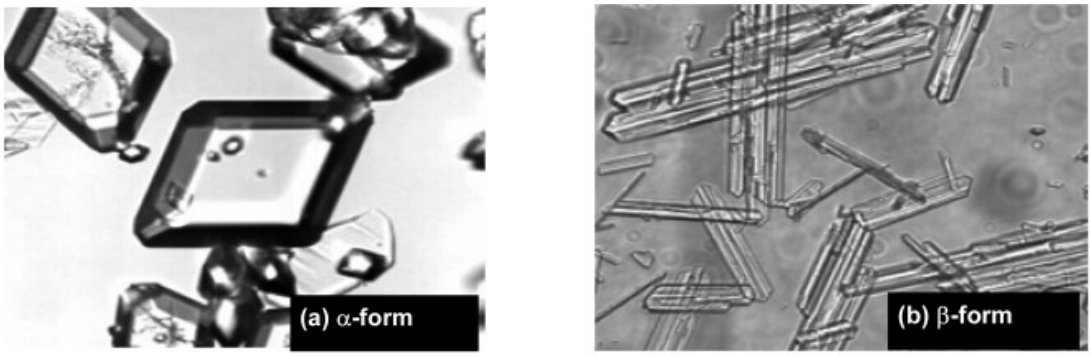

Figure 4.3: Polymorphic forms of L-glutamic Acid: On the left α L-glutamic Acid: On the right β L-glutamic Acid (Borissova et al., 2008).

In industry, however, the α-form is preferred due to its robustness if it is compared to β-form that can break during the downstream processes (Ferrari and Davey, 2004).

4.2.2 Glycine

Glycine (Chemical formula $C_2H_5NO_2$, Molar Mass 75.07 g/ mol) is the simplest amino acid that exists in all life forms on Earth and is widely used in food, pharmaceutical, fertiliser and rubber industries. It has one basic amine group and one carboxylic acid group as depicted in Figure 4.4.

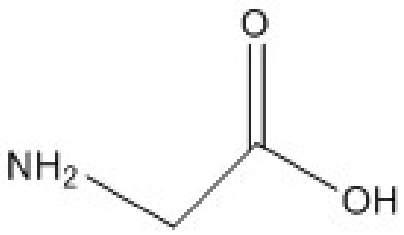

Figure 4.4: Molecular structure of Glycine.

Molecules of glycine in aqueous solutions are in a zwitterionic form, however, it can crystallise in five polymorphic forms α, β, γ, ε and δ where the intermolecular hydrogen bonds dominate the crystalline form. The ε and δ-glycine can only be formed at high pressure (Dowling, 2012). The transitions among the other three polymorphic form of glycine are illustrated in Figure 4.5 (Srinivasan, 2008).

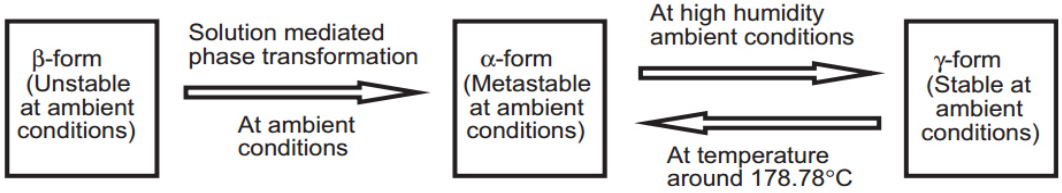

Figure 4.5: Polymorphic phase transformations of glycine as observed in (Srinivasan, 2008).

Figure 4.6 presents α and γ polymorphic forms of glycine crystals. The α-form crystals, which are transparent and prism-like, are grown from aqueous solutions by slow cooling crystallisation. At ambient conditions, they have a tendency to transit, due to their metastability, to γ-form that is trigonal and white in colour. But, if they are of large size, they maintain their form without any transformation for several months (Srinivasan, 2008).

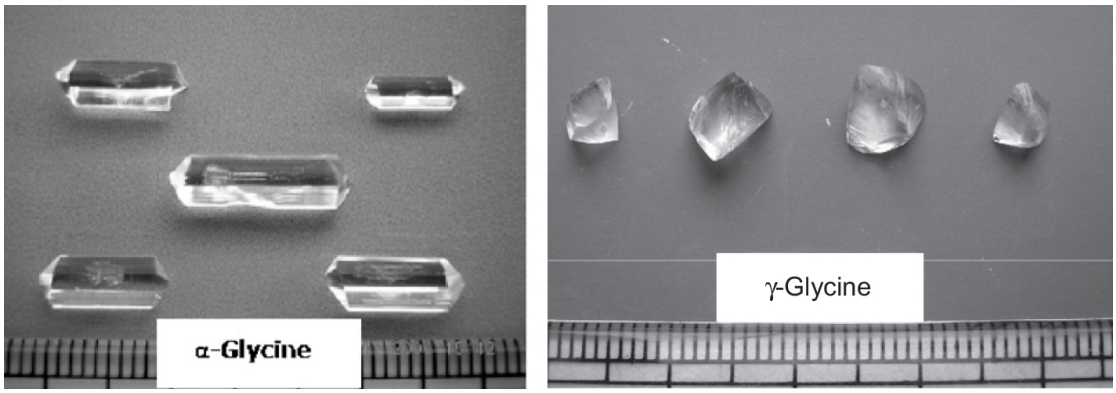

Figure 4.6: (left) α-glycine crystals grown from solution with 5 g of NaCl concentration in 100 ml of DD water. (Right) Grown γ-glycine single crystals from solution with 8 g of NaCl concentration in 100 ml of DD water by slow evaporation method (Srinivasan, 2008).

As mentioned earlier, the two materials selected for this study are glycine and LGA, because they have different solubility; glycine has higher solubility in water than LGA. This can be clearly seen in Figure 4.7 which illustrates the solubility data of LGA and glycine in water at different temperatures. The slope of solubility curves for glycine and LGA were found to be 0.6 wt.%/°C and 0.07 wt.%/°C, respectively.

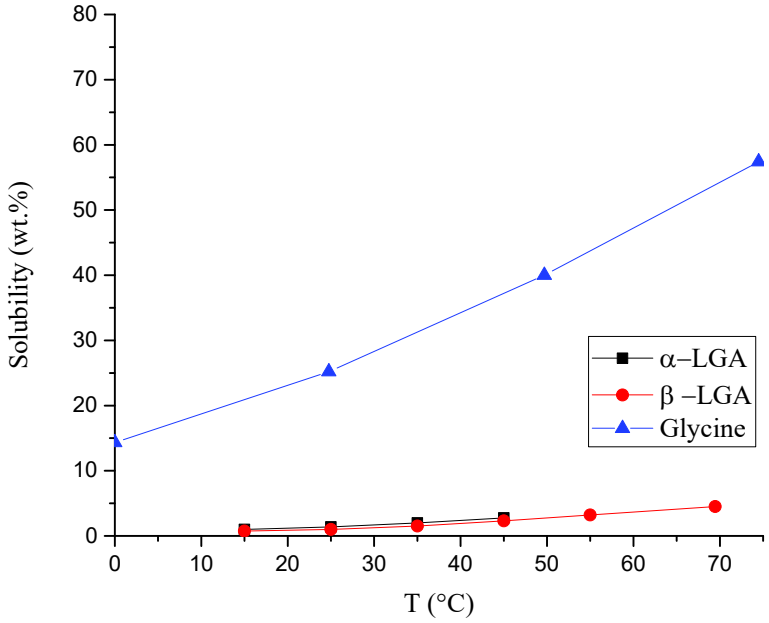

Figure 4.7: Solubility wt.% of (α - LGA, ß - LGA, and glycine) in water as a function of temperature. Data has been derived from (Mullin, 2001; Liang, 2002).

4.3 Experimental Set-up

Batch cooling crystallisation experiments were carried out using the same experimental set-up explained in detail in chapter 3 (section 3.2). The retreat curve impeller (RCI) was chosen because of its ability to offer a gentle mixing, good heat transfer and represent impellers that can be found in larger scale crystallisers. There was also a reference list of literature documenting the mixing characteristics from a RCI. Conventional Rushton turbine and pitched blade turbine have been used for L-glutamic acid crystallisation experiments before (Liang, 2002), however these impellers represent more laboratory scale impellers rather than those used in industry. Two RCI of different materials, Perspex and stainless steel, were used for the investigation of impeller material effect in the current work. Liang (2002) had shown that impellers of different materials would affect the crystallisation of L-glutamic acid. Experimental results obtained under this thesis work would therefore be directly comparable to the work by Liang.

The vessel was placed inside a rectangular tank which has walls of black colour to reduce light refraction in order to improve the quality of the image captured. Placing the cylindrical jacketed vessel within the rectangular tank reduced the issues with refraction for the optical system. Heating-cooling cycles for the crystallisation experiments were carried out using a MATLAB programme running on PC connected via RS232 port to the water bath (Haake-F6-C40).

The crystals images were captured using a DFK 23G274 GigE colour industrial camera from "The Imaging Source Europe GmbH" along with its IC Capture 2.2 software. The camera has a resolution of 1600x1200, a maximum frame rate of 20 images per second and a field of view (24x18 mm) for the camera positioning and lenses calibration employed. The camera was placed outside the rectangular tank wall 17 cm away from the centre of the vessel perpendicular to a 50W LED light used to provide illumination as required. This light was positioned 34cm from the vessel centre. A picture of the experimental set-up for the crystallisation experiments using the optical system is shown in Figure 4.8.

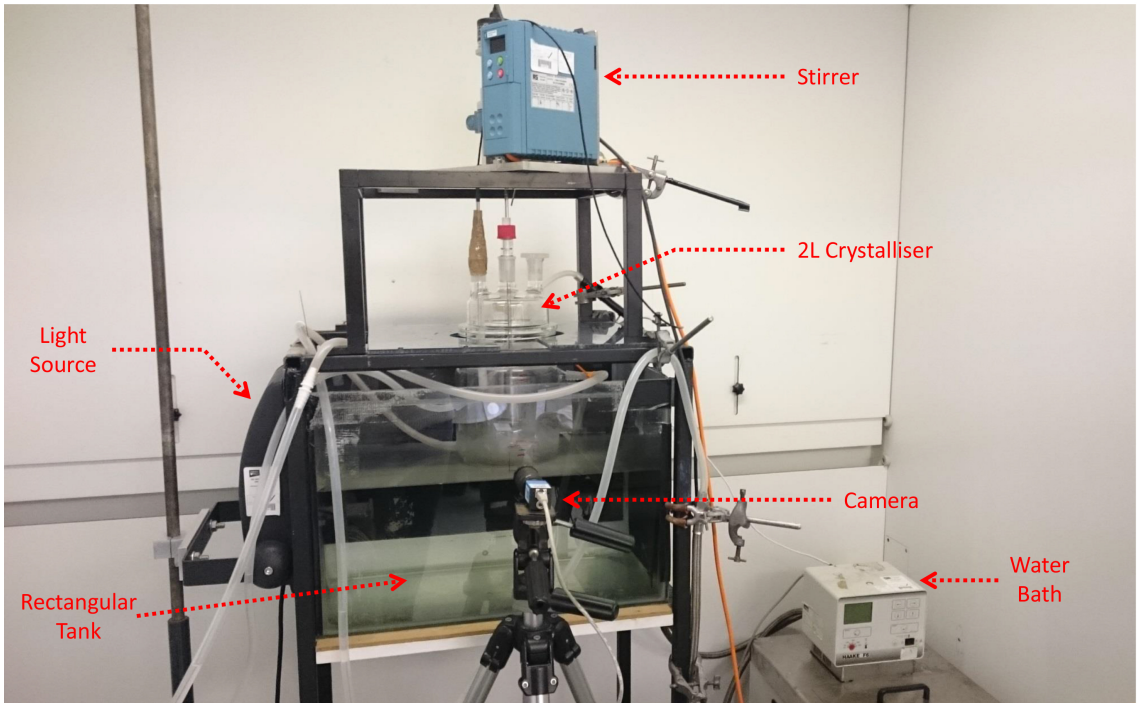

Figure 4.8: Picture of the laboratory unit.

4.4 Experimental Procedure

Prior to start each experiment, the vessel, the impeller, the baffle and the thermometer were washed properly with water to remove any particles left from previous runs. A solution of 80g of L-glutamic acid (Sigma-Aldrich Company Ltd. Specification,

98.5+%, FCC) dissolved in 2 L of distilled water (saturated at 64˚C) was prepared for each experiment at room temperature. A high resolution semi micro analytical balance (AND HR-202i) was utilised to weigh the LGA powder.

For the experiments of the MSZW measurement, freshly prepared L-glutamic acid solution (4wt%) was heated up from room temperature to 80˚C (about 15˚C above saturation temperature) at a constant rate, and then the temperature was held at 80˚C for 70 minutes to ensure that all the crystals dissolved. The solution was then cooled to 20˚C at the same rate as the heating stage. The heating and cooling cycles were carried out using a MATLAB program written specifically to change the water bath temperature according to the rate required, to record vessel and water bath temperatures, to take images and process them (see section 4.6 for more details).

The focusing area of the camera that was set proved to be important. Viewing the entire vessel proved difficult due to reflections from the rotating impeller and external sources. After some trial and error experiments, the most appropriate position to view the solution was to focus on the area located to the left hand portion of the vessel between the impeller and the vessel sidewall to avoid any reflection. This position also corresponded to the area below the impeller which accumulated crystals quickly once the nucleation had taken place. Both the images and the vessel temperature were recorded every 30 seconds during the heating and cooling cycles and saved to external hard drive. To validate the method and the procedure, each experiment was repeated twice to check the repeatability.

4.5 Image Analysis

The recorded images for each run were analysed using the developed MATLAB programme that calculates the white pixels percentage value in each image in order to determine the dissolution and crystallisation temperatures. Due to the camera resolution, each image consisted of 1600 columns and 1200 rows of pixels. The captured images were of RGB format which were converted into grey scale, where each pixel given an intensity value between 0 (black representing the clear solution) and 255(white representing the crystals).

Figure 4.9 shows a typical graph of white pixel percentage as a function of temperature for the heating/cooling cycle. Before starting the heating stage, the image was totally white due to the presence of undissolved crystals. During the heating stage, the crystals started to dissolve and the percentage of the white pixels decreased until the recorded image became mostly black. In most experiments, some white pixels were seen which were due to air bubbles trapped in the fluid within the jacket. For the reverse process of heating, the starting image was black as there were no crystals present. As the cooling process continued forward, the crystals began to nucleate and grow, and the white pixels percentage increased until the image became totally white when the recording was stopped. Due to the area viewed by the camera, this procedure could not observe the entire vessel and therefore the camera system here matches those experiments which use point type immersion probes (turbidity, FBRM, ATIR, etc.) that only look at a small volume of the crystalliser.

In a similar procedure to experiments using turbidity, the dissolution temperature (T_{dis}) in this work was determined from the camera images when the white pixels percentage dropped by 20% from the one for cloudy solution (100%). Whereas, the crystallisation temperature (T_{cry}) was defined when the white pixels percentage rose by 20% from the value for clear solution (0%). However, the value for the clear solution was found to vary above zero due to the presence of air bubbles which formed when the jacket fluid was heated up. Using a base image when the solution was clear, the impact of the bubbles was removed and hence this effect was not taken into consideration when T_{cry} was determined. Therefore, the MSZW (ΔT_{max}) can be calculated for specific experimental conditions via equation (4.1):

$$\Delta T_{max} = T_{sat} - T_{cry} \quad \textbf{(4.1)}$$

Where T_{sat} is the saturation temperature of the solution and T_{cry} is the crystallisation temperature of the solution.

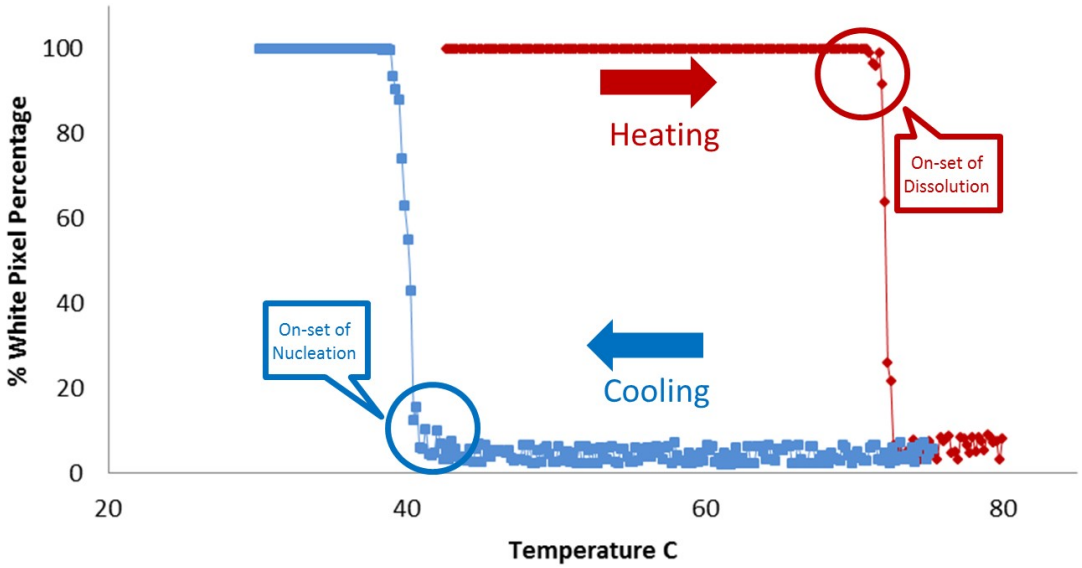

Figure 4.9: White pixel percentage as a function of temperature for LGA crystallisation run using stainless steel impeller @ (0.2 ˚C /min, 200 rpm).

A number of repeated conditions were done and the measured crystallisation temperature was found to vary from batch to batch by a maximum of ± 1˚C. Thus, each run was repeated twice and the average was considered as the measured crystallisation temperature. Figure 4.10 shows some images captured by the optical technique during the cooling stage of the crystallisation process at different times. At the beginning, the solution was clear (the image was black) (4.10a). As time progresses, the crystals started to form and grow (4.10b). At the end of the run, the image became totally white (4.10c).

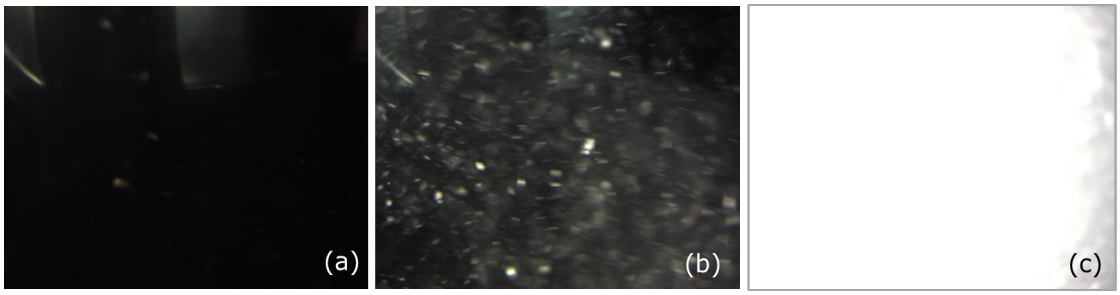

Figure 4.10: Captured images showing baseline (a), start of crystallisation (b) and end of crystallisation (c).

In image 4.10c, the right hand side of the image is not completely white due to the direction of the light source which illuminates the left hand portion of the image. The high concentration of crystals formed reflects the light causing a darker section to appear on the far right.

It is worth noting that for the camera positioning and lenses calibration employed, the smallest detectable crystal (*SDC*) size was calculated to be 15µm:

$$SDC = \frac{Image\ Width}{Horizontal\ Resolution} = \frac{24.1\ mm}{1600\ pixel} = 15\ \mu m$$

The image scale was determined by grabbing images for a probe of known diameter using the same camera positioning and lenses calibration applied in the experiments. Table 4.1 shows how the smallest detectable crystal (SDC) size can be affected by the camera resolution and position.

Table 4.1: Camera position and resolution effects on smallest detectable crystal (µm) (Brown, 2012).

Smallest detectable crystal (µm)				
Captured area width (mm)	Horizontal resolution (px)			
	736	1024	1392	1600
10	14	10	7	6
20	27	20	14	13
32	43	31	23	20
40	54	39	29	25
50	68	49	36	31

Therefore, for the camera positioning and lenses calibration employed in this work, the crystal size should be at least 15 µm to be detected resulting in post nucleation determination.

However, with higher camera resolution and smaller capture area, the nucleation point and much smaller crstal size can be dectected more accurately due to the decrease in the smallest dectectable size which is the size of 1 pixel. In addition, this improvement in camera specfication allows a clearer imaging of the individuel crystal which helps determine the crystal's shape. Table 4.2 shows the resolution and pixel size of the current cameras avaialable at (TheImagingSource, 2016).

Table 4.2: New cameras' specifications from (TheImagingSource, 2016).

Model	Resolution	Pixel Size [μm]
DFK 27A(B)UP031	2592 x 1944	2.2
DFK 27A(B)UJ003	3856 x 2764	1.67
DFM 73AUC04-ML	2592 x 1944	1.4

4.6 The Developed MATLAB Code for Heating/Cooling Cycle Control and Image Processing

For the experiments of MSZW measurement, a MATLAB programme was developed to change the water bath temperature at a designated rate and simultaneously record the water bath and vessel temperatures as well as take and process images at intervals of 30 seconds. The communication between a PC running MATLAB and the Haake water bath was achieved through the built-in RS232 port. The main code steps are shown in Figure 4.11 and described below:

1. Create and configure serial port object and connect it to the water bath in order to send command to and read data from.
2. Define the constants that include high temperature (T_H) and low temperature (T_L), holding time after heating stage (H_1) and heating/cooling rate (H/C Rate).
3. Go into a loop that heats the vessel from its starting temperature to T_H at the desired heating rate, and then hold the vessel at T_H for a set time to ensure all crystals were dissolved.
4. During the heating loop, record the current vessel and water bath temperatures as well as process the captured image at a specified interval and write their values to an excel file. The image processing algorithm included the conversion of the image from RGB format into grey scale, count the number of white pixels based on a threshold value and then calculate the white pixels percentage value W% (as a percentage of the total viewing screen size). Produce a plot of the vessel temperature and the W% as a function of time during the heating cycle.
5. Start the cooling process by setting the bath set point to a calculated value using the desired cooling rate.
6. Duplicate step 4 above when the vessel is cooled. Continue recording until the vessel reached temperature T_L, see Appendix A.

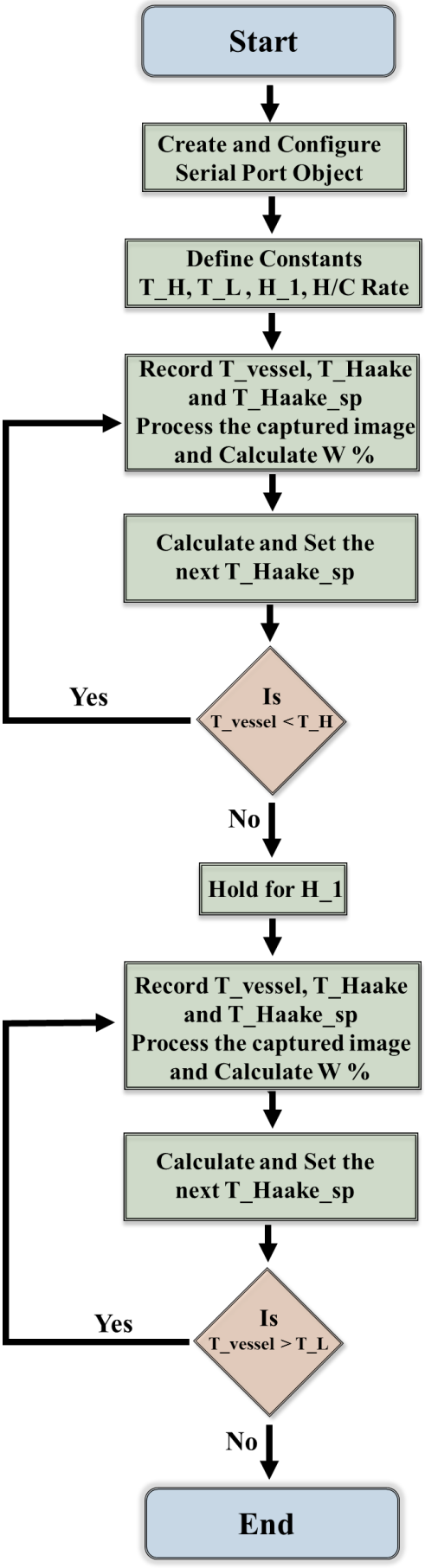

Figure 4.11: Flow-chart of the developed programme for heating/cooling cycle.

4.7 Results and Discussion for L-glutamic Acid Experiments

4.7.1 Comparing the Optical System with Turbidity for MSZW Measurements

To validate the feasibility of using the on-line video imaging system for monitoring crystallisation processes, the MSZW of 4.5wt% L-glutamic acid solution (saturated at 70˚C) in the 2L crystalliser was measured at heating/cooling rates: 0.2 and 0.3 ˚C/min using Perspex RCI at a constant stirring speed of 200 rpm. These operating conditions are the same as the ones used in previous studies using the turbidmetric fiber-optic probe (Liang, 2002) . The results are listed in Table 4.3.

Table 4.3: Comparison between MSZW measurement results using on-line video imaging system and previous work using turbidity probe.

Cooling Rate [˚C/min]	Stirrer Speed [rpm]	T_{cry} current work [˚C]	T_{cry} (Liang,2002) [˚C]	MSZW Current work [˚C]	MSZW (Liang,2002) [˚C]
0.2	200	48.9	44	21.1	26
0.3	200	39.1	32	30.9	38

As shown above, the MSZW measured in this work is narrower than that reported by (Liang,2002) for the same operating conditions. The video camera detects the presence of crystals at higher temperatures than reported by Liang which means the camera system was detecting crystals before the system used by Liang.

4.7.2 Impeller Material Effect

Liang reports that the MSZW and crystallisation temperature are affected by the type of material the impeller is made from. To test this, two experiments were done using impeller of different materials (Perspex and stainless steel) and the results are shown in Table 4.4.

Table 4.4: Results for MSZW measurement using on-line video imaging system in 2L vessel at cooling rate of 0.2C/min and stirrer speed of 200 rpm for both types of impellers.

Cooling Rate [˚C/min]	Stirrer Speed [rpm]	Stirrer Material	Crystallisation Temperature, T_{cry} [˚C]	MSZW T_{sat} - T_{cry} [˚C]
0.2	200	Perspex	40.6	23.4
0.2	200	Stainless Steel	42.5	21.5

These results are comparable with those of Liang where the stainless steel was found to nucleate the solution sooner. Liang suggested that the contact angle of a LGA sample may explain this.

4.7.2.1 Contact Angle Measurements

The contact angle of water droplets on different solid flat surfaces was measured using a USB digital microscope with 400X magnification (type: Veho-VMS-004) connected to a PC using MicroCapture-veho-vms004 software to save the captured images. The purpose of this measurement was to investigate the effect of the impeller material on the nucleation point based on the contact angle obtained. The water droplet was formed on various solid surfaces of different materials: stainless steel, Perspex, Aluminium, and glass slide using microsyringe (40µm). A pictorial representation of the experimental procedure is shown in Figure 4.12. To obtain reliable data, the measurement was repeated five times for each material.

Figure 4.12: Contact Angle measurement apparatus.

Figure 4.13 presents the contact angle measurement of water droplet on different flat solid surfaces.

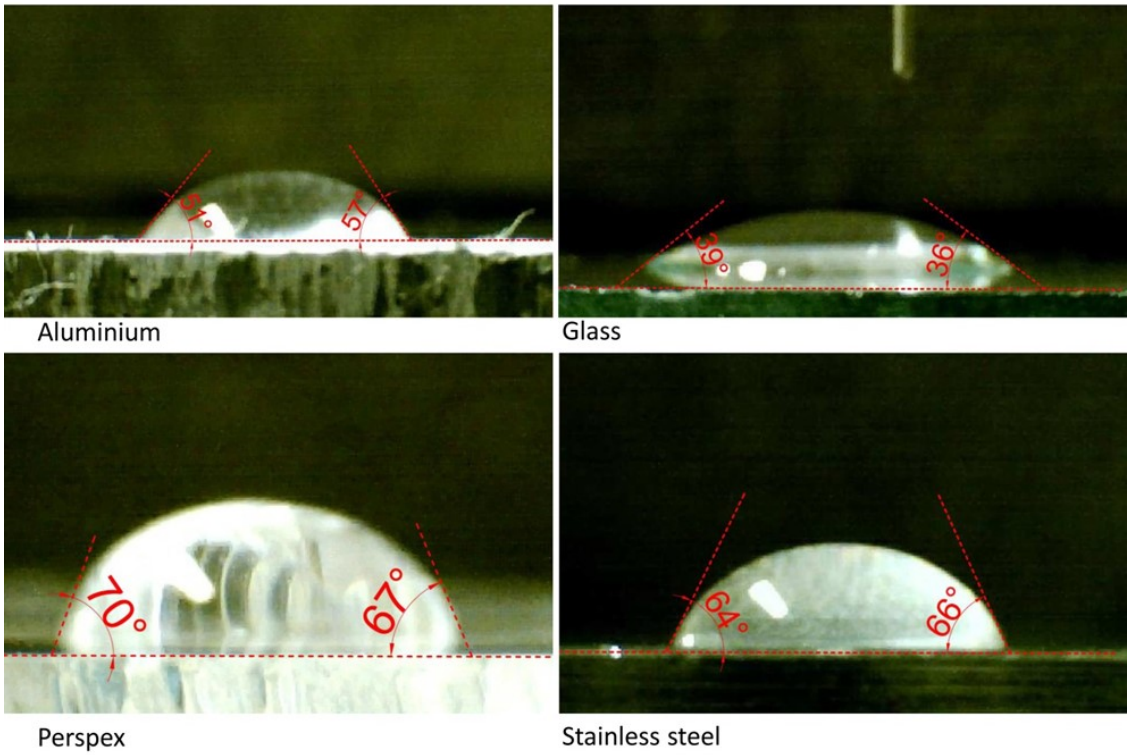

Figure 4.13: The contact angle of water droplet on various solid surfaces.

It can be observed in Figure 4.13, that the measured contact angle of water droplet on the Perspex surface is greater than that on the stainless steel one. In accordance with the nucleation theory, the ratio of free energy change of heterogeneous and homogenous nucleation ϕ is less than unity and can be calculated based on the contact angle value θ using equation (4.2) (Mullin, 1997).

$$\Phi = \frac{(2+\cos\theta)\ (1-\cos\theta)^{\,2}}{4} \qquad \textbf{(4.2)}$$

According to Figure 4.13 and equation (4.2), the free energy change needed to form a nucleus on stainless steel surface is less than that on a Perspex one, hence the stainless steel impeller would produce nuclei sooner than the polymer base. This is supported by the crystallisation temperature recorded in Table 4.4 with the crystal using stainless steel impeller appearing before crystals using Perspex impeller.

4.7.3 Metastable Zone Width Measurement

Observation the experiments presented in section 4.7.2 was challenging due to reflection from the light source hitting the impeller and the stainless steel shaft. In order to reduce this reflection, the impeller and the shaft were painted black. To investigate if

this had an impact on the crystallisation behaviour, a series of experiments to measure the MSZW of L-glutamic acid over a range of different operating conditions were conducted as follows:

1. The effect of the cooling rate where three different cooling rates: 0.2, 0.3 and 0.4˚C/min at constant stirrer speed of 200rpm were investigated.
2. The influence of stirring speed where four agitation speeds: 200, 250, 300 and 400 rpm at 0.2˚C/min cooling rate were applied.

Table 4.5 shows the MSZWs, determined using the on-line video imaging system according to equation (4.1) mentioned in section 4.5, of a 4 wt% L-glutamic acid solution in the 2 L crystalliser equipped with a retreat curve impeller and a single baffle at different cooling rates and stirring speeds.

Table 4.5: Results for MSZW measurement using on-line video imaging system in 2L vessel at various cooling rates and agitation speeds.

Cooling Rate [˚C/min]	Stirrer Speed [rpm]	Impeller Material	T_{dis} [˚C]	T_{cry} [˚C]	MSZW T_{sat}-T_{cry} [˚C]	S C/C* [-]
0.2	200	Painted Perspex	70.9	40.3	23.7	1.74
0.2	250	Painted Perspex	72.3	42.9	21.1	1.60
0.2	300	Painted Perspex	72.2	43.7	20.3	1.56
0.2	400	Painted Perspex	71.1	42	22	1.65
0.3	200	Painted Perspex	71.5	38	26	1.88
0.3	250	Painted Perspex	71.3	39.5	24.5	1.79
0.3	300	Painted Perspex	72.2	39.1	24.9	1.81
0.3	400	Painted Perspex	72.3	38.4	25.6	1.86
0.4	200	Painted Perspex	71.8	29.3	34.7	2.53
0.4	300	Painted Perspex	71.2	32.6	31.4	2.26
0.4	400	Painted Perspex	71.6	31	33	2.38
0.2	200	Painted SS	71.8	40.4	23.6	1.74
0.2	250	Painted SS	72.1	42	22	1.65
0.2	300	Painted SS	72.2	45.5	18.5	1.48
0.2	400	Painted SS	70.2	44.9	19.1	1.51
0.3	200	Painted SS	71.9	37	27	1.94
0.3	250	Painted SS	72.0	37.9	26.1	1.89
0.3	300	Painted SS	72.1	40.5	23.5	1.73
0.3	400	Painted SS	71.3	39.6	24.4	1.78
0.4	200	Painted SS	71.8	29.2	34.8	2.54
0.4	300	Painted SS	71.2	31.8	32.2	2.32
0.4	400	Painted SS	70.2	34.8	29.2	2.09

Alongside the material effect, surface roughness also plays a role in enhancing the nucleation due to the smaller contact angle formed on rough surface compared with smooth one (Liang, 2002).

The impellers in all runs listed in Table 4.5 were painted. It was observed that the surface of the painted stainless steel RCI was smoother than that of Perspex RCI in some areas. The surface roughness of the painted stainless steel and Perspex impellers was measured using a Taylor Hobson roughness measurement device. This device gives the arithmetic mean of the departures of the profile from the mean line (Ra) and this is an internationally recognised method of measuring roughness of metals. The measurements of roughness parameter (Ra) for both impellers are listed in Table 4.6.

Table 4.6: Values for roughness parameter Ra for Perspex and stainless steel RCIs.

Impeller Material	Ra on the tip of impeller [μm]	Ra between impeller tip and hub [μm]
Painted Perspex	0.45	4.2
Painted Stainless Steel	1	0.6

Table 4.6 shows that the surface roughness varies between the two impellers especially between the area on the impeller tips and the area between tip and hub. This may suggest that regions with high roughness may allow crystals to attach easier than regions which are smoother.

As shown in Table 4.5, the MSZW at the same operating conditions for both painted Perspex and painted stainless steel impellers are quite similar. For unpainted impellers the MSZW was 21.5˚C for stainless steel (at 0.2˚C/min and 200 rpm) and 23.4˚C for the Perspex (see Table 4.4). However, from Table 4.5 the MSZW was 23.6 ˚C and 23.7 ˚C for painted stainless steel and Perspex respectively. Therefore, it is considered that the painting affected the surface characteristics and then either impeller can be used for subsequent experiments. Nevertheless, it is seen in Table 4.5 that there are differences in the MSZWs for the two painted impellers at higher stirring speed. The different crystallisation behaviour must be related to the hydrodynamics produced by these two impellers.

Photographs of both impellers at the end of the crystallisation runs are presented in Figure 4.14 and show the formation of crystal deposits on the surface of impeller shaft and tips. This indicates that crystals form on the impeller at these regions and then these deposited crystals can break off allowing seed crystals to enter the solution. Thus, it is worth pointing out that the nucleation processes in all the experiments done in this work

are a surface-induced heterogeneous nucleation mechanism which is in line with findings of other researchers (Liang et al., 2004).

It is also seen that more crystals are attached to the surface which has a measured roughness higher than other areas, i.e. the edge, the joint, the top and bottom of the blades revealing again that the surface roughness can enhance the nucleation process.

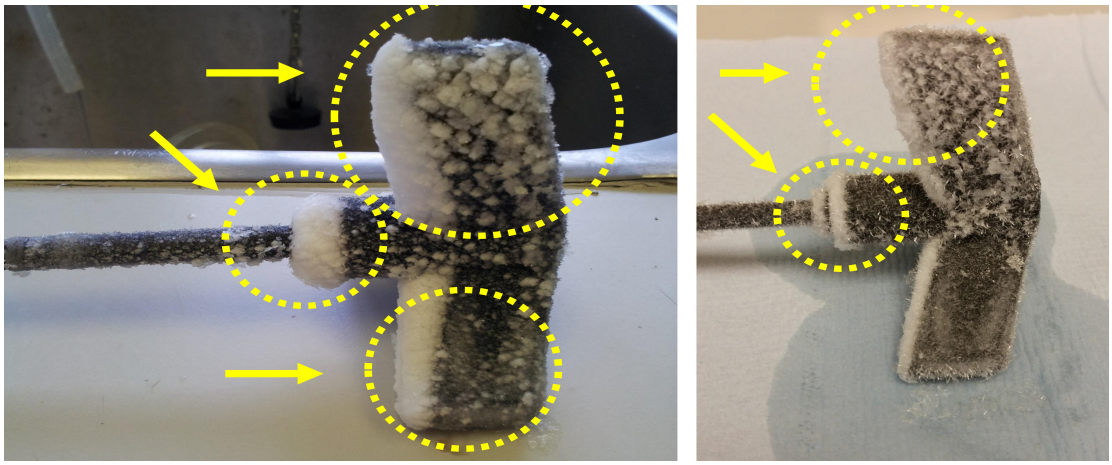

Figure 4.14: Photos of retreat curve impeller at the end of the crystallisation process, showing the encrustation on the surface of : (left) Painted Stainless Steel impeller, (right) Painted Perspex impeller.

Overall, the comparison between painted impellers of stainless steel and Perspex are quantitatively similar;

- Crystal deposits are seen on both, at regions where the roughness is highest.
- The deposits are small in size; there are no large crystals on the impeller.

4.7.3.1 Cooling Rate and Stirring Speed Effects

The effect of cooling rate on apparent MSZW at different stirring speeds for painted Perspex impeller, based on the results presented in Table 4.5, is depicted in Figure 4.15.

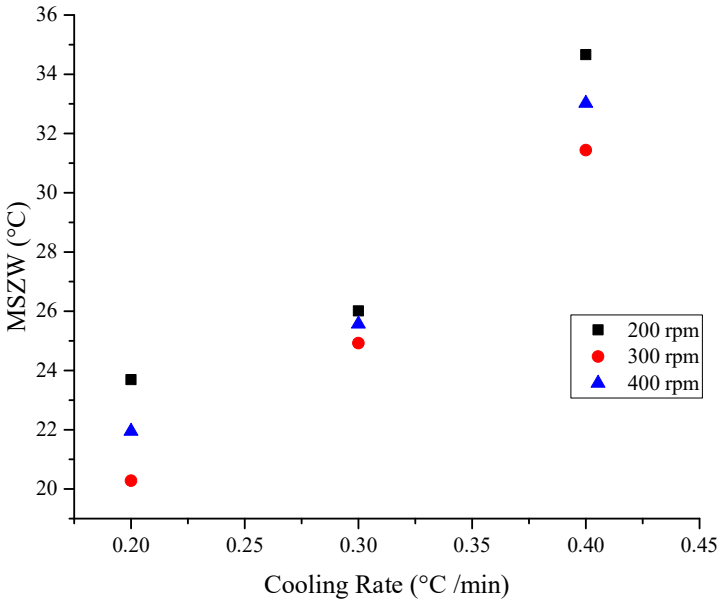

Figure 4.15: The effect of cooling rate on apparent MSZW at different stirring speeds for painted Perspex impeller.

It can be clearly seen in Figure 4.15 that the apparent MSZW widens significantly as the cooling rate increases. This finding is in good agreement with the nucleation theory where the faster the cooling rate is, the lower the crystallisation temperature will be to achieve a quasi-steady-state distribution of molecular clusters and form stable nuclei (Mullin, 2001). Thus, the MSZW becomes wider with higher cooling rate.

The dependency of MSZW on agitation speed at different cooling rates for both impellers, based on the data listed in Table 4.5, is illustrated in Figure 4.16.

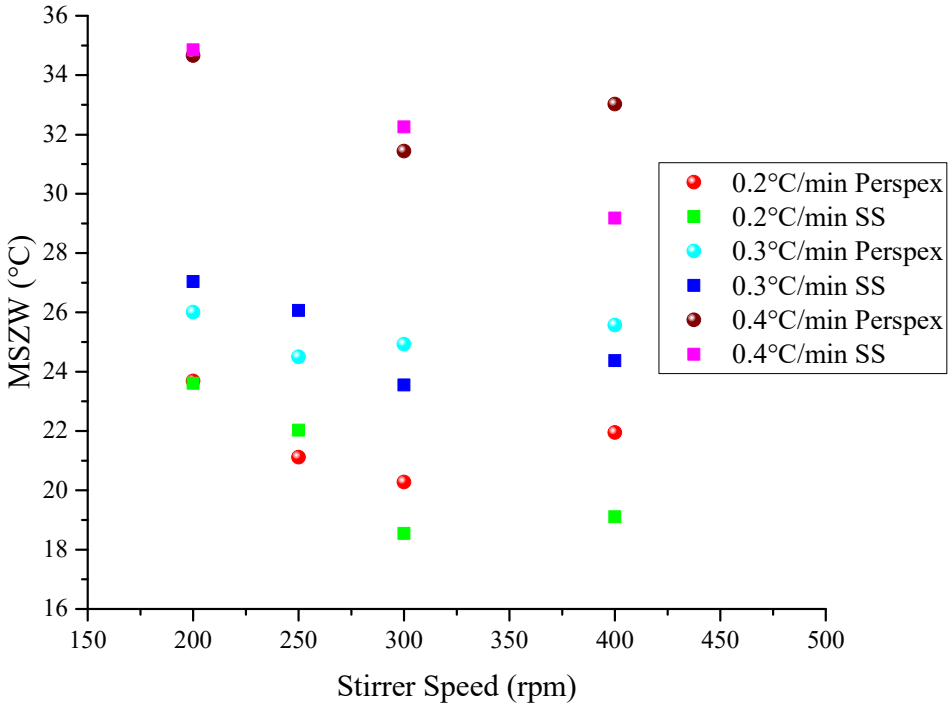

Figure 4.16: The dependence of MSZW on stirring speed at different cooling rates in 2L crystalliser for both impellers.

It is noteworthy that MSZW decreases with increasing the stirring speed which means that higher speeds enhance the nucleation process. However, the MSZW increases again when the stirring speed reaches 400rpm where it seems that the nucleation is retarded. This effect on MSZW is less pronounced for stainless steel RCI. The hindering impact can be explained due to the central vortex formation which starts to draw air into the solution at 400rpm. Air bubbles were found around the impeller shaft as seen in Figure 4.17. (Liang et al., 2004) found that the nucleation process starts at the surface of the impeller so the presence of air bubbles may affect the mixing efficiency and have strong influence on diffusional mass transfer in the area surrounding the nuclei and therefore affect the critical molecular cluster which promotes the inhibiting of nucleation process.

However, it could be that air bubbles introduced into the unit act as seeds or allow LGA molecules to align on the surface and form solid and in this case promote the nucleation. This can explain the results seen in Figure 4.16.

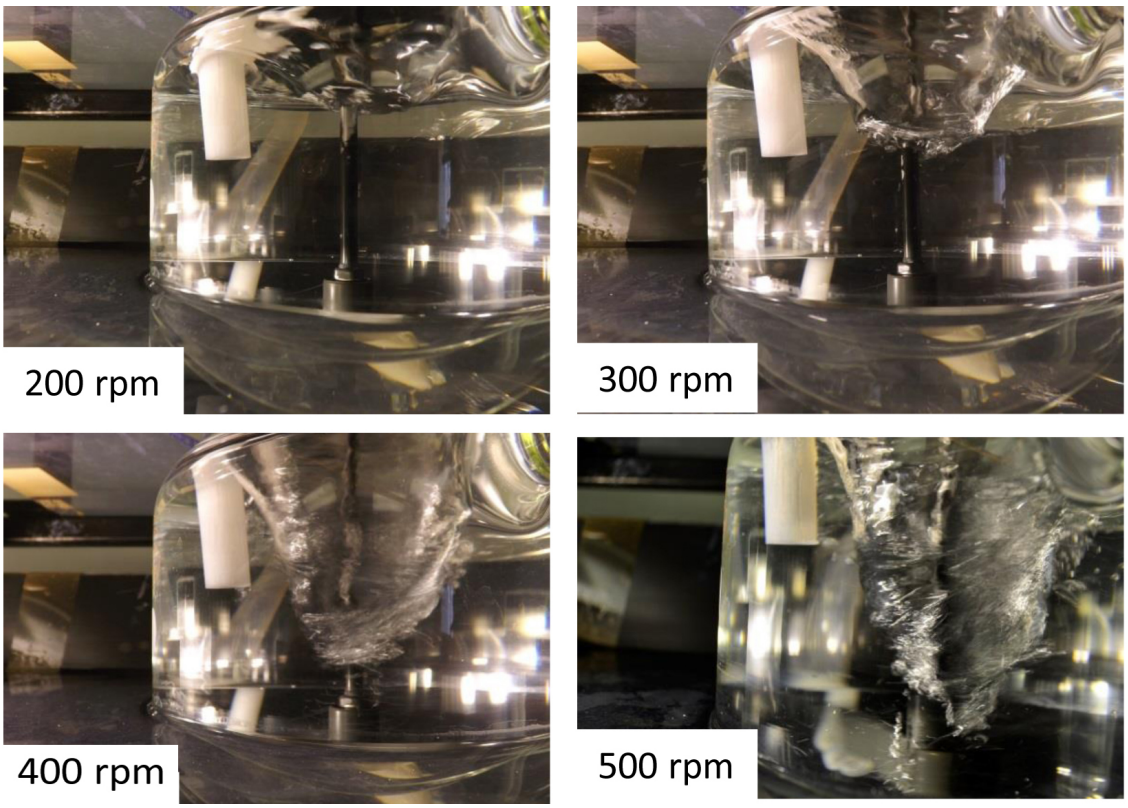

Figure 4.17: Images of the formation of central vortex in 2L crystalliser with increasing the agitation speed for Perspex impeller.

4.7.4 Nucleation Kinetic Parameters

The nucleation kinetic parameters can be quite readily calculated from the measured MSZW data using Nývlt's method (Nývlt, 1968). The method is summarised by plotting the logarithm of the measured MSZW verses the logarithm of the cooling rate which produces a straight line as shown in Figure 4.18. The slope of the straight line is the nucleation order m, whereas the nucleation rate constant K can be evaluated from the intercept (Liang, 2002).

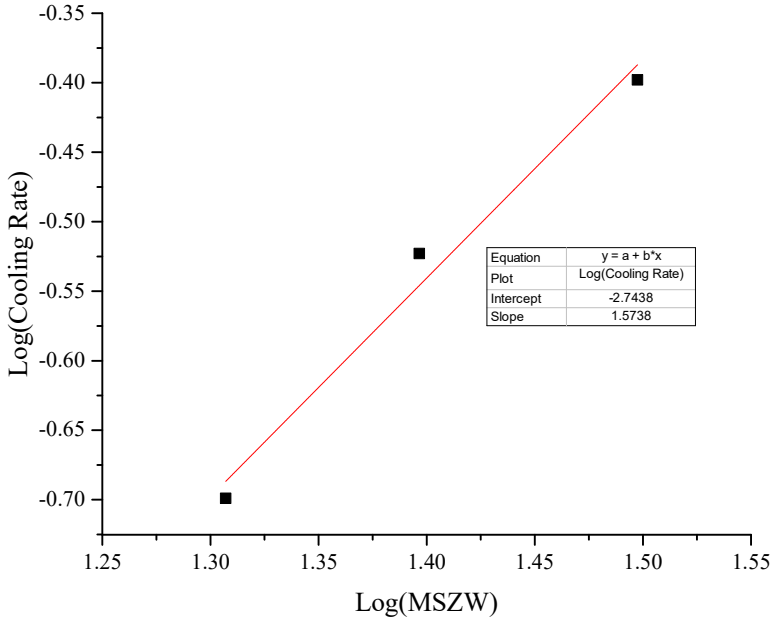

Figure 4.18: The plot of log cooling rate against log MSZW for Perspex impeller at 300 rpm.

The variation of nucleation order and nucleation rate constant as a function of stirring speed for the painted Perspex impeller is given in Figure 4.19.

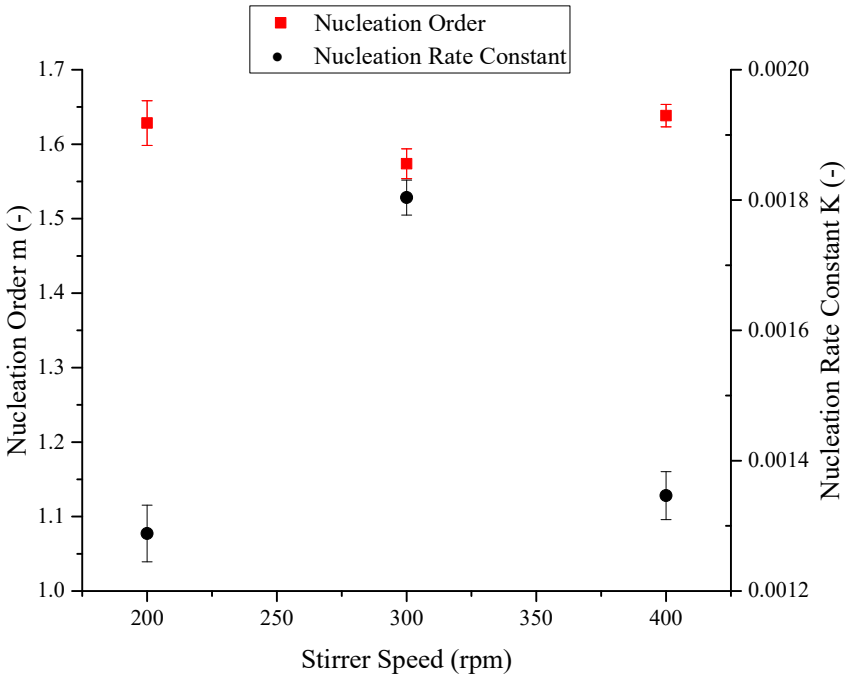

Figure 4.19: Nucleation order and Nucleation rate constant as a function of stirrer speed for painted Perspex impeller.

It can be seen that the nucleation order (m) does not depend on the stirring speed; the value for LGA was measured between 1.57 and 1.64. According to Nývlt, the value of nucleation order (m) is related to the molecular weight of the solute and does not depend on the presence of the solid phase or temperature. In other words, it is inversely proportional to the number of molecules needed for forming a critical nucleus (Nývlt, 1968). The nucleation order has a physical importance for the crystallising system; it reflects the state of the solid-liquid interface. Therefore, the low value of m represents strong solid-liquid interfaces which eases the formation of stable nuclei, while the high value of m means weak solid-liquid interfaces which makes the formation of stable nuclei difficult (Sangwal, 2009b). As it can be seen from Figure 4.19, the calculated value for the nucleation order is relatively small which suggests quite strong solid-liquid interfaces (Nývlt, 1968).

It can also be noted from Figure 4.19 that the nucleation rate constant increases with increasing the agitation speed, however by increasing the speed above 300 rpm the value starts to decrease which matches trends with those previously reported (Liang et al., 2004).

As the measurement of MSZW is a common measurement to take and data for LGA at 2 L scale has been published, it is useful to show here data taken from the imaging system. Table 4.7 summarises the measured nucleation order based on the PVI system with literature values using turbidity probe and FBRM. Nucleation order measured in this study was higher than FBRM data recorded by Patchigolla but of similar order to that measured by Liang. The PVI values are higher by 6% from those using a turbidity probe.

Table 4.7: A comparison between the measured nucleation order using PVI system and the literature values.

Nucleation order PVI(Current Work)	Nucleation order FBRM(Patchigolla, 2007)	Nucleation order Turbidity probe(Liang, 2002)
1.57-1.64	0.84-1.3	1.48-1.54

4.7.5 Mass Transfer Rate Recorded Using the Optical Technique

After the successful application of the optical technique to detect the nucleation event and measure the MSZW at different operating conditions, this technique was used to

calculate the overall mass transfer rate of LGA crystals. The same experimental set-up and camera calibration mentioned in section 4.3 were applied. The recorded images from the start of the cooling stage until the solution became cloudy (totally white) were processed using MATLAB code which summated the pixels of each column of the recorded image resulting in intensity distribution curve that represents the distribution of the crystals in the processed image (Golnabi, 2006).

The programme then calculated the area under the distribution curve that is referred to as the intensity distribution integral (IDI) (see Appendix B). Figure 4.20 shows the IDI values against time for LGA crystallised at a particular operating condition.

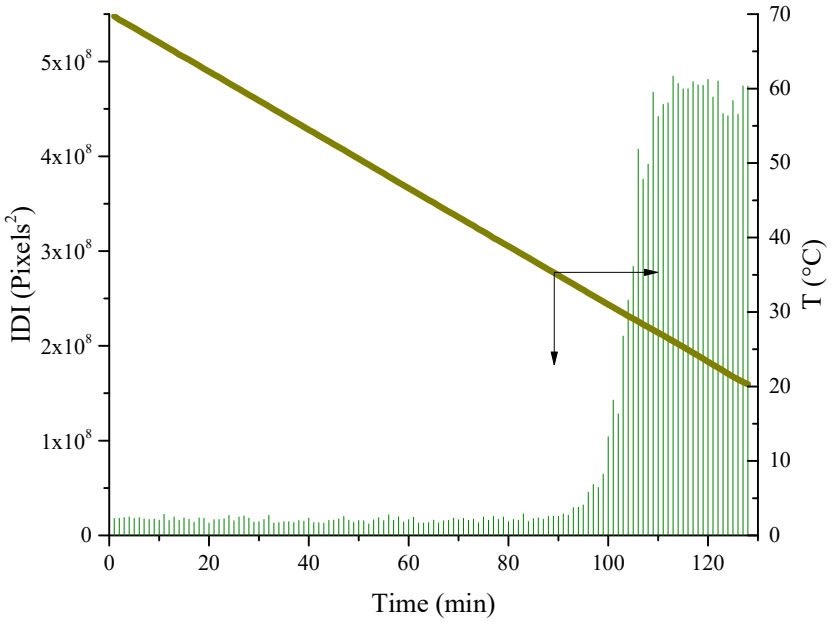

Figure 4.20: IDI values as a function of crystallisation time for painted Perspex impeller at 0.4°C/min and 300 rpm.

It can clearly be seen in Figure 4.20 that the IDI value increases with time up to a maximum value when the solution becomes cloudy. After this maximum value, fluctuation in the IDI values can be observed which is explained by crystal overlapping within the observation area due to high crystal mass generated.

As the concentration of LGA crystals, C_c (g/ml) can be calculated at any time during the crystallisation stage from equation (4.3) (Brown, 2012).

$$C_C = \frac{\left(\frac{(IDI - IDI_{Min})}{(IDI_{Max} - IDI_{Min})}\, m_{r,LGA}\right)}{V} \quad \textbf{(4.3)}$$

Where

IDI: Area under intensity distribution curve at any time, (pixel^2).

IDI_{Max} : Maximum area under the intensity distribution curve , (pixel^2).

IDI_{Min} : Minimum area under the intensity distribution curve, pixel^2, representing 0 g/ml crystal concentration.

V: Vessel volume, (ml).

$m_{r,LGA}$: Mass of recovered LGA crystals, (g); this mass was measured by filtering and drying the collected slurry.

The instantaneous solute mass transfer rate, G_i (g/min), can then easily be determined by equation (4.4) (Brown, 2012).

$$G_i = \frac{(C_{c2} - C_{c1})}{T_{c2} - T_{c1}}\, V_{ave} \quad \textbf{(4.4)}$$

Where C_{c2} is the crystal concentration at time 2, g/ml, C_{c1} is the crystal concentration at time 1, g/ml, T_{C2} , T_{C1} are time 2 and 1 respectively, min and V_{ave} is the vessel volume, ml.

Therefore, the overall solute mass transfer rate can be calculated using equation (4.5) (Brown, 2012) which averages the instantaneous mass transfer rates evaluated using equation (4.4) over the crystallisation period.

$$G_{ave} = \frac{\left(\sum_{T_{c1}}^{T_{c2}} G_i\right)}{n} \quad \textbf{(4.5)}$$

Where *n* is the number of data points between T_{c1} and T_{c2}.

Utilising equation (4.5), the data for the overall mass transfer rate of LGA crystallised at 300 rpm stirring speed and different cooling rates is displayed in Table 4.8.

Table 4.8: The values of the overall solute mass transfer rate (from solution to solid) calculated using equation (4.5) at different cooling rate.

Cooling Rate [˚C/min]	0.2	0.3	0.4
Overall solute mass transfer rate [g/min]	2.15	3.11	3.49

In terms of the effect of the cooling rate on the overall solute mass transfer rate, Table 4.8 shows that there is a direct proportional relationship. This finding is consistent with the literature where higher cooling rate can generate higher supersaturation rate which is the driving force for crystallisation process.

In order to validate the data obtained for the solute mass transfer rate from the optical method, the overall solute mass transfer rate calculated using equation (4.5) can be compared to the overall solute mass transfer rate obtained from recovered mass using equation (4.6) (Brown, 2012).

$$G_{ave} = \frac{P_r}{T_{c2} - T_{c1}} \tag{4.6}$$

Comparison between the solute mass transfer rate obtained by the image analysis method and that by the recovered mass method is shown in Figure 4.21.

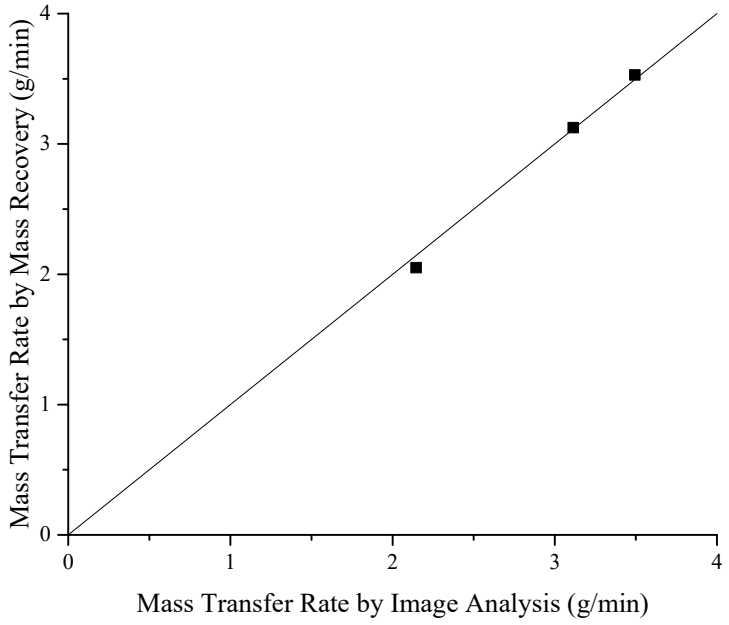

Figure 4.21: Deviation between image and experimental solute mass transfer rates.

It can clearly be noticed that the deviation between the two set of data is too small which provides the confidence in applying the optical technique for evaluating the crystallisation parameters.

It is worth noting that the use of the current optical method only allowed measuring the overall solute mass transfer rate. No crystal shape or polymorph transition has been detected. This has an advantage of not being sensitive to the image resolution. However, higher camera resolution, smaller capture area and more advanced image processing tools are needed for measuring crystal size and identifying polymorphic information.

4.8 Results and Discussion for Glycine Experiments

4.8.1 Linear Cooling Rate Experiments

The optical technique was also utilised to monitor the cooling crystallisation of glycine. The same experimental set-up and camera calibration explained in section 4.3 were used. The experiments were conducted using a solution of glycine (Fisher Scientific. Specification, >=98.5% CAS 56-40-6) of concentration of 38g/100 g distilled water (saturated at 46˚C) prepared at room temperature. Prior to starting the experiment, the vessel, the impeller, the baffle and the thermometer were washed properly with water to remove any particles left from previous runs.

In each run, the solution was heated up to 62˚C (about 15˚C above saturation temperature) at constant rate followed by holding stage for 30 minutes to guarantee that all the crystals dissolved. Then, the solution was cooled down at the same rate as the heating one. The heating/cooling cycle was implemented for three different heating/ cooling rates: 0.1, 0.2, and 0.3˚C/min at 200 rpm stirring speed using Perspex retreat curve impeller. Simultaneously, water bath and vessel temperatures were recorded and images were taken and processed at intervals of 30 seconds.

4.8.1.1 Metastable Zone Width Measurement

MSZW of glycine for a particular operating condition was calculated using equation (4.1). The method is described in detail in section 4.5. The dependency of MSZW on cooling rate is illustrated in Table 4.9.

Table 4.9: Results for MSZW measurement using on-line video imaging system in 2L reactor at various cooling rates.

Cooling Rate [˚C/min]	Stirrer Speed [rpm]	Crystallisation Temperature, T_{cry} [˚C]	MSZW T_{sat} - T_{cry} [˚C]	Supersaturation C/C* [-]
0.1	200	43.1	2.9	1.04
0.2	200	42.0	4.0	1.06
0.3	200	39.6	6.4	1.11

The values of MSZW exhibit a high degree of agreement with those previously reported (Louhi-Kultanen et al., 2006). As expected, the higher the cooling rate is, the wider the MSZW becomes. This is similar to the trends observed by previous researchers for different materials (Liang, 2002; Rajoub, 2014) as well as corresponding with the nucleation theory (Mullin, 1997). Noteworthy is that glycine has narrower MSZW than L-glutamic acid as shown in Tables 4.3 and 4.9. This can be explained by the higher solubility of glycine in water compared with L-glutamic acid which means more material is crystallised as temperature decreases.

4.8.1.2 Nucleation Kinetic Parameters

The nucleation kinetic parameters were evaluated from MSZW data according to equation (4.7) (Kashchiev et al., 2010a):

$$\ln q = \ln q_0 + (n+1) \ln u_c \tag{4.7}$$

Therefore, a plot of the logarithm of cooling rate (q) versus the logarithm of relative critical undercooling (u_c) was constructed as shown in Figure 4.22. The relative critical undercooling (u_c) is calculated by:

$$u_c = \frac{T_{sat} - T_{cry}}{T_{sat}} \tag{4.8}$$

As shown in Figure 4.22, the slope of the best-fit straight line of the data (n+1) is less than 3, suggesting that the glycine crystals were formed by the instantaneous nucleation mechanism (IN). This means that all the nuclei emerged simultaneously at the start of the crystallisation process and thereafter they grew into crystals (Kashchiev et al., 2010a).

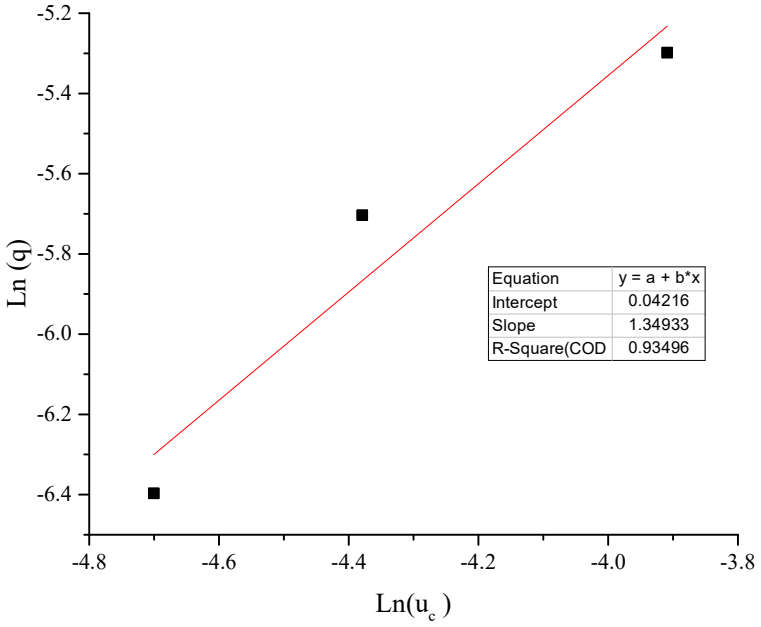

Figure 4.22: The plot of ln q vs. ln u_c for glycine cooling crystallisation data using Perspex impeller at 200 rpm.

The value of the intercept can be used to calculate the concentration C_0 of instantly formed nuclei in the solution according to equation (4.9) (Kashchiev et al., 2010a).

$$q_0 = [k_v\, C_0 /(n+1)^d\, \alpha_{det}]^{1/md}\, a^n K_G T_{sat} \qquad \textbf{(4.9)}$$

Where k_v is the growth shape factor (i.e. $4\pi/3$ for spheres), m is related to the growth mechanism (i.e. m=1 for growth controlled by the diffusion of the solute via the layer around the crystal), d =3 is for three dimensional growth of spheres, K_G is crystal growth parameter, α_{det} is the crystal volume fraction and a is the molecular latent heat of crystallisation.

The parameters values of equation (4.9) together with the calculated value of C_0 are given in Table 4.10.

Table 4.10: Summary of the glycine cooling crystallisation parameters values obtained from the analysis of the polythermal data.

q_0 [K/s]	k_v [-]	n [-]	d [-]	m [-]	α_{det} [-]	a [-]	K_G [m/s]	T_{sat} [K]	C_0 [m^{-3}]
1.04	$4\pi/3$	0.35	3	1	10^{-6}	5.32	10^{-8}	319	$3.6X10^9$

The calculated value of C_0 is quite reasonable as it corresponds to 7×10^6 crystals in solution of volume of 2×10^{-3} m^3.

It can also be clearly seen that the nucleation order of glycine is lower than that of LGA (see Figure 4.18 in section 4.7.4). (Sangwal, 2009b) found that the nucleation order value is inversely proportional to the solubility of the solute. Taking into account that the solubility of LGA in water is lower than that of glycine (see Figure 4.7), this can verify our findings which are in a good agreement with previous observations of other researchers (Sangwal, 2009b).

4.8.2 Crash Cooling Experiments

In an attempt to show whether the jacket's fluid temperature is of importance on the crystallisation process inside the vessel, crash cooling experiments to different lower temperatures were carried out. In these experiments, two water baths, the Grant as a hot source and the Haake as a cold source were used. The same experimental set-up and camera calibration explained in detail in section 4.3 were used. Computer controlled solenoid valves allowed one bath to be switched into the jacket, see section 3.4.

At the start of each run, the glycine solution was heated to 61 ºC to dissolve all the crystals using the Grant and then followed by rapid cooling down to a different set of temperatures via Haake bath. The camera was used to detect the first signs of crystals. Table 4.11 summarises the measured crystallisation temperatures (T_{cry}) for the performed experiments and the time elapsed since switch point to spontaneous nucleation. The crystallisation temperature was defined as the point at which white pixel percentage (W%) rose by 10% from the value for clear solution. The same criterion was used to measure T_{cry} for all runs in this chapter.

Table 4.11: Summary of crash cool crystallisation runs of glycine of concentration of 38g/100g from aqueous solution in 2 L beaver-tail baffled crystalliser agitated by Perspex RCI at 200 rpm.

T_sp of cold bath [˚C]	Measured T_{cry} [˚C]	Time for spontaneous Nucleation since switch point [min]	S C/C* [-]
39	40	23	1.1
30	35	15.33	1.2
25	32.7	13.5	1.25

Crash cooling gives a nonlinear cooling profile which becomes steeper for a lower temperature of the cold bath. As clearly seen in Table 4.11, the lower the cold bath temperature, the faster the solution nucleates and that the nucleation temperature is lower. In explanation, the temperature gradient at the vessel wall would increase as a result of lower jacket temperature which means higher supersaturation generated. Supersaturation is the main driving force for crystallisation process, thus higher supersaturation leads to higher nucleation rate which causes the solution to nucleate faster. This finding is well in agreement with the classical nucleation theory (Mullin, 1997) and previous researches (Liang, 2002; Groen, 2001a). However, a lower cold bath temperature led to lower crystallisation temperature as shown in Table 4.11. The explanation of this result can be that higher effective cooling rate was achieved with lower bath temperature which in turn widened the apparent MSZW. This agrees with the nucleation theory which states that the faster the cooling rate, the lower the crystallisation temperature will be to achieve a quasi-steady-state distribution of molecular clusters and form stable nuclei. This means the MSZW becomes wider with higher cooling rate (Mullin, 2001). Thus, the results here from crash cooling experiments are as expected.

In order to calculate the nucleation parameters for the case of isothermal method (i.e. crash cooling), a plot of Ln $\{\tau[S(S-1)^{md}]^{1/(1+md)}\}$ vs. $1/T^3$ $(\text{Ln } S)^2$ was generated using the data given in Table 4.11, see Figure 4.23. The linear relationship was found by assuming m = 0.5 and d = 1 which refers to crystal growth governed by diffusion in one dimension (Kashchiev, 2000). The derivation of this relationship is explained in detail in (Corzo et al., 2014).

From the slope of the best-fit straight line of the data shown in Figure 4.23, the effective interfacial tension γ_{eff} can be calculated from equation (4.10) as:

$$Slope = \frac{16\,\pi\, v_0^2\, \gamma_{eff}^3}{3(1+md)k^3} \qquad \textbf{(4.10)}$$

Where k is Boltzmann constant (1.38×10^{-23} J/K) and v_0 is the volume of glycine molecule in the crystal (7.27×10^{-29} m^3).

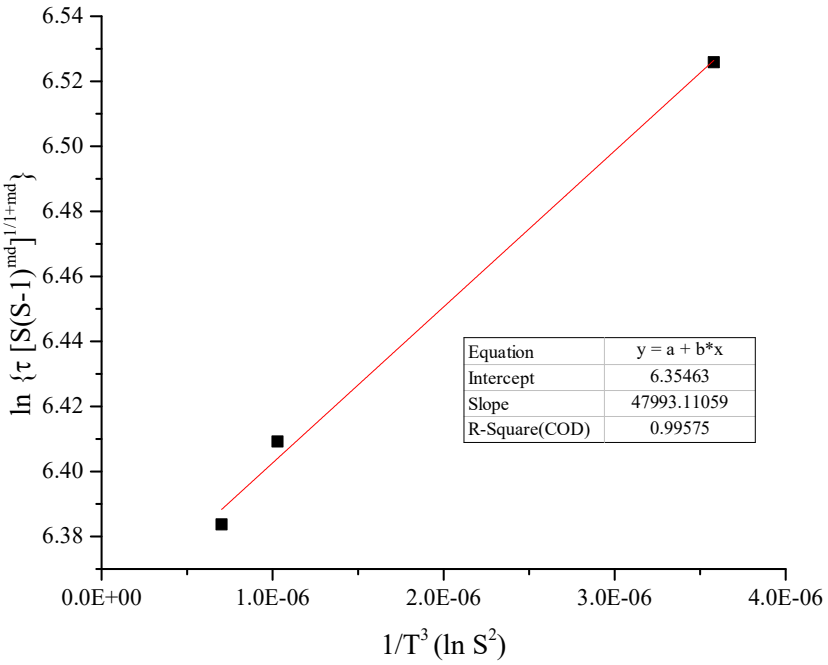

Figure 4.23: Plot of experimental data in Ln {τ[S(S-1) ^{md}] $^{1/(1+md)}$} vs. 1/T^3 (Ln S) ^{2} coordinates for the crash cooling runs of glycine in water.

The critical radius of the nucleus (r^*) and the number of molecules in the critical nucleus (i^*) can then be obtained from equations (4.11) and (4.12), respectively (Corzo et al., 2014):

$$r^* = \frac{2\, v_0\ \gamma_{eff}}{k\, T \ln S} \tag{4.11}$$

$$i^* = \frac{4\,\pi\,(r^*)^3}{3v_0} \tag{4.12}$$

The calculated values of γ_{eff}, r^* and i^* are shown in Table 4.12. The results showed that the lower the supersaturation generated by the crash cooling, the larger the nucleus formed which is in good agreement with the literature (Mullin, 2001; Khan et al., 2011). This finding is also supported by the values of the number of molecules in the critical nucleus (i^*).

Table 4.12: Nucleation parameters obtained according to the isothermal method for glycine solution.

S [-]	γ_{eff} [mJ/m^2]	r^* [nm]	i^* [-]
1.1	1.23	3.63	2590
1.2	1.23	2.17	552
1.25	1.23	1.90	369

4.8.3 The Effect of Applying Different Cooling Modes on the Crystallisation of Glycine

Traditionally, crash and linear cooling profiles are used in crystallisation processes. In this PhD work, however, a switching technique between hot and cold water baths was introduced as mentioned above. Therefore, this section discusses the difference between the conventional cooling profiles and cooling which results from the switching technique in terms of their effect on the nucleation temperature of glycine. The same experimental set-up and camera calibration explained in detail in sections 3.4 and 4.3 were used. All the runs here included three stages: heating up to dissolve all the crystals, holding to ensure that all the crystals dissolved and finally cooling down using different profiles which are:

1. Run A: Linear cooling rate of 0.1 ºC/min.
2. Run B: Linear cooling rate of 0.3 ºC/min.
3. Run C: Switching between hot bath (Grant at 46 ºC) and cold bath (Haake at 30 ºC) at frequency rate of 1:1 (Grant: Haake →40s: 40s).
4. Run D: Crash cooling to 30 ºC.

The key similarity among these runs is that they would cool down the vessel from 46 ºC to 30 ºC, but this will be at different cooling profiles.

A MATLAB programme was written specifically to run these stages and record all the required parameters. Simultaneously, water baths and vessel temperatures were recorded as well as images were taken and processed at intervals of 10 seconds.

Comparison between the vessel temperature and the W% change for the different cooling modes are shown in Figure 4.24.

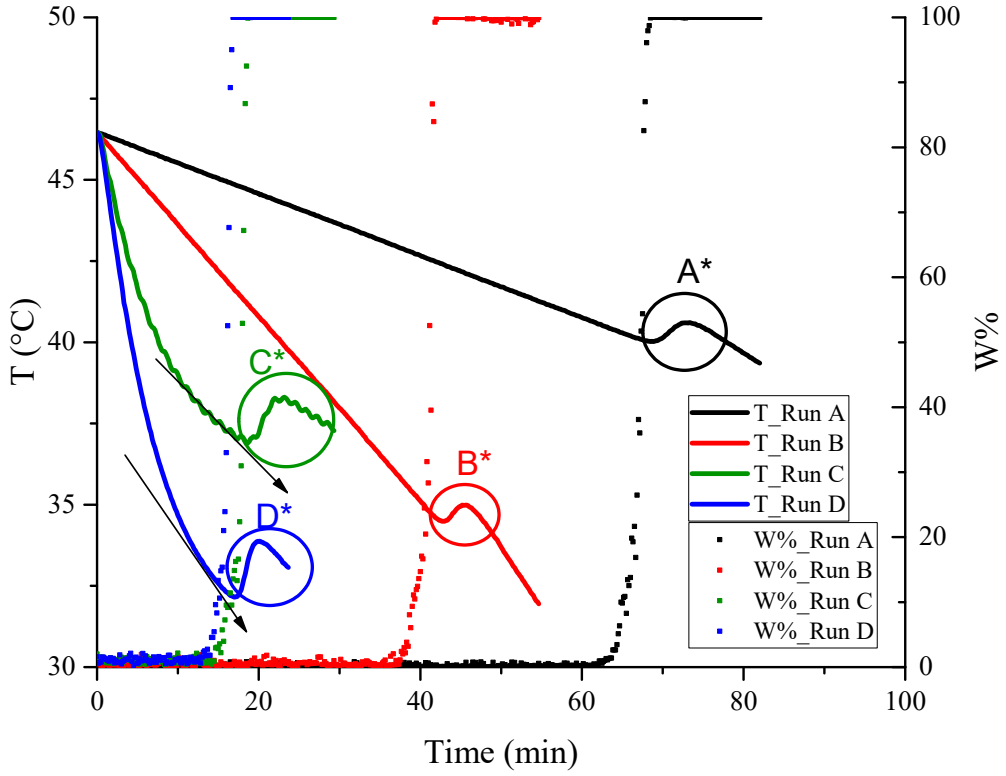

Figure 4.24: The vessel temperature and W% change profiles of different cooling profiles for aqueous glycine solution in 2 L beaver-tail baffled crystalliser agitated by Perspex RCI at 200 rpm.

The effective cooling rate, the crystallisation temperature and the time taken to spontaneously nucleate for the different cooling profiles are listed in Table 4.13.

Table 4.13: Summary of different cooling modes results for aqueous solution of glycine of concentration of 36g/100g in 2L beaver-tail baffled crystalliser agitated by Perspex RCI at 200 rpm.

Run [-]	Effective cooling rate [˚C/min]	T_{cry} [˚C]	Time for spontaneous Nucleation [min]	S C/C* [-]
A	0.1	40.3	57	1.04
B	0.3	35.4	35.5	1.13
C	0.21*	37.3	16	1.10
D	0.5*	32.7	14.7	1.19

*: **at the arrows, see Figure 4.24.**

It can be seen clearly from the results in Figure 4.24 and Table 4.13 that for runs A and B the lower the cooling rate, the higher the crystallisation temperature and the longer the time taken are. This is as expected and in a good agreement with the literature (Mullin, 1997). The crash cooling produced an effective higher cooling rate than 0.3 ºC/min and therefore crystallisation temperature was the lowest and the time was the shortest. The switching mechanism in turn had a higher crystallisation temperature than crash cooling and 0.3 ºC/min linear cooling due to its lower effective cooling rate of 0.21 ºC/min but the point at which crystals were detected was only 1.5 minutes different from the crash cooling case. In explanation, both switching mechanism and crash cool give nonlinear cooling profile which is very steep at the beginning (i.e. the cooling rates are 0.7 and 0.9 ºC/min, respectively) and then becomes less steep (i.e. the cooling rates are 0.21 and 0.5 ºC/min, respectively). This could explain why the time was shorter in the case of switching and crash cooling than that of 0.1 and 0.3 ºC/min linear cooling rates.

In addition, a temperature rise ranging from 0.5-2 ºC can be seen after the rapid increase in W% as a result of the spontaneous nucleation, as shown in Figure 4.24 (Region A^*, B^*, C^*, D^*) respectively. The reason behind this observation can be the release of crystallisation enthalpy that caused the vessel solution to reheat.

4.8.4 A Comparison between the Effect of Crash Cooling and the Switching Technique on the Crystallisation of Glycine

A nonlinear cooling profile is generated from both the switching system and crash cool as clearly shown in Figure 4.24. However, there is a difference between them, that the crash cooling gives uncontrollable profile while the switching profile is controlled by selecting the hot and cold bath temperatures set point and the switching frequency. Therefore, switching method adds an additional level of control not possible with one water bath. To investigate more about the influence of the switching system on the nucleation behaviour of glycine compared with crash cool, a further set of experiments were conducted as follows:

1. Run 1: Crash cooling from 55 ºC to 45 ºC.
2. Run 2: Switching between hot bath (Grant at 55ºC) and cold bath (Haake at 45ºC) at frequency rate of 1:1 (Grant: Haake →40s: 40s).
3. Run 3: Crash cooling from 55 ºC to 49 ºC.

The purpose of these experiments is twofold, firstly to compare again the switching and the crash cooling profiles over the same range of temperature (55 - 45 ºC) and their effect on glycine crystallisation and secondly to check any advantage of the switching mechanism over the crash cool if both produce the same cooling profile (Runs 2 and 3).

The vessel temperature and the W% change as a result of applying different cooling modes are shown in Figure 4.25.

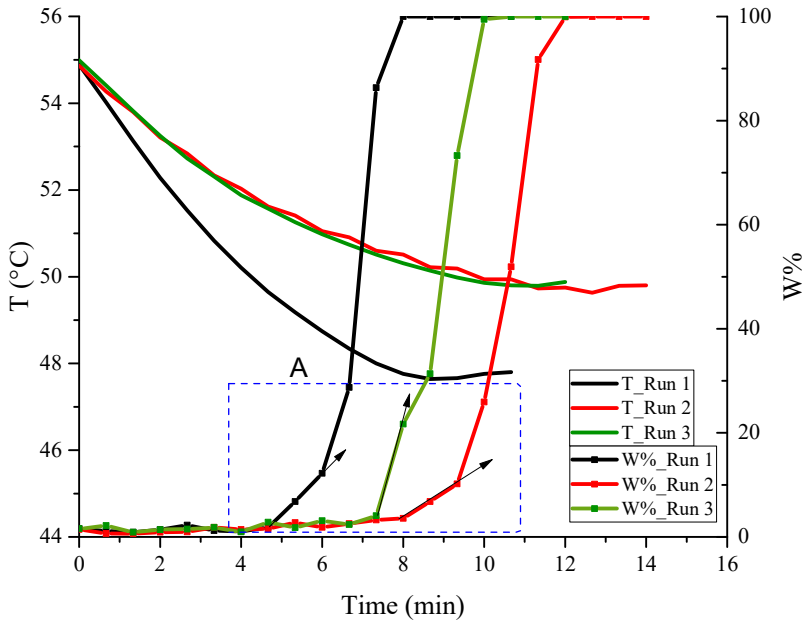

Figure 4.25: A comparison of the vessel temperature and W% profiles between crash cooling to different lower temperatures and switching method.

A comparison between the effective cooling rate, crystallisation temperature and the time taken to spontaneously nucleate for crash cooling and switching runs are listed in Table 4.14.

Table 4.14: Comparison between the effect of switching and crash cooling to different lower temperatures runs on the crystallisation of glycine of concentration of 49g/100g.

Run Number [-]	Effective cooling rate [˚C/min]	T_{cry} [˚C]	Time for spontaneous Nucleation [min]	S C/C* [-]
Run 1	0.94	48.7	6.0	1.24
Run 2	0.51	50.2	9.3	1.21
Run 3	0.53	50.4	7.5	1.21

As seen in Table 4.14, the findings for Runs 1 and 2 showed similar trends to what observed earlier in section 4.8.3, i.e. the higher the cooling rate, the lower the crystallisation temperature and the shorter the time taken are. Regarding the switching at 45:55 ˚C (run 2) and crash cooling at 49 ˚C (run 3), both produce the same cooling curve of 0.5 ˚C/min effective cooling rate and thus the crystallisation temperature is the same. However, a delay of about 2 minutes in nucleation point is seen between the two runs. This could be due to the impact of hot source presence. Adding to that, by looking at the W% change for all the runs, it can be noted that the W% change of switching is not as sharp as the crash cooling runs (see Figure 4.25, region A). This indicates that switching also has influence on crystal growth as a result of the hot source presence that can play role in dissolving the fines making the W% change at a lower rate. This observation means that if the switching frequency is manipulated, it will give a level of control for W% change that is not possible with one water bath (i.e. the case of traditional cooling profiles: linear and crash). The above findings and discussion show that switching does have an effect on both nucleation point (as seen in Runs 1and 2) and growth rate (as shown in Runs 2 and 3). This technique will be studied in more detail in next section.

4.8.5 The Effect of Switching Duration on the Crystallisation of Glycine

As found in sections 4.8.3 and 4.8.4, the switching technique between hot and cold baths did have different effect on glycine crystallisation when compared to the linear and crash cooling profiles. Therefore, it was of interest to explore deeply about this technique and how both its frequency (the ratio of hot source duration to the cold one) and duration (the time of each bath being active) can affect the crystallisation of glycine.

In an attempt to investigate the effect of switching duration, a set of experiments were carried out. Each one of them consisted of three stages which were: heating, holding and switching. A MATLAB programme was written specifically to change the water bath temperature at a designated rate during the heating stage in order to dissolve all the crystals and alter the water flow through the vessel jacket at a designated rate between the hot and cold baths during the switching stage via six solenoid valves.

The switching durations tested here were: (Grant: Haake →40s:40s, 60s:60s, 80s:80s and 100s:100s). As clearly seen, the switching frequency was 1:1 for all of these experiments. The hot source was Grant bath at 57ºC while the cold source was Haake bath at 45ºC. Figure 4.26 demonstrates the vessel temperature and W% change over the switching stage as a consequence of applying various switching durations.

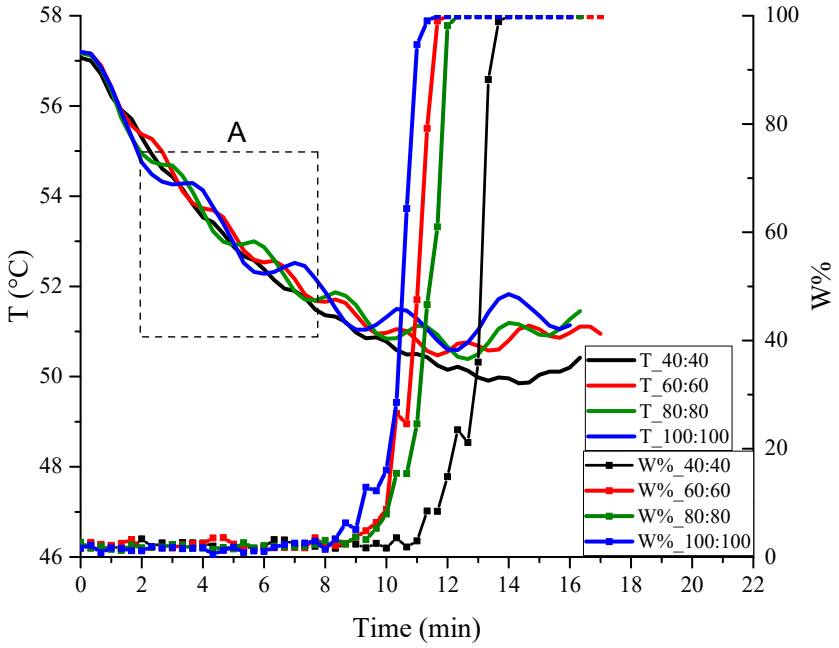

Figure 4.26: The vessel temperature and W% change over the switching stage as a consequence of using various switching durations for aqueous glycine solution in 2 L beaver-tail baffled crystalliser agitated by Perspex RCI at 200 rpm.

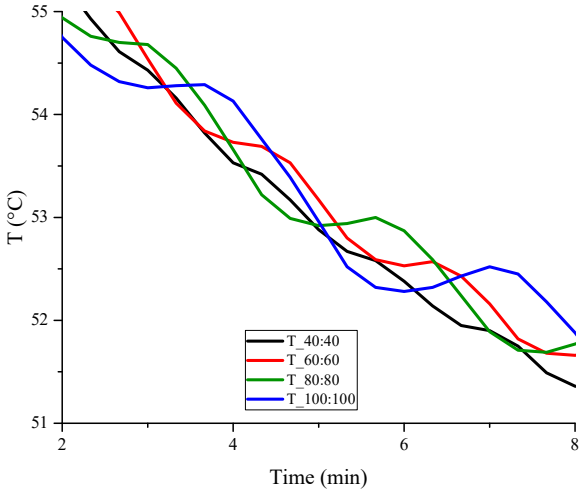

Figure 4.27: Enlargement of region A in Figure 4.26 that shows the solution temperature change as a result of applying various switching durations closely and clearly.

A comparison between crystallisation temperature and the time taken to spontaneously nucleate for different switching duration runs are listed in Table 4.15.

Table 4.15: Comparison among different switching duration runs on the crystallisation of glycine of concentration of 49g/100g.

Run [-]	Switching Duration [Grant: Haake]→[Hot: Cold] [s]	T_{cry} [˚C]	Time for spontaneous Nucleation since switch point [min]	S C/C* [-]
1	40:40	50.2	12	1.21
2	60:60	51	10.3	1.2
3	80:80	50.9	10.33	1.2
4	100:100	51	9.33	1.2

It can be noted from the results in Figure 4.26 and Table 4.15 that:

- The same switching frequency (1:1) but with different durations showed similar temperature profiles and therefore had the same cooling rate which gives the same crystallisation temperature. This is to be expected since the same amount of heat is removed regardless of the duration.
- The time needed for spontaneous nucleation is different and dependent on the duration that the cold water bath is connected to the vessel. Run 4 had the cold source switched to the vessel for longer period (100s) than any other run and hence the time to form crystals is shorter than other runs.

To see if the oscillatory vessel temperature profile as a result of applying different switching durations (e.g. 80s:80s and 100s:100s) can also be predicted using the mathematical model developed in chapter 3, the fourth order Runge-Kutta method was used to solve equation (3.16) in MATLAB. The experimental and model results for the switching duration 80s:80s and 100s:100s are plotted in Figures 4.28 and 4.29, respectively.

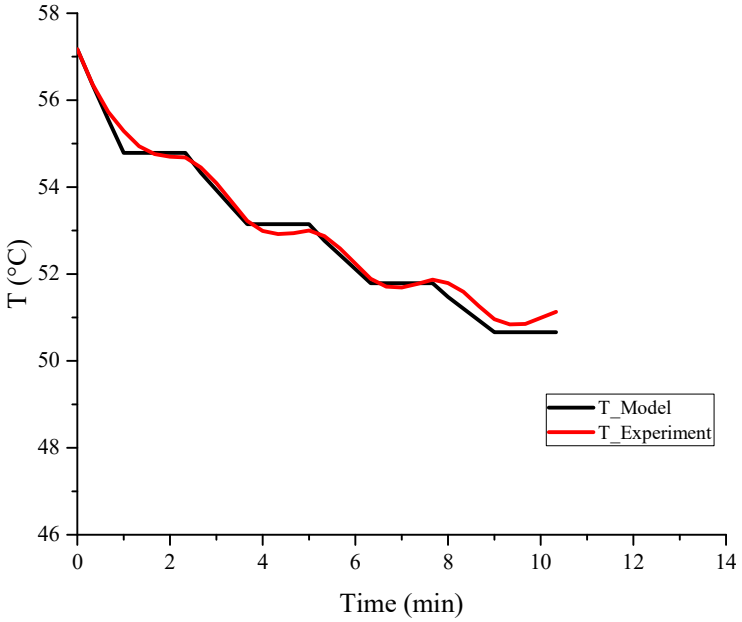

Figure 4.28: A comparison between the experimental data and the model results of the vessel temperature for switching duration of Hot: Cold→80s:80s.

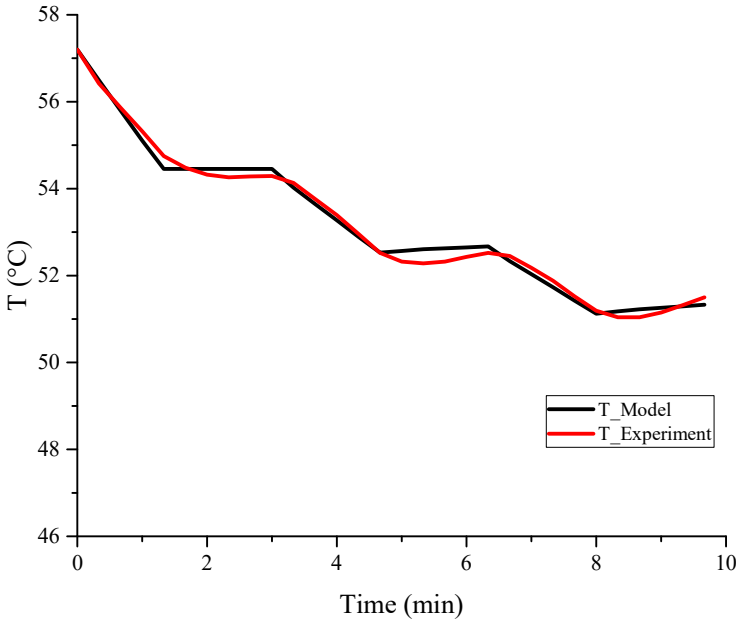

Figure 4.29: A comparison between the experimental data and the model results of the vessel temperature for switching duration of Hot: Cold→100s:100s.

As can be seen in Figures 4.28 and 4.29, the model results matched well the experimental data. The optimised value of U was 250 $W.m^{-2}$ K^{-1} for the cold water bath and 50 $W.m^{-2}$ K^{-1} for the hot bath. This would suggest that the jacket fluid itself does

have a big influence on the resistance to heat transfer which in turn depends on the heat exchange system.

4.8.6 The Effect of Switching Frequency on the Crystallisation of Glycine

Moving on to study the effect of switching frequency, further set of experiments was performed. The different switching frequencies and durations examined here were: (Grant: Haake → 20s:40s, 40s:80s, 20s:60s, and 40s:120s). The hot source was Grant bath at 55 ºC while the cold source was Haake bath at 45 ºC. The profiles of vessel temperature and W% change over the switching stage as a result of applying various switching frequencies and durations are shown in Figure 4.30.

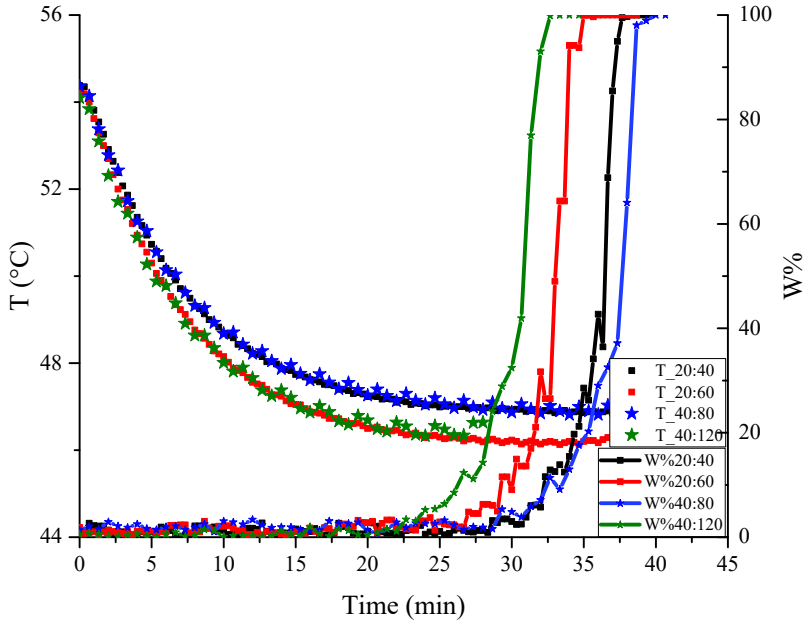

Figure 4.30: A comparison of vessel temperature and W% change over the switching stage among different switching frequencies and durations.

As seen in Figure 4.30, the same switching frequencies show identical temperature profiles. This is to be expected since the same amount of heat is removed regardless of the duration. However, switching ratio of 1:3 led to a cool down of the vessel to a lower temperature compared with that of 1:2 because the cold source was active for longer period. The crystallisation temperature did not differ much as a result of applying different switching frequencies and durations. In contrast, the time needed for spontaneous nucleation varied as shown clearly in Table 4.16.

Table 4.16: A comparison of crystallisation temperature and time for nucleation between different switching frequencies and durations for glycine solution of concentration of 40g/100g.

Run [-]	Switching Duration [Grant: Haake]→[Hot: Cold] [s]	T_{cry} [˚C]	Time for spontaneous nucleation since switch point [min]	S C/C* [-]
1	20:40	46.9	32.7	1.04
2	40:80	46.8	34.0	1.04
3	20:60	46.2	30.3	1.05
4	40:120	46.4	26.3	1.05

Table 4.16 shows several key features using the switching method:

1. Shifting frequencies that give the same ratio between hot and cold baths produce the same crystallisation temperature. Runs 1 & 2 and runs 3 & 4 have the same ratio and therefore the same cooling rate which gives the same crystallisation temperature.
2. The crystallisation temperatures detected are very similar (less than 0.5 ºC differences) yet can be detected using the camera system.
3. That the time that crystals was observed, and hence the growth rates are different and dependent on the duration that the cold water bath is connected to the vessel. Run 4 had the cold bath switched to the vessel for longer than any other run and hence the time to achieve crystals is shorter than other runs.

The above findings showed that the switching profile is controlled by its frequency and in turn affects how the W% changes. This can give a level of control which was the basis to develop a control system that is able to produce good quality of crystals in terms of size and presence of fines as will be seen in detail in chapter 5.

To investigate the impact of the oscillatory temperature profile produced by the switching technique on the nucleation kinetics, the same method explained in detail in section 4.8.1 was applied. Therefore, a plot of the logarithm of cooling rate (q) versus the logarithm of relative critical undercooling (u_c) was constructed.

The values of the slope, intercept together with the other parameters values used to calculate the concentration C_0 of instantly formed nuclei in the solution are listed in Table 4.17.

Table 4.17: Summary of the glycine cooling crystallisation parameters values obtained from the analysis of the switching data.

q_0 [K/s]	k_v [-]	Slope [-]	d [-]	m [-]	α_{det} [-]	*a* [-]	K_G [m/s]	T_{sat} [K]	C_0 [m^{-3}]
2.32	4π/3	1.82	3	1	10^{-6}	5.32	10^{-8}	323	$9X10^9$

As seen in Table 4.17, the slope of the best-fit straight line of the data (n+1) is less than 3, suggesting that the glycine crystals were formed by the instantaneous nucleation mechanism (IN) which is the same mechanism as that occurred using the polythermal method.

The calculated value of C_0 is quite reasonable as it corresponds to 18×10^6 crystals in solution of volume of 2×10^{-3} m^3. However, if compared with that of the polythermal method, it can be noted that the value of the switching method is double suggesting that switching technique allowed more nuclei to be formed.

4.8.7 The Effect of Varying the Hot and Cold Sources Temperatures Set Point on the Crystallisation of Glycine

As mentioned before, the switching technique is based on the presence of two sources; hot and cold. To investigate if the temperature set point of these sources has any impact, the switching ratio of 1:3 runs were repeated with the hot source (Grant) at a lower temperature of 50 ºC. A comparison of vessel temperature and W% change profiles over the switching stage between runs of different hot source temperatures set point is illustrated in Figure 4.31.

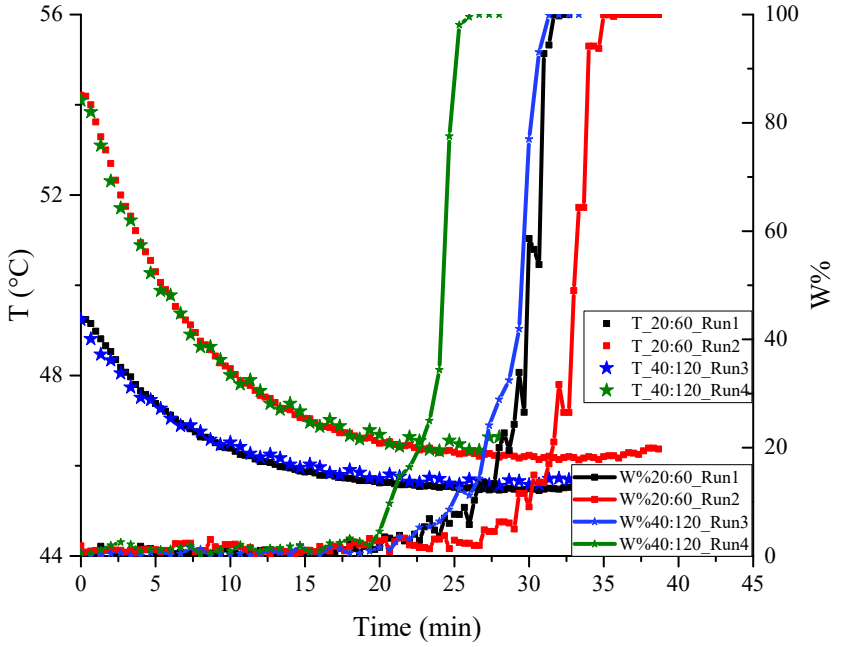

Figure 4.31: The profiles of vessel temperature and W% change over the switching stage for the same switching frequencies but different durations as a result of different temperature set point for the hot source (Grant bath).

It can be seen explicitly from Figure 4.31 that the two runs of switching ratio of 1:3 with the hot source at 50 ºC have similar temperature and W% profiles. This suggests that lowering the Grant bath temperature set point resulted in negating its effect as a hot source and therefore no effect of the switching duration is seen which is different from what observed in the case of higher Grant bath temperature set point. It can be said that the lower hot bath temperature set point made the switching look like a crash cool run.

Moving on to the effect of cold source temperature set point, a set of experiments of 1:1 and 1:3 switching ratios with different cold source temperature set point of 45 ºC and 42 ºC were performed. A comparison of vessel temperature and W% change profiles over the switching stage between runs of different cold source set point temperatures is depicted in Figure 4.32.

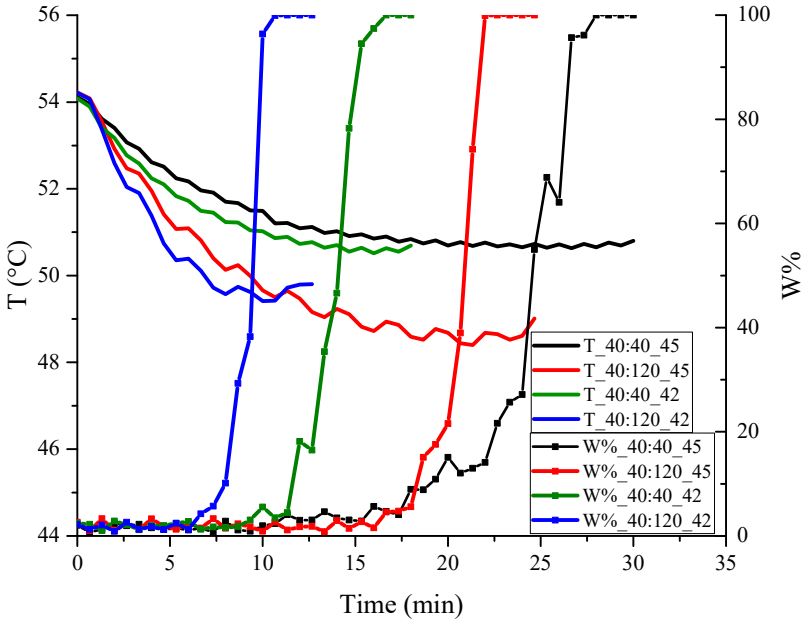

Figure 4.32: The profiles of vessel temperature and W% change over the switching stage for the same switching durations but different frequencies as a result of different temperature set point for the cold source (Grant bath).

In Figure 4.32, it is worth noting that a lower temperature set point of the cold bath drove the solution to nucleate much faster for both frequencies than a higher one. However, the crystallisation temperature did not vary much for 1:1 switching ratio, but by 1ºC for the ratio of (1:3) as summarised in Table 4.18.

Table 4.18: A comparison of crystallisation temperature and time needed for nucleation between different temperatures set point of the cold source for glycine of concentration of 49g/100g.

Run [-]	Cold bath T_SP [˚C]	Switching Duration [Haake: Grant]→[Hot: Cold] [s]	T_{cry} [˚C]	Time needed for nucleation [min]	S C/C* [-]
1	45	40:40	50.8	19.3	1.20
2	45	40:120	48.6	18	1.24
3	42	40:40	50.7	12	1.20
4	42	40:120	49.6	8	1.22

The results in Table 4.18 show that the time needed to form crystals, and hence the growth rates are different and dependent on both the duration that the cold water bath is connected to the vessel and its temperature set point. Run 4 had the cold bath switched

to the vessel for longer than any other run as well as the lower cold bath temperature set point and hence the time to achieve crystals is shorter than other runs.

The observed shorter time for nucleation for runs with lower cold source temperature can be again explained by a higher temperature difference at the vessel wall and thus higher supersaturation leading to faster nucleation. The effect of having different cold bath T_SP on the crystallisation temperature is more visible for a 1:3 switching ratio as the cold bath is active for longer period.

4.8.8 Repeatability Extent of Switching Technique

To determine the reproducibility of the switching technique, the runs for a 40s:40s and 100s:100s switching duration were repeated. The hot source was Grant bath at 65 ºC, whereas the cold source was Haake at 45 ºC. Figures 4.33 and 4.34 portray the vessel temperature in company with those of the W% change, switching and Haake and Grant temperatures as a result of using 40s:40s and 100s:100s switching durations respectively.

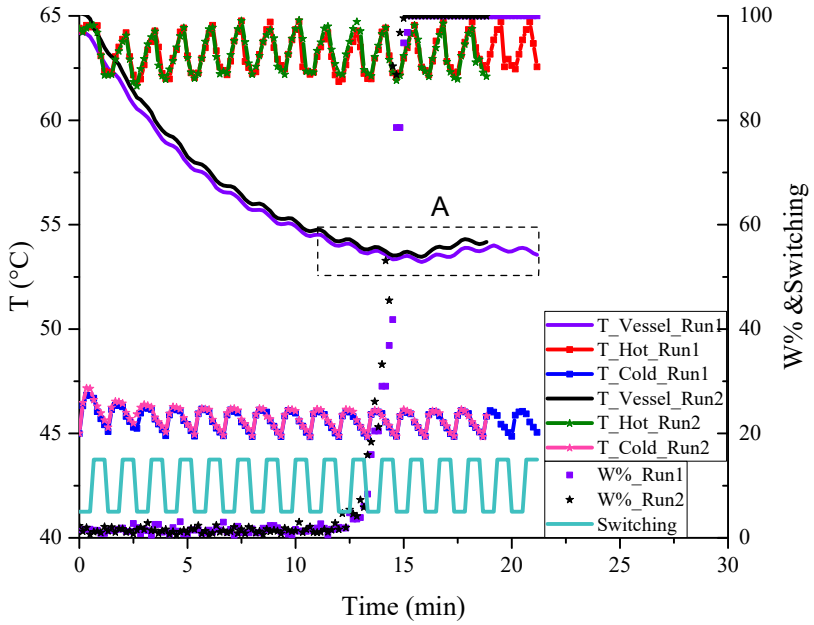

Figure 4.33: A comparison of Vessel , Haake and Grant water baths temperatures and W% profiles between two runs of 40:40 switching duration.

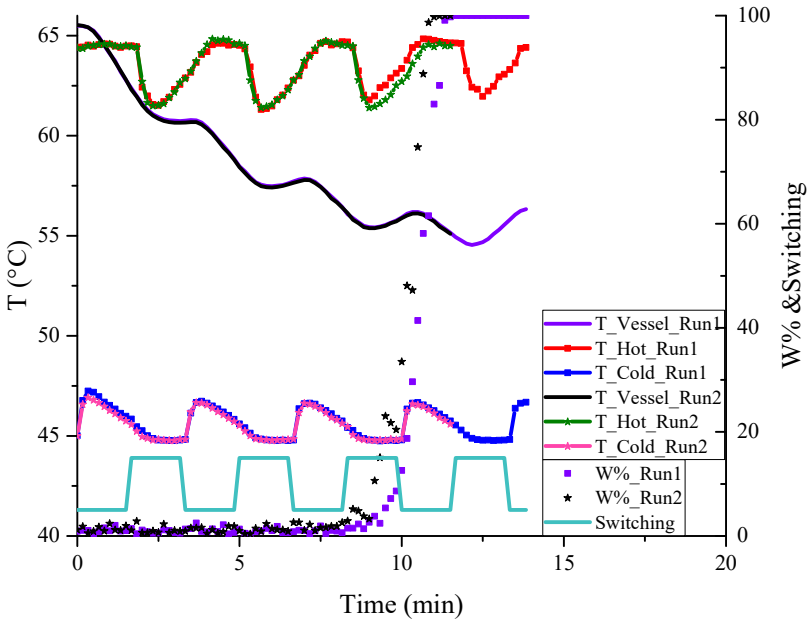

Figure 4.34: A comparison of Vessel, Haake and Grant water baths temperatures and W% profiles between two runs of 100:100 switching duration.

As depicted in Figures 4.33 and 4.34, the results are shown explicitly the good repeatability of the developed switching technique which is of paramount importance for technique validation. Also of interest is the observation of temperature increase of 0.8ºC after the rapid rise in W% as shown in Figure 4.35 which is enlargement of region A in Figure 4.33.

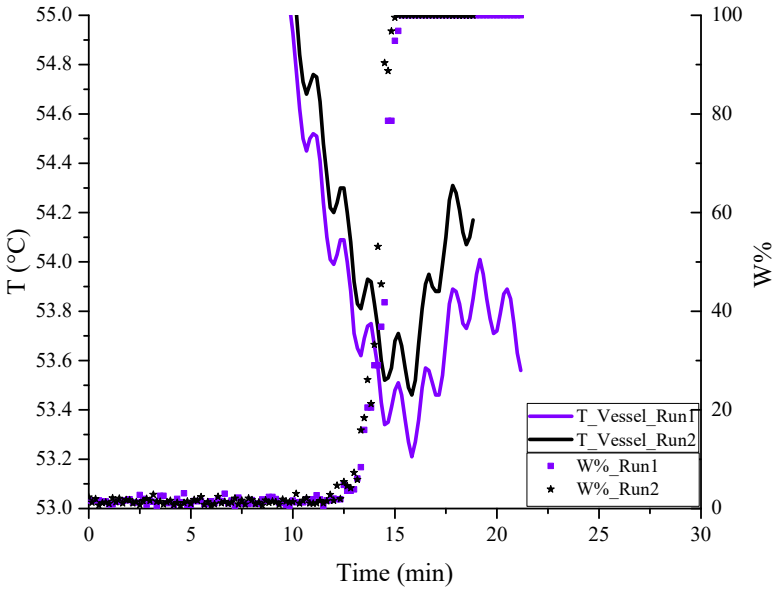

Figure 4.35: Enlargement of region A in Figure 4.33 that shows the solution temperature increase due to crystallisation heat.

This can be clarified by the release of crystallisation enthalpy that resulted in reheating the vessel solution. This finding is in good agreement with that previously reported (Groen, 2001a).

As some runs were conducted using the same solution, undesired events, such as, accidental seeding from encrustation on the crystalliser's wall were noted. For larger industrial scale crystallisers, a local increase in the liquid level due to vortex or evaporation can create a deposit on the inside wall. If this deposit breaks free, it can act as seeds. To check the robustness of the technique in case of accidental seeding presence, runs with 40s:40s and 100s:100s switching durations were examined. A comparison of vessel temperature and W% change profiles over the switching stage between runs of different switching durations as a consequence of accidental seeding is shown in Figure 4.36.

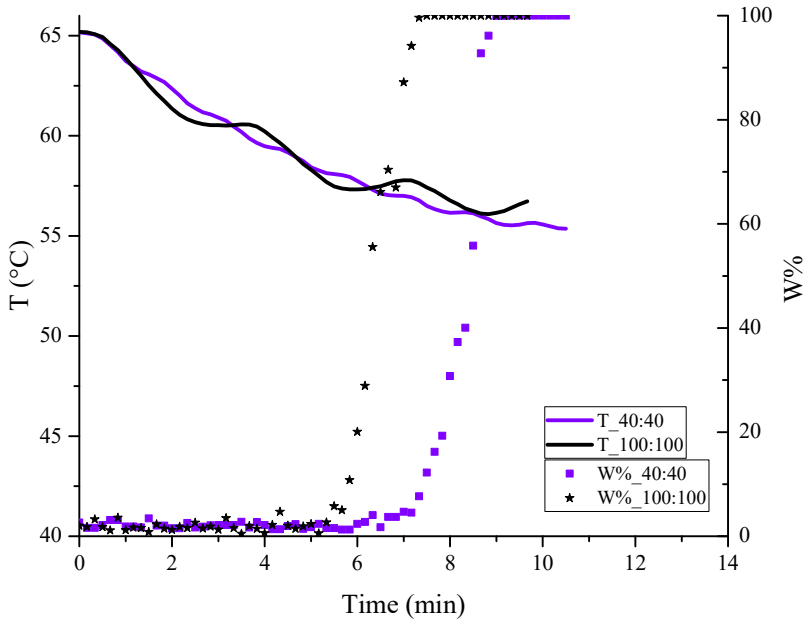

Figure 4.36: The profiles of vessel temperature and W% change over the switching stage for the same switching frequency but different durations in the case of accidental seeding from crust on the crystalliser wall.

The crystallisation temperature and time needed for increase of 10% in W% varied from 56.5ºC to 57.3ºC and from 7.5min to 5.8 min respectively as the switching duration rose from 40sec to 100sec, again matching trends reported in section 4.8.5 for runs without accidental seeding.

4.9 Conclusion

This chapter showed that the developed on-line video imaging system was successfully applied to characterise the cooling crystallisation of LGA and glycine. The MSZW for both materials was evaluated at different operating conditions. The effect of the cooling rate, stirrer speed and impeller materiel has been investigated. The results matched trends previously reported using different techniques such as FBRM (Rajoub, 2014) and turbidity probe (Liang, 2002).

In addition, the nucleation kinetics parameters for both the polythermal and isothermal data of glycine experiments were calculated according to KBHR method, and they are in good agreement with those previously observed. Interestingly, the nucleation order dependency on the solute solubility was demonstrated, again matching trends previously presented. This chapter showed that the developed imaging system can also be used to measure the instantaneous and overall mass transfer rate of LGA by analysing the images recorded.

All these findings prove that a relatively cheap on-line video imaging system (about £2K) can be a good technique for monitoring cooling crystallisation when compared with other much more expensive techniques, for example, FBRM and turbidity probe.

This chapter also studied the switching of the water flow through the crystalliser jacket between hot and cold water baths using six solenoid valves in order to vary the temperature of aqueous glycine solution in 2 L beaver-tail baffled crystalliser agitated by Perspex RCI at 200 rpm and see how this can affect the crystallisation of glycine.

The main variables examined were the switching frequency and duration as well as the temperature set point of the two baths. It was found that the switching duration had a little effect on glycine nucleation time and temperature. In contrast, the switching frequency had impact which was more obvious when the ratio became higher either for the cold bath duration to the hot one or vice versa. Moreover, the temperature set point of the hot and cold baths showed to be of great potential for switching effectiveness. It was concluded from a series of pre-trials that the temperature set point should be above the saturation temperature of the solution for the hot source and within MSZ for the cold one. Added to that, the heat transfer model developed in chapter 3 showed its ability to predict the vessel temperature in the case of applying different switching durations.

For the first time, a comparison of the switching technique, crash cooling and constant linear cooling rate effects on the nucleation point of glycine was presented. It was found that the switching mechanism gives controllable profile by selecting the hot and cold bath temperatures set point and the switching frequency. Therefore, switching method adds an additional level of control not possible with one water bath which is used in traditional cooling profiles (crash and linear). Adding to that, the presence of hot source that induces the dissolution at the vessel wall prevents a rapid change in W% after the nucleation occurs if compared with the traditional cooling profiles.

This chapter gave valuable insight into the role of switching technique for inducing the crystal formation and dissolution at the vessel wall. These findings provided good ground to develop a control system that improves the quality of LGA and glycine crystals formed in batch cooling crystallisation as shown in chapter 5.

This successful application of the switching technique and the developed imaging system for monitoring crystallisation process, as shown in this chapter, gives motivation to apply these techniques later on to control the cooling crystallisation of LGA and glycine which will be discussed in detail in Chapter 5.

Chapter 5
Controlling the Crystallisation of LGA and Glycine in Batch Cooling Crystalliser Using Online Video Imaging and Switching Techniques

This chapter presents the developed strategy for controlling the crystallisation of LGA and glycine. LGA and glycine have a number of different characteristics that make them suitable candidates to demonstrate the principle of the cooling method used in this work. As outlined in chapter 4, the measured variable is the white percentage "W%_actual" which is related to the number and size of crystals produced, and the manipulated variable is the switching frequency of the hot and cold sources. In addition to performing trial runs, the sensitivity and robustness of the developed control approach are examined by changing the trajectory set point that the measured variable should follow and investigating the effect it has on the crystal size distribution produced.

The overall quality of the crystals in terms of size and presence of fines appears improved over conventional methods. Section 5.2 will discuss the control strategy in further detail; sections 5.3 and 5.4 will show the control system working with glycine and LGA, respectively. Section 5.5 will present images that show the size and general quality of the crystals produced and estimation of the crystal size distribution from analysing the crystals' images will be reported. Finally, section 5.7 will show the ability of the developed heat transfer model to predict the vessel temperature during the control stage and section 5.8 will demonstrate the importance and the robustness of the developed control strategy.

5.1 Introduction

Controlling the shape, size and often polymorphic form of crystals produced during the separation stages of a liquid phase process is of great importance in the field of chemical industries especially the pharmaceutical ones. As the quality of the crystalline product (i.e. its shape, size and form) has a big impact on the efficiency of the downstream processes such as filtration, milling and drying (Mullin, 2001). Added to that, through better control of crystal formation, companies aim to improve product

effectiveness in terms of bioavailability and stability; for example, in the pharmaceutical industry this optimises the dissolution rate of the drugs in order to gain the maximum benefit (Variankaval et al., 2008). Accordingly, the control of crystallisation process has its significance for meeting the product specifications, such as crystal size distribution, shape, purity and morphology within industrial production.

Different control strategies based on either model approach or direct design approach have been developed, as shown in detail in chapter 2, to attain the desired crystal shape and CSD with the possibility of repeatability from batch to batch.

In the light of the above observations, this chapter will be devoted to present the implementation of the control strategy developed in this work on the cooling crystallisation of LGA-water and glycine-water systems to grow for the first time crystals with larger size through combining the developed PVI system with the switching technique. The switching method was employed to change the wall temperature between hot and cold using two water baths: one is a hot source and the other is a cold source. This has the effect of inducing crystal formation and dissolution close to the vessel wall.

5.2 Control Strategy Based on the Combination of the Optical System and the Switching Technique

In chapter 4, the switching system between two temperature sources (one hot and one cold) was described and the impact of the switching frequency on the crystallisation of glycine was discussed. The next stage in using switching was to develop a closed feedback system using the optical imaging as a measurement target and the switching frequency as the manipulated variable. Through a series of experiments described in this section, it will be shown how the switching method can improve the quality of crystals formed in a self-seeded cooling crystallisation process through dissolving the smaller nuclei via the hot source and allowing the larger ones to further grow by means of the cold source.

All the experiments performed in this chapter consisted of four stages, which are, described in general by Figure 5.1:

- Heating to a holding temperature T_H (e.g.70˚C) to dissolve all crystals.

- Holding temperature at T_H for 30 minutes to ensure that all crystals dissolved.
- Cooling down by switching to the cold bath (set at T_L) until the presence of crystals was detected by an increase in the white percentage of the image captured online by the camera (i.e. W%_actual typically > 5%).
- A control stage that will be explained below in detail.

The initial heating through to the final controlled cooling was programmed into a MATLAB (2013b) code, (see Appendix D for a listing of the control code).

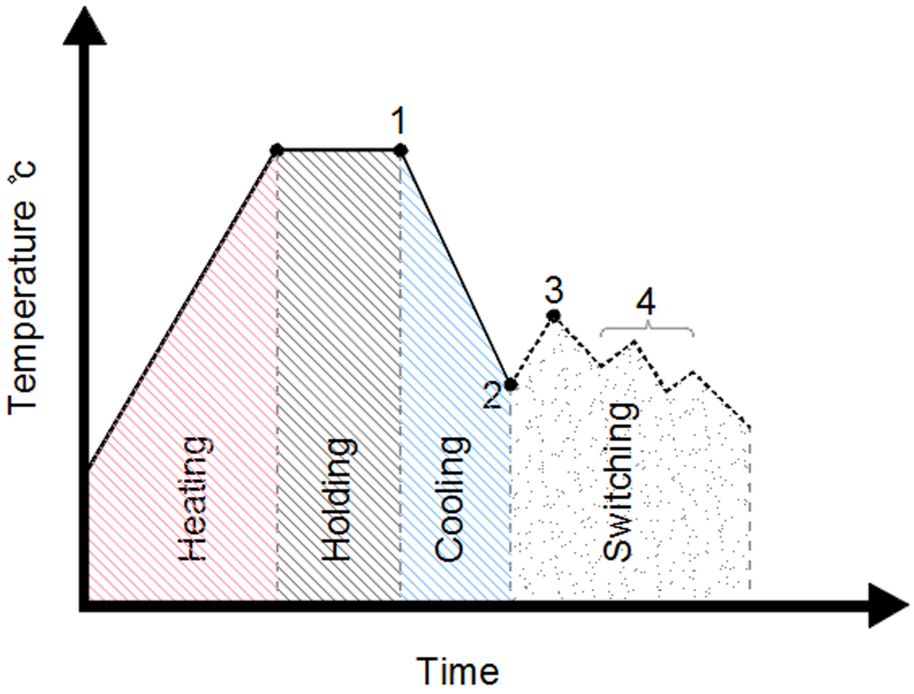

Figure 5.1: Schematic representation of the stages involved in all control experiments.

5.2.1 The Stages of Control Strategy Development

The system to switch between two water baths was outlined in chapter 3. To implement this in a control application, a formal closed-loop control system was developed. Development of the closed-loop system followed a number of trails eventually leading to the system incorporated into the current code version. To develop the control algorithm, a number of assumptions were made:

1. The white percentage W%_actual is a measure of both the number and size of crystals at any time in the camera's field of view. Hence, starting from a clear

solution, an increase in W%_actual from 0 to some number is attributed to the formation of new nuclei and growth to a sufficient size as to be detectable.

2. The presence of air bubbles and other artefacts such as reflections from internal components can artificially increase or decrease the value of measured W%_actual.

3. That to have crystals growing, the W%_actual value itself must change with time. The range will be between 0 and 100.

4. From experiments described in chapter 4, a rapid increase in W%_actual indicates a spontaneous nucleation event (SNE). This event would be primary nucleation although secondary nucleation cannot be ruled out.

In order to regulate the growth of crystals, the rate at which the W%_actual changes is the controlled variable. With this in mind, the algorithm calculates the variable "SLOPE" which is the W%_actual change within a specific duration. To establish the working range of controllable SLOPE's, information from experiments outlined in chapter 4 was used. A series of experiments were then performed adjusting the target SLOPE required. To terminate the control stage, a variable called the "intensity distribution integral value (IDI)" for a totally white image was used.

During the development of the control loop, a threshold condition (i.e. target SLOPE) was introduced. At the start of the control stage, the system would sometimes exhibit rapid increases in W%_actual. To avoid this situation occurring in subsequent tests, a test on the measured SLOPE variable was needed to switch to the hot bath source and monitor the W%_actual until the system regained control. To facilitate that, this could only be reduced by rapid heating until W%_actual level returned to some pre-set value. Therefore, upon detection of such an event, the control system was programmed to return the W%_actual value to its setting before the system lost control.

Adding this condition (i.e. rapid heating to return W%_actual to its value before the occurrence of the sharp increase) in the control system was not sufficient, because choosing a constant value (i.e. W%_actual value before the sudden increase) to reactivate the SLOPE check condition led to the dissolution of more crystals than

required resulting in longer control stage, notably in the case of frequent sudden increase in the W%_actual happened. Accordingly, it was concluded that the W%_actual should follow a predefined profile, the so-called the trajectory of white pixels percentage set-point "W%_SP". Consequently, when a rapid increase in the W%_actual happens during the control stage, the software detects that, deactivates the SLOPE check and switches to the hot bath to dissolve the crystals. The SLOPE check is reactivated when the difference between the W%_actual and W%_SP values becomes less than or equal to 5%; this value (5%) was chosen to avoid the dissolution of more crystals than needed. This method is explained in detail in section 5.2.3 and illustrated in Figure 5.4.

5.2.2 The Final Developed Control Approach Applied for LGA and Glycine Control Experiments

As mentioned above, the control method developed in this work was based on setting a predefined profile for W%_actual change, the so-called W%_SP profile. Thus, the W%_actual of the image captured for the crystals formed should follow this profile. The images were recorded online by the developed optical system; see chapter 4 (section 4.5), and analysed to calculate the W%_actual during the entire duration of the crystallisation process. Maintaining the W%_actual close to the W%_SP value was implemented using the automated feedback control system that switches the flow through the crystalliser jacket between hot and cold water baths to directly dissolve the undesired fines generated or grow the larger crystals.

As discussed in chapter 4, some initial trails were required to determine the temperature set point of both water baths to ensure that they can operate effectively as hot and cold sources. This was due to the differences in heating and cooling power combined with differences in pumping rate of the utility fluid. However, it was found that the temperature set point of the hot source should be above the saturation temperature of the solution and within the MSZ for the cold one.

A typical operating profile of the crystallisation process using the developed control system is shown in Figure 5.2. It can be seen that the clear solution was cooled down until the primary nucleation took place to generate seeds internally and then the control

stage started where heating and cooling cycles were carried out to keep the W%_ actual at its target (W%_SP), see Table 5.1 for detailed explanation.

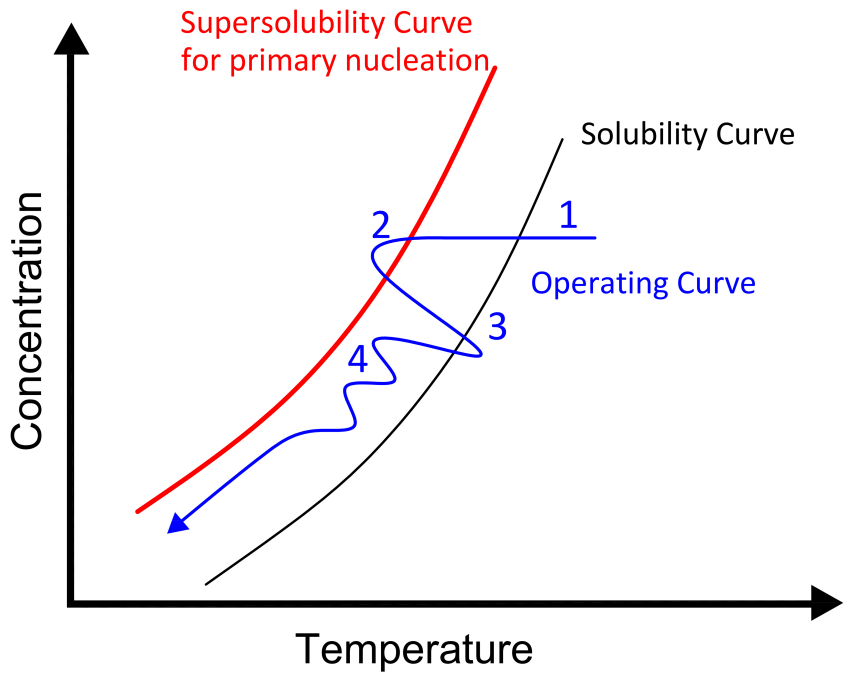

Figure 5.2: A typical operating profile for the developed control strategy.

Table 5.1: Explanation of Figure 5.2 steps.

Point	Description
1	Initial clear solution above its saturation temperature. The control system is programmed to drop the temperature by switching to the cold bath set at T_L. This imitates crash cooling. As the solution moves through the MSZ, primary nucleation will take place.
2	There will be a rapid increase in W%_ actual as primary nucleation takes place. The software detects this event and switches to the hot bath to dissolve the crystals.
3	The control system is programmed to decrease the W%_ actual by not less than 10% by switching to the hot bath. The aim of that is to dissolve the fines formed by primary nucleation (Point 2) but leave a few crystals as seeds (Point 3).
4	Switching between hot and cold baths to allow the W%_ actual to follow the W%_SP profile.

Compared to a traditional small-scale laboratory cooling system, the switching system is more akin to the setup industry can use. Figure 5.3 compares the schematic block

diagram of the developed control system for the cooling crystallisation of both LGA and glycine with that of traditional control system. As known, the number of control "handles" available to manipulate the crystallisation system is limited and therefore switching can introduce a viable method for further manipulation of the process.

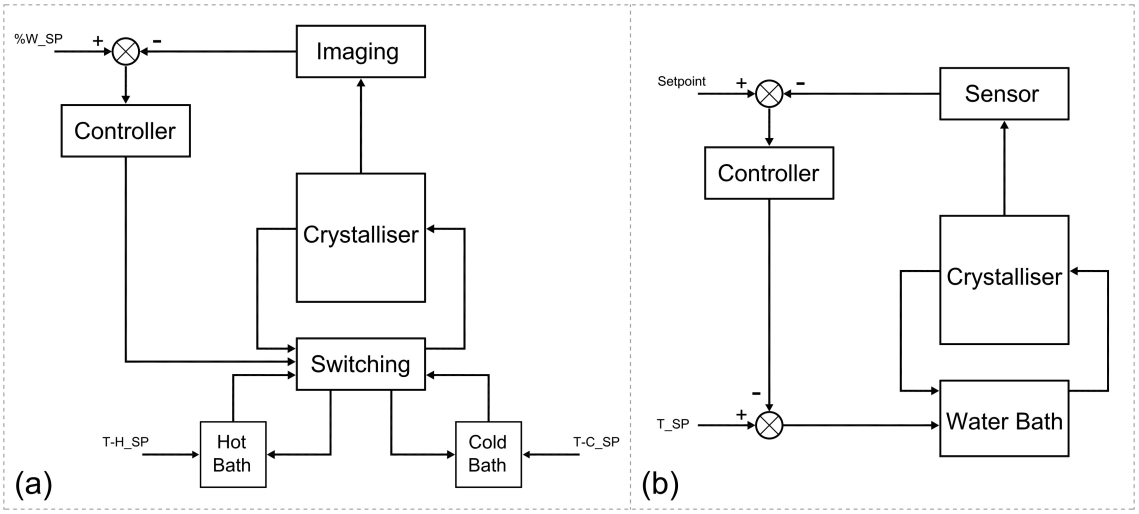

Figure 5.3: Comparison between the schematic block diagrams of (a) the developed control system and (b) the traditional control system, both for batch cooling crystallisation.

With reference to Figure 5.3 (a), the W%_ actual measured by the imaging system is compared to W%_SP. Based on the error signal, the controller sends a command to the switching unit to either switch to the hot bath or the cold one to change the crystalliser temperature accordingly. However, in the traditional control system, Figure 5.3 (b), the crystalliser temperature is changed also based on the error signal between the measured variable (by the sensor) and the set point, but by adjusting the water bath temperature set point. As a result, immediate heating and cooling rates may not be easy to achieve as this would depend on the power of the heater/ cooler system. By using the switching system between two water baths (i.e. hot and cold), changing the crystalliser temperature would be much faster.

5.2.3 Measurement-Based Control Strategy:

This section outlines the philosophy behind the switching control system. The W%_actual of the image captured by the optical technique at the beginning of the control stage which represents the seeds internally generated is assigned to W%_base. This is the initial point of a straight line that W%_actual should follow; the target W%_SP trajectory. Images were then recorded every few seconds (this depends on the

system under investigation; 20 seconds for glycine and 30 seconds for LGA) and analysed to find W%_actual. So-called SLOPE, which is the W%_actual change between two successive images (W%_actual(i) – W%_actual(i-1)) within a specific duration , was calculated. Based on that, commands were sent to the solenoid valves to either switch to the hot bath if SLOPE was greater than what it should be, or switch to the cold bath if SLOPE was equal or less than what is supposed to be. In parallel, the W%_actual was compared with the target W%_SP. A difference of 5% between W%_actual and W%_SP was added as a condition to stop heating and reactivate the SLOPE check to avoid undesirable decrease in W%_actual below its target (W%_SP) due to extra heat from the hot bath. Different W%_SP trajectories were applied as will be shown in sections 5.3.2 and 5.4.2. A flow-chart of the developed control mechanism and underlying calculations are provided in Figure 5.4.

The control system developed in this thesis has its own advantages, for example, it is model-free, thus no information about the system kinetics is required beforehand and thus the operating profile is mainly based on the required target (W%_SP). There is some pre-work to determine the hot and cold bath set points however this is a relatively straightforward process. In addition, there is no need for external seeding as this strategy could be applied successfully to an unseeded crystallisation process. It provides in-situ fines removal without any need for external equipment or recycle loop. Finally, the optical technique used as a monitoring tool for the control system is much cheaper than the other commercially available devices, such as FBRM with a cost of around £2000.

Cycling temperature between two limits has been documented before (Saleemi, 2011; Abu Bakar, 2010) , although this reported, the method used a standard set point control bath and tried to keep the conditions within the MSZ.

Glycine in water and LGA in water were chosen as model systems in this work because of the big difference in their solubility curves. Glycine has stronger relationship between temperature and concentration than LGA. This makes them represent two different systems where the rate of temperature change (heating and cooling) has more effect on glycine than it does with LGA.

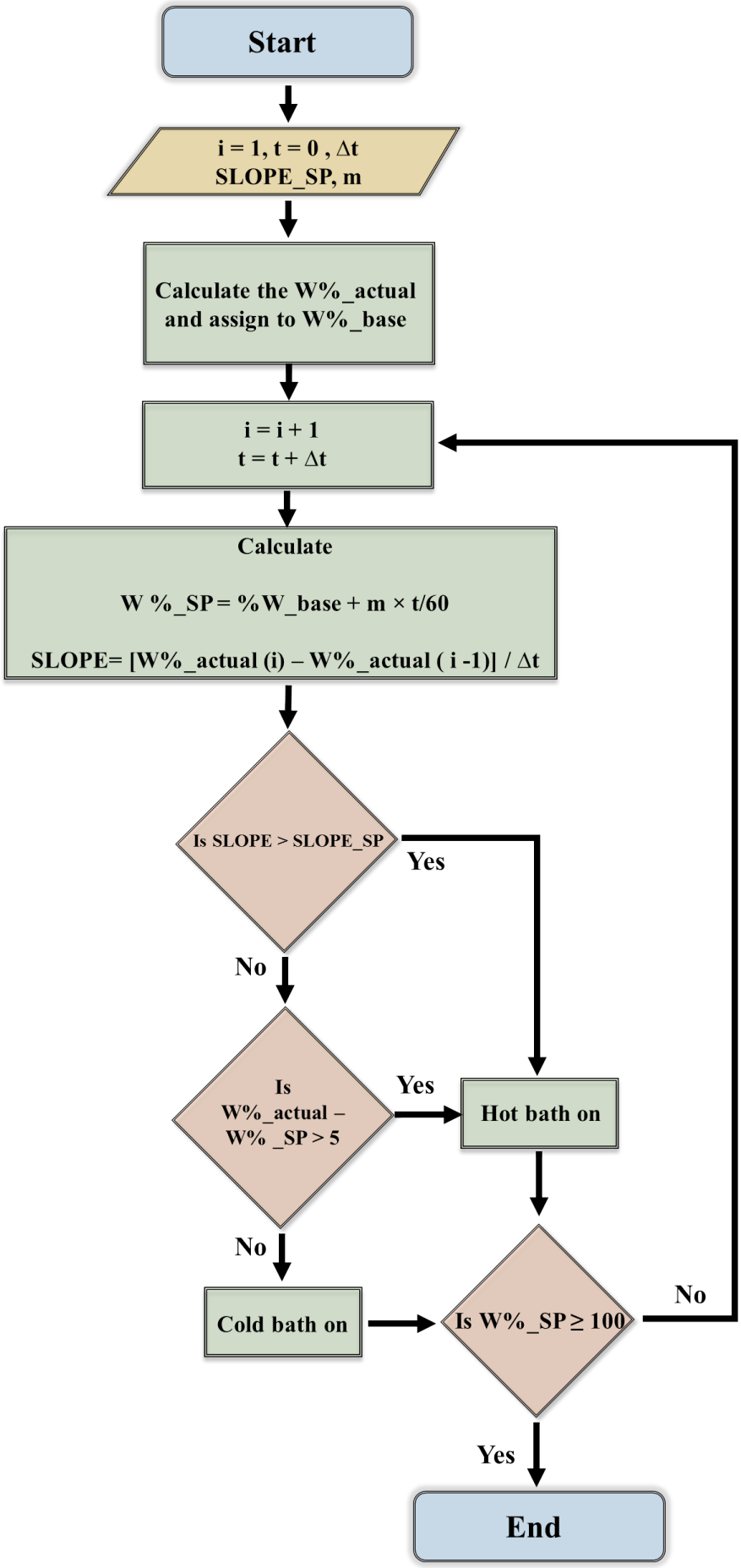

Figure 5.4: Flow-chart of the developed control system for batch cooling crystallisation.

5.3 Temperature Cycling Control Approach for Cooling Crystallisation of Glycine

5.3.1 Experimental Procedure

To carry out the experiments in this chapter, the experimental set-up and camera calibration described in detail in sections 3.4 and 4.3 were employed. A solution of glycine of a concentration of 38 g/ 100 mL of distilled water was prepared at room temperature. This solution was placed in the 2 litre crystalliser which was sealed with a glass cover. Stirring speed was set to 200 rpm to ensure good mixing using a Perspex RCI. A single baffle was used to avoid vortex formation. The camera position was set to focus on the area located between the impeller and the vessel bottom to capture any sedimentation of large crystals formed. The hot source was a Grant water bath operating with a temperature set point of 60˚C, while a Haake water bath was the cold source operating with a temperature set point of 40˚C. These temperature set points were determined through a series of pre-trials.

During the whole run, continuous readings of temperatures were recorded from both water baths and the vessel internal temperature. Images were taken and processed at intervals of 20 seconds. This time interval corresponds to the time at which the slope condition is checked.

5.3.2 Results and Discussion

Different experiments were conducted with the aim to examine the effect of different targets of W%_SP trajectories and different values of variable SLOPE which is the W%_actual change between two successive images (W%_actual(i) – W%_actual(i-1)) over 20 seconds on the robustness and sensitivity of the developed control system described in detail in section 5.2.3 and the quality of the crystals produced. These conditions are summarised in Table 5.2. The target trajectory of W%_SP is calculated by:

$$\mathrm{W\%\_SP} = \mathrm{W\%\_base} + \mathrm{m} * \mathrm{dt}/60 \qquad \textbf{(5.1)}$$

Where *dt* is the time difference between two readings; i.e. 20 seconds for glycine and *m* is the gradient of W%_SP line; i.e. a set-point set by the user, % /min.

Table 5.2: Summary of the different conditions applied to glycine control experiments.

Run Number [-]	m [% /min]	SLOPE_SP [Δ% /20 sec]
1	2	1
2	1	1
3	1	0.5
4	0.5	1
5	0.5	0.5

The vessel and two water baths temperatures, W%_actual and W%_SP profiles and on/off baths during the control stage, for the different conditions mentioned in Table 5.2, are shown in Figure 5.5.

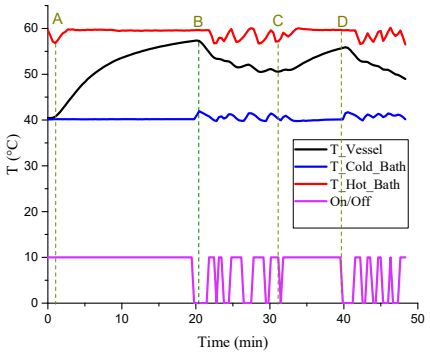

(a) Run 1

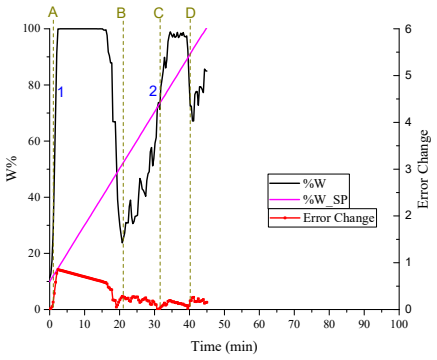

(b) Run 1

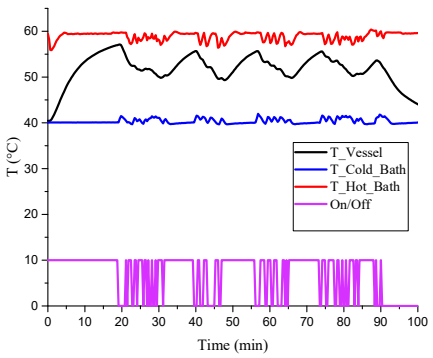

(a) Run 2

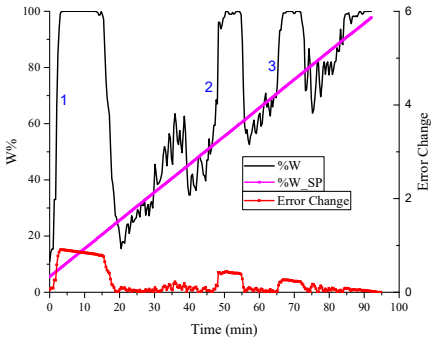

(b) Run 2

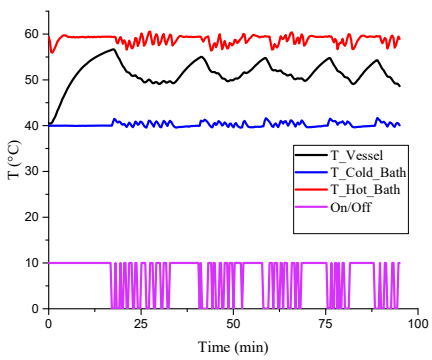

(a) Run 3

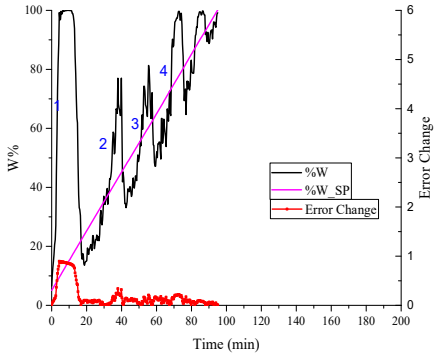

(b) Run 3

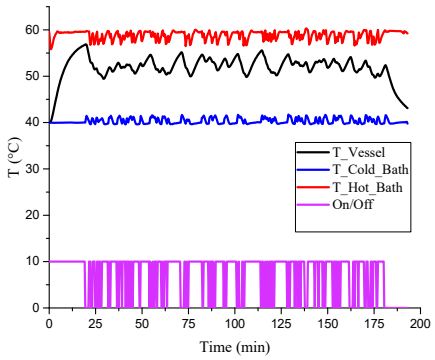

(a) Run 4

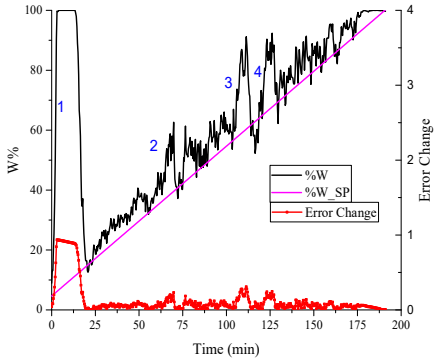

--------(b) Run 4

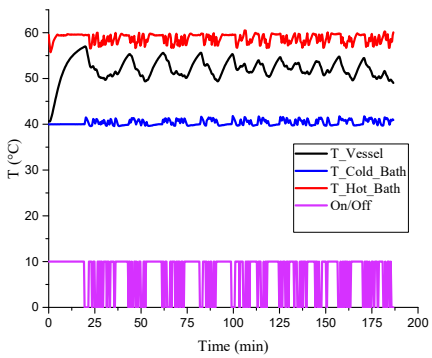

(a) Run 5

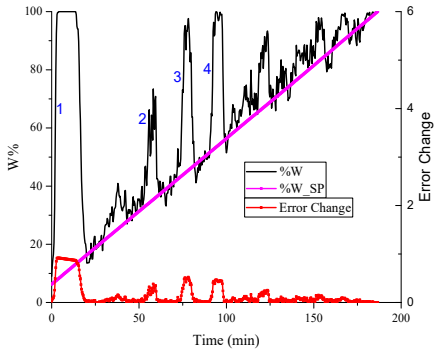

--------(b) Run 5

Figure 5.5: Profiles of vessel and water baths temperatures and On/Off baths (on the left (a)) and W%_actual and W%_SP (on the right (b)) for the control stage of the different conditions summarised in Table 5.2.

With reference to Figure 5.5 Run 1, the two plots show the measured temperatures and the W%_actual values together with the target W%_SP. Point A corresponds to the condition where the reactor temperature drops to 40 °C and spontaneous nucleation takes place. As clearly shown in Figure 5.5 (Run 1, (b)), there is a sudden increase (sharp peak) in W%_actual which is a result of significant primary nucleation and thus

the system switched to heating stage (i.e. the hot bath was on). As a consequence, the vessel temperature started to increase in order to dissolve the fines and follow the W%_SP again, see Figure 5.5 (Run1, (a)). What is clear is that even with the hot and cold switching, the rate of nucleation is higher than the rate at which temperature can change as can be clearly noted from the slope at point A, see Figure 5.5 (Run1, (a) for the temperature and (b) for W%). As the temperature approaches 60 °C, the W%_actual starts to fall to point B. However, the heating dissolved more crystals than needed and the W%_actual dropped to 25% which is 25% less than the W%_SP value (section A-B).

A switching sequence between the hot and cold baths was observed in section B-C based on the SLOPE value. During region B-C, the temperature was higher than that at point A hence the rate of formation of new crystals or the growth of existing ones, was lower hence the rate of change in W%_actual during this time was slower and appears to be controlled. However, as the target rate of W%_SP change was high, the W%_actual was not able to follow the target trajectory leading to a further spontaneous process at point C. This could be a secondary nucleation event since the presence of crystals and temperature condition could only explain the rapid rise in W%_actual. The control system detected this second rapid increase and switched the baths in order to reduce the W%_actual value. Point D shows the system trying to regain control.

From run 1, the initial setting of m to be 2 was clearly too large for the current water bath configuration. Consequently, enough time was not available to grow larger crystals and instead more fines generated that form and dissolve much more quickly. Reducing this value to 1 and below resulted in a better control situation, as seen in runs 2-5. Although there were also some sudden increases in W%_actual, the system was able to bring it back to its target. In other words, the lower the value of m, the better the W%_actual followed the W%_SP. Table 5.3 lists the actual value of W%_actual slope with the target value for the different runs, the time in which each run was controllable, the overall cooling rate during the control stage and the peaks' slope.

Table 5.3: Summary of the target and actual values of m for the different operating conditions as well as the control duration, overall cooling rate and peaks' slope.

Run Number [-]	Target value of m [% /min]	Actual value of m [% /min]	Duration of control [min]	Overall Cooling rate ºC/min	Spike Slope [%/min]
1	2	2.8	24.5	0.22	1) 37 2) 8
2	1	1.02	71.4	0.07	1) 28.2 2) 13.8 3) 13.9
3	1	1.1	77.5	0.1	1) 22 2) 5.2 3) 5 4) 8
4	0.5	0.49	170	0.069	1) 31 2) 3.8 3) 3.2
5	0.5	0.47	165	0.05	1) 33.1 2) 4.5 3) 10.9 4) 12.5

As seen in Table 5.3, a very slow overall cooling rate was produced by the switching technique. This cooling rate is directly proportional to the target value of m. Therefore, a lower value of m would grow larger crystals. This is supported by the crystals' images in section 5.5.

Another interesting point is that the slope of the first spike in each graph is much higher than the slope of the other spikes. The difference in rate of change means that different mechanisms happened. This can be explained because of the primary nucleation that caused the first peak while the other resulted from secondary nucleation as crystals already existed.

Regarding the second variable (SLOPE), its values (0.5, 1) were chosen to be the minimum changes in W%_actual that the camera can detect without continuous on/off switching; this is based on information from experiments outlined in chapter 4.

The results in this work suggest that the developed control system induces an enhanced form of Ostwald ripening through accelerating the growth of large crystals at the expense of the small ones, together with the dissolution of fine material.

5.4 Temperature Cycling Control Approach for Cooling Crystallisation of LGA

5.4.1 Experimental method

A solution of 60g of LGA dissolved in 2 L of distilled water was prepared for each experiment at room temperature. The same experimental set-up, camera calibration and operating conditions mentioned in section 5.3.1 were used with the exception of that hot source (Grant water bath) was set at 70˚C, while the cold source (Haake water bath) was at 15˚C. These temperatures limits were determined through a series of pre-trials to ensure that the upper temperature is able to dissolve the fines quickly and the lower temperature is enough to generate nucleation. The MATLAB code developed for glycine control experiments was applied to monitor and control the whole experiment of LGA. Water baths and vessel temperatures were recorded as well as images were taken and processed at intervals of 30 seconds.

5.4.2 Results and Discussion

Similar to glycine experiments, different targets of W%_SP trajectories and different values of variable SLOPE which is the W%_actual change between two successive images (W%_actual(i) – W%_actual(i-1)) over 30 seconds were examined and are summarised in Table 5.4.

Table 5.4: The different conditions applied to LGA control experiments.

Run Number [-]	M [% /min]	SLOPE_SP [Δ% /30 sec]
1	0.7	1
2	0.5	1
3	0.5	3
4	0.35	1

The vessel and two water baths temperatures, W%_actual and W%_SP profiles and on/off baths during the control stage, for the different conditions mentioned in Table 5.4, are shown in Figure 5.6.

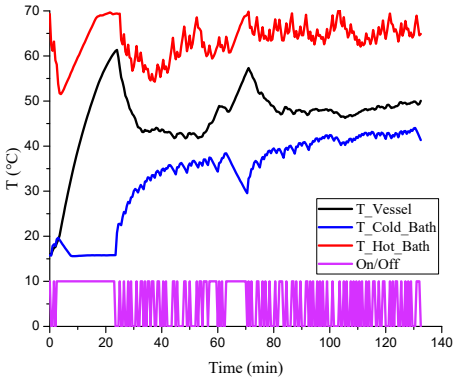

(a) Run 1

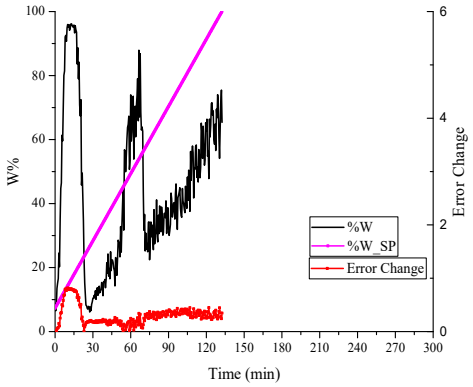

(b) Run 1

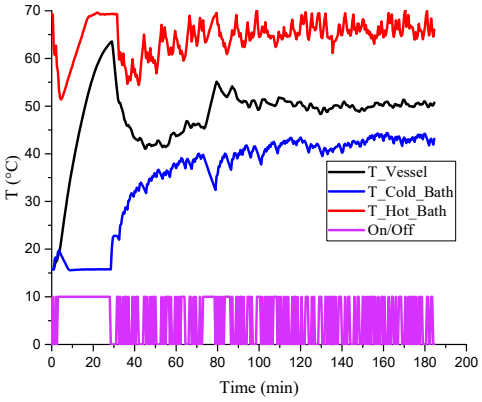

(a) Run 2

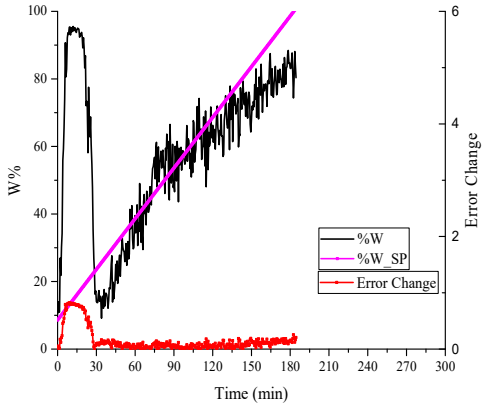

(b) Run 2

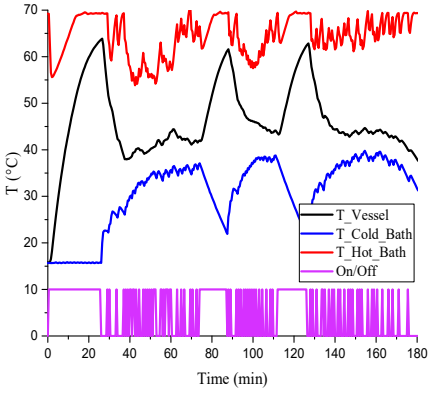

(a) Run 3

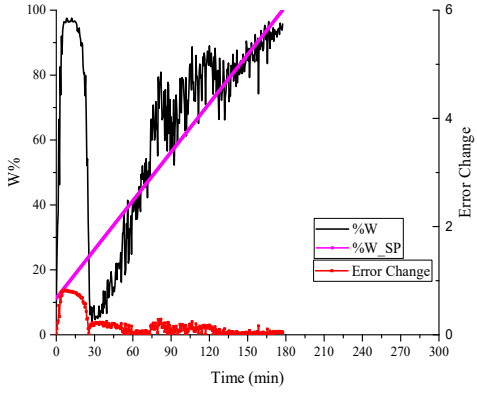

(b) Run 3

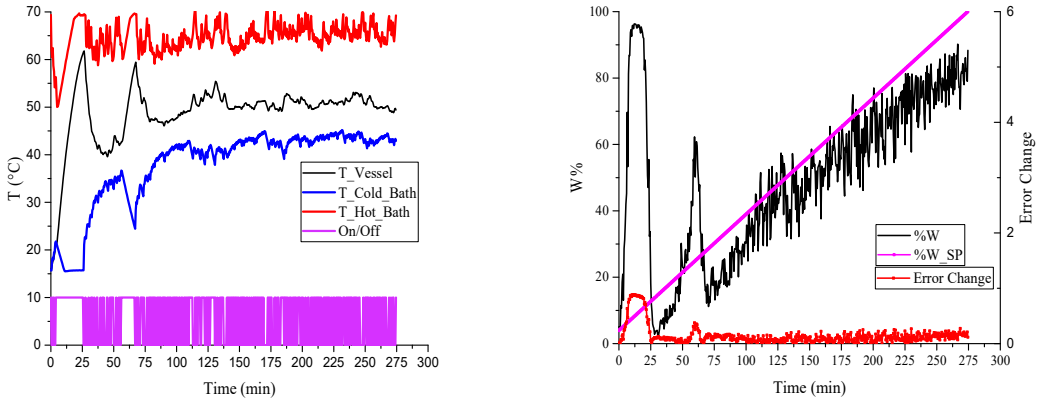

(a) Run 4 (b) Run 4

Figure 5.6: Profiles of vessel and water baths temperatures and On/Off baths (on the left (a)) and W%_actual and W%_SP (on the right (b)) for the control stage of the different conditions summarised in Table 5.4.

Similar to glycine, Figure 5.6 shows that the lower the target (m), the better the W%_actual followed the W%_SP profile. Though, a sudden increase (sharp peak) in W%_actual value was observed as a result of fines formation, the system was able to bring it back to its target.

By comparing runs 2 and 3 which have the same target (m=0.5%/min) but different values of SLOPE (1 and 3 respectively) , it can be noticed that there is an overshoot in W%_actual between 40-80% in run 3 that is not seen in run 2 with lower SLOPE. Therefore, it is worth pointing out that both variables (i.e. target value of m and SLOPE) can affect the performance of the control system and care needed to be taken in choosing these values. This represents a limitation of the technique but can be overcome by an initial series of pre-trial experiments.

With reference to Figure 5.6, an overshoot in W%_actual can be seen at the beginning of the control stage due to uncontrolled primary nucleation. Despite the fact that the control programme was able to dissolve some of the nuclei formed by switching to the hot water bath and returned the W%_actual back to W%_SP trajectory, uncontrolled growth occurred during this period. To maximise the period in which the growth is under control, the control programme, described in section 5.2.3, was modified: a condition was added to the code before the control stage to heat up the solution in order to dissolve the fines that caused the sharp increase in W%_actual and keep only 10% as

seeds. Table 5.5 summarises the conditions for the experiments conducted to investigate the impact of changing the MATLAB code.

Table 5.5: The different conditions applied to LGA control experiments using the modified code.

Run Number [-]	m [% /min]	SLOPE [Δ% /30 sec]
1	0.7	1
2	0.35	1
3	0.2	1

The vessel and two water baths temperatures, W%_actual and W%_SP profiles and on/off baths during the control stage, for the different conditions mentioned in Table 5.5, are shown in Figure 5.7.

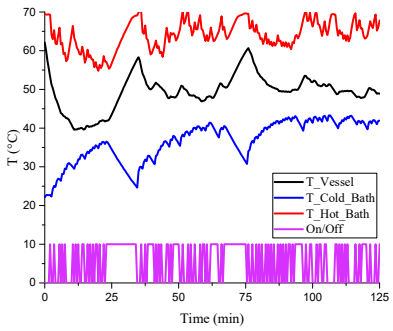

(a) Run 1

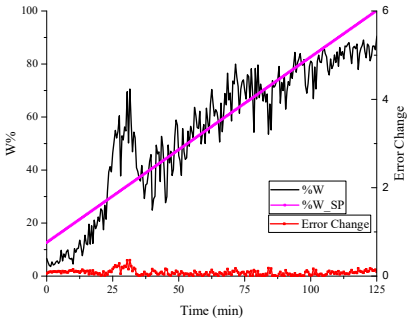

(b) Run 1

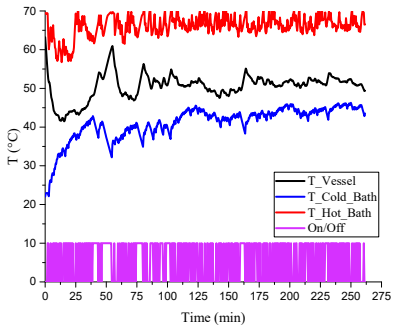

(a) Run 2

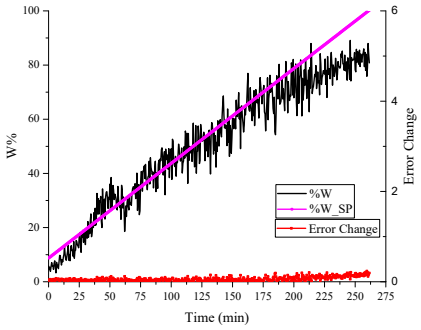

(b) Run 2

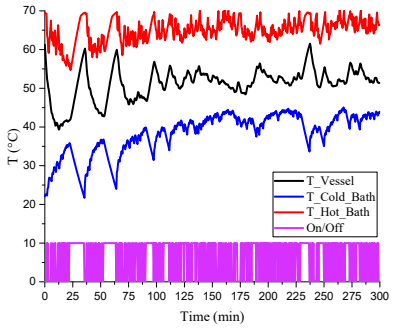

(a) Run 3

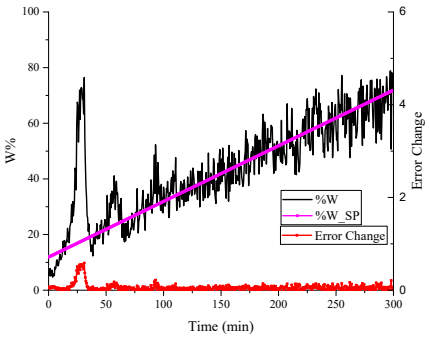

(b) Run 3

Figure 5.7: Profiles of vessel and water baths temperatures and On/Off baths (on the left (a)) and W%_actual and W%_SP (on the right (b)) for the control stage of the different conditions, shown in Table 5.5.

As seen in Figure 5.7, the modified code gave better control than the original code (Figure 5.6) for the different targets of m. In other words, the W%_actual followed the W%_SP trajectory. This will be verified in section 5.5.2 by looking at the quality of the crystals formed in both cases (original and modified codes). Table 5.6 lists the actual value of W%_actual slope with the target value for different runs as well as the time in which the run was controllable and the overall cooling rate.

Table 5.6: Summary of the target and actual values of m, the control duration and overall cooling rate for the different operating conditions outlined in Table 5.5 using the modified code.

Target m [% /min]	Actual m [% /min]	Duration of Control [min]	Overall Cooling Rate [ºC/min]
0.7	0.65	125	0.09
0.35	0.3	261	0.045
0.2	0.19	262.5*	0.022

*: to achieve only 72% for W%_SP

5.5 Crystal Shape Quality

5.5.1 Glycine Crystals

There is a difference in the size of crystals formed as a result of applying different targets of m; the lower the value of m, the bigger the crystal size is, as shown in Figure 5.8. The crystals' images below are extracted from a video recording the crystallisation process using Sony mobile phone camera.

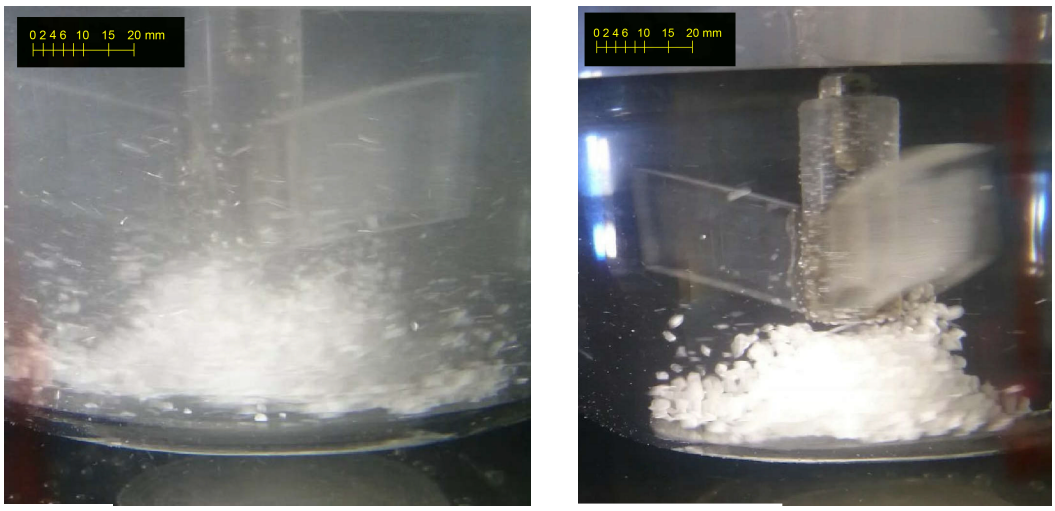

(a) (b)

Figure 5.8: Crystalliser's images at the end of the runs showing glycine crystals for different targets of m: (a) 1 %/min, and (b) 0.5 %/min.

With reference to Figure 5.8, both images were captured at the end of the runs: image (a) at (W%_SP=98% and T_vessel=50.4ºC), and image (b) (W%_SP=97% and T_vessel=50.07ºC). This means that both images are at the same end point and can be compared. Image (a) has more fines (shown by the cloudy solution) than image (b), while larger crystal's size (4.7 mm) is identified in image (b) compared with 2.7 mm in image (a). All these observations confirm the effect of the target value of m on the size of the crystals formed; with lower m, larger crystals can grow. To verify the benefits of the proposed control system, an image of the crystals was taken at room temperature as shown in Figure 5.9. It can be clearly noted that crystals of large size are formed.

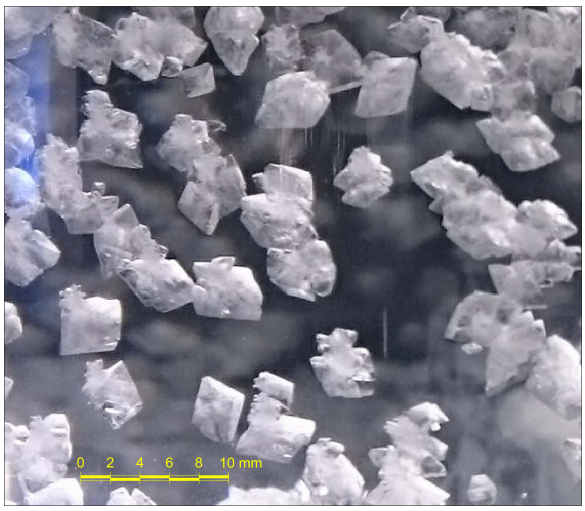

Figure 5.9: Image of Glycine's crystals at room temperature.

5.5.2 LGA Crystals

Similar findings to glycine runs were observed for LGA regarding the effect of the target value of m on the crystal size formed. Figure 5.10 presents images of the crystals captured at the end of each run using the developed optical technique. Due to the limitations of focus and characteristics of the camera, visualising small crystals of micron scale was not possible. The actual size of the crystals shown on the images in Figure 5.10 was calculated from the image width which in turn was determined by inserting a shape of known diameter into the camera's field of view at the same distance to avoid re-focusing the camera.

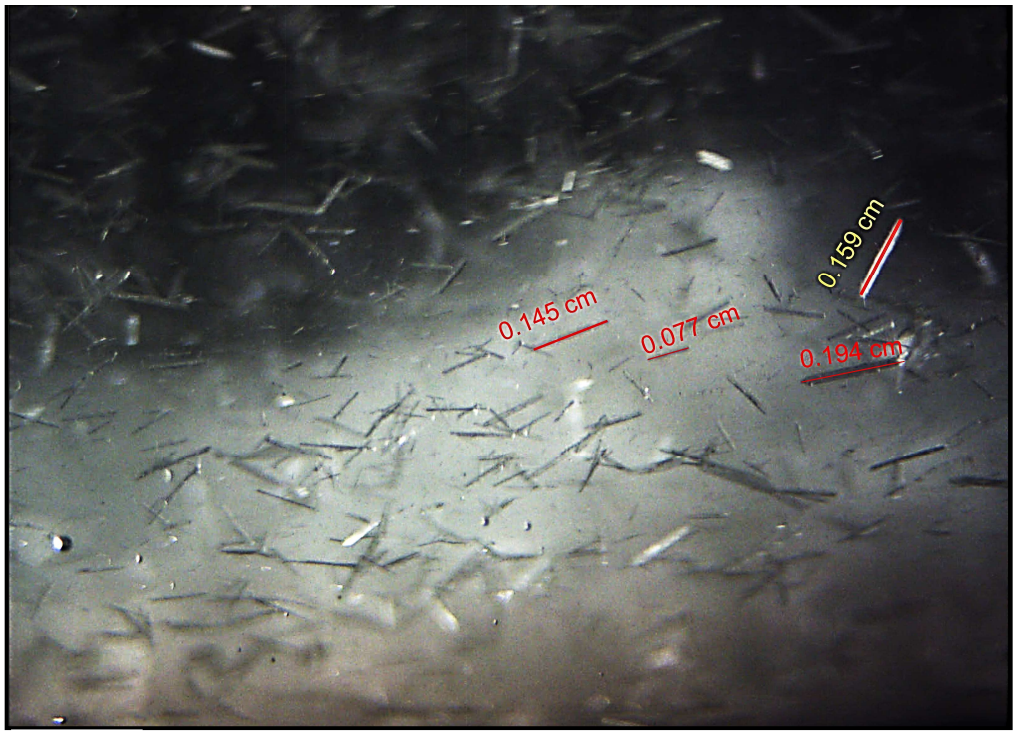

(a)

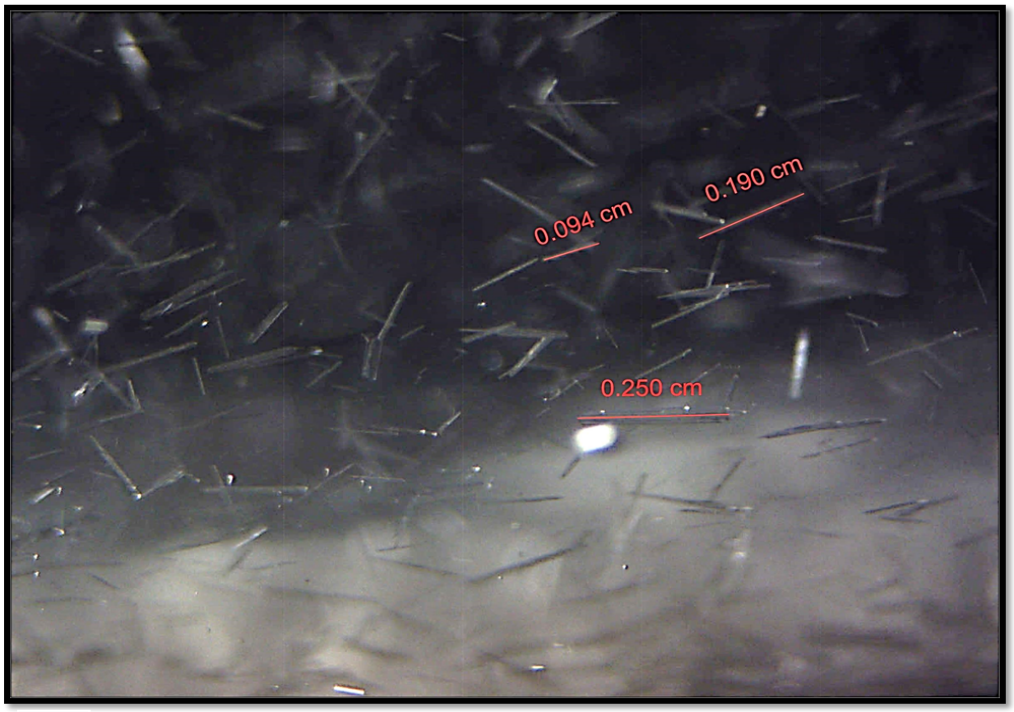

(b)

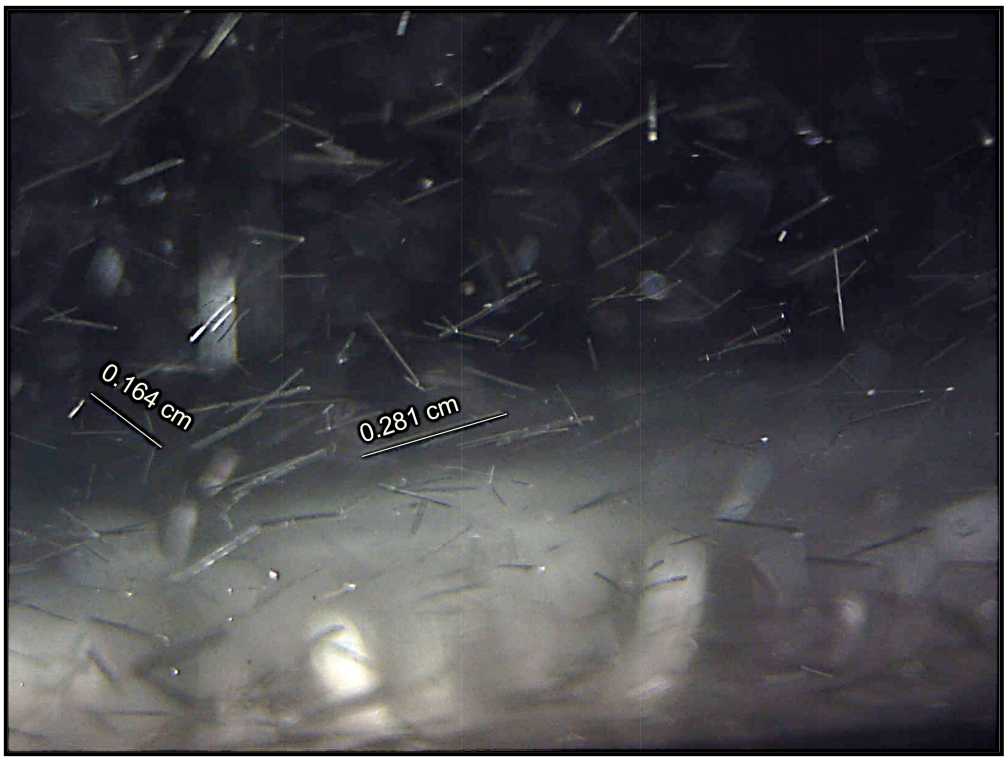

(c)

Figure 5.10: Crystals' images at the end of (a) Run 1:0.7 %/min, (b) Run 2: 0.35 %/min, and Run 3: (c) 0.2 %/min; these runs are shown in Figure 5.7.

It is worth noting that a lower value of m is preferable as it allowed growing much larger crystals than a higher value. Equating the W%_actual measurement to temperature, a slow growth of crystals would correspond to a small rate of temperature

change. This would be consistent with the classical cooling crystallisation where a slow linear cooling could result in controlled growth of crystals. As seen in Figure 5.10, crystals of average size 3mm can be formed. These are far larger than crystals of 200µm reported by (Mougin, 2001) for linear cooling rate of 0.1ºC/min.

In addition, using the modified code (see section 5.4.2) led to better crystals' quality (larger size) than using the original one for the same value of m. This can be clearly seen in Figure 5.11 which shows the crystals' images captured at the end of the run: (a-b) for m= 0.7%/min using the original and modified codes respectively, and (c-d) for m= 0.35%/min using the original and modified codes respectively.

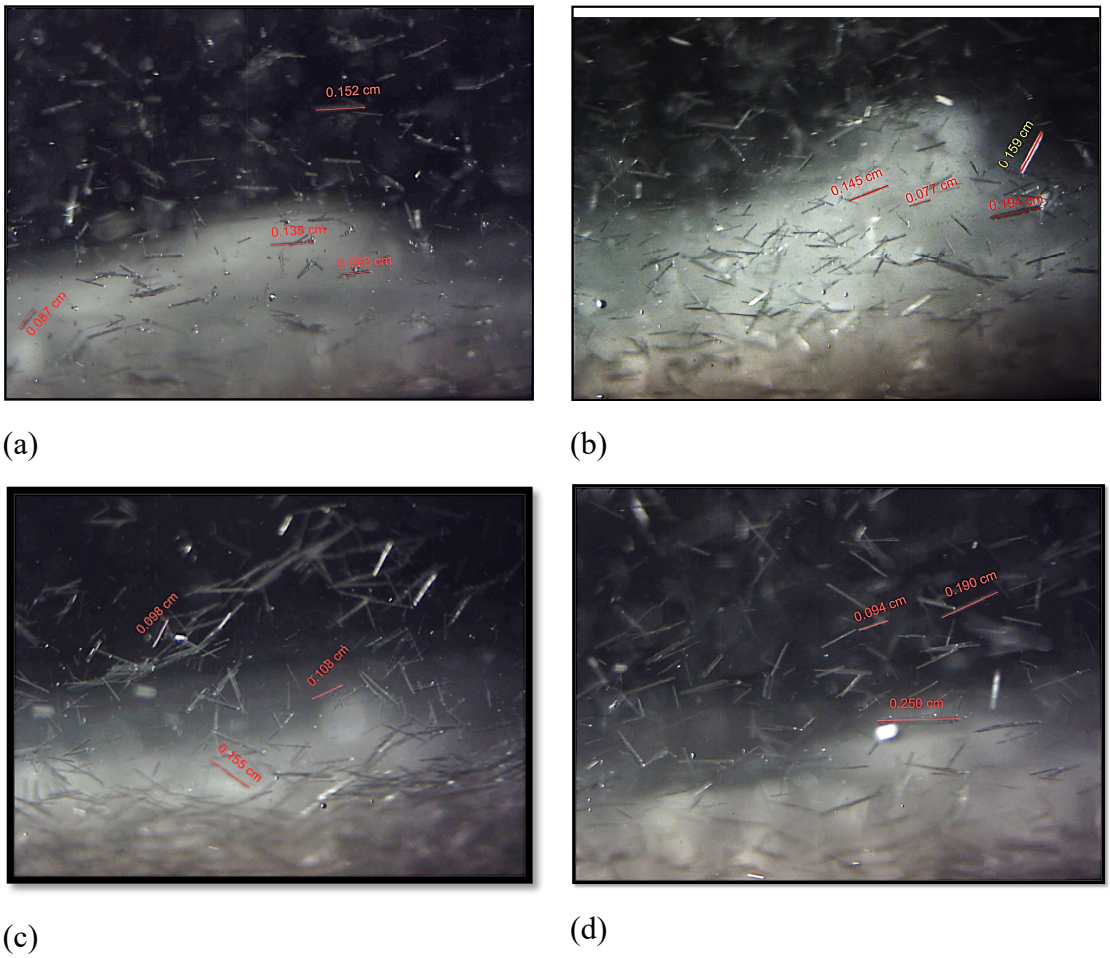

(a) (b)

(c) (d)

Figure 5.11: LGA Crystals' images at the end of different runs: (on the left (a&c)) using original code, (on the right (b&d)) using modified code.

In order to prove further the robustness of the developed control system, the crystals' images for the different operating conditions, shown in Figure 5.10, were analysed

where the number of the crystals was counted and their size was measured. Figure 5.12 presents the variation in the crystal size for the different conditions.

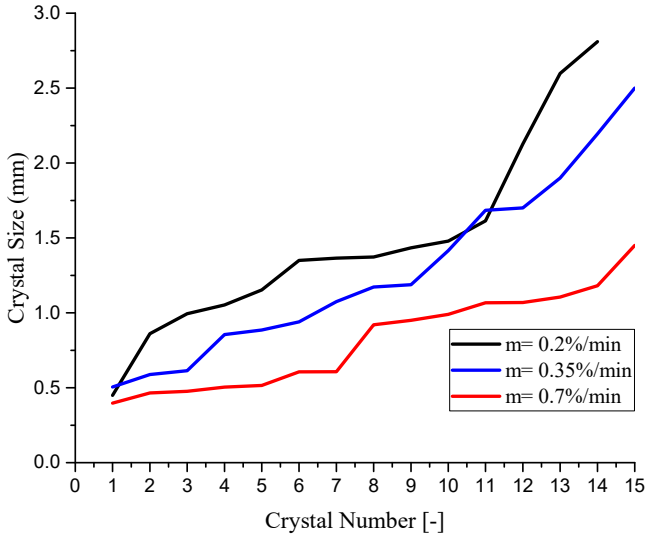

Figure 5.12: Crystals' size retrieved from image analysis for the different values of target m.

As can be clearly seen in Figure 5.12, the lower the value of m (i.e. the slope of the target trajectory), the larger the size of the crystals is. To estimate the number of crystals formed as a result of setting different values of m, the mean crystal size for each condition was calculated from the data plotted in Figure 5.12 and then the volume of each crystal was evaluated. The overall volume of the crystals grown was also determined from the mass of the crystals and the density. The calculated values are given in Table 5.7.

Table 5.7: Summary of the calculated crystals' number and mean size for the different control parameters.

m [%/min]	0.2	0.35	0.7
Mean Crystal Size [mm]	1.5	1.3	0.8
Volume of each Crystal [mm^3]	0.01	0.008	0.005
Total volume [mm^3]	7740	6849	4726
Number of crystals	4.9×10^5	8.1×10^5	14.9×10^5

The results shown in Figure 5.12 and Table 5.7 confirm the effect of the developed control system parameters on the quality of the products. This adds to the validity of the proposed control strategy as a way for improving the crystal quality.

5.6 Approximate Growth Rate Calculation from Control Runs

An estimate of the overall linear growth rate was calculated from the maximum size of the crystal and the time spent to grow the crystal to that size. Tables 5.8 and 5.9 display the results of LGA and glycine growth rates at different control conditions, respectively.

Table 5.8: Summary of the LGA approximate growth rate calculation at different conditions, for runs shown in Figure 5.7.

Change Rate of W%_SP m [%/min]	Maximum Crystal Size [mm]	Time Needed [min]	Approximate Overall Growth Rate [μm/s]
0.7	1.94	148	0.21
0.35	2.5	285	0.145
0.2	2.81	320	0.146

The growth rate was calculated from the maximum length of the crystal in the captured image divided by the time needed to grow that crystal. The calculated values of LGA growth rate are in the range 14×10^{-8} to 21×10^{-8} m/s, whereas the literature values are: 9×10^{-8} m/s for relative supersaturation σ =0.6 (Kitamura and Ishizu, 2000), 1.04×10^{-8} m/s for seeded natural cooling crystallisation (Patchigolla, 2007) with maximum crystal length of 1cm, $(2.44 - 3.14) \times 10^{-8}$ m/s (Wang et al., 2005), 6×10^{-8} m/s (Mougin, 2001) both for linear cooling of 0.1˚C/min with maximum crystal length of 200 μm and a maximum growth rate of 2.4×10^{-6} m/s for α-LGA retrieved by FBRM data (Rajoub, 2014). From this analysis, it would seem that the growth rates achieved here are slightly larger by factors between 2 and 7. The high value of the growth rate can be supported by the crystals images (see section 5.5.2) and explained as a result of the switching technique which accelerated the growth of the larger crystals at the expense of the tiny ones. However, less number of crystals but with much larger size was grown in this case compared to those reported in the literature. An important feature is that in this system the ending temperature for the crystallisation process is higher than that used by the previous workers mentioned above.

Table 5.9: Summary of the approximate glycine growth rate calculation at different conditions compared with the values in the literature.

Change Rate of W%_SP m [%/min]	Maximum Crystal Size [mm]	Control Duration [min]	Approximate Overall Growth Rate [μm/s]
1	2.7	95	0.46
0.5	4.7	184	0.43
(Moscosa-Santillan et al., 2000)	1.3	204	0.11
(Doki et al., 2004)	0.702	210	0.06
(Chew et al., 2007b)	0.257	135	0.03
(Han et al., 2012)	N/A	N/A	0.9

From Table 5.9, it can be seen that the approximate growth rates calculated for glycine are within the range reported in the literature. The high value of the growth rate can be explained as a result of the switching technique which accelerated the growth of the larger crystals at the expense of the undesired fine crystals. However, fewer crystals were grown in this case. It is worth mentioning that the final temperature of the crystallisation process in this PhD work is higher than those of the works reported in the literature.

5.7 Prediction of the Oscillatory Temperature Profile during the Control Stage using the Developed Heat Transfer Model

The mathematical heat transfer model developed in chapter 3 was also used to predict the oscillatory vessel temperature profile during the control stage of both glycine and LGA. This was done by solving equation (3.16) in MATLAB via the fourth order Runge-Kutta method. The experimental and model results for the control runs of glycine and LGA are plotted in Figures 5.13 and 5.14, respectively.

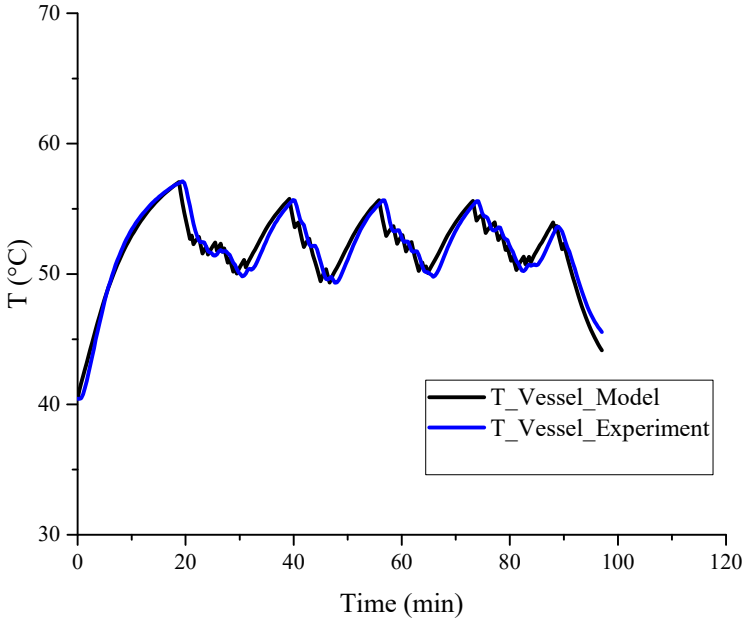

Figure 5.13: A comparison between the experimental data and the model results of the vessel temperature for glycine control run of m=1%/min.

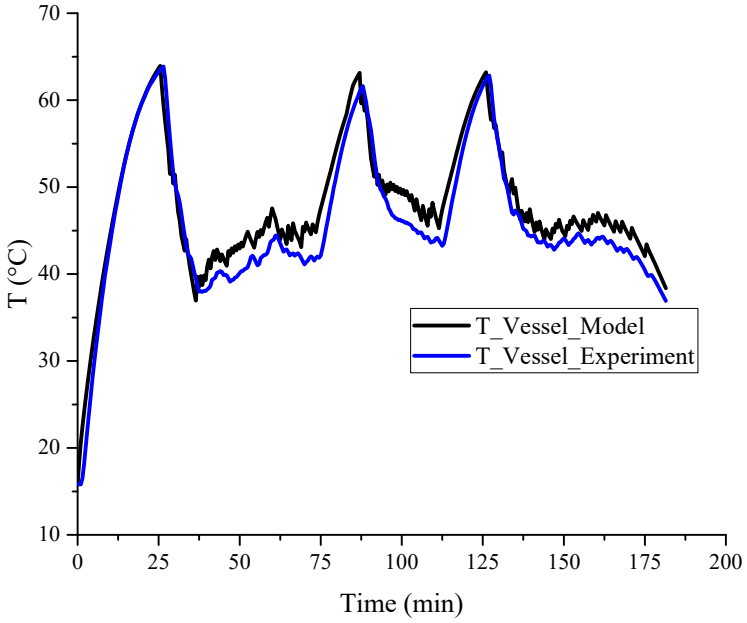

Figure 5.14: A comparison between the experimental data and the model results of the vessel temperature for LGA control run of m=0.5%/min.

As can be seen in Figures 5.13 and 5.14, the model results matched well the experimental data. The optimised value of U was 350 $W.m^{-2}$ K^{-1} for the cold water bath and 200 $W.m^{-2}$ K^{-1} for the hot bath. This would suggest that the jacket fluid itself does

have a big influence on the resistance to heat transfer which in turn depends on the heat exchange system.

5.8 Validation of the Developed Control Strategy

5.8.1 Repeatability

Crystallisation is often classed as a "black art" and this highlights a level of uncertainty in the re-predictability of primary nucleation. A series of experiments to determine the repeatability of the switching system were devised. The W%_actual and W%_SP profiles of the control stage for the two cases used are shown in Figure 5.15.

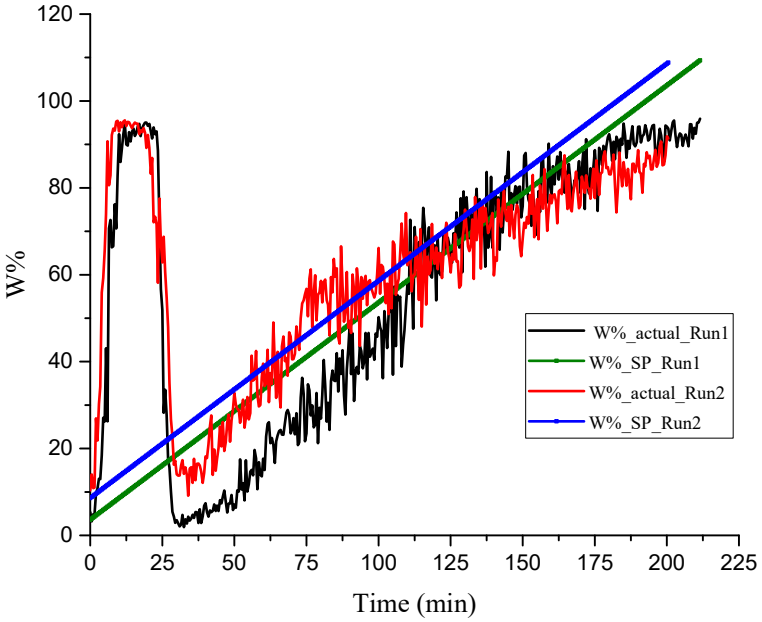

Figure 5.15: A comparison between W%_actual and W%_SP profiles of two runs of LGA for W%_SP gradient (m) of 0.5 %/min.

The results in Figure 5.15 show that there is a slight difference in the W%_actual values during the initial cooling-heating cycle (between 0- 25 minutes), but the overall actual values of the rate of change of W%_actual (in the range 30-200 minutes) are 0.4%/min for run 1 and 0.6 %/min for run 2; while the target value is 0.5%/min. Therefore, it can be said that the switching technique was able to reproduce the same profile of W%_actual with a difference of 20% from the target. This difference can be explained due to the fact that runs had one uncontrolled crystallisation event at the beginning of the curve (between 0-25 minutes) before being brought back under control. This can be

improved by starting the control stage after the sharp increase in W%_actual using the modified code; see section 5.4.2.

5.8.2 Comparison between Linear and Controlled Cooling Profiles

To show another significance of the developed control strategy, a comparison between controlled run using the developed strategy and linear cooling run in terms of the vessel temperature and W%_actual profiles; see Figure 5.16, and the size of crystals formed; see Figure 5.17, is made.

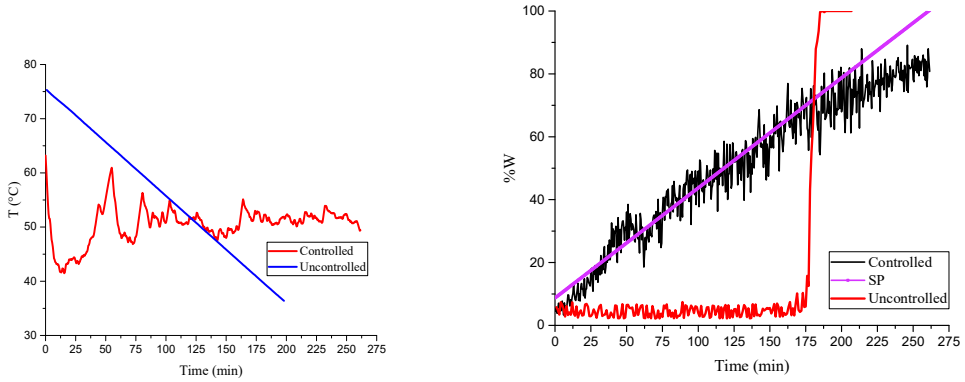

(a) (b)

Figure 5.16: Comparison between controlled (m=0.35 %/min) and linear cooling (0.2º C/min) runs for (a) Vessel temperature profile and (b) W%_actual profile.

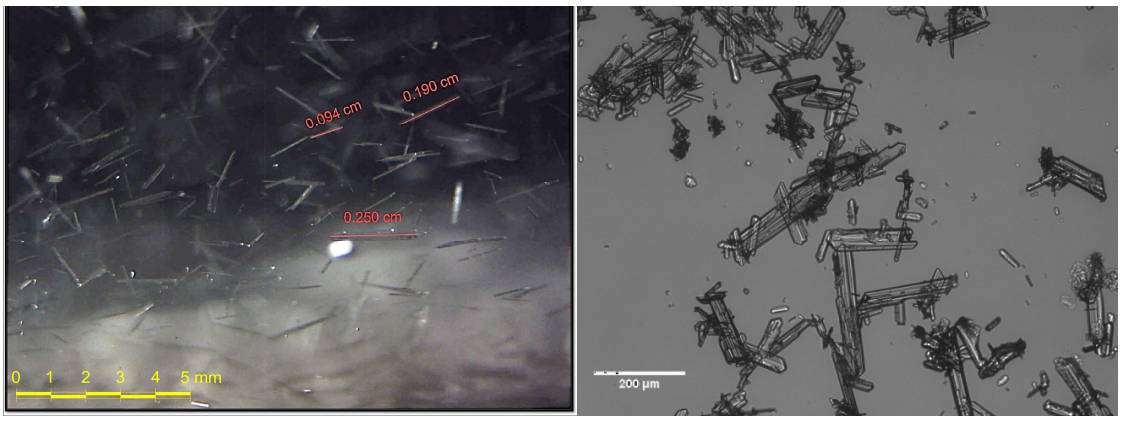

(a) **(b)**

Figure 5.17: Comparison between (a) controlled and (b) linear cooling runs for crystals' size.

With reference to Figure 5.16 (a), the crystalliser's temperature for the linear cooling run was cooled down from 75 to 36 ºC at a constant rate of 0.2º C/min. During the first 175 minutes of the cooling stage, the W%_actual was about 5% due to the presence of air bubbles and other artefacts such as reflections from internal components, but no

crystals were detected. After that, the W%_actual started to increase rapidly because the spontaneous nucleation took place reaching 100% in 12 minutes. This means that the linear cooling profile imposed resulted in uncontrolled primary nucleation which leads to a large number of small crystals in the final solution. This is supported by the photograph (b) in Figure 5.17 which shows crystals of small size in the final solution.

However, for the controlled run (Figure 5.16 (a)), once the nuclei were produced by the spontaneous nucleation, the system then regulated this in a controlled manner where the switching system produced a very slow overall cooling rate of about 0.09 ºC/min so that far larger crystals from the solution were grown. This is backed up by looking at Figure 5.17 (Photograph (a)) which shows far larger crystals. The lower portion of the image is out of focus but suggests that there are a significant number of crystals below the impeller. These crystals would also be of large size since they collect below the impeller and hence are not sufficiently small to be re-dispersed.

In the controlled system, the ending temperature is still high (48.55º C). This means that there is still a lot of solute left in the solution at the end of the process compared to the ones that drop the temperature to 20º C. But the system developed in this PhD was able to grow far larger seeds than that reported previously. Therefore, the solution was then cooled at a linear cooling rate of 0.2ºC/min to 20ºC; these larger seeds (from 2500 microns) continued to grow even larger as shown in Figure 5.18 in which crystal of 4mm can be seen.

Figure 5.18: Picture of β-LGA crystal at end of the run.

This finding is supported by the work of (Khan et al., 2011). In their work, cooling crystallisation experiment was conducted at a linear cooling rate of 0.3ºC/min using external dry seeds ($D_{0.5}$=132 µm and $D_{4,3}$=196 µm). The optical microscopic images of the final product showed larger crystals which confirmed the growth of the seeds (to about 600 microns). Added to that, the work of (Zhang et al., 2016) showed that the quality of the seeds (i.e. their size and shape) did have a big impact on the quality of LGA products as narrow seed size distribution led to produce larger and uniform crystals. This can also verify the outcome of the control experiment where much larger crystals were grown from the large seeds produced during the control stage, as shown in Figure 5.18.

Moreover, (Mougin, 2001) reported that a linear cooling rate of 0.1º C/min can grow crystals of maximum size of 200µm. A simple calculation of the time needed to cool the current system at this rate from (71-20º C) will be 510 minutes. However, using the developed system, the time will be 472 minutes (this time includes the cooling stage to form nuclei, switching stage to grow larger seeds and linear cooling to room temperature) and much larger crystals can grow. This shows an advantage of the developed system over the traditional linear cooling methods.

5.8.3 Degradation Phenomenon of LGA Solutions

As stated in section 5.8.1, the repeatability of the developed strategy was verified. However, the control runs of LGA, when they were carried out using old solutions instead of fresh ones, were uncontrollable. A comparison between fresh and old solutions runs for the same condition ((a) m= 0.5 % /min and (b) m= 0.35 % /min) is illustrated in Figure 5.19.

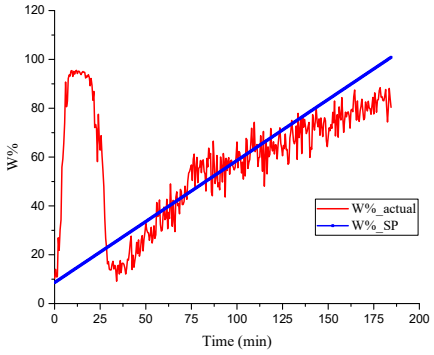

(a)Fresh Solution

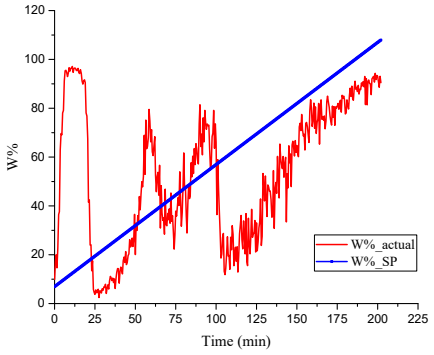

(a) After 9 days

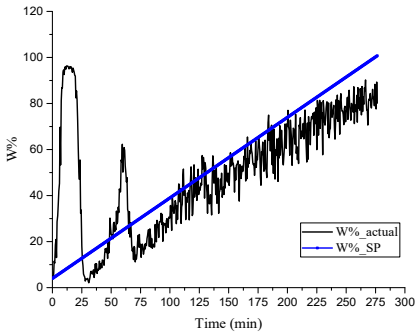

(b)Fresh Solution

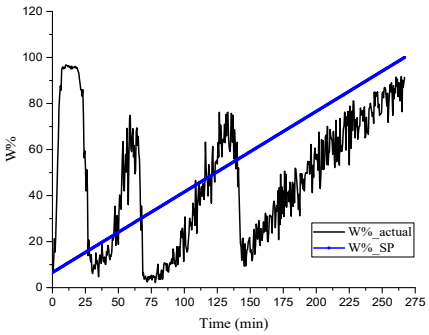

(b) After 7 days

Figure 5.19: A comparison between W%_actual and W%_SP profiles of fresh and old LGA solutions runs for two different value of m: (a) 0.5 % /min and (b) 0.35 % /min.

With reference to Figure 5.19 Run (a), the two plots show the W%_actual together with the W%_SP for fresh solution (on the left) and the same solution after 9 days (on the right). As can be seen in the case of the fresh solution, a rapid rise in W%_actual was observed at the beginning of the control stage due to the occurrence of uncontrolled spontaneous nucleation, but the W%_actual did follow again the W%_SP trajectory. However, for the same solution after 9 days, the W%_actual was not able to follow the W%_SP trajectory after its first sharp increase and more overshoot and undershoot were observed. It seems that the nature of the solution changed, and the crystals formed contained much more fines that could dissolve much quickly when the hot bath was on causing the W%_actual dropped far below the W%_SP trajectory. The same observation is seen in Run (b); for the fresh solution, the W%_actual followed the W%_SP trajectory whereas for the same solution after 7 days, it did not do. This can be explained by the degradation phenomenon of LGA solution as the aqueous LGA solution can convert into pyrrolidone carboxylic acid slowly at room temperature as stated in "Sigma Aldrich Product Information Sheet". Moreover, LGA is poorly soluble material and therefore is prone to ageing that can be a chemical change (Nývlt, 1985). To verify that the solution nature was changed, the run of the old solution was repeated at the same condition and the results for both runs are shown in Figure 5.20.

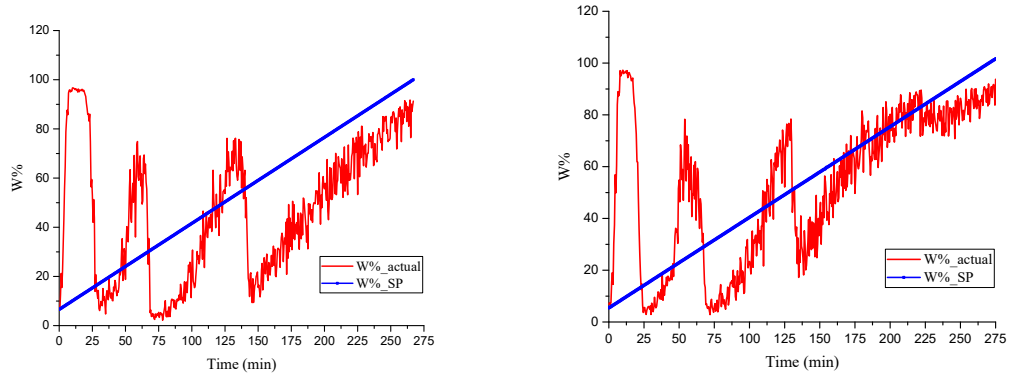

(a) After 7 days **(b) After 8 days**

Figure 5.20: A comparison between W%_actual and W%_SP profiles of old LGA solutions runs for the same condition; m = 0.35 % /min.

As clearly seen in Figure 5.20, in both runs, the same profile of the W%_actual was obtained. The repeatability confirmed the degradation phenomenon of aqueous LGA solutions and also the ability of the developed strategy to pick up this phenomenon of LGA. This degradation was not observed in glycine experiments even though old solutions were used.

5.9 Conclusion

This chapter demonstrated the successful implementation of the control strategy developed in this work on unseeded cooling crystallisation of LGA-water and glycine-water as model systems. The strategy combined the optical technique (camera) as a measurement tool to give input signal for the feedback control system with the switching technique as a manipulated tool**.** The camera is non-intrusive tool which has its advantages over the other techniques that include placing a probe within the crystalliser which causes serious problems; for example changing the hydrodynamics of the system, the contamination if not cleaned properly or the presence of artefacts on the probe's window that can give a wrong signal for the controller. Furthermore, the generation of nuclei and further growth were achieved by a switching method using two water baths: one is hot source and another is cold source. This technique can accordingly change the vessel temperature and overcome the phenomenon of formation large number of fine crystals much faster than linear rate using one water bath.

The sensitivity and robustness of the developed control approach were examined by changing the trajectory set point that the measured variable (W%_actual) should follow and investigating the effect it had on the crystal's size produced.

The results showed that the novel control strategy was capable to promote the growth of large crystals at the expense of undesired fine crystals that could form due to secondary nucleation or breakage. The crystals size at the end of control run was larger than that obtained from uncontrolled run.

Furthermore, the developed control strategy is simple; no modelling is required and not expensive to implement the complete system.

Chapter 6
Conclusion and Recommendations for Future Works

This chapter outlines the main findings that can be drawn from the work carried out in this thesis. In addition, proposals for future works on further improvement of the developed control system and the possibility of extending its application to larger scale and continuous mode are suggested.

6.1 Conclusions

The main conclusions that arise from the experimental work presented in this thesis are summarised as follows:

6.1.1 On-line Monitoring of Batch Cooling Crystallisation Using the Developed Process Video Imaging (PVI) System

A low cost PVI system was developed and used to monitor batch cooling crystallisation of two different chemicals; L-glutamic acid and glycine in solution with water. LGA and glycine were chosen due to their different solubility curves; glycine has a stronger relation to temperature than LGA; meaning that minor changes in temperature can result in more deposition of solids. In addition, these materials have been studied by others and the key crystallisation behaviour has been reported in the literature. This provided data to validate the results obtained in this work using the developed PVI system.

In this thesis, the apparent MSZW for LGA was calculated at various operating conditions including the linear cooling rate, agitation speed and impeller material. The results were found to agree with the current literature in that:

- The MSZW widened as the cooling rate increased. The apparent MSZW changes as a function of cooling rate because primary nucleation occurs at lower temperatures as cooling rate is increased. The value of MSZW measured using the PVI system was narrower than that measured by turbidity probe (Liang, 2002), suggesting PVI is more sensitive than turbidity probe methods.
- The MSZW decreased as the stirring speed increased. However, it started to increase again when the speed was at 400 rpm due to the formation of central vortex which retarded the occurrence of nucleation.

- The MSZW in the case of using stainless steel impeller was narrower than that for an impeller constructed from Perspex. Applying paint to both stainless steel and Perspex impellers tended to make the crystallisation temperature the same for the same agitation speed. However, at higher stirring speed, differences in the MSZWs for the two painted impellers were seen. This different crystallisation behaviour must be related to the hydrodynamics produced by these two impellers.

The above findings are in a good agreement with those previously reported using different techniques such as FBRM (Rajoub, 2014) and turbidity probe (Liang, 2002).

Nucleation kinetics parameters for both the polythermal and isothermal data were calculated according to KBHR method, again with numerical values of the order similar to those previously quoted in literature (Liang et al., 2004; Patchigolla, 2007; Sangwal, 2009b). An interesting point was the observation of nucleation order dependence on the solute solubility; the results showed an inverse relation between nucleation order and solubility, in other words, the glycine with higher solubility had a lower value of nucleation order than LGA. This observation was in agreement with trends stated previously by other researchers (Sangwal, 2009b).

All the above findings showed the feasibility of the developed PVI as on-line monitoring technique for crystallisation process of both fast and slow growing systems; glycine and LGA respectively. Repeatability of the PVI system was found to be good with virtually no difference in MSZW when experiments were repeated under exactly the same conditions. The PVI system did suffer from being able to detect relatively large crystals, but the method could be improved by using higher resolution cameras or through focusing on a smaller viewing area. As such the PVI method becomes no different from a turbidity probe.

6.1.2 Studying the Effect of Changing the Temperature Conditions at the Crystalliser's Wall by Introducing Rapid Heating and Rapid Cooling via Switching Technique on the Cooling Crystallisation of Glycine

Cooling crystallisation is normally performed by controlling the temperature of the fluid inside the crystalliser by manipulating the temperature of the thermal fluid in the jacket.

Therefore the number of control "handles" available to manipulate the crystallisation is limited to a) imposing a linear or non-linear cooling profile, or b) changing the agitator speed. Seeding, addition of anti-solvent or habit modification material is considered in this thesis to be adding foreign material into the mixture and therefore not useful in direct control.

In addition, the mixing inside batch vessels fitted with retreat curve impellers is known to be not uniform. CFD simulations presented by (Liang, 2002; Bentham, 2015) and others, show that the flow is circulatory with fluid pulled down to the impeller in the centre of the vessel, and be reflected up from the base to travel up towards the surface close to the vessel inside wall. There is also an area of stagnation directly below the impeller. CFD and heat transfer simulations showed that there is a very small temperature difference close to the cool inner wall during cooling crystallisation. To offer an alternative method of manipulating the crystallisation, a novel switching method has been developed. This switching method induces a rapid change in the temperature of the crystalliser wall. Therefore, of significant interest was to investigate the effect of the temperature conditions at the wall of the vessel on crystallisation behaviour. In response to this, the influence of switching technique supplying hot and cold water to the crystalliser's jacket on the cooling crystallisation of glycine was studied for the first time.

Key variables studied included the switching frequency and duration as well as the temperature set point of the two water baths used to provide the hot and cold sources. Using two water baths mimics the system often used to control industrial crystallisers, rather than the single water bath that is often used in laboratory experiments. The results showed:

1. That switching between a hot and cold source produced a ramp type temperature profile within the crystalliser. This is due to the inherent lag in heat transfer. A model using a simple heat balance observed potential changes in the overall heat transfer coefficient suggesting a higher rate of heat transfer is achieved using the switching system than a single water bath.

2. That by switching between two water baths, the average temperature within the crystalliser once the system has stabilised (i.e. at steady state) is the average of

the two baths temperatures. Additional cold can therefore be achieved by lowering either the set point of the cold bath or the frequency (i.e. the ratio of the hot bath to the cold one). Due to the heat transfer characteristics inherent in this system (i.e. $U.A/\dot{M}.c_p$), switching resulted in an oscillation in the vessel temperature rather than steady average temperature. However, at lower switching frequencies, a lower level of fluctuation will be seen in vessel temperature.

3. For the primary nucleation temperature of glycine and in principle for LGA, the impact of switching frequency was to change the induction time before the first crystals were observed, but the initiation point of crystallisation i.e. the temperature the PVI system indicated primary nucleation was of similar value to when linear cooling profile was applied. The higher the ratio of cold: hot, the shorter the time became and vice versa. This is explained by the cold source being (ON) for the longest period which caused larger temperature gradient adjacent to the vessel wall causing higher supersaturation and inducing faster nucleation.

4. The temperature set point of each water bath has a significant impact on the conditions within the crystalliser; the higher the set point of hot bath, the longer the time for nucleation (slow down) whilst the lower the set point of cold bath, the faster the nucleation took place (speed up).

5. The same switching frequency (1:1) but with different durations showed similar temperature profiles and therefore had the same crystallisation temperature. This is expected since the same amount of heat is removed regardless of the duration. However, shorter induction time was observed for the longest duration that the cold bath was connected to the vessel.

6. That a controlled cooling profile can be achieved from the switching technique by selecting the switching frequency and the temperature set point of the hot and cold baths which is not possible by the crash cooling. Closer inspection of the vessel temperature achieved under switching shows that it is possible to have a rapid non-linear cooling profile followed by an approximately linear profile

which gives an additional method to initiate crystallisation as opposed to linear or crash cooling. Section 4.8.3 discusses this for glycine.

7. Interestingly, the switching technique showed an impact on the growth stage (after the primary nucleation occurred) where the W% did not change as sharp as the traditional cooling profiles runs displaying the role of the hot source in dissolving the fines. This observation means that if the switching frequency is manipulated, it will give a level of control for W% change that is not possible with one water bath as the case in traditional cooling profiles.

6.1.3 Developing Control Strategy that Improves the Quality of LGA and Glycine Crystals by Combining PVI and Switching Techniques:

A control approach that integrated PVI system with switching technique was successfully developed and implemented on cooling crystallisation of LGA-water and glycine-water systems. This approach was based on following target profile of the white pixels percentage change (W%_SP) through changing the temperature of crystalliser's wall via the new switching method. Using two baths in switching creates a system that has a faster response time to changes detected within the crystalliser than using one water bath. The novel switching system therefore has the advantage to respond quickly to primary and subsequently secondary nucleation of unseeded and self-seeded crystallisation.

The results of the experiments covered in chapter 5 demonstrate that the combined PVI-switching system:

- Has the ability to detect the initial primary nucleation event and re-dissolve many of the new nuclei. The system dissolves the smaller nuclei, allowing any larger sized initial crystals to remain. The control system then let the large crystals to grow at a slow cooling rate. Any further nucleation events, which are due to secondary nucleation, are captured and the new crystals from that are dissolved leaving the larger growing crystals;

- Yields high quality seed crystals in terms of size and a lower concentration of fines. Potentially, the large seed crystals would provide more than adequate solution for further growth using a linear cooling profile. The large crystals observed from analysis of PVI images at the end of the control stage were

several orders of magnitude larger than crystals normally seen in batch crystallisation. The PVI-switching control system essentially enhances processes such as Ostwald ripening, in comparison with those using the conventional methods;

- Applies successfully on both low growing system (LGA-water) and fast growing system (glycine-water), displaying the robustness of the developed approach;

- The parameters that create a stable PVI-switching system depend on the solubility characteristics of the solute involved. The minimum values of these parameters are 0.5 %/min and 0.2%/min for glycine and LGA respectively;

- The combined switching- PVI technique has proved to be highly reproducible. As a consequence the technique shows that for LGA if the same solution is used repeatedly (more than 3 times), the solution degrades. The degradation phenomenon of aqueous LGA is a known problem.

All the above findings confirmed the validity of relatively inexpensive developed PVI technique for monitoring crystallisation process. Adding to that, the developed control system that combined PVI and switching techniques, offered a simple but effective method to improve the product quality which is, in turn, of economic importance in terms of minimising the operation time and cost.

6.2 Proposals for Future Works

Based on the results demonstrated in this thesis, further investigation of some aspects can be recommended for future works which are:

- To monitor and control other model systems, for instance, salicylic acid which has lower solubility than LGA, adipic acid with solubility lies between LGA and glycine, monosodium glutamate (MSG) with high solubility and long induction time. In addition, only cooling crystallisation has been explored here, and therefore, it is important to apply the developed system to other crystallisation methods, such as anti-solvent crystallisation which is

also utilised in many processes. Examples of systems can be studied are: LGA in methanol-water mixture, glycine in ethanol-water, etc.

- To link the switching system to other monitoring techniques: ATIR and FBRM. This would give more information about the solution supersaturation and the number of particles present in, leading to develop more robust control approach.

- The developed switching technique was capable to respond to the initial nucleation faster than a current one water bath system. Therefore, it would be of interest to understand the relationship between the kinetics for nucleation and that for the heat transfer, assuming that both of them are the dominant kinetic features, through coupled dynamic heat transfer and population balance modelling.

- To scale up the crystallisation process and investigate how the smaller focused area of the camera can be capable to give reliable information to control the crystallisation process as well as the efficiency of the switching mechanism as already known that the time constant will be much higher than that for laboratory scale.

- The camera positioning and lenses calibration employed in this work offered a good monitoring technique where MSZW and nucleation kinetics parameters were successfully determined. On the other hand, no crystal's shape or morphology was defined. Therefore, it will be of potential to improve the camera specifications which could allow a clearer imaging of the individual crystal and help on-line measurement of crystal's shape and morphology.

- Recently, there are growing trends to move crystallisation process from batch to continuous operation and thus extending the application of the developed control system to continuous crystalliser will be of great importance for industrial implementation.

References

Aamir, E., Nagy, Z. & Rielly, C. 2010a. Evaluation of the effect of seed preparation method on the product crystal size distribution for batch cooling crystallization processes. *Crystal growth & design,* 10**,** 4728-4740.

Aamir, E., Nagy, Z. K. & Rielly, C. D. 2010b. Optimal seed recipe design for crystal size distribution control for batch cooling crystallisation processes. *Chemical Engineering Science,* 65**,** 3602-3614.

Abbas, A., Nobbs, D. & Romagnoli, J. A. 2002a. Investigation of on-line optical particle characterization in reaction and cooling crystallization systems. Current state of the art. *IOP Science* 13**,** 249-256.

Abbas, A., Nobbs, D. & Romagnoli, J. A. 2002b. Investigation of on-line optical particle characterization in reaction and cooling crystallization systems. Current state of the art. *Measurement Science and Technology,* 13**,** 349.

Abu Bakar, M. R. 2010. *Process analytical technology based approaches for the monitoring and control of size and polymorphic form in pharmaceutical crystallisation processes.* PhD, Loughborough University.

Abu Bakar, M. R., Nagy, Z. K. & Rielly, C. D. 2010. Investigation of the effect of temperature cycling on surface features of sulfathiazole crystals during seeded batch cooling crystallization. *Crystal growth & design,* 10**,** 3892-3900.

Abu Bakar, M. R., Nagy, Z. K., Saleemi, A. N. & Rielly, C. D. 2009. The impact of direct nucleation control on crystal size distribution in pharmaceutical crystallization processes. *Crystal Growth and Design,* 9**,** 1378-1384.

Al-Jibbouri, S., Strege, C. & Ulrich, J. 2002. Crystallization kinetics of epsomite influenced by pH-value and impurities. *Journal of crystal growth,* 236**,** 400-406.

Alvarez, A. J. 2007. Development of Crystallization Processes for Pharmaceutical Applications.

Artisan 2000. Instruction Manual F6 and N6 Circulator including all Baths. *In:* CORPORATION, A. S. (ed.).

Bakar, M. R. A., Nagy, Z. K. & Rielly, C. D. 2009. Seeded batch cooling crystallization with temperature cycling for the control of size uniformity and polymorphic purity of sulfathiazole crystals. *Organic Process Research & Development,* 13**,** 1343-1356.

Baldan, A. 2002. Review progress in Ostwald ripening theories and their applications to nickel-base superalloys Part I: Ostwald ripening theories. *Journal of materials science,* 37**,** 2171-2202.

Barrett, P. & Becker, R. Nucleation, solubility, and polymorph identification: The interrelationship as monitored with lasentec FBRM. ABSTRACTS OF PAPERS OF THE AMERICAN CHEMICAL SOCIETY, 2002. AMER CHEMICAL SOC 1155 16TH ST, NW, WASHINGTON, DC 20036 USA, U641-U642.

Barrett, P. & Glennon, B. 2002. Characterizing the metastable zone width and solubility curve using Lasentec FBRM and PVM. *Chemical Engineering Research and Design,* 80**,** 799-805.

Barrett, P., Smith, B., Worlitschek, J., Bracken, V., O'Sullivan, B. & O'Grady, D. 2005. A review of the use of process analytical technology for the understanding and optimization of production batch crystallization processes. *Organic Process Research & Development,* 9**,** 348-355.

Becker, R. & Döring, W. 1935. Kinetische behandlung der keimbildung in übersättigten dämpfen. *Annalen der Physik,* 416**,** 719-752.

Beckmann, W. 2000. Seeding the desired polymorph: background, possibilities, limitations, and case studies. *Organic process research & development,* 4**,** 372-383.

Bentham, E. J. 2015. *Conjugate Transfer Processes in a Pilot-Scale Unbaffled Agitated Vessel with a Plain Jacket.* PhD, University of Leeds.

Berthoud, A. L. 1912. *Theorie de la formation des faces d'un cristal*.

Borissova, A., Jammoal, Y., Javed, K., Lai, X., Mahmud, T., Penchev, R., Roberts, K. & Wood, W. 2005. Modeling the precipitation of L-glutamic acid via acidification of monosodium glutamate. *Crystal growth & design,* 5**,** 845-854.

Borissova, A., Khan, S., Mahmud, T., Roberts, K. J., Andrews, J., Dallin, P., Chen, Z.-P. & Morris, J. 2008. In situ measurement of solution concentration during the batch cooling crystallization of l-glutamic acid using ATR-FTIR spectroscopy coupled with chemometrics. *Crystal Growth and Design,* 9**,** 692-706.

BORISSOVA, A., KHAN, S., MAHMUD, T., ROBERTS, K. J., ANDREWS, J., DALLIN, P., CHEN, Z.-P. & MORRIS, J. 2009. In Situ Measurement of Solution Concentration during the Batch Cooling Crystallization of L-Glutamic Acid using ATR-FTIR Spectroscopy Coupled with Chemometrics. *Crystal growth & design,* 9**,** 692-706.

Braatz, R. D. 2002. Advanced control of crystallization processes. *Annual reviews in control,* 26**,** 87-99.

Braatz, R. D., Fujiwara, M., Ma, D. L., Togkalidou, T. & Tafti, D. K. 2002. Simulation and new sensor technologies for industrial crystallization: A review. *International Journal of Modern Physics B,* 16**,** 346-353.

Bravi, M., Di Cave, S., Mazzarotta, B. & Verdone, N. 2003. Relating the attrition behaviour of crystals in a stirred vessel to their mechanical properties. *chemical engineering journal,* 94**,** 223-229.

Brown, C. J. 2012. *Characterization of crystallization processes with video imaging.* PhD, Heriot-Watt University.

BrukerOptics. 2011. *Attenuated Total Reflection (ATR) – a versatile tool for FTIR spectroscopy* [Online]. Available: https://goo.gl/pb9fFw.

Buonacucina, C. 2010. *Mixing and suspension studies in an industrial batch crystalliser.* Master of Philosophy, Heriot-Watt University.

Burton, W.-K., Cabrera, N. & Frank, F. 1951. The growth of crystals and the equilibrium structure of their surfaces. *Philosophical Transactions of the Royal Society of London A: Mathematical, Physical and Engineering Sciences,* 243**,** 299-358.

Caillet, A., Rivoire, A., Galvan, J.-M., Puel, F. & Fevotte, G. 2007. Crystallization of monohydrate citric acid. 1. In situ monitoring through the joint use of Raman spectroscopy and image analysis. *Crystal Growth & Design,* 7**,** 2080-2087.

Cashell, C., Corcoran, D. & Hodnett, B. 2004. Control of polymorphism and crystal size of L-glutamic acid in the absence of additives. *Journal of crystal growth,* 273**,** 258-265.

Chawla, G. & Bansal, A. K. 2004. Challenges in polymorphism of pharmaceuticals. *CRIPS,* 5**,** 9-12.

Chen, C.-C. & Song, Y. 2004. Solubility modeling with a nonrandom two-liquid segment activity coefficient model. *Industrial & engineering chemistry research,* 43**,** 8354-8362.

Chen, J., Sarma, B., Evans, J. M. & Myerson, A. S. 2011. Pharmaceutical crystallization. *Crystal Growth & Design,* 11**,** 887-895.

Chew, J. W., Black, S. N., Chow, P. S. & Tan, R. B. 2007a. Comparison between open-loop temperature control and closed-loop supersaturation control for cooling

crystallization of glycine. *Industrial & engineering chemistry research,* 46**,** 830-838.

Chew, J. W., Chow, P. S. & Tan, R. B. 2007b. Automated in-line technique using FBRM to achieve consistent product quality in cooling crystallization. *Crystal growth & design,* 7**,** 1416-1422.

Choudhury, S., Utiger, L., Riesen, R. & Groth, U. 2016. Heat Transport in Agitated Vessels: Estimating the Heat Transfer Coefficient. Schwerzenbach, Switzerland: Mettler-Toledo GmbH AutoChem.

Chung, S. H., Ma, D. L. & Braatz, R. D. 2000. Optimal model-based experimental design in batch crystallization. *Chemometrics and Intelligent Laboratory Systems,* 50**,** 83-90.

Corzo, D. M. C., Borissova, A., Hammond, R. B., Kashchiev, D., Roberts, K. J., Lewtas, K. & More, I. 2014. Nucleation mechanism and kinetics from the analysis of polythermal crystallisation data: methyl stearate from kerosene solutions. *CrystEngComm,* 16**,** 974-991.

Costa, C. B. & Maciel Filho, R. 2005. Evaluation of optimisation techniques and control variable formulations for a batch cooling crystallization process. *Chemical engineering science,* 60**,** 5312-5322.

Costa, C. B. B., Maciel, M. R. W. & Maciel Filho, R. 2007. Considerations on the crystallization modeling: Population balance solution. *Computers & chemical engineering,* 31**,** 206-218.

De Dietrich Process Systems, I. 2015. Introductory Guide to Glass-lined Steel Equipment. De Dietrich Process Systems, Inc.

Deneau, E. & Steele, G. 2005. An in-line study of oiling out and crystallization. *Organic process research & development,* 9**,** 943-950.

Desikan, S., Parsons, R. L., Davis, W. P., Ward, J. E., Marshall, W. J. & Toma, P. H. 2005. Process development challenges to accommodate a late-appearing stable polymorph: A case study on the polymorphism and crystallization of a fast-track drug development compound. *Organic process research & development,* 9**,** 933-942.

Doki, N., Kubota, N., Sato, A. & Yokota, M. 2001. Effect of cooling mode on product crystal size in seeded batch crystallization of potassium alum. *Chemical Engineering Journal,* 81**,** 313-316.

Doki, N., Seki, H., Takano, K., Asatani, H., Yokota, M. & Kubota, N. 2004. Process control of seeded batch cooling crystallization of the metastable α-form glycine using an in-situ ATR-FTIR spectrometer and an in-situ FBRM particle counter. *crystal growth & design,* 4**,** 949-953.

Donnelly, A., White, G., Wilkinson, D., Mahmud, T. & Roberts, K. J. 2005. CFD Modelling. Chemicals Behaving Badly II.

Dowling, R. J. 2012. A Study of the Nucleation and Growth of glycine and DL-alanine.

Dunuwila, D. D. & Berglund, K. A. 1997. ATR FTIR spectroscopy for in situ measurement of supersaturation. *Journal of Crystal Growth,* 179**,** 185-193.

Eggers, J., Kempkes, M. & Mazzotti, M. 2008. Measurement of size and shape distributions of particles through image analysis. *Chemical Engineering Science,* 63**,** 5513-5521.

Erdemir, D., Lee, A. Y. & Myerson, A. S. 2009. Nucleation of crystals from solution: classical and two-step models. *Accounts of chemical research,* 42**,** 621-629.

Feng, L. & Berglund, K. A. 2002. ATR-FTIR for determining optimal cooling curves for batch crystallization of succinic acid. *Crystal growth & design,* 2**,** 449-452.

Ferrari, E. S. & Davey, R. J. 2004. Solution-mediated transformation of α to β L-glutamic acid: Rate enhancement due to secondary nucleation. *Crystal growth & design,* 4**,** 1061-1068.

Févotte, G. 2002. New perspectives for the on-line monitoring of pharmaceutical crystallization processes using in situ infrared spectroscopy. *International journal of pharmaceutics,* 241**,** 263-278.

Forgione, M., Mesbah, A., Bombois, X. & Van den Hof, P. M. Iterative learning control of supersaturation in batch cooling crystallization. American Control Conference (ACC), 2012, 2012. IEEE, 6455-6460.

Freundlich, H. & Hatfield, H. S. 1926. Colloid and capillary chemistry.

Fujiwara, M., Chow, P. S., Ma, D. L. & Braatz, R. D. 2002. Paracetamol crystallization using laser backscattering and ATR-FTIR spectroscopy: metastability, agglomeration, and control. *Crystal Growth & Design,* 2**,** 363-370.

Fujiwara, M., Nagy, Z. K., Chew, J. W. & Braatz, R. D. 2005. First-principles and direct design approaches for the control of pharmaceutical crystallization. *Journal of Process Control,* 15**,** 493-504.

Garside, J. 1985. Industrial crystallization from solution. *Chemical Engineering Science,* 40**,** 3-26.

Garside, J. & Davey, R. 2000. From Molecules to Crystallizers—An Introduction to Crystallization Ch. 3. Oxford Univ. Press.

Garside, J. & Davey, R. J. 1980. Invited review secondary contact nucleation: kinetics, growth and scale-up. *Chemical Engineering Communications,* 4**,** 393-424.

Garside, J., Mersmann, A. & Nývlt, J. 2002. *Measurement of crystal growth and nucleation rates*, IChemE.

Gibbs, J. W., Bumstead, H. A. & Longley, W. R. 1928. *The collected works of J. Willard Gibbs*, Longmans, Green and Company.

Gmehling, J. G., Anderson, T. F. & Prausnitz, J. M. 1978. Solid-liquid equilibria using UNIFAC. *Industrial & Engineering Chemistry Fundamentals,* 17**,** 269-273.

Golnabi, H. 2006. Precise CCD image analysis for planar laser-induced fluorescence experiments. *Optics & Laser Technology,* 38**,** 152-161.

Graber, T., Taboada, M., Alvarez, M. & Schmidt, E. 1999. Determination of mass transfer coefficients for crystal growth of nitrate salts. *Crystal Research and Technology,* 34**,** 1269-1277.

Grant 2010. Low temperature bath/circulator R series: Operating Manual. *In:* SCIENTIFIC, G. (ed.) 5 ed.

Groen, H. 2001a. *On-line monitoring and control of supersaturation in batch crystallisers for organic fine chemical products using ATR FTIR spectroscopy.* PhD.

Groen, H. 2001b. On-line monitoring and control of supersaturation in batch crystallisers for organic fine chemical products using ATR FTIR spectroscopy.

Groen, H. & Roberts, K. J. 2001. Nucleation, growth, and pseudo-polymorphic behavior of citric acid as monitored in situ by attenuated total reflection Fourier transform infrared spectroscopy. *The Journal of Physical Chemistry B,* 105**,** 10723-10730.

Grön, H., Borissova, A. & Roberts, K. J. 2003. In-process ATR-FTIR spectroscopy for closed-loop supersaturation control of a batch crystallizer producing monosodium glutamate crystals of defined size. *Industrial & engineering chemistry research,* 42**,** 198-206.

Guo, Z., Zhang, M., Li, H., Wang, J. & Kougoulos, E. 2005. Effect of ultrasound on anti-solvent crystallization process. *Journal of Crystal Growth,* 273**,** 555-563.

Gürbüz, H. & Özdemir, B. 2003. Experimental determination of the metastable zone width of borax decahydrate by ultrasonic velocity measurement. *Journal of Crystal Growth,* 252**,** 343-349.

Gutwald, T. & Mersmann, A. 1990. Batch cooling crystallization at constant supersaturation: technique and experimental results. *Chemical Engineering & Technology,* 13**,** 229-237.

Han, G., Chow, P. S. & Tan, R. B. 2012. Direct comparison of α-and γ-glycine growth rates in acidic and basic solutions: New insights into glycine polymorphism. *Crystal Growth & Design,* 12**,** 2213-2220.

Harner, R. S., Ressler, R. J., Briggs, R. L., Hitt, J. E., Larsen, P. A. & Frank, T. C. 2008. Use of a fiber-optic turbidity probe to monitor and control commercial-scale unseeded batch crystallizations. *Organic Process Research & Development,* 13**,** 114-124.

Hermann, T. 2003. Industrial production of amino acids by coryneform bacteria. *Journal of biotechnology,* 104**,** 155-172.

Hermanto, M. W., Braatz, R. D. & Chiu, M. S. 2011. Integrated batch-to-batch and nonlinear model predictive control for polymorphic transformation in pharmaceutical crystallization. *AIChE journal,* 57**,** 1008-1019.

Hermanto, M. W., Chow, P. S. & Tan, R. B. 2010. Implementation of focused beam reflectance measurement (FBRM) in antisolvent crystallization to achieve consistent product quality. *Crystal Growth & Design,* 10**,** 3668-3674.

Hixson, A. & Knox, K. 1951. Effect of agitation on rate of growth of single crystals. *Industrial & Engineering Chemistry,* 43**,** 2144-2151.

Jiang, S. 2012. *An examination of sonocrystallization kinetics of l-glutamic acid.* PhD, University of Leeds.

Jones, A. 1974. Optimal operation of a batch cooling crystallizer. *Chemical Engineering Science,* 29**,** 1075-1087.

Jones, A. G. & Mullin, J. 1974. Programmed cooling crystallization of potassium sulphate solutions. *Chemical Engineering Science,* 29**,** 105-118.

Kadam, S. S., Kramer, H. J. & ter Horst, J. H. 2011. Combination of a single primary nucleation event and secondary nucleation in crystallization processes. *Crystal Growth & Design,* 11**,** 1271-1277.

Kashchiev, D. 2000. *Nucleation*, Butterworth-Heinemann.

Kashchiev, D., Borissova, A., Hammond, R. B. & Roberts, K. J. 2010a. Dependence of the critical undercooling for crystallization on the cooling rate. *The Journal of Physical Chemistry B,* 114**,** 5441-5446.

Kashchiev, D., Borissova, A., Hammond, R. B. & Roberts, K. J. 2010b. Effect of cooling rate on the critical undercooling for crystallization. *Journal of Crystal Growth,* 312**,** 698-704.

Keane, R. D. & Adrian, R. J. 1992. Theory of cross-correlation analysis of PIV images. *Applied scientific research,* 49**,** 191-215.

Kempkes, M., Vetter, T. & Mazzotti, M. 2010. Measurement of 3D particle size distributions by stereoscopic imaging. *Chemical Engineering Science,* 65**,** 1362-1373.

Khan, S. 2008. *Application of on-line ATR-FTIR spectroscopy for monitoring, controlling and scaling-up the batch crystallisation of L-glutamic acid.* PhD, University of Leeds.

Khan, S., Ma, C. Y., Mahmud, T., Penchev, R. Y., Roberts, K. J., Morris, J., Özkan, L., White, G., Grieve, B. & Hall, A. 2011. In-process monitoring and control of supersaturation in seeded batch cooling crystallisation of l-glutamic acid: from laboratory to industrial pilot plant. *Organic Process Research & Development,* 15**,** 540-555.

Kim, K.-J. & Mersmann, A. 2001. Estimation of metastable zone width in different nucleation processes. *Chemical Engineering Science,* 56**,** 2315-2324.

Kim, S., Lotz, B., Lindrud, M., Girard, K., Moore, T., Nagarajan, K., Alvarez, M., Lee, T., Nikfar, F. & Davidovich, M. 2005. Control of the particle properties of a drug substance by crystallization engineering and the effect on drug product formulation. *Organic process research & development,* 9**,** 894-901.

Kim, S., Wei, C. & Kiang, S. 2003. Crystallization process development of an active pharmaceutical ingredient and particle engineering via the use of ultrasonics and temperature cycling. *Organic process research & development,* 7**,** 997-1001.

Kitamura, M. 2002a. Controlling factor of polymorphism in crystallization process. *Journal of Crystal Growth,* 237–239, Part 3**,** 2205-2214.

Kitamura, M. 2002b. Controlling factor of polymorphism in crystallization process. *Journal of Crystal Growth,* 237**,** 2205-2214.

Kitamura, M. & Ishizu, T. 2000. Growth kinetics and morphological change of polymorphs of L-glutamic acid. *Journal of crystal growth,* 209**,** 138-145.

Korovessi, E. & Linninger, A. A. 2005. *Batch processes*, CRC Press.

Korovessi, E. L., A. A. 2005. *Batch Processes*, CRC.

Kougoulos, E., Jones, A., Jennings, K. & Wood-Kaczmar, M. 2005. Use of focused beam reflectance measurement (FBRM) and process video imaging (PVI) in a modified mixed suspension mixed product removal (MSMPR) cooling crystallizer. *Journal of Crystal Growth,* 273**,** 529-534.

Kubota, N. 2008. A new interpretation of metastable zone widths measured for unseeded solutions. *Journal of Crystal Growth,* 310**,** 629-634.

Kubota, N., Doki, N., Yokota, M. & Sato, A. 2001. Seeding policy in batch cooling crystallization. *Powder technology,* 121**,** 31-38.

Lafferrere, L., Hoff, C. & Veesler, S. 2004. In situ monitoring of the impact of liquid-liquid phase separation on drug crystallization by seeding. *Crystal growth & design,* 4**,** 1175-1180.

Lai, W. T. 1996. Particle image velocimetry- A new approach in experimental fluid research. *Three-dimensional velocity and vorticity measuring and image analysis techniques***,** 61-92.

Lakghomi, B., Kolahchian, E., Jalali, A. & Farhadi, F. 2008. Coil and Jacket's Effects on Internal Flow Behavior & Heat Transfer in Stirred Tanks. *World Academy of Science, Engineering and Technology, International Journal of Chemical, Molecular, Nuclear, Materials and Metallurgical Engineering,* 2**,** 383-387.

Larsen, P., Rawlings, J. & Ferrier, N. 2007. Model-based object recognition to measure crystal size and shape distributions from in situ video images. *Chemical Engineering Science,* 62**,** 1430-1441.

Larsen, P. A. & Rawlings, J. B. 2008. Assessing the reliability of particle number density measurements obtained by image analysis. *Particle & Particle Systems Characterization,* 25**,** 420-433.

Lee, M.-y. & Parkinson, G. M. 1999. Growth rates of gibbsite single crystals determined using in situ optical microscopy. *Journal of crystal growth,* 198**,** 270-274.

Lewiner, F., Fevotte, G., Klein, J. & Puel, F. 2001a. Improving batch cooling seeded crystallization of an organic weed-killer using on-line ATR FTIR measurement of supersaturation. *Journal of Crystal Growth,* 226**,** 348-362.

Lewiner, F., Fevotte, G., Klein, J. & Puel, F. 2002. An online strategy to increase the average crystal size during organic batch cooling crystallization. *Industrial & engineering chemistry research,* 41**,** 1321-1328.

Lewiner, F., Klein, J., Puel, F. & Fevotte, G. 2001b. On-line ATR FTIR measurement of supersaturation during solution crystallization processes. Calibration and applications on three solute/solvent systems. *Chemical Engineering Science,* 56**,** 2069-2084.

Liang, J. K. 2002. *Process scale dependence of L-glutamic acid batch crystallised from aqueous solution in relation to reactor internals, reactant mixing and process conditions.* PhD, Heriot-Watt University.

Liang, K., White, G., Wilkinson, D., Ford, L. J., Roberts, K. J. & Wood, W. M. 2004. An examination into the effect of stirrer material and agitation rate on the nucleation of L-glutamic acid batch crystallized from supersaturated aqueous solutions. *Crystal growth & design,* 4**,** 1039-1044.

Liotta, V. Automated metastable zones. Lasentec Users Forum, 2001. 25-28.

Liotta, V. & Sabesan, V. 2004. Monitoring and feedback control of supersaturation using ATR-FTIR to produce an active pharmaceutical ingredient of a desired crystal size. *Organic process research & development,* 8**,** 488-494.

Llinàs, A. & Goodman, J. M. 2008. Polymorph control: past, present and future. *Drug Discovery Today,* 13**,** 198-210.

Löffelmann, M. & Mersmann, A. 2002. How to measure supersaturation? *Chemical Engineering Science,* 57**,** 4301-4310.

Louhi-Kultanen, M., Karjalainen, M., Rantanen, J., Huhtanen, M. & Kallas, J. 2006. Crystallization of glycine with ultrasound. *International journal of pharmaceutics,* 320**,** 23-29.

Lung-Somarriba, B. L. M., Moscosa-Santillan, M., Porte, C. & Delacroix, A. 2004. Effect of seeded surface area on crystal size distribution in glycine batch cooling crystallization: a seeding methodology. *Journal of crystal growth,* 270**,** 624-632.

Lyczko, N., Espitalier, F., Louisnard, O. & Schwartzentruber, J. 2002. Effect of ultrasound on the induction time and the metastable zone widths of potassium sulphate. *Chemical Engineering Journal,* 86**,** 233-241.

Mangin, D., Puel, F. & Veesler, S. 2009. Polymorphism in processes of crystallization in solution: a practical review. *Organic Process Research & Development,* 13**,** 1241-1253.

Marciniak, B. 2002. Density and ultrasonic velocity of undersaturated and supersaturated solutions of fluoranthene in trichloroethylene, and study of their metastable zone width. *Journal of Crystal Growth,* 236**,** 347-356.

McConville, F. X. 2002. The pilot plant real book. *FXM Engineering and Design, Worcester, MA*.

McConville, F. X. 2007. *The Pilot Plant Real Book,* Worcester, FXM Engineering and Design

Mersmann, A. & Bartosch, K. 1998. How to predict the metastable zone width. *Journal of crystal growth,* 183**,** 240-250.

Mettler-Toledo AutoChem, I. 2011. Best practices for crystallization development. A review of modern techniques. *Mettler-Toledo AutoChem* http://goo.gl/xlENct. Columbia, USA.

Mitchell, N. A. & Frawley, P. J. 2010. Nucleation kinetics of paracetamol–ethanol solutions from metastable zone widths. *Journal of Crystal Growth,* 312**,** 2740-2746.

Mo, Y., Dang, L. & Wei, H. 2011. Solubility of α-form and β-form of l-glutamic acid in different aqueous solvent mixtures. *Fluid Phase Equilibria,* 300**,** 105-109.

Mohan, R., Boateng, K. A. & Myerson, A. S. 2000. Estimation of crystal growth kinetics using differential scanning calorimetry. *Journal of crystal growth,* 212**,** 489-499.

Monnier, O., Fevotte, G., Hoff, C. & Klein, J. 1997. Model identification of batch cooling crystallizations through calorimetry and image analysis. *chemical engineering science,* 52**,** 1125-1139.

Moscosa-Santillan, M., Bals, O., Fauduet, H., Porte, C. & Delacroix, A. 2000. Study of batch crystallization and determination of an alternative temperature-time profile by on-line turbidity analysis—application to glycine crystallization. *Chemical engineering science,* 55**,** 3759-3770.

Mougin, P. M.-J. 2001. *In situ and on-line ultrasonic attenuation spectroscopy for particle sizing during the crystallisation of organic fine chemicals.* PhD, Heriot-Watt University.
Moynihan, H. A. & Kelly, D. M. 2012. *Phenacetin Crystallization: Cooling Regimes and Crystal Morphology*, InTech Open Access Publisher.
Mullin, J. & Jancic, S. 1979. Interpretation of metastable zone widths. *Transactions of the Institution of Chemical Engineers,* 57**,** 188-193.
Mullin, J. & Nývlt, J. 1971. Programmed cooling of batch crystallizers. *Chemical Engineering Science,* 26**,** 369-377.
Mullin, J. W. 1997. *Crystallization,* Oxford Butterworth-Heinemann.
Mullin, J. W. 2001. *Crystallization,* Oxford Butterworth-Heinemann.
Myerson, A. 2002. *Handbook of industrial crystallization*, Butterworth-Heinemann.
Nagy, Z., Fujiwara, M. & Braatz, R. Optimal control of combined cooling and anti-solvent pharmaceutical crystallization. BIWIC 2006: 13th International Workshop on Industrial Crystallization, September 13-15, 2006, Delft University of Technology, Delft, The Netherlands, 2006. IOS Press, 16.
Nagy, Z. K. & Braatz, R. D. 2004. Open-loop and closed-loop robust optimal control of batch processes using distributional and worst-case analysis. *Journal of process control,* 14**,** 411-422.
Nagy, Z. K., Fujiwara, M., Woo, X. Y. & Braatz, R. D. 2008. Determination of the kinetic parameters for the crystallization of paracetamol from water using metastable zone width experiments. *Industrial & Engineering Chemistry Research,* 47**,** 1245-1252.
Nernst, W. 1904. Theory of reaction velocity in heterogenous systems. *Zeit. physikal. Chem,* 47**,** 52-55.
Ness, J. & White, E. Collision nucleation in an agitated crystallizer. Chemical Engineering Progress Symposium Series, 1976. 153.
Ni, X. & Liao, A. 2008. Effects of cooling rate and solution concentration on solution crystallization of L-glutamic acid in an oscillatory baffled crystallizer. *Crystal Growth and Design,* 8**,** 2875-2881.
Ni, X. & Liao, A. 2010. Effects of mixing, seeding, material of baffles and final temperature on solution crystallization of l-glutamic acid in an oscillatory baffled crystallizer. *Chemical Engineering Journal,* 156**,** 226-233.
Noyes, A. A. & Whitney, W. R. 1897. The rate of solution of solid substances in their own solutions. *Journal of the American Chemical Society,* 19**,** 930-934.
Nývlt, J. 1968. Kinetics of nucleation in solutions. *Journal of Crystal Growth,* 3**,** 377-383.
Nývlt, J. 1985. *The kinetics of industrial crystallization*, Elsevier Science Ltd.
Nývlt, J., Sohnel, O., Matuchova, M. & Broul, M. 1985. The kinetics of industrial crystallization Elsevier. Amsterdam.
O'Rourke, A. M. & MacLoughlin, P. 2005. A comparison of measurement techniques used in the analysis of evolving liquid–liquid dispersions. *Chemical Engineering and Processing: Process Intensification,* 44**,** 885-894.
Ostwald, W. 1900. On the assumed isomerism of red and yellow mercury oxide and the surface-tension of solid bodies. *Z. Phys. Chem,* 34**,** 495.
Ostwald, W. 1901. Blocking of Ostwald ripening allowing long-term stabilization. *Phys. Chem,* 37**,** 385.
Patchigolla, K. 2007. *Particle process measurements: shape and size with crystal growth and nucleation kinetics.* PhD, Heriot-Watt University.
Patience, D. B. 2002. *Crystal engineering through parti-cle size and shape, monitoring, modeling and control.* PhD, University of Wisconsin.

Perry, R. H. & Green, D. W. 1999. *Perry's chemical engineers' handbook*, McGraw-Hill Professional.
Pöllänen, K. 2006. Monitoring of crystallization processes by using infrared spectroscopy and multivariate methods. *Acta UniversitatisLappeenrantaensis*.
Pons, M.-N., Milferstedt, K. & Morgenroth, E. 2006. Modeling of chord length distributions. *Chemical Engineering Science,* 61**,** 3962-3973.
Qu, H., Pöllänen, K., Louhi-Kultanen, M., Kilpiö, T., Oinas, P. & Kallas, J. 2005. Batch cooling crystallization study based on in-line measurement of supersaturation and crystal size distribution. *Journal of Crystal Growth,* 275**,** e1857-e1862.
Raffel, M., Willert, C. E., Wereley, S. T. & Kompenhans, J. 2007. *Particle Image Velocimetry: A Practical Guide,* New York, Springer.
Rajoub, N. 2014. *Monitoring of crystallization and kinetics in batch crystalliser by FBRM and PIV.* PhD, Heriot-Watt University.
Randolph, A. D. & Sikdar, S. K. 1974. Effect of a soft impeller coating on the net formation of secondary nuclei. *AIChE Journal,* 20**,** 410-412.
Raphael, M. & Rohani, S. 1996. On-line estimation of solids concentrations and mean particle size using a turbidimetry method. *Powder technology,* 89**,** 157-163.
Rawlings, J. B., Miller, S. M. & Witkowski, W. R. 1993. Model identification and control of solution crystallization processes: a review. *Industrial & Engineering Chemistry Research,* 32**,** 1275-1296.
Richmond, W., Jones, R. & Fawell, P. 1998. The relationship between particle aggregation and rheology in mixed silica–titania suspensions. *Chemical Engineering Journal,* 71**,** 67-75.
Rodríguez-hornedo, N. & Murphy, D. 1999. Significance of controlling crystallization mechanisms and kinetics in pharmaceutical systems. *Journal of pharmaceutical sciences,* 88**,** 651-660.
Saleemi, A., Rielly, C. & Nagy, Z. K. 2012. Automated direct nucleation control for in situ dynamic fines removal in batch cooling crystallization. *CrystEngComm,* 14**,** 2196-2203.
Saleemi, A. N. 2011. *Strategic feedback control of pharmaceutical crystallization systems.* PhD, Loughborough University.
Sangwal, K. 2009a. Novel approach to analyze metastable zone width determined by the polythermal method: physical interpretation of various parameters. *Crystal Growth and Design,* 9**,** 942-950.
Sangwal, K. 2009b. A novel self-consistent Nývlt-like equation for metastable zone width determined by the polythermal method. *Crystal Research and Technology,* 44**,** 231-247.
Sangwal, K. 2011. Recent developments in understanding of the metastable zone width of different solute− solvent systems. *Journal of Crystal Growth,* 318**,** 103-109.
Sangwal, K. & Mielniczek-Brzóska, E. 2004. Effect of impurities on metastable zone width for the growth of ammonium oxalate monohydrate crystals from aqueous solutions. *Journal of Crystal Growth,* 267**,** 662-675.
Sanzida, N. & Nagy, Z. K. 2013. Iterative learning control for the systematic design of supersaturation controlled batch cooling crystallisation processes. *Computers & Chemical Engineering,* 59**,** 111-121.
Scheel, H. & Elwell, D. 1975. Crystal Growth from High-Temperature Solutions. *Crystal Growth from High Temperature Solutions*.
Schöll, J., Bonalumi, D., Vicum, L., Mazzotti, M. & Müller, M. 2006. In situ monitoring and modeling of the solvent-mediated polymorphic transformation of L-glutamic acid. *Crystal Growth & Design,* 6**,** 881-891.
Seidell, A. 1940. Solubilities of inorganic and metal organic compounds.

Sharp, K. & Adrian, R. 2001. PIV study of small-scale flow structure around a Rushton turbine. *AIChE Journal,* 47**,** 766-778.

Sharp, K. V., Kim, K. C. & Adrian, R. 2000. Dissipation estimation around a Rushton turbine using particle image velocimetry. *Laser Techniques Applied to Fluid Mechanics.* Springer.

Simon, L. L., Nagy, Z. K. & Hungerbuhler, K. 2009a. Comparison of external bulk video imaging with focused beam reflectance measurement and ultra-violet visible spectroscopy for metastable zone identification in food and pharmaceutical crystallization processes. *Chemical Engineering Science,* 64**,** 3344-3351.

Simon, L. L., Nagy, Z. K. & Hungerbuhler, K. 2009b. Endoscopy-based in situ bulk video imaging of batch crystallization processes. *Organic Process Research & Development,* 13**,** 1254-1261.

Simon, L. L., Oucherif, K. A., Nagy, Z. K. & Hungerbuhler, K. 2010. Histogram matching, hypothesis testing, and statistical control-chart-assisted nucleation detection using bulk video imaging for optimal switching between nucleation and seed conditioning steps. *Industrial & engineering chemistry research,* 49**,** 9932-9944.

Smith, C. A. & Corripio, A. B. 1985. *Principles and practice of automatic process control*, Wiley New York.

Srinivasan, K. 2008. Crystal growth of α and γ glycine polymorphs and their polymorphic phase transformations. *Journal of Crystal Growth,* 311**,** 156-162.

Stephen, H., Stephen, T. & Silcock, H. L. 1963. *Solubilities of inorganic and organic compounds*, Pergamon Press.

Stephenson, G. A., Forbes, R. A. & Reutzel-Edens, S. M. 2001. Characterization of the solid state: quantitative issues. *Advanced drug delivery reviews,* 48**,** 67-90.

Tavare, N. & Garside, J. 1986. Simultaneous estimation of crystal nucleation and growth kinetics from batch experiments. *Chemical engineering research & design,* 64**,** 109-118.

TheImagingSource. 2016. *The Imaging Source Technology Based on Standards* [Online]. Available: https://www.theimagingsource.com/ [Accessed May 2016].

Thompson, R. W. & Robson, K. 2001. Nucleation, growth, and seeding in zeolite synthesis. *Verifield Syntheses of Zeolitic Materials, Elsevier, Amsterdam***,** 21-23.

Titiz-Sargut, S. & Ulrich, J. 2003. Application of a protected ultrasound sensor for the determination of the width of the metastable zone. *Chemical Engineering and Processing: Process Intensification,* 42**,** 841-846.

Trifkovic, M., Sheikhzadeh, M. & Rohani, S. 2009. Determination of metastable zone width for combined anti-solvent/cooling crystallization. *Journal of Crystal Growth,* 311**,** 3640-3650.

Uhl, V. W. & Gray, J. B. 1966. Mixing, Theory and Practice, vol. 1. *l-172. Academic Press, New York***,** 11.

Valeton, J. 1924. I. Wachstum und Auflösung der Kristalle. III. *Zeitschrift für Kristallographie-Crystalline Materials,* 60**,** 1-38.

Variankaval, N., Cote, A. S. & Doherty, M. F. 2008. From form to function: crystallization of active pharmaceutical ingredients. *AIChE Journal,* 54**,** 1682-1688.

Vekilov, P. G. 2010. Nucleation. *Crystal growth & design,* 10**,** 5007-5019.

Volmer, M. 1939. Kinetik der phasenbildung.

Wang, X., Calderon De Anda, J., Roberts, K., Li, R., Thomson, G. & White, G. 2005. Advances in on-line monitoring and control of the morphological and polymorphic forms of organic crystals grown from solution. *KONA (Powder and Particle),* 23**,** 69-85.

Wilkinson, M., Jennings, K. & Hardy, M. 2000. Non-invasive video imaging for interrogating pharmaceutical crystallization processes. *Microscopy and microanalysis-New York-,* 6**,** 996-997.

Wilkinson, M., Jennings, K., Plant, R., Logan, R. & Drayson, B. 2003. Particle size and shape measured for process monitoring using high-speed image analysis. *Particulate Systems Analysis—2003, Harrogate*.

Wirth, M. & Baritaud, T. 1996. A cross correlation PIV technique using electro-optical image separation. *Experiments in fluids,* 21**,** 410-416.

Woo, X. Y., Nagy, Z. K., Tan, R. B. & Braatz, R. D. 2009. Adaptive Concentration Control of Cooling and Antisolvent Crystallization with Laser Backscattering Measurement. *Crystal Growth & Design,* 9**,** 182-191.

Worlitschek, J. & de Buhr, J. 2005. Crystallization Studies with Focused Beam Reflectance Measurement and MultiMax. *Application Note, AutoChem, MultiMax, Mettler Toledo: Columbia, MD, USA*.

Worlitschek, J. & Mazzotti, M. 2004. Model-based optimization of particle size distribution in batch-cooling crystallization of paracetamol. *Crystal Growth & Design,* 4**,** 891-903.

Yang, G., Louhi-Kultanen, M., Sha, Z., Kubota, N. & Kallas, J. 2006. A model for the prediction of supersaturation level in batch cooling crystallization. *Journal of chemical engineering of Japan,* 39**,** 426-436.

Yu, Z. Q., Chow, P. S. & Tan, R. B. 2006a. Application of attenuated total reflectance-Fourier transform infrared (ATR-FTIR) technique in the monitoring and control of anti-solvent crystallization. *Industrial & engineering chemistry research,* 45**,** 438-444.

Yu, Z. Q., Chow, P. S. & Tan, R. B. 2006b. Seeding and constant-supersaturation control by ATR-FTIR in anti-solvent crystallization. *Organic Process Research & Development,* 10**,** 717-722.

Zhang, F., Liu, T., Huo, Y., Guan, R. & Wang, X. Z. 2016. Investigation of the operating conditions to morphology evolution of β-l-glutamic acid during seeded cooling crystallization. *Journal of Crystal Growth*.

Zhang, J., Nguyan, J., Xiong, Z. & Morris, J. Iterative learning control of a crystallisation process using batch wise updated linearised models. Control and Decision Conference, 2009. CCDC'09. Chinese, 2009. IEEE, 1734-1739.

Zhang, S., Wang, F., He, D. & Jia, R. 2012. Batch-to-batch control of particle size distribution in cobalt oxalate synthesis process based on hybrid model. *Powder technology,* 224**,** 253-259.

Zhang, X.-Y., Févotte, G., Zhong, L., Qian, G., Zhou, X.-G. & Yuan, W.-K. 2010. Crystallization of zinc lactate in presence of malic acid. *Journal of Crystal Growth,* 312**,** 2747-2755.

Zhou, G. X., Fujiwara, M., Woo, X. Y., Rusli, E., Tung, H.-H., Starbuck, C., Davidson, O., Ge, Z. & Braatz, R. D. 2006. Direct design of pharmaceutical antisolvent crystallization through concentration control. *Crystal Growth & Design,* 6**,** 892-898.

Appendices

Appendix A

```
% The Developed MATLAB Code for Heating/Cooling Cycle Control and Image
% Processing for MSZW Measurement Experiments
%--------------------------------------------------------------------
close all;                  % close all figures
clc;                        % clear the command window
clear all;                  % clear all workspace variables
fclose('all');              % close all open files
delete(instrfindall);       % Reset Com Port
delete(timerfindall);       % Delete Timers
warning('off','all');
% ************************************************
% Constants
% ************************************************
T_H = 80;                           % Maximum Temperature in C
T_S = 20;                           % Minimum Temperature in C
H_1 = 70*60;                        % Holding Time after Heating Stage
Heating_Rate = 0.3;                 % Heating Rate C/min
Cooling_Rate = 0.3;                 % Cooling Rate C/min
bath_update_master_1=30         % Number of seconds allowed for updating the water
bath temperature
bath_update_master_2=30         % Number of seconds allowed for updating the water
bath temperature

% ************************************************
%Heating Stage:
% *************
disp('Starting the bath')
t0 = clock;                         % Read the current date and time
pause(15);                          % Hold for 15 seconds
% Read the current vessel temperature:
ans=read_bath('F2');
T_Vessel = decode_bath(ans);
figure
bath_last_update_time_1=0       % Hold the clock value since the bath was last updated
disp('In Heating Mode')
T_sp = T_Vessel;
T_start = T_sp;                     % Starting point for Temperature
% Write the set point temperature in a way that can be sent to water bath
Set_T_sp=round(T_sp*100); Set_T_sp=num2str(Set_T_sp);Ini='S  0';
Set_T_sp=strcat(Ini,Set_T_sp);
read_bath(Set_T_sp);
A = [{'Time', 'T_VESSEL','T_sp'}];    % matrix for writing header for excel file
while abs(T_Vessel - T_H)>1
t00 =clock;                                 % read the current date and time
Elapsed_time = etime(t00,t0);           % Time elapsed between date vectors
if Elapsed_time-bath_last_update_time_1>bath_update_master_1
```

```
disp('Waiting to reach T_H')
% Now we plot out values and update the bath
disp('Updating bath')
time = etime(t00,t0);           % Time elapsed between date vectors
old_T_Vessel=T_Vessel;
% plotting time vs Vessel temperature
plot(time,T_Vessel,'*k','MarkerSize',10,'LineWidth',2)
xlabel('Time(seconds)')
ylabel('Temperature (C)')
title('Plot of Time vs Vessel temperature')
hold on
% Increase the water bath temperature at a specific rate
if T_sp < T_H
T_sp = T_start +(Heating_Rate /60* Elapsed_time );
Set_T_sp=round(T_sp*100); Set_T_sp=num2str(Set_T_sp);Ini='S  0';
Set_T_sp=strcat(Ini,Set_T_sp);
ans=read_bath(Set_T_sp);
   else
disp('End of heating loop')
T_sp = T_H
Set_T_sp=round(T_sp*100); Set_T_sp=num2str(Set_T_sp);Ini='S  0';
Set_T_sp=strcat(Ini,Set_T_sp);
end
% Writing to excel file
A = [A;[{ time, T_Vessel,T_sp}]];
fid = fopen('Heating_Stage_Data.csv','wt');
fprintf(fid, '%s,%s,%s\n', A{1,:});
[row, col] = size(A);
for i=2:row
fprintf(fid, '%d,%d,%d\n', A{i,:});
end
fclose(fid);
plot(time,T_sp,'+k','MarkerSize',10,'LineWidth',2)
hold on
ans=read_bath(Set_T_sp);
% Now ask for the current vessel temperature from the extenal pt100
pause(5);                                   % Pause just in case
ans=read_bath('F2');
T_Vessel = decode_bath(ans)                 % Now read the vessel temperature
bath_last_update_time_1=Elapsed_time; % This stores the last time the bath was
updated
old_T_Vessel=T_Vessel;
if  ~isfloat(T_Vessel)                % check if water bath temperature is float or not
T_Vessel = old_T_Vessel;
end
end
end
% Holding Stage
disp('Holding for H_1')
pause(H_1)                            % Hold for H_1
t1 = clock;                           % read the current date and time
ans=read_bath('F2');
```

```
T_Vessel = decode_bath(ans)            % Now read the vessel temperature
% Create the delays in updating the water bath to avoid communications errors
bath_last_update_time_2=0              % Holds the clock value since the bath was last
updated
% ***********************************************
% Cooling Stage:
% **************
disp('In cooling mode')
T_sp = T_H;
A = [{'Time', 'T_VESSEL' , 'T_sp'}];       % matrix for writing the header for excel file
while T_Vessel - T_S >0.3
t2 = clock;                                % read the current date and time
Elapsed_time = etime(t2,t1);               % Time elapsed between date vectors
 if Elapsed_time-bath_last_update_time_2>bath_update_master_2
% Now we plot out values and update the bath
disp('Updating bath')
time=etime(t2,t0);                         % Time elapsed between date vectors
% Plotting time vs Vessel temperature
plot(time,T_Vessel,'*g','MarkerSize',10,'LineWidth',2)
hold on
% Decrease the water bath temperature at a specific rate
if T_sp > T_S
T_sp = T_H - (Cooling_Rate /60* Elapsed_time );
Set_T_sp=round(T_sp*100); Set_T_sp=num2str(Set_T_sp);Ini='S  0';
Set_T_sp=strcat(Ini,Set_T_sp);
ans=read_bath(Set_T_sp);
else
disp('End of cooling loop')
T_sp = T_S
Set_T_sp=round(T_sp*100); Set_T_sp=num2str(Set_T_sp);Ini='S  0';
Set_T_sp=strcat(Ini,Set_T_sp);
end
W%rite to excel file
A =[A; [{time,T_Vessel,T_sp}]];
fid = fopen('Cooling_Stage_Data.csv','wt');
fprintf(fid, '%s,%s,%s\n', A{1,:});
[row, col] = size(A);
for i=2:row
fprintf(fid, '%d,%d,%d\n', A{i,:});
end
fclose(fid);
plot(time,T_sp,'+g','MarkerSize',10,'LineWidth',2)
hold on
ans=read_bath(Set_T_sp);
% Now ask for the current vessel temperature from the extenal pt100
pause(5);                                  % Pause just in case
ans=read_bath('F2');
old_water_bath_T=T_Vessel;
T_Vessel = decode_bath(ans)                % Now read the vessel temperature
bath_last_update_time_2=Elapsed_time; % This stores the last time the bath was
updated
if  ~isfloat(T_Vessel) || T_Vessel ==0
```

```
T_Vessel = old_T_Vessel;
end
end
end
disp('Run finished')
fclose(s1)
```

Appendix B

```
% Function to calculate the Intensity Distribution Integral term (IDI) of the images:
%-------------------------------------------
function Cal_IDI = find_IDI( directory, isavarege)
dir_content=dir(strcat(directory , '/*.bmp'))
[nfiles n]=size(dir_content)                % Find the number of images in the directory
if  nfiles==0
message=sprintf('there is no image in the specified directory');
disp(message);
else
IDI_Value = [];
for frame=1:nfiles
image=sprintf('%s',dir_content(frame).name)
message=sprintf('Reading Frame %d %s',frame,image)
im_1=imread(strcat(strcat(directory, '/'), image));
im = rgb2gray(im_1);
A=sum(im,1);
IDI=trapz(A)            % Calculate the area underneath the curve of A by trapezoid rule
IDI_Value = [IDI_Value; IDI];
end
if isavarege
Cal_IDI= mean(IDI_Value);
else
Cal_IDI= IDI_Value
end
status=xlswrite('IDI_Values.xls',IDI_Value);
message=sprintf('Finished');
disp(message);
end
end
```

Appendix C

```
% Programme for running switching experiments:
%-----------------------------------------------
close all;                    % close all figures
clc;                          % clear the command window
clear all;                    % clear all workspace variables
fclose('all');                % close all open files
delete(instrfindall);         % Reset Com Port
delete(timerfindall);         % Delete Timers
warning('off','all');
% ************************************************
% Constants
% ************************************************
T_H=70;                       % Maximum Temperature in C
H_1 = 15*60;                  % Holding Time after Heating Stage
H_2 = 15*60;                  % Holding Time after Cooling Stage
bath_update_master=20;  % Number of seconds allowed for updating the water bath
temperature
bath_update_master_1=20;
bath_update_master_2=20;
% ************************************************
% Heating Stage:
% *************
disp('Starting the bath')
t0 = clock;                   % Read the current date and time
ans=read_bath('F2');          % Read the current vessel temperature
T_Vessel=decode_bath(ans);
figure
bath_T= read_bath('F1');   % Read the current Haake bath temperature
T_Haake= decode_bath(bath_T);
% Set the cold source (Haake bath) at its set point
T_sp=45;
% Write the temperature set point in a way that can be sent to water bath
Set_T_sp=round(T_sp*100); Set_T_sp=num2str(Set_T_sp);Ini='S  0';
Set_T_sp=strcat(Ini,Set_T_sp);
read_bath(Set_T_sp);
bath_last_update_time=0   % Holds the clock value since the bath was last updated
disp('In Heating Mode')
A = [{'Time', 'T_Vessel','T_Haake','T_Grant','W%'}]; % matrix for writing header for
excel file
%Reading the temperatures of Haake and Grant baths through a Pico Technology TC-
%08 USB Data Logger fitted with thermocouple type K
Temperature=['K';'K']
tc08Handle=tc08connect(Temperature)
Tem=tc08query(tc08Handle);
T_HAAKE= Tem(1,1)
T_GRANT= Tem(2,1)
dir_name = 'data_06112015';                    % the name of the images file
White_percentage= do_process(dir_name,0,1) %Calculate the W% of the last image
captured
while  abs(T_Vessel - T_H)>0.5
t00 =clock;                                    % read the current date and time
```

```
Elapsed_time = etime(t00,t0);                    % Time elapsed between date vectors
if Elapsed_time-bath_last_update_time>bath_update_master % Create the delays in
updating the water bath to avoid communications error
disp('Waiting to reach T_H')
disp('Updating bath')
time = etime(t00,t0);              % Time elapsed between date vectors
old_T_Vessel=T_Vessel;
% plotting time vs vessel temperature
plot(time,T_Vessel,'*k','MarkerSize',10,'LineWidth',2)
xlabel('Time(seconds)')
ylabel('Temperature (C)')
title('Plot of Time vs temperature')
hold on
% Writing to excel bath
A = [A;[{ time,T_Vessel ,T_HAAKE,T_GRANT,White_percentage}]];
fid = fopen('Heating_Stage_Data.csv','wt');
fprintf(fid, '%s,%s,%s,%s,%s\n', A{1,:});
[row, col] = size(A);
for i=2:row
fprintf(fid, '%d,%d,%d,%d,%d\n', A{i,:});
end
fclose(fid);
% Plotting time vs water bath(Grant) temperature
plot(time,T_GRANT,'+k','MarkerSize',10,'LineWidth',2)
hold on
%Reading the temperatures of Haake and Grant baths through a Pico Technology
TC-08 USB Data Logger fitted with thermocouple type K
Temperature=['K';'K']
tc08Handle=tc08connect(Temperature)
Tem=tc08query(tc08Handle);
T_HAAKE= Tem(1,1)
T_GRANT= Tem(2,1)
ans=read_bath('F2'); % Read the current vessel temperature
T_Vessel=decode_bath(ans)
dir_name = 'data_06112015';
White_percentage= do_process(dir_name,0,1)
bath_last_update_time=Elapsed_time; % This stores the last time the bath was updated
if  ~isfloat(T_Vessel)                    % check if water bath temperature is float or not
T_Vessel = old_T_Vessel;
end
end
end
% Holding Stage:
disp('Holding for H_1')
pause(H_1)                    % Hold for H_1
%-----------------------------------------------------
% Cooling Stage:
%***************
Valve(0,0,1,0)                % vessel is connected to Grant water bath (Hot source)
Bath_on='Grant';
t3 = clock;                   % read the current date and time
ans=read_bath('F2');          % Now read the vessel temperature
```

```
T_Vessel = decode_bath(ans)
pause(2);                       % Pause just in case
bath_T=read_bath('F1');         % Now read the Haake water bath temperature
T_Haake = decode_bath(bath_T);
% Set the cold source (Haake bath) at its set point
T_sp=45;
Set_T_sp=round(T_sp*100); Set_T_sp=num2str(Set_T_sp);Ini='S  0';
Set_T_sp=strcat(Ini,Set_T_sp);
read_bath(Set_T_sp);
bath_last_update_time_2=0       % Holds the clock value since the bath was last updated
disp('In cooling Mode')
A = [{'Time', 'T_vessel' ,'T_Haake', 'W%','Bath_on'}]; % matrix for writing the header
for excel file
B = [{'Time', 'T_vessel','T_Haake','T_Grant'}];
dir_name = 'data_06112015';
White_percentage= do_process(dir_name,0,1)
Temperature=['K';'K']
tc08Handle=tc08connect(Temperature)
Tem=tc08query(tc08Handle);
T_HAAKE= Tem(1,1)
T_GRANT= Tem(2,1)
while  abs(T_Vessel - 55)>0.5
t4 = clock;                             % read the current date and time
Elapsed_time = etime(t4,t3);            % Time elapsed between date vectors
if Elapsed_time-bath_last_update_time_2>bath_update_master_2
disp('Updating bath')
time=etime(t4,t0);                      % Time elapsed between date vectors
B = [B;[{ time,T_Vessel ,T_HAAKE,T_GRANT}]];
fid = fopen('Temperatures_Data_CoolingStage.csv','wt');
fprintf(fid, '%s,%s,%s,%s\n', B{1,:});
[row, col] = size(B);
for i=2:row
fprintf(fid, '%d,%d,%d,%d\n', B{i,:});
end
fclose(fid);
% Plotting time vs vessel temperature
plot(time,T_Vessel,'*b','MarkerSize',10,'LineWidth',2)
hold on
% Plotting time vs W%
plot(time,White_percentage,'+r','MarkerSize',10,'LineWidth',2)
hold on
T_sp=45;
pause(2);                                       % Pause just in case
ans=read_bath('F2');
T_Vessel = decode_bath(ans)
pause(2);
bath_T=read_bath('F1');
T_Haake = decode_bath(bath_T);
dir_name = 'data_06112015';
White_percentage= do_process(dir_name,0,1)
Temperature=['K';'K']
tc08Handle=tc08connect(Temperature)
```

```
Tem=tc08query(tc08Handle);
T_HAAKE= Tem(1,1)
T_GRANT= Tem(2,1)
A =[A; [{time,T_Vessel,T_Haake,White_percentage,Bath_on}]];
fid = fopen('Cooling_Stage_Data.csv','wt');
fprintf(fid, '%s,%s,%s,%s,%s\n', A{1,:});
[row, col] = size(A);
for i=2:row
fprintf(fid, '%d,%d,%d,%d,%s\n', A{i,:});
end
fclose(fid);
bath_last_update_time_2=Elapsed_time;
end
end
disp('Holding for H_2')
pause(H_2)
%-----------------------------------------------
%Switching Stage:
%*****************
Valve(0,0,1,0)                  % Vessel is connected to the hot water bath (Grant)
Bath_on='Grant';
t3 = clock;                     % read the current date and time
ans=read_bath('F2');
T_Vessel = decode_bath(ans)
pause(2);
bath_T=read_bath('F1');
T_Haake = decode_bath(bath_T);
bath_last_update_time_1=0       % Holds the clock value since the bath was last updated
disp('In switching Mode')
T_sp = 45;
A = [{'Time', 'T_Vessel' ,'T_Haake', 'W%','Bath_on'}];
B = [{'Time', 'T_Vessel','T_Haake','T_Grant'}];
dir_name = 'data_06112015';
White_percentage= do_process(dir_name,0,1)
Temperature=['K';'K']
tc08Handle=tc08connect(Temperature)
Tem=tc08query(tc08Handle);
T_HAAKE= Tem(1,1)
T_GRANT= Tem(2,1)
counter_1=0;
counter_2=0;
while White_percentage < 100
t4 = clock;                             % read the current date and time
Elapsed_time = etime(t4,t3);            % Time elapsed between date vectors
if Elapsed_time-bath_last_update_time_1>bath_update_master_1
disp('Updating bath')
time=etime(t4,t0);                      % Time elapsed between date vectors
B = [B;[{ time,T_Vessel ,T_HAAKE,T_GRANT}]];
fid = fopen('Temperatures_Data_SwitchingStage.csv','wt');
fprintf(fid, '%s,%s,%s,%s\n', B{1,:});
[row, col] = size(B);
for i=2:row
```

```
fprintf(fid, '%d,%d,%d,%d\n', B{i,:});
end
fclose(fid);
% Plotting time vs vessel temperature
plot(time,T_Vessel,'*b','MarkerSize',10,'LineWidth',2)
hold on
% Plotting time vs W%
plot(time,White_percentage,'+r','MarkerSize',10,'LineWidth',2)
hold on
if  rem(counter_1,2) == 0
if (strcmp(Bath_on,'Grant')==1)
Valve(0,0,0,1)                  % vessel is connected to cold water bath
end
Bath_on='Haake';
counter_2=counter_2+1;
elseif rem(counter_1,2) == 1
Valve(0,0,1,0)                  % vessel is connected to hot water bath
Bath_on='Grant';
counter_1=counter_1+1;
end
ans=read_bath('F2');
T_Vessel = decode_bath(ans)
pause(2);
bath_T=read_bath('F1');
T_Haake = decode_bath(bath_T);
dir_name = 'data_06112015';
White_percentage= do_process(dir_name,0,1)
Temperature=['K';'K']
tc08Handle=tc08connect(Temperature)
Tem=tc08query(tc08Handle);
T_HAAKE= Tem(1,1)
T_GRANT= Tem(2,1)
A =[A; [{Time,T_Vessel,T_Haake,White_percentage,Bath_on}]];
fid = fopen('Switching_Stage_Data.csv','wt');
fprintf(fid, '%s,%s,%s,%s,%s\n', A{1,:});
[row, col] = size(A);
for i=2:row
fprintf(fid, '%d,%d,%d,%d,%s\n', A{i,:});
end
fclose(fid);
if counter_2==2
counter_1=counter_1+1;
counter_2=0;
end
bath_last_update_time_1=Elapsed_time;
end
end
disp('Run finished')
```

Appendix D

```
% MATLAB Code for the Developed Control Approach Applied for LGA and Glycine
Control Experiments:
%-----------------------------------------------------------------------------------------------
close all;                  % close all figures
clc;                        % clear the command window
clear all;                  % clear all workspace variables
fclose('all');              % close all open files
delete(instrfindall);       % Reset Com Port
delete(timerfindall);       % Delete Timers
warning('off','all');
% ************************************************
% Constants
% ************************************************
T_H = 70;                               % Maximum Temperature in C
H_1 = 30*60;                            % Holding Time after Heating Stage
Cooling_Rate_stage_1=0.2;
bath_update_master_1= 30;               % Number of seconds allowed for updating the
water bath temperature
bath_update_master_2= 30;
bath_update_master_3= 30;
bath_update_master_4= 30;
disp('Starting the bath')
t0 = clock;                             % read the current date and time
pause(15);                              % Hold for 15 seconds
% Read the current Vessel and Haake bath temperatures:
ans=read_bath('F2');
T_Vessel=decode_bath(ans)
figure
bath_T= read_bath('F1');
T_Haake = decode_bath(bath_T)
% Write the set point temperature in a way that can be sent to water bath
T_sp = 20;                              %  Temperature set-point of Haake water bath
Set_T_sp=round(T_sp*100); Set_T_sp=num2str(Set_T_sp);Ini='S  0';
Set_T_sp=strcat(Ini,Set_T_sp);
read_bath(Set_T_sp);
bath_last_update_time_1=0      % Holds the clock value since the bath was last updated
disp('In Heating Mode')
A = [{'Time', 'T_vessel','T_Haake','T_Grant'}];
%Reading the temperatures of Haake and Grant baths through a Pico Technology TC-
08 USB Data Logger fitted with thermocouple type K
Temperature=['K';'K']
tc08Handle=tc08connect(Temperature)
Tem=tc08query(tc08Handle);
T_HAAKE= Tem(1,1)
T_GRANT= Tem(2,1)
% *************
% Heating Stage:
% *************
while  abs(T_Vessel - T_H)>1
t6 =clock;                                  % read the current date and time
Elapsed_time = etime(t6,t0);                % Time elapsed between date vectors
```

```
if Elapsed_time-bath_last_update_time_1>bath_update_master_1  % Create the delays
in updating the water bath to avoid communications error
disp('Waiting to reach T_H')
% Now we plot out values and update the bath
disp('Updating bath')
time = etime(t6,t0);        % Time elapsed between date vectors
old_T_Vessel=T_Vessel;
% plotting time vs vessel temperature
plot(time,T_Vessel,'*k','MarkerSize',10,'LineWidth',2)
xlabel('Time(seconds)')
ylabel('Temperature (C)')
title('Plot of Time vs vessel temperature')
hold on
% writing to excel file
A = [A;[{ time,T_Vessel,T_HAAKE,T_GRANT}]];
fid = fopen('Temperature_Data_HeatingStage.csv','wt');
fprintf(fid, '%s,%s,%s,%s\n', A{1,:});
[row, col] = size(A);
for i=2:row
fprintf(fid, '%d,%d,%d,%d\n', A{i,:});
end
fclose(fid);
plot(time,T_GRANT,'+k','MarkerSize',10,'LineWidth',2)
hold on
%Reading the temperatures of Haake and Grant baths through a Pico TechnologyTC-08
USB Data Logger fitted with thermocouple type K
Temperature=['K';'K']
tc08Handle=tc08connect(Temperature)
Tem=tc08query(tc08Handle);
T_HAAKE= Tem(1,1)
T_GRANT= Tem(2,1)
% Read the current vessel temperature:
ans=read_bath('F2');
T_Vessel=decode_bath(ans)
bath_last_update_time_1=Elapsed_time;
if  ~isfloat(T_Vessel)            % check if vessel temperature is float or not
T_Vessel = old_T_Vessel;
end
end
end
% Write the set point temperature in a way that can be sent to water bath
T_sp= 15;               %  Temperature set-point of Haake water bath as Cold Source
Set_T_sp=round(T_sp*100); Set_T_sp=num2str(Set_T_sp);Ini='S  0';
Set_T_sp=strcat(Ini,Set_T_sp);
read_bath(Set_T_sp);
% Holding Stage:
disp('Holding for H_1')
pause(H_1)                        % Hold for H_1

% Cooling Stage:
%***************
Valve(0,0,0,1)                    % vessel is connected to COLD water bath: Haake bath
```

```
Bath_on='Haake';
t7 = clock;                          % read the current date and time
ans=read_bath('F2');                 % Now read the vessel temperature
T_Vessel = decode_bath(ans)
pause(2);                            % Pause just in case
bath_T=read_bath('F1');              % Now read the Haake temperature
T_Haake = decode_bath(bath_T);
% Write the set point temperature in a way that can be sent to water bath
T_sp=15;                        %Temperature set-point of Haake water bath as Cold Source
Set_T_sp=round(T_sp*100); Set_T_sp=num2str(Set_T_sp);Ini='S  0';
Set_T_sp=strcat(Ini,Set_T_sp);
read_bath(Set_T_sp);
% Create the delays in updating the water bath to avoid communications error
bath_last_update_time_2=0
disp('In cooling Mode')
A = [{'Time', 'T_Vessel' ,'T_Haake', 'W%','Bath_on'}];
B = [{'Time', 'T_Vessel','T_Haake','T_Grant'}];
dir_name = 'data_28012016';                          % the name of the images file
White_percentage= do_process(dir_name,0,1)     %Calculate the W% of the last image
captured
%Reading the temperatures of Haake and Grant baths through a Pico Technology TC-
08 USB Data Logger fitted with thermocouple type K
Temperature=['K';'K']
tc08Handle=tc08connect(Temperature)
Tem=tc08query(tc08Handle);
T_HAAKE= Tem(1,1)
T_GRANT= Tem(2,1)
while White_percentage < 5
t3 = clock;                          % read the current date and time
Elapsed_time = etime(t3,t7);     % Time elapsed between date vectors
if Elapsed_time-bath_last_update_time_2>bath_update_master_2
disp('Updating bath')
time=etime(t3,t0);                   % Time elapsed between date vectors
% Writing to excel file
B = [B;[{ time,T_Vessel ,T_HAAKE,T_GRANT}]];
fid = fopen('Temperatures_Data_CoolingStage.csv','wt');
fprintf(fid, '%s,%s,%s,%s\n', B{1,:});
[row, col] = size(B);
for i=2:row
fprintf(fid, '%d,%d,%d,%d\n', B{i,:});
end
fclose(fid);
% Plotting time vs VESSEL temperature and white percentage
plot(time,T_Vessel,'*b','MarkerSize',10,'LineWidth',2)
hold on
plot(time,White_percentage,'+r','MarkerSize',10,'LineWidth',2)
hold on
Time=etime(t3,t0);                   % Time elapsed between date vectors
ans=read_bath('F2');                 % Now read the vessel temperature
T_Vessel = decode_bath(ans)
pause(2);
bath_T=read_bath('F1');                          % Now read the Haake temperature
```

```
T_Haake = decode_bath(bath_T);
dir_name = 'data_28012016';                    % Images file name
White_percentage= do_process(dir_name,0,1) % Calculate the white percentage of the
current image
%Reading the temperatures of Haake and Grant baths through a Pico Technology TC-
08 USB Data Logger fitted with thermocouple type K
Temperature=['K';'K']
tc08Handle=tc08connect(Temperature)
Tem=tc08query(tc08Handle);
T_HAAKE= Tem(1,1)
T_GRANT= Tem(2,1)
% Writing to excel file
A =[A; [{Time,T_Vessel,T_Haake,White_percentage,Bath_on}]];
fid = fopen('Cooling_Stage_Data.csv','wt');
fprintf(fid, '%s,%s,%s,%s,%s\n', A{1,:});
[row, col] = size(A);
for i=2:row
fprintf(fid, '%d,%d,%d,%d,%s\n', A{i,:});
end
fclose(fid);
bath_last_update_time_2=Elapsed_time;
end
end
%---------------------------------
%reset stage
Valve(0,0,1,0)                    % vessel is connected to HOT water bath
Bath_on='Grant';
t4 = clock;                       % read the current date and time
ans=read_bath('F2');
T_Vessel = decode_bath(ans)       % Now read the vessel temperature
pause(2);
bath_T=read_bath('F1');           % Now read the Haake temperature
T_Haake = decode_bath(bath_T);
T_sp=15;
Set_T_sp=round(T_sp*100); Set_T_sp=num2str(Set_T_sp);Ini='S  0';
Set_T_sp=strcat(Ini,Set_T_sp);
read_bath(Set_T_sp);
bath_last_update_time_3=0
disp('In reset Mode')
T_sp = 15;
A = [{'Time', 'T_Vessel' ,'T_Haake', 'W%','Bath_on'}];
B = [{'Time', 'T_Vessel','T_Haake','T_Grant'}];
dir_name = 'data_28012016';
White_percentage= do_process(dir_name,0,1)     %Calculate the white percentage of
the current image
%Reading the temperatures of Haake and Grant baths through a Pico Technology TC-
08 USB Data Logger fitted with thermocouple type K
Temperature=['K';'K']
tc08Handle=tc08connect(Temperature)
Tem=tc08query(tc08Handle);
T_HAAKE= Tem(1,1)
T_GRANT= Tem(2,1)
```

```
while (T_Vessel < 60)||( White_percentage > 10 )  % To remove the rapid increase in
W% due to spontaneous nucleation
t5 = clock;                                       % read the current date and time
Elapsed_time = etime(t5,t4);                      % Time elapsed between date vectors
if Elapsed_time-bath_last_update_time_3>bath_update_master_3
disp('Updating bath')
time=etime(t5,t0);                                % Time elapsed between date vectors
B = [B;[{ time,T_Vessel ,T_HAAKE,T_GRANT}]];
fid = fopen('Temperature_Data_ResetStage.csv','wt');
fprintf(fid, '%s,%s,%s,%s\n', B{1,:});
[row, col] = size(B);
for i=2:row
fprintf(fid, '%d,%d,%d,%d\n', B{i,:});
end
fclose(fid);
% Plotting time vs vessel temperature
plot(time,T_Vessel,'*g','MarkerSize',10,'LineWidth',2)
hold on
% Plotting time vs W%
plot(time,White_percentage,'+b','MarkerSize',10,'LineWidth',2)
hold on
Time=etime(t5,t0);
pause(2);
ans=read_bath('F2');
T_Vessel = decode_bath(ans)
pause(2);
bath_T=read_bath('F1');
T_Haake = decode_bath(bath_T);
dir_name = 'data_28012016';
White_percentage= do_process(dir_name,0,1)
Temperature=['K';'K']
tc08Handle=tc08connect(Temperature)
Tem=tc08query(tc08Handle);
T_HAAKE= Tem(1,1)
T_GRANT= Tem(2,1)
A =[A; [{Time,T_Vessel,T_Haake,White_percentage,Bath_on}]];
fid = fopen('reset_stage_Data.csv','wt');
fprintf(fid, '%s,%s,%s,%s,%s\n', A{1,:});
[row, col] = size(A);
for i=2:row
fprintf(fid, '%d,%d,%d,%d,%s\n', A{i,:});
end
fclose(fid);
bath_last_update_time_3=Elapsed_time;
end
end
%---------------------------------
%control stage:
%***************
Valve(0,0,0,1)                    % vessel is connected to COLD water bath
Bath_on='Haake';
% Initial variables:
```

```
Control_type='A'
Mode='Auto'
t6 = clock;                         % read the current date and time
ans=read_bath('F2');                % Now read the vessel temperature
T_Vessel = decode_bath(ans)
pause(2);
bath_T=read_bath('F1');             % Now read the Haake temperature
T_Haake = decode_bath(bath_T);
T_sp=15;
Set_T_sp=round(T_sp*100); Set_T_sp=num2str(Set_T_sp);Ini='S  0';
Set_T_sp=strcat(Ini,Set_T_sp);
read_bath(Set_T_sp);
% Create the delays in updating the water bath to avoid communications error
bath_last_update_time_4=0
disp('In control stage')
A = [{'Time', 'T_vessel' ,'T_Haake',
'T_sp','Slope','W%_actual','Control_type','Bath_on','Mode','W%_SP'}];
B = [{'Time', 'T_vessel','T_Haake','T_Grant'}];
dir_name = 'data_28012016';
White_percentage_base= do_process(dir_name,0,1)        % calculate the W%_base
W_sp =0
while W_SP < 100
t7 = clock;                                           % read the current date and time
Elapsed_time = etime(t7,t6);                          % Time elapsed between date vectors
if Elapsed_time-bath_last_update_time_4>bath_update_master_4
dt=Elapsed_time;
disp('Updating bath')
time=etime(t7,t0);
dir_name = 'data_28012016';
White_percentage= do_process(dir_name,1,1)
old_T_Vessel=T_Vessel;
ans=read_bath('F2');                                  % Now read the vessel temperature
T_Vessel = decode_bath(ans)
pause(2);
bath_T=read_bath('F1');                               % Now read the HAAKE temperature
T_Haake = decode_bath(bath_T);
Temperature=['K';'K']
tc08Handle=tc08connect(Temperature)
Tem=tc08query(tc08Handle);
T_HAAKE= Tem(1,1)
T_GRANT= Tem(2,1)
B = [B;[{ time,T_Vessel,T_HAAKE,T_GRANT}]];
fid = fopen('Temperatures_Data_ControlStage.csv','wt');
fprintf(fid, '%s,%s,%s,%s\n', B{1,:});
[row, col] = size(B);
for i=2:row
fprintf(fid, '%d,%d,%d,%d\n', B{i,:});
end
fclose(fid);
% Plotting time vs Vessel temperature
plot(time,T_Vessel,'*b','MarkerSize',10,'LineWidth',2)
hold on
```

```
read_bath(Set_T_sp);
% Plotting time vs W%
plot(time,White_percentage,'+r','MarkerSize',10,'LineWidth',2)
hold on
dir_name = 'data_28012016';
whitepercentage=do_process(dir_name, 0,2); %Calculate the W% of the last 10 images
in the file
n=length(whitepercentage);
average_values_start = mean(whitepercentage(n-3:n-2));
average_values_final = mean(whitepercentage(n-1:n));
Slope=( average_values_final-average_values_start)       %Calculate SLOPE value

% Conditions to switch between HOT and COLD baths:
%-----------------------------------------------------------------
if ((Slope <= 1) &&(strcmp(Bath_on,'Grant')==1) &&(strcmp(Control_type,'A')==1))
Valve(0,0,0,1)                                  % vessel is connected to COLD water bath
Bath_on='Haake';
elseif ((Slope <= 1) &&(strcmp(Bath_on,'Haake')==1))
T_sp = 15;
Set_T_sp=round(T_sp*100); Set_T_sp=num2str(Set_T_sp);Ini='S  0';
Set_T_sp=strcat(Ini,Set_T_sp);
ans=read_bath(Set_T_sp);
elseif ((Slope > 1)&& (strcmp(Bath_on,'Haake')==1))
Valve(0,0,1,0)                                  % vessel is connected to HOT water bath
Bath_on='Grant';
elseif  ((Slope > 1)&& (strcmp(Bath_on,'Grant')==1))
Control_type ='M'
Mode = 'Manual'
end
dir_name = 'data_28012016';
White_percentage= do_process(dir_name,1,1)
% Calculate the W%_SP Trajectory:
W_SP= White_percentage_base+ (0.2*(dt/60))

if (((White_percentage - W_SP)< 5) &&(strcmp(Control_type,'M')==1)) % Condition
to avoid dissolve more crystals than needed
Control_type ='A'
Mode = 'Auto'
end
%Write all the parameters to excel file
A =[A;
[{time,T_Vessel,T_Haake,T_sp,Slope,White_percentage,Control_type,Bath_on,Mode,
W_SP}]];
fid = fopen('control_stage_Data.csv','wt');
fprintf(fid, '%s,%s,%s,%s,%s,%s,%s,%s,%s,%s\n', A{1,:});
[row, col] = size(A);
for i=2:row
fprintf(fid, '%d,%d,%d,%d,%d,%d,%s,%s,%s,%d\n', A{i,:});
end
fclose(fid);
bath_last_update_time_4=Elapsed_time;
if  ~isfloat(T_Vessel) || T_Vessel ==0
```

```
T_Vessel = old_T_Vessel;
end
end
end
disp('Run finished')
```

Appendix E

Functions called in the main programmes listed in Appendices A, B, C and D are:

Function 1:

```
% Decode the string from the bath into a temperature:
%-------------------------------------------------------------
function temperature_from_bath = decode_bath( from_bath)
if from_bath=='$'
temperature_from_bath=0;
else
temperature_from_bath=sscanf(from_bath,'%f');
end
end
```

Function 2:

```
%A function to read the current temperature from the HAKKE water bath
%-------------------------------------------------------------------
function message_from_bath = read_bath(message_to_bath)
s1 = serial('COM1','BaudRate',2400,'DataBits',8);
set (s1,'Terminator','CR','InputBufferSize',256);
fopen(s1);
fprintf(s1,message_to_bath);
ans=fscanf(s1,'%s');
fclose(s1);
message_from_bath=ans;
end
```

Function 3:

```
% Function to calculate the W% of the images:
%-----------------------------------------------------
function white_pixel_percentage=do_process(directory, isavarege,variable)
dir_content=dir(strcat(directory , '/*.bmp'))
[nfiles n]=size(dir_content)                % Find the number of images in the directory
if nfiles==0
message=sprintf('there is no image in the specified directory');
disp(message);
else
white_percentages = [];
switch variable
case 1
frame=nfiles;
image=sprintf('%s',dir_content(frame).name);
message=sprintf('Reading Frame %d %s',frame,image);
disp(message);
im_1=imread(strcat(strcat(directory, '/'), image));
im = rgb2gray(im_1);
im_sub=im2double(im);
[n m] = size(im_sub);
counter_white=0;
for i=1:n
```

```
for j=1:m
if im_sub(i,j)>0.1
counter_white=counter_white+1;
end
end
end
white_percentage= (counter_white/(n * m))*100
message=sprintf('White_percentage %s %d %%',image,white_percentage);
disp(message);
white_percentages = [white_percentages; white_percentage]
if isavarege
white_pixel_percentage= mean(white_percentages)
else
white_pixel_percentage= white_percentage
end
xlsFile = 'White_percentage.xls';
try
data = xlsread(xlsFile);
catch ex
data = [];
end
status=xlswrite(xlsFile,[data; white_percentages]);
message=sprintf('Finished');
disp(message);
case 2
for frame=nfiles-9:nfiles
image=sprintf('%s',dir_content(frame).name);
message=sprintf('Reading Frame %d %s',frame,image);
disp(message);
im_1=imread(strcat(strcat(directory, '/'), image));
im = rgb2gray(im_1);
im_sub=im2double(im);
[n m] = size(im_sub);
counter_white=0;
for i=1:n
for j=1:m
if im_sub(i,j)>0.1
counter_white=counter_white+1;
end
end
end
white_percentage= (counter_white/(n * m))*100
message=sprintf('White_percentage %s %d %%',image,white_percentage);
disp(message);
white_percentages = [white_percentages; white_percentage]
end
if isavarege
white_pixel_percentage= mean(white_percentages)
else
white_pixel_percentage= white_percentages
end
xlsFile = 'White_percentage_control.xls';
```

```
try
data = xlsread(xlsFile);
catch ex
data = [];
end
status=xlswrite(xlsFile,[data; white_percentages]);
message=sprintf('Finished');
disp(message);
end
end
end
```

Function 4:

```
%A Function to Control the Valves through USB:
%-------------------------------------------
function Valve(v3,v2,v1,v0)
daqregister('mcc')                % Register the board , register hDAQ adaptor
dio=digitalio('mcc',0)            % constructs a digital I/O object associated with adaptor
                                  % ('mcc', #) #: Board number
hline = addline(dio,0:3,0,'Out');   % Add lines and assign their statues to the object
 % addline(dio,Lines numbers(0:7),Port number(0=A,1=B),'Out'/'In')
putvalue(dio, [0 0 0 0])        % Assign values to the lines: putvalue(dio, [A3 A2 A1 A0])
start(dio)                        % Start
putvalue(dio, [v3 v2 v1 v0])        % Assign another values
delete (dio)                        % Delete the object before next run
end
```